Emulsion-derived (PolyHIPE) foams for structural materials applications

Carnachan, Ross James

Emulsion-derived (PolyHIPE) Foams For Structural Materials Applications

A thesis submitted to the University of Durham in accordance with the regulations governing the award of the degree of Doctor of Philosophy

Ross James Carnachan

Department of Chemistry
University of Durham
Durham

May 2004

Declaration

The material contained within this thesis has not previously been submitted to the University of Durham or any other University. The research reported within this thesis has been conducted by the author unless indicated otherwise.

Ross Carnachan
May 2004

Abstract

Emulsion-derived (PolyHIPE) Foams for Structural Materials Applications.

Ross James Carnachan

The simplest type of sandwich composite consists of two, thin, stiff strong sheets of dense material separated by a thick layer of low density material. The first major structure to incorporate sandwich panels was the Second World War "Mosquito aircraft" which consisted of a balsa wood core with plywood faces.

The cellular materials used for sandwich core applications can generally be divided into two categories; honeycomb structures and polymer foams. Other cellular cores which exist are balsa wood and corrugated cores. Honeycomb materials generally have a hexagonal cellular shape, and are the core material of choice for advanced composites.

In this thesis it was the aim to prepare open-cellular PolyHIPE foam core materials by the polymerisation of the continuous phase of a high internal phase emulsion (HIPE). To assess whether PolyHIPE materials are viable as core materials their flexural, compressive and shear properties were evaluated against the current commercially used core materials. It was shown that it was possible to improve the flexural, compressive and shear properties of a styrene/DVB PolyHIPE material by the addition of fibres to the material and the use of an optimised surfactant system (OSS).

It was also shown that by the addition of monomers such as; butyl acrylate, 2-ethylhexyl acrylate, butyl methacrylate and methyl methacrylate to the monomer phase that the compressive properties of the S/DVB material could be varied.

It was also possible to prepare a fibre-free and fibre-reinforced resorcinol-formaldehyde-based material, which had greater compressive and shear properties compared to the styrene/DVB material.

Also a PolyHIPE material containing poly (ϵ-caprolactone) diacrylate showed shape-memory properties and an elongated cell structure after deformation and cooling. This elongated cell structure could lead to possible anisotropic behaviour.

Finally it was concluded that the best mechanically performing PolyHIPE materials prepared competed well with the shear and compressive strength of the commercial honeycomb and foam core materials examined.

Acknowledgements

I would like to acknowledge the financial support from Qinetiq and especially my dad while I was writing up. I would not be at this stage otherwise.

I would like to thank Wrigley's fibres, Rhodia Chemicals and Borden Chemicals.

I would also like to thank my supervisors Dr Neil Cameron and Dr Martin Swan for their continued support during my Ph.D.

I would like to thank a number of technical staff at the chemistry department; Jim and especially Neil in the mechanical work shop for putting together the PVC mould and cutting my large blocks of PolyHIPE, Doug Carswell for DSC and TGA analysis and Stuart Eggleston for his continued help with the ESEM.

Thanks to my friends and colleagues in the NRC group past and present, Craig F, Jane, Kelly F, Wendy, Andrea, Audrey, Alistair Reid, Peter, Chun-tian, Moira and Alex.
To my following friends here in Durham and GSAFC, for making my past three years here so enjoyable; Amy, Zoe, Ian S, Paul P, Steve B, Stephen O, John Malget, Craig M, Bruce, Alan, Troll, Dave H, Dave (Poly), Alister, Jacquie, Esther, Damo, Brian, Neil, Dave E, Kelly L, Claire M, Claire P, Vicci, Ian K, Katie, Simon, Alex (50's), Michael, Cameron and Mr & Mrs Nixon (especially Martin for supplying me with lots of cheap beer for the last three years).

Finally to my family, mum, dad, Doug, Greg and Grant for all you support over the past three years.

Abbreviations

ASTM	American society for testing and materials
AIBN	2'2-Azo-bis-(isobutyronitrile)
BA	n-Butyl acrylate
BMA	Butyl methacrylate
BSED	Back scattering emission detector
C	Carbon
CEB	2-Chloroethyl benzene
CFC	Chloro-fluoro-carbon
CTAB	Cetyltrimethylammonium bromide
DCM	Dichloromethane
DDBSS	Dodecylbenzenesulfonic acid, sodium salt
DMTA	Dynamic mechanical thermal analysis
DSC	Differential Scanning Calorimetry
DVB	Divinylbenzene
EGDMA	Ethyleneglycol dimethacrylate
EHA	2-Ethylhexyl acrylate
EHMA	2-Ethylhexyl methacrylate
ESEM	Environmental scanning electron microscope
FRC	Fibre-reinforced composite
FRP	Fibre-reinforced polymer
H	Hydrogen
HCl	Hydrochloric acid
HDPE	High density poly (ethylene)

HIPE	High internal phase emulsion
HIPS	High impact polystyrene
HLB	Hydrophile-lipophile balance
K	Kevlar
LDPE	Low density poly (ethylene)
MALDI-tof	Matrix assisted laser desorption of ionisation-time of flight
MMA	Methyl methacrylate
M_n	Number average molecular weight
N	Nitrogen
NMR	Nuclear magnetic resonance
OSS	Optimised surfactant system
PAN	Polyacrylonitrile
PB	Poly (butadiene)
PCL	Poly (ϵ-caprolactone)
PCLDA	Poly (ϵ-caprolactone) diacrylate
PE	Polyethylene
PES	Poly (ethersulfone)
PEO	Poly (ethylene oxide)
PMI	Polymethacrylimide
PP	Polypropylene
PPS	Poly (phenylsulfone)
PS	Polystyrene
PTFE	Poly (tetrafluoroethylene)
PUR	Polyurethane
PVC	Poly (vinyl chloride)

RF	Resorcinol/formaldehyde
S	Styrene
S80	Span 80
S20	Span 20
SAN	Styrene/acrylonitrile
SEM	Scanning electron microscope/micrograph
TGA	Thermo-gravimetric analysis
TMPTM	Trimethylolpropane trimethacrylate
T_g	Glass transition temperature
T_m	Crystalline melting temperature
T_{trans}	Transition temperature
T_{perm}	Highest thermal transition
UF	Urea/formaldehyde
V	Viscose
VBC	Vinyl benzyl chloride

Contents

Chapter 1

Introduction

1.1 Introduction to mechanical behaviour

The mechanical properties of polymers are important in any application where they are used as structural materials [1]. The wide use of plastics, rubbers and fibres is dependent on their mechanical properties rather than their chemical behaviour. The interest is in understanding why one polymer, for example, is tough or brittle compared to one that is a rubber. It is essential to know how the mechanical behaviour is related to the chemical structure to tailor the material properties for specific applications.

1.1.1 Definition of mechanical terms

Mechanical behaviour involves the deformation of a material by applied forces. A homogenous, isotropic, elastic material has the simplest mechanical properties.

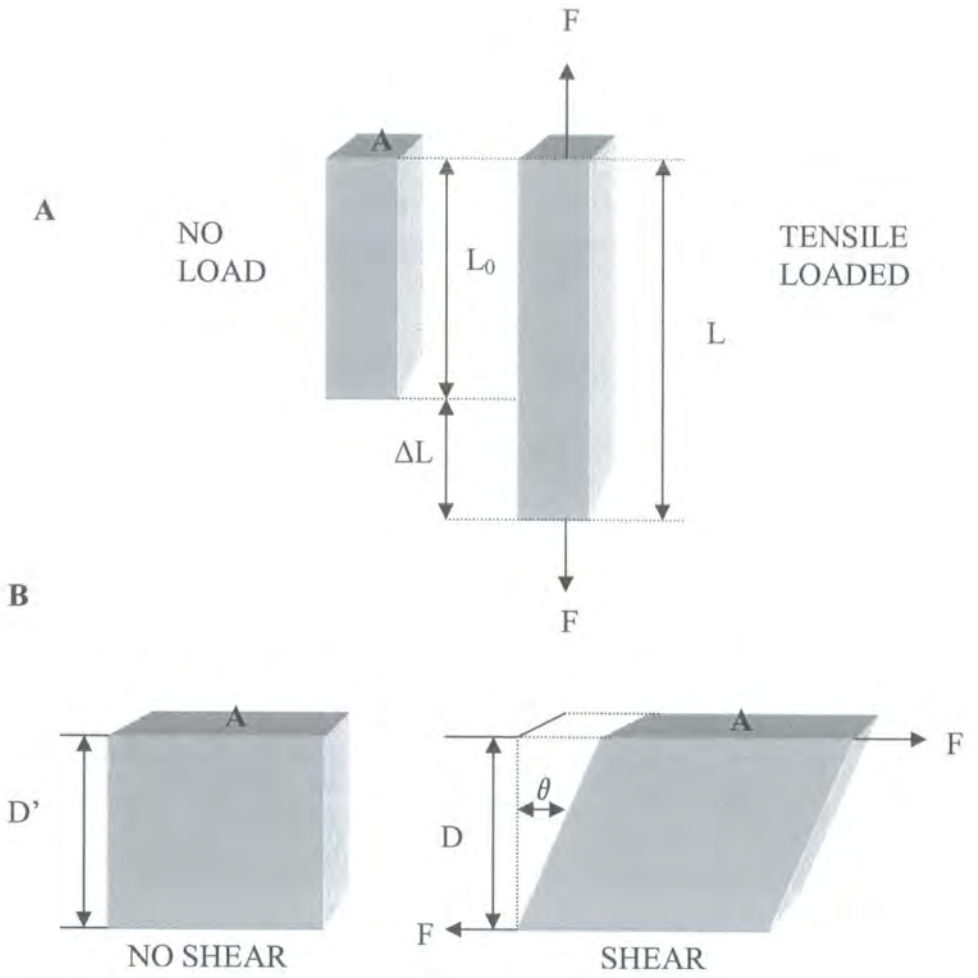

Figure 1.1 *(a) Tensile stretching of a bar, (b) shear of a rectangular block.*

Figure 1.1 (a) shows schematically the stretching of a bar by a tensile load. The bar has an original length L_0 and a cross-sectional area A. A tensile force increases the length of the bar by an amount ΔL to give a stretched length L. Young's modulus, E, for a material which obeys Hooke's law, is defined as the ratio of tensile stress to tensile strain and is is given by the expression in **equation 1.1**.

$$E = \frac{\text{Tensile stress } \sigma}{\text{Tensile strain } \epsilon} = \frac{\text{Force per unit area}}{\text{Stretch per unit length}} \qquad \textbf{Equation 1.1}$$

Therefore,

$$E = \frac{F/A}{\Delta L / L_0} = \frac{\sigma}{\varepsilon} \qquad \textbf{Equation 1.2}$$

The stress is defined as the force per unit area and the strain or elongation defined as $\Delta L/L_0$ for small elongations, for large deformations/elongations other definitions are available. All of the definitions give the same values at low extensions. **Equations 1.1** and **1.2** can also be applied when the bar is decreased in length by a compressive force. The shearing of a rectangular block is shown in **figure 1.1 (b)**. The rigidity or shear modulus G is defined as the ratio of shearing stress to shearing strain.

$$G = \frac{\text{shear stress } \sigma_s}{\text{Shear strain } \epsilon_s} = \frac{\text{shear force per unit area}}{\text{shear per unit distance between shearing surfaces}} \qquad \textbf{Equation 1.3}$$

or

$$G = \frac{F/A}{S/D} = \frac{F}{A\tan\theta} = \frac{\sigma_s}{\varepsilon_s} \qquad \textbf{Equation 1.4}$$

When a material is stretched it's cross-sectional area changes as well as its length. Poisson's ratio, ν is the constant relating the changes in dimensions and is defined in **equation 1.5**.

$$\nu = \frac{\text{change in width per unit of width}}{\text{change in length per unit length}} = \frac{\Delta C/C}{\Delta L/L_0} \qquad \textbf{Equation 1.5}$$

If the volume of a material remains constant when stretched then the Poisson's ratio will 0.5. In general most materials increase in volume when subjected to a tensile stress and their Poisson's ratio lies between 0.2 and 0.5. It is also possible for ν to be negative and this breeds a class of material known as "auxetic" [(2)]. A negative Poisson's ratio is simply an extension of the increase in volume exhibited by a material that has a positive Poisson's ratio less than 0.5.

The moduli are not independent of one another and follow the relationship shown in **equation 1.6** for isotropic materials.

$$E = 2G(1+\nu) \qquad \textbf{Equation 1.6}$$

Metals have far greater moduli than rigid polymers such as polystyrene, which provides a limitation of plastics for many applications. However, plastic materials are much lighter than metals so that when a comparison is made on equal weights, polymers compare favourably with metals.

1.1.2 Viscoelastic materials

The theory discussed in **1.1.1** is only applicable for perfectly elastic materials where the strain is proportional to stress and obeys Hooke's law, i.e., they behave like perfect springs. A given load stretches the material a certain amount, when the load is removed the material shrinks back to its original length.

Polymers are not perfectly elastic materials and can display all the intermediate range of properties between an elastic solid and a viscous liquid [3], depending on the temperature and the time scale. This behaviour of a viscous liquid and an elastic solid is known as viscoelasticity. Newton's law of viscosity defines the viscosity η as the stress σ proportional to the velocity gradient of the liquid (**see equation 1.7**).

$$\sigma = \eta \frac{\partial V}{\partial y} \qquad \textbf{Equation 1.7}$$

Creep measurements can be used to evaluate viscoelastic materials. A load is applied to a test specimen and its length (strain) is measured as a function of time. In addition to the initial elongation characteristic of an elastic material, the elongation increases with time for a viscoelastic material. The creep behaviour is generally investigated as a function of temperature to evaluate the material properly.

With stress-relaxation tests the specimen is stretched to a given value, and the stress required to hold the length constant is measured as a function time. The most widely used test is the stress-strain test, which can be done over a wide range of temperatures. The material is stretched or compressed at a given strain rate until the sample breaks or

yields. The area under the stress-strain curve is proportional to the energy absorbed in breaking the material.

1.2 Transitions in polymers

To learn more about the mechanical properties of polymers it is important to learn about the types of transitions that can occur, such as crystal melting and the glass transition. These transitions and the temperature at which they transpire govern the mechanical behaviour of polymers.

1.2.1 Glass transition temperature

At sufficiently low temperatures all polymers are hard rigid solids. As the temperature increases the polymer obtains sufficient thermal energy to enable the chains to move freely and the sample behaves like a viscous liquid [4]. When the polymer is completely amorphous the chains are arranged in an entirely random fashion. If the polymer is a glass and is heated beyond its glass transition temperature, T_g, it then becomes rubber-like in nature. A further increase in temperature would lead to a change from rubbery to a viscous liquid. The defining factor in determining T_g is the flexibility of the polymer chain. This is shown by the decrease in T_g from poly(methyl acrylate) (3 °C), to poly(ethyl acrylate) (-22 °C) to poly(n-butyl acrylate) (- 56 °C) the T_g decreases as the number of carbon atoms and the flexibility of the side group increases [1]. However as the chain length increases beyond a certain value, crystallisation of the side chain occurs and T_g starts to increase once more. It is difficult to separate chain flexibility from steric hindrance and the size of the side group attached to the polymer backbone. Steric hindrance increases the glass transition temperature. This is shown by the difference between poly(methyl acrylate) (3 °C) and poly(methyl methacrylate) (120 °C), which is largely due to the steric effect of the methyl group [1]. Cross-linking will also increase the T_g of a material due the restriction of chain movement. The addition

of plasticisers to plastics can lower the T_g by acting as a lubricant where the small molecules ease the movement of the polymer chains by pushing them further apart [4]. Poly(vinyl chloride) (PVC) is an example of a polymer, which contains 30 to 40 mass percent of plasticsers to improve the flexibility of the material.

Copolymers, which are made up of two or more types of monomer, have a glass transition temperature intermediate between those of the homopolymers. Fox gave a simple expression, which in certain circumstances can describe this relationship [1], [5],

$$\frac{1}{T_g} = \frac{W_1}{T_{g1}} + \frac{W_2}{T_{g2}} + \ldots\ldots\ldots \frac{W_i}{T_{gi}} \qquad \textbf{Equation 1.8}$$

where W_i is the fraction of monomer i in the copolymer with a glass transition temperature T_{gi} in degrees Kelvin.

1.2.2 Melting temperature

In a perfectly crystalline polymer all the chains are incorporated into regions of a three-dimensional ordered structure, which are called crystallites and no glass transition would be observed. The crystallites within a polymer generally melt over a temperature range, but the temperature above which these crystallites cannot exist is called the melting temperature, T_m. The longer the sequence of polymer chains the higher the melting point and therefore the melting point is dependent on the molecular weight. At lower molar mass the number of chain ends relatively free to move is greater therefore there is less energy required to stimulate chain motion and melting. Intermolecular forces can also have an effect on the melting temperature. Any interaction between chains in a crystal lattice will hold the structure together more firmly and raise the melting temperature. As with the glass transition temperature, flexibility and stiffness of the polymer chain can also affect the T_m. Substitution of a flexible and non-polar side group on to the polymer chain will lower the T_m. However, substitution of bulky

and rigid side groups, such as the phenyl group, will raise the T_m. Perfectly crystalline polymers are generally never encountered; instead, polymers with areas of ordered and disordered regions are found. Semi-crystalline polymers show both a T_g and T_m corresponding to regions of disordered and ordered structure, respectively.

1.3 Cellular solids

1.3.1 Introduction

A cellular solid is a solid made up of an interconnected network of struts, which can form the faces or edges of a cell [6]. The simplest structure is the two-dimensional hexagonal structure of a honeycomb. In most cases the cells are three-dimensional polyhedra, and such structures are generally referred to as foams. If the material or solid of which the foam is made is contained in the cell edges only and the cells are interconnected through open faces the foam is referred to as open-cell. If the cell faces contain the material also the foam is said to be closed-cell. Gibson and Ashby [6] describe the most important feature of a cellular solid as being the relative density ρ^*/ρ_s, which is the density of the cellular material ρ^* divided by the density of the solid of which the cell edges or faces are made, ρ_s. Generally polymers are foamed by introducing gas bubbles into the liquid monomer or hot polymer and then solidifying by cross-linking or cooling. The physical blowing agents used are generally gases such as carbon dioxide or nitrogen. Low melting point liquids such as chlorofluorocarbons (CFCs) which volatise on heating to produce vapour bubbles can also be mixed in to the polymer. Chemical blowing agents can also be used and these are generally additives, which either decompose on heating or combine to release gas. The foams produced can either be open or closed-cell (**see figure 1.2**). There are many applications of cellular materials, the examples of which are thermal insulation,

packaging and structural use. Cellular materials are also common in nature with wood, cork, bone, sponge and coral providing an example (**see figure 1.3**)

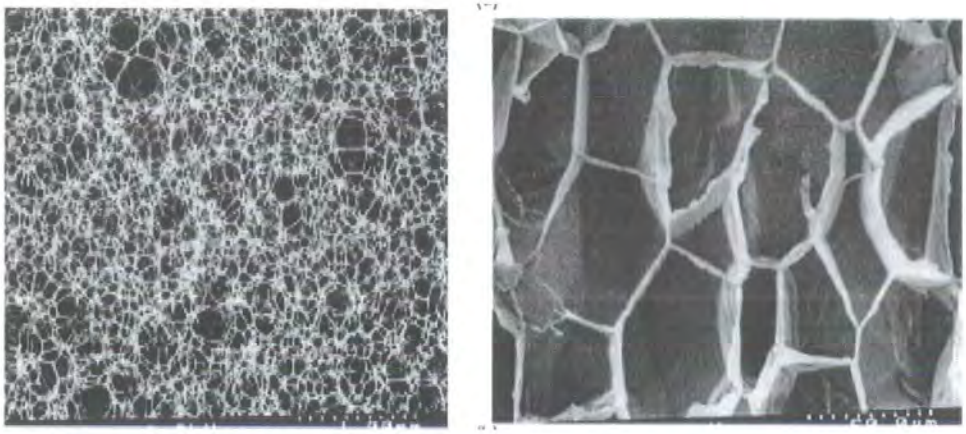

(a) (b)

Figure 1.2 *Three-dimensional cellular foam materials (a) open-cell melamine, (b) closed-cell Polystyrene* [7].

Natural foams such as cork and balsa have closed-cells, which are almost as regular as honeycomb materials. Sponge and cancellous bone are open-networks of struts. Materials such as coral or cuttlefish bone are anisotropic where the cells are elongated or aligned in a particular dimension. Many natural materials exhibit anisotropic properties largely caused by the elongated shape of their cells.

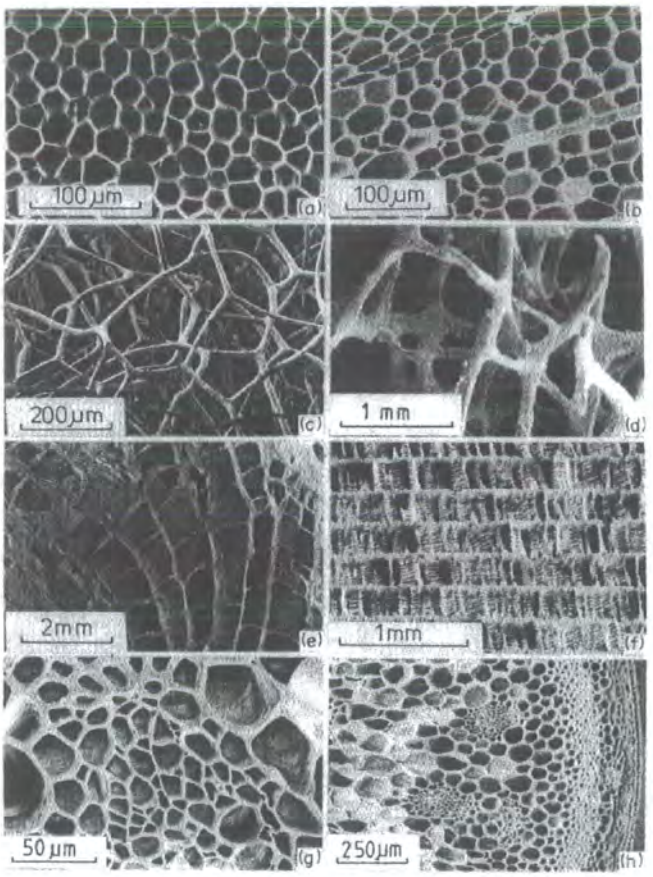

Figure 1.3 *Natural cellular materials, (a) cork, (b) balsa wood, (c) sponge, (d) cancellous bone, (e) coral, (f) cuttlefish, (g) iris leaf, (h) stalk of a plant* [6].

1.3.2 High internal phase emulsions (HIPEs) and PolyHIPE materials

1.3.2.1 High internal phase emulsions

The main aim of the research was to produce lightweight cellular materials by the use of a high internal phase emulsion (HIPE) as a template to be used as a structural core material. The lightweight cellular material produced from the polymerisation of the continuous phase of a HIPE is referred to as a PolyHIPE [8].

HIPEs are defined as emulsions with an internal (droplet) phase volume of greater than 74.05 % [9]. This figure represents the maximum volume, which can be occupied by uniform spheres. Above this volume fraction the droplets present in the HIPE are polydisperse in size and/or deformed into polyhedra to maximise packing efficiency. HIPEs can be prepared in either normal (oil-in-water, o/w) or inverse (water-in-oil, w/o) forms.

The preparation of a stable HIPE requires an emulsifying agent/surfactant and this needs to be insoluble in the droplet phase to prevent emulsion inversion at high internal phase volumes.

Surfactants are molecules possessing both hydrophilic and hydrophobic groups. Surfactants diffuse from the phase they are dissolved in to the interface between the two phases. They are classified in accordance with the charge on the part of the molecule absorbed to the interface; anionic, cationic, non-ionic or amphoteric. The major attraction between two or more droplets is van der Waals long-range forces, against which ionic surfactants provide an electrostatic barrier. Non-ionic surfactants contain a hydrophilic polar head and in the majority of cases the hydrophobic part consists of a long hydrocarbon chain. The HLB (hydrohile-lipohile balance) number, introduced by Griffin in 1949 [10] classifies surfactants, and in particular non-ionic surfactants. This is based on the weight fractions of hydrophobic and hydrophilic groups present in the molecule. For blends of two or more surfactants, the HLB value can be determined by an additive formula [10], [11],

$$HLB_{mix} = \sum X_i (HLB)_i \qquad \textbf{Equation 1.9}$$

where HLB_{mix} is the HLB value of the surfactant mixture, and X_i and the HLB_i are the weight fraction and HLB number of component i.

There are three main processes that cause emulsion instability: coagulation (flocculation), coalescence and creaming [12], [13]. Coalescence is the formation of large droplets due to the rupture of thin films between the adjacent droplets, and eventually can lead to complete phase separation of the emulsion. Creaming is the formation of a concentrated layer either above or below the bulk emulsion, due to density differences between the two phases. Emulsion droplets come into contact with each other due to Brownian motion. Coagulation (flocculation) is the coming together of droplets due to

Brownian motion. Coagulation can lead to the formation of larger droplets and coalescence.

By forming a thin film around the dispersed phase, the surfactant provides a barrier against coalescence and lowers the interfacial tension of the system. A high viscosity of the continuous phase can reduce creaming and flocculation by impeding Brownian motion, which can allow the droplets to come in contact with one another. However an increase in the viscosity of the continuous phase can lead to inefficient mixing of the two phases and a low volume fraction of internal phase incorporated into the emulsion [14]. Aronson and Petko [15] found that the addition of electrolytes to the aqueous phase helped stabilise w/o HIPEs. This was due to the salt reducing the solubility of the aqueous phase and reducing coalescence and Ostwald ripening. Ostwald ripening is a process where large drops grow at the expense of smaller droplets, as the larger droplets are energetically more favourable. However they concluded that even though Ostwald ripening contributed to HIPE destabilisation and was prevented by the presence of the electrolyte, the dominating effect was coalescence. Kizling and Kronenberg [16] proposed that electrolytes could reduce the rate of coalescence by lowering the van der Waals interactions through polarisbility or increasing the refractive index of the aqueous phase towards that of the oil phase.

1.3.2.2 Preparation of PolyHIPE materials

The polymerisation of the continuous phase of a HIPE by the routes of free radical addition or step growth polymerisation (e.g polycondensation [17]) results in the production of a porous material called a PolyHIPE. Generally the internal phase can be removed leaving a porous and permeable material.

The majority of the research described in this thesis is fairly novel. There has been limited research into the mechanical strengthening of PolyHIPE materials. There are also only a few examples in the journal and patent literature of PolyHIPE materials templated from o/w HIPEs [17], [153], [154] and the research discussed later in **chapter 9** describes the first PolyHIPE material to possess what is known as shape-memory properties.

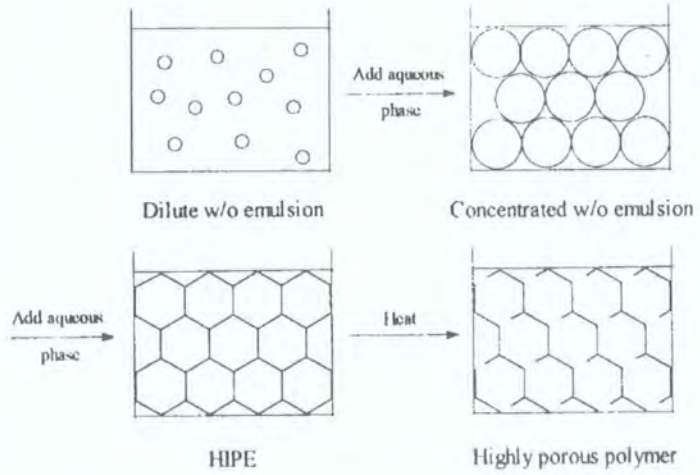

Figure 1.4 *Schematic of PolyHIPE preparation* [13]

The procedure used to prepare PolyHIPEs is schematically shown in **figure 1.4** and consists of adding, slowly, the droplet phase to the monomeric continuous phase containing the surfactant with constant agitation to form the HIPE. This is followed by curing of the monomers in some way (thermal, UV, redox or addition of catalyst). The porous monolith can then be washed in a Soxhlet apparatus with a lower alcohol and then dried *in vacuo* to leave the lightweight porous material.

1.3.2.2.1 Kinetics of free radical polymerisation

Free radical addition polymerisation is a polymer-forming process in which a macromolecular chain is produced by a single chain reaction. The reaction is composed

of a number of elementary free radical reactions: initiation (radical formation), propagation and termination and transfer reactions.

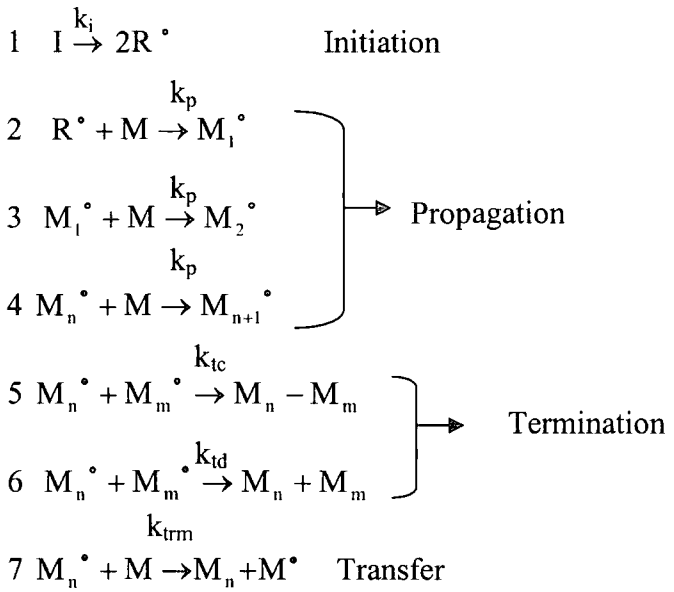

Where $R^{\bullet}$ = primary radical, I = initiator, M = monomer, $M_1^{\bullet}$ = monomer radical, $M_n^{\bullet}$ = polymer radical, M_n and M_m = inactive dead polymer.

k_i = rate constant for initiation,
k_p = rate constant for propagation,
k_{tc} = rate constant for combination termination,
k_{td} = rate constant for disproportionation termination,
k_{trm} = rate constant for transfer to monomer.

It is assumed that the formation of radicals occurs with 100 % efficiency and that most of the monomer is consumed in the propagation step rather than in the initiation, termination or transfer steps.

Assuming a stationary state in radicals applies ($R^{\bullet}$ and $M^{\bullet}$ remain small and constant) the rate of polymerisation, R_p can be described by **equation 1.10**.

$$R_p = k_p \left(\frac{k_i}{k_t}\right)^{1/2} [I]^{1/2}[M] \qquad \textbf{Equation 1.10}$$

In emulsion polymerisation the radicals initiate polymerisation in the micelles and as the monomer is consumed it is replenished by diffusion of more monomer from the macrodroplets which act as a reservoir. The polymer particles formed can contain up to 50 % by weight of monomer until the macrodroplets are consumed. Hence the rate of polymerisation within a particle is constant over a long period of time but will begin to fall as the monomer content of the polymer particles falls. This is quite different to normal solution radical polymerisation.

Radicals are generated at around 10^{13} cm^3s^{-1} and on average a new radical enters a polymer particle or micelle every 10 seconds. From the size of the micelle and the rate constant for radical termination it can be shown that half the micelle polymer particles have a growing radical in them and half do not. Therefore the rate of polymerisation per cm^3 of emulsion, R_p, can be described by **equation 1.11**.

$$R_p = k_p[M]N/2 \qquad \textbf{Equation 1.11}$$

Where N = number of polymer containing micelles per cm^3.

1.3.2.2.2 Kinetics of step-growth polymerisation

Step growth polymerisations involve some type of organic condensation reaction between two monomer molecules to form a dimer and then a repetition of this condensation process many times. The kinetic behaviour is quite different to that of chain reactions.

In the case of a polyesterification reaction in the presence of a strong acid catalyst, it can be shown that the number average degree of polymerisation, $\overline{DP}_N$, can be described by **equation 1.12**.

$$\overline{DP}_N = \frac{1}{1-p} \qquad \textbf{Equation 1.12}$$

Where, p, is the extent of the reaction (the fraction of each functional group reacted in time, t.). Thus it is shown that as time goes on the average molecular weight of the polymer increases as the extent of the reaction increases. This is different to chain (free radical) polymerisation reactions where the molecular weight average is established very quickly (~ 2-5 % monomer conversion) and remains fixed during the reaction. Another difference between chain and step growth reactions is that in the latter high levels of conversion are needed before any significant molecular weight in the polymer is observed.

1.3.2.3 Poly(styrene/divinylbenzene) PolyHIPE materials

The system of styrene and divinylbenzene was the original focus of Barby and Haq's Unilever Patent [8]. The non-ionic surfactant sorbitan monooleate (Span 80) was used and the polymerisation was initiated thermally with potassium persulfate. Monomers such as p-butylstyrene and butyl methacrylate were also used to prepare other porous materials. **Figure 1.5** shows a SEM image of the morphology of a S/DVB PolyHIPE material similar to that prepared by Barby and Haq.

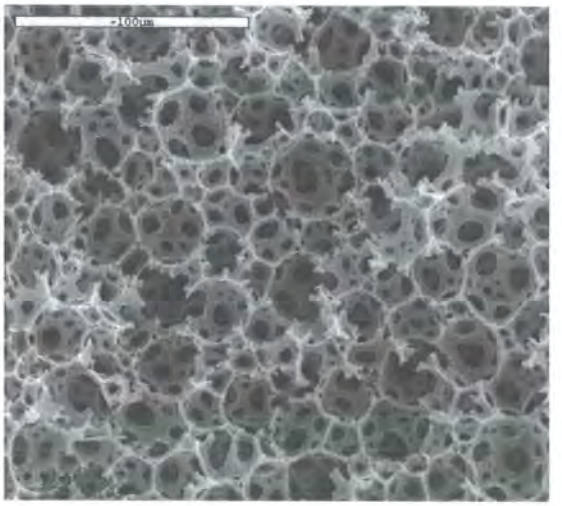

Figure 1.5 *Morphology of a S/DVB PolyHIPE material.*

The full patent [8] also describes the ability of the PolyHIPE material to absorb amounts of liquids up to 30 times its weight by capillary action. Early applications such as absorbents for spillage treatment were also discussed [18], [19].

Another application investigated for poly(styrene/DVB) PolyHIPE materials was as filter bodies. Gregory et al [20] produced PolyHIPE discs, which were compressed before their filtration characteristics were tested. These filters were able to remove effectively 95 % of polystyrene particles of diameter 1-5 μm from aqueous solution. Work by Bhumgara [21] described the production of materials for cross-flow microfiltration. Poly (styrene/DVB) PolyHIPEs have also been prepared as stationary phases for HPLC [22]. The monoliths were prepared in moulds and placed in HPLC

columns and were held in place by either applying air pressure or by immobilising with an epoxy resin. Williams and Wrobleski [23] suggested using PS/DVB PolyHIPEs to entrap intact particles of cosmic dust.

1.3.2.4 Elastomeric and other PolyHIPE materials

At Proctor and Gamble, Dyer and co-workers [24] investigated the production of rubbery PolyHIPE materials by copolymerisation of conjugated polyenes. Another route of producing elastomeric foams involves the copolymerisation of a hydrophobic elastomer such as 2-ethylhexyl acrylate (EHA). This route was first explored by workers at Unilever [25], [26]. A HIPE composed of a monomer phase consisting of styrene, DVB and EHA could be prepared in the same way using the same aqueous phase composition and surfactant to those involving styrene and DVB i.e. the EHA does not compromise emulsion stability. The patent describes materials with high levels of EHA (> 60 %) as elastomeric at room temperature. The same patent also describes the use of n-butyl acrylate to produce the same type of materials. These EHA containing PolyHIPE materials can be used for insulation purposes (thermal, acoustic or mechanical) [27], [28]. Proctor and Gamble described another use for EHA containing PolyHIPE materials [29]. They found that membranes of such foams could be use as efficient stain removers. The addition of styrene as a toughening monomer (at a level of 35 % w/w) was crucial to the application. Chang et al. [30] impregnated a porous felt mat substrate with an EHA-containing HIPE and subsequent curing led to a high efficiency filter. These were found to operate at lower pressure drops than other high efficiency filters.

Cameron and Sherrington [31] conducted a study of the thermal properties of EHA-derived PolyHIPE foams and those including the monomer 2-ethylhexylmethacrylate (EHMA). Both sets of materials were found to have a non-linear relationship between

composition and T_g, which was explained by considering the influence of EH(M)A units on chain flexibility and free volume and the likely comonomer unit sequencing.

All the EHA containing materials discussed so far have been prepared with sorbitan monooleate (Span 80) as surfactant. It has been reported in the literature that Span 80 may not be the optimum surfactant for preparing these HIPEs. Beshouri [32] describes the use of two different sorbitan esters in the preparation of EHA-derived emulsions. The resulting emulsions were far more stable than those prepared with the single surfactant and could be obtained at higher internal phase volumes. Other subsequent work by Beshouri [33] shows the use of mixtures of sorbitan esters with a glycerol monofatty acid ester cosurfactant leading to further optimisation of emulsion stability. Work done at Proctor and Gamble [34] also provided alternative surfactants to Span 80; they found that stable HIPEs with uniform droplet size could be prepared using polyglycerol aliphatic ether surfactants. Other optimised surfactant systems have also been reported for EHA containing HIPEs. A mixture of a cationic surfactant, with either a sorbitan ester [35] or an anionic surfactant [36] was found to produce a stable HIPE which could be formed at a water:oil ratio of up to 60:1. Another advantage of this system is that less surfactant overall is used (around 6% w/w) compared to the normal 20 % w/w of Span 80. The emulsions could also be cured at higher temperatures such as 100 °C without any emulsion collapse.

Reducing the curing time required to produce PolyHIPE materials can be advantageous not only in reducing emulsion breakdown and coalescence but also from an economic perspective. Brownscombe et al. [37], [38] discuss the pre-polymerisation of the HIPE monomer phase as an attempt to achieve this. The same group has also used provided a multi-step cure strategy for the same purpose [39]. Another way is to cure the emulsion at elevated temperatures [40], [41]. As little as 4 minutes were required to cure HIPEs of

EHA, DVB and hexanediol diacrylate at 182 °C in a stainless steel pressure vessel. Alternative initiators to $K_2S_2O_8$ that can produce radicals by other means can also be used. A Japanese group [42] has used a redox initiator combination such as ascorbic acid and Fe (II) salt with H_2O_2 to yield fully cured HIPEs in around one hour. A wide range of oil soluble initiators can also be employed, leading to solid foams. Desmarais [43] claimed that degassing the aqueous phase before HIPE formation leads to a defect free PolyHIPE monolith when used with a high polymerisation temperature.

Williams et al. [44-48] impregnated S/DVB PolyHIPE materials with silica aerogels, resorcinol-formaldehyde and phloroglucinol-formaldehyde foams or polystyrene by filling under vacuum. The composites produced had the properties of both the base materials used. PolyHIPE materials have also been produced from methacrylonitrile and have been used as precursors for monolithic porous carbons [49]. Cooper et al. [50] have developed the use of supercritical CO_2-in-water HIPEs stabilised by poly(vinyl alcohol) to prepare PolyHIPE materials from hydrophilic monomers such as acrylamide and 2-hydroxyethyl acrylate. Recently the use of ring opening methathesis polymerisation (ROMP) to produce microcellular PolyHIPE foams from a norbornene derivative using a Grubbs catalyst has also been described [51].

The vast majority of PolyHIPE materials are generally prepared by addition polymerisation, however within the patent literature the production of porous monoliths by step-growth polymerisation has also been described [17]. The types of curing chemistries used ranged from resorcinol-formaldehyde, urea-formaldehyde, melamine-formaldehyde to amine cured epoxies.

A number of organic/inorganic composite emulsion-derived foams have also been prepared. Mork et al. [52] detailed the addition of various filler materials (clay particles, iron powder, hollow ceramic spheres and $Al(OH)_3$ to styrene/EHA/DVB foams to

enhance flame retardancy. The $Al(OH)_3$-impregnated material, unlike the unfilled material, was difficult to ignite and quickly self extinguished. Silverstein et al. [53] have prepared inorganic/organic composite foam materials. A siloxymethacrylate monomer was copolymerised with styrene and DVB. Subsequent hydrolysis of the trimethoxysilyl groups, due to the increasing acidity of the aqueous phase arising from the decomposition of the potassium persulfate initiator, formed the inorganic network.

1.3.2.5 Chemical modification of PolyHIPE materials

Electrophilic aromatic substitution has been performed on PolyHIPE materials, where the most common modification carried out is sulfonation. Haq's patent [54] described the sulfonation of polystyrene/DVB PolyHIPE discs with agents such as H_2SO_4 and oleum, yielding materials with degrees of sulfonation of up to 95 %. Cameron et al. [55] found that a more hydrophobic sulfonating species, such as lauroyl sulfonate in cyclohexane, yielded a lower level of surface functionalisation but a more uniformly sulfonated monolith. Nitration has also been performed using ammonium nitrate and trifluoroacetic acid anhydride [56] giving a degree of substitution of 8.07 % (corresponding to a degree of nitration of 5.4 $mmolg^{-1}$). Again as described in the previous work the use of a more hydrophobic nitrating agent (tetrabutyl ammonium nitrate) [55] resulted in a uniform degree of modification of large monoliths.

PolyHIPE materials produced from the hydrophobic monomer 4-vinylbenzyl chloride can easily be modified by a variety of nucleophiles. Workers at Unilever [57-60] describe the modification of polyVBC monoliths with a variety of agents, including amines, carboxylates and alkoxides. PolyVBC monoliths have been surface-grafted with poly(4-vinyl pyridine) for the removal of heavy metals from solution [61] PolyVBC-co-DVB materials have also been successfully modified with tris(2-aminoethyl) amine [62].

This PolyVBC derivative successfully scavenged 4-chlorobenzoyl chloride from solution.

Cross-linked foams prepared from high levels of divinylbenzene possess a certain level of unreacted residual double bonds, up to 45 % (mol) of the amount present at the start of the curing process when 80 % DVB is used [63]. These residual double bonds can be further modified to introduce useful functionality. This method has been explored by Deleuze et al. [64-66]. The PolyDVB monoliths were modified by various reactions including hydroboration and oxidation to yield primary alcohols. The chemical modification reactions were performed under batch and flow-through conditions.

1.3.2.6 Control of morphology and properties

1.3.2.6.1 Cellular structure

PolyHIPE monoliths can be either open- or closed-cell materials. To produce closed-cell materials, the monomer films surrounding the emulsion droplets form polymer membranes, trapping the contents of the droplet within the foam. This forms a high-density material where the aqueous phase is difficult to remove from the material. The latter have an open and interconnected structure where each void is connected to some or all of its neighbours. The open-cell materials produced are highly permeable and of low density, where the density is determined by the internal phase volume used.

Williams and Wrobleski[67] investigated the factors that controlled the cellular morphology of S/DVB PolyHIPE foams. They found that the cellular structure was independent of the ratio of aqueous to oil phase but was affected by the amount of surfactant in the monomer phase. Closed-cell materials were formed at low (<5 % w/w) surfactant concentration. Cameron et al. [68] showed by performing scanning electron microscopy (SEM) on frozen samples of HIPE that had been cured for different lengths of time, that appearance of adjacent cavities coincided with gel-time. The dependence

on surfactant concentration on this process is due to its effect on the thickness of the films separating emulsion droplets. At higher surfactant concentrations the films become thinner, thus on curing, vinyl monomers undergo a volume contraction and this shrinkage results in the production of interconnects between the voids.

1.3.2.6.2 Void and interconnect size

There have been a number of factors discussed in the literature that have been shown to affect the average size of the PolyHIPE voids and interconnects. The investigation by Aronson and Petko on the effect of electrolytes on emulsion stability has already been discussed [15]. Gregory et al [69] investigated the influence of the ionic strength of the aqueous phase and found that increasing the concentration of $CaCl_2$ increased both the size and number of interconnecting holes. Williams et al [70] also observed a drop in average void size with increasing either the DVB content in the organic phase or surfactant content. They also provided further evidence for the influence of salt content on void and interconnect size by adding increasing amounts of K_2SO_4 to HIPEs that were prepared with AIBN rather than $K_2S_2O_8$ as initiator. They observed a 10-fold decrease in interconnect to void ratio.

The reduction in void and increase in interconnect size are generally related to emulsion stability. The modes of emulsion instability have already been discussed in **1.3.2.1**. Larger droplets are produced through lower emulsion stability; and more stable emulsions have thinner films separating adjacent droplets; therefore the foam material will have larger interconnects. If the surfactant concentration is increased or the organic phase is made more hydrophobic and the aqueous phase more polar the emulsion stability will increase. Work performed by Barbetta et al. [71] provided a good indication that this reasoning is correct. They noticed that foam materials prepared from DVB and 4-vinylbenzyl chloride (VBC) showed a drop in void size with increasing VBC content.

They performed experiments involving monolayers of mixtures corresponding to the monomer phase spread on to a solution of identical composition to the aqueous phase. They found that VBC was absorbed at the (air-water) interface. This suggested that the VBC was exhibiting cosurfactant behaviour and explained the reduction in void size observed. A similar effect was reported for monoliths produced from HIPEs containing chlorinated solvents in the organic phase [72].

1.3.2.6.3 Surface area

PolyHIPE materials have low surface areas due to the void sizes being in the range of microns to tens of microns, but by replacing some of the monomer in the organic phase with a hydrophobic solvent, it is possible to increase the surface area of the material [73]. The materials produced have dual porosity; large voids which are characteristic of PolyHIPE materials, and much smaller pores caused by phase separation of polymer from solution during cure. By using toluene as a porogen, in a 1:1 ratio relative to the monomer content and a high DVB content (80 %), PolyHIPE materials were prepared with surface areas of 350 m^2g^{-1}. Recently [72] PolyHIPE materials with surface areas of 550 m^2g^{-1} have been prepared by using different porogenic solvents such as 2-chloroethylbenzene (CEB).

1.3.2.6.4 Thermal and mechanical stability

S/DVB PolyHIPE materials have relatively low thermo-oxidative properties that can limit their use in structural and other applications. The thermal behaviour and performance can be improved by including maleimide-based monomers. With increasing amounts of ethyl maleimide incorporated into the S/DVB material there was an increase in T_g as determined by dynamic thermal analysis (DMTA), to above 200 ° C [72]. There were higher T_g values (220 °C) obtained when bismaleimide was used as cross-linker instead of DVB [74] Increasing the maleimide content also led to an

increase in the thermo-oxidative properties of the material as shown by thermogravimetric analysis [75]. Duke et al. [76] also investigated the effect of N-substituent size on the thermal properties of the alkyl maleimide. The investigation indicated that the smaller or bulkier substituents N-cyclohexylmaleimide or ethylmaleimide produced materials with the highest T_g values while the T_g was decreased with the larger N-propyl and N-butyl maleimide groups. Cameron et al. [77] also reported producing PolyHIPE materials by the copolymerisation of maleimide-terminated poly(ether sulfone) with styrene, DVB or a bis(vinyl ether) macromonomer. The PolyHIPE materials produced had far greater thermo-oxidative properties than the S/DVB material. The inorganic/organic composite PolyHIPE material produced by Silverstein et al. [53] using a siloxymethacrylate monomer was also reported to show greater thermo-oxidative properties than the standard S/DVB material due to the formation of a SiO_2 layer, which prevented further degradation of the organic network. In the presence of a nitrogen atmosphere the silyl based PolyHIPE material showed a decrease in thermal performance compared to the S/DVB PolyHIPE material.

Improving the mechanical properties of PolyHIPE materials has not been widely investigated in the literature. However there are some examples in the patent literature [78], [79]. Mats consisting of thermally bonded bundles of fibres were impregnated with S/DVB HIPEs and then cured. The composite materials produced were found to have higher fracture strength than the S/DVB foam with no reinforcing material present. More recently Dyer and co-workers [80] prepared fibre-reinforced S/DVB/EHA-based PolyHIPE materials by the addition of fibres prior to and after HIPE preparation. They found that the materials prepared with compatible fibres (activated carbon and PE) had higher modulus values compared to the fibre free material and the PolyHIPE materials prepared with non-compatible fibres (cellulose).

The effect on morphology with increasing Span 80 concentration has already been discussed [67]. Williams in the same paper also investigated the effect on the compressive properties of the S/DVB material with increasing surfactant (Span 80) concentration. They found that there was a maximum crush strength for foams prepared with 10 % surfactant. The value then decreases as the amount of surfactant is increased. A similar behaviour is observed for Young's modulus. They suggest that the strut type foams are weakened through plasticisation by the surfactant.

1.4 Mechanical properties of foams

Man made foams produced on a large industrial scale, are used for absorbing the energy of impacts (packaging etc), for example as cores of sandwich panels. and the use of these materials requires us to understand their mechanical properties. The basic mechanical behaviour of polymer materials has already been discussed in **1.1**. Gibson and Ashby [6] give an excellent overview of the mechanical behaviour of foam materials and describe their behaviour as similar to that of honeycomb materials. The mechanical behaviour of foam materials is related to their structure and the properties of the material from which the cell walls are made, the degree to which the cell walls are open or closed, their shape (anisotropy ratio) and the relative density of the material. They model the material using a cubic array of unit cells.

Figure 1.6 shows the stress/strain curves from three different foam materials under a compressive strain. Cell wall bending controls the linear elastic region and if the cells are closed by cell wall stretching. Young's modulus E* is the initial slope (elastic region) of the stress/strain curve. The plateau represents the collapse of the cells by elastic buckling (**see figure 1.7 (a)**) in elastomeric foams, by brittle crushing in an elastic- brittle foam (**see figure 1.7 (b)**) and by formation of plastic hinges that yield in elastic-plastic foams (**see figure 1.7 (c)**). When all the cells have collapsed, further

strain compresses the foam structure itself and this accounts for the region of rapidly increasing stress. This is called densification.

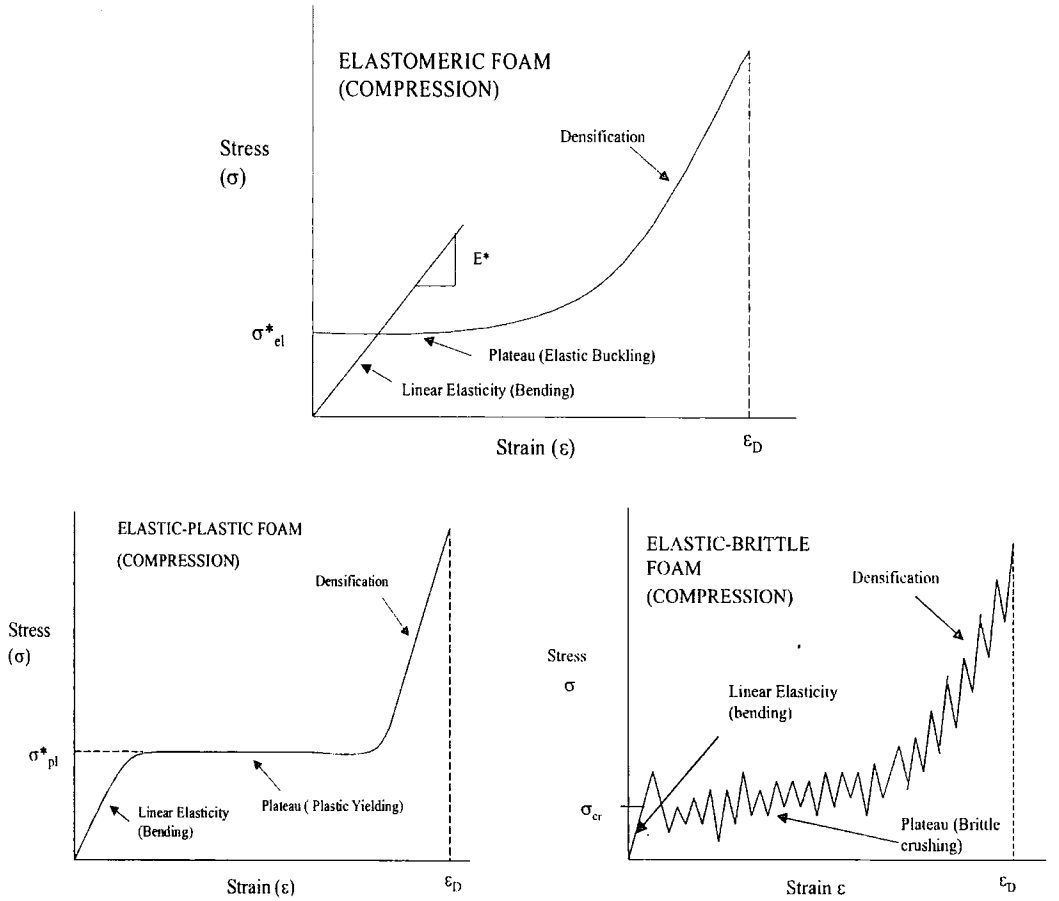

Figure 1.6 *Compressive stress/strain curves for a) elastomeric foam; b) an elastic/plastic foam, c) an elastic-brittle foam*

Gibson and Ashby determined that Young's modulus in the linear-elastic region for all three types of open-cell foams is related to the density by **equation 1.13** where C_1 is a constant, which includes all the geometric constants of proportionality.

$$\frac{E^*}{E_s} = C_1\left(\frac{\rho^*}{\rho_s}\right)^2 \qquad \textbf{Equation 1.13}$$

For an elastomeric foam, they determined that the yield strength, σ^*_{el},was also related to a $(\rho^*/\rho_s)^2$ factor, but at high relative densities the corrected version is given by **equation 1.14**.

$$\frac{\sigma_{el}^{*}}{\sigma_s} = C'_4\left(\frac{\rho^*}{\rho_s}\right)^2\left(1+\left(\frac{\rho^*}{\rho_s}\right)^{1/2}\right)^2 \qquad \textbf{Equation 1.14}$$

For an elastic-plastic foam material they determined that the plastic yield stress, σ^*_{pl} was proportional to $(\rho^*/\rho_s)^{3/2}$ with the density corrected form shown in **equation 1.15**. Plastic collapse transpires when the moment exerted on the cell walls is greater than the fully plastic moment of the cell edges, producing plastic hinges (**see figure 1.7 (c)**)

$$\frac{\sigma_{pl}^{*}}{\sigma_{ys}} = C'_5\left(\frac{\rho^*}{\rho_S}\right)^{3/2}\left(1+\left(\frac{\rho^*}{\rho_S}\right)^{1/2}\right)^2 \qquad \textbf{Equation 1.15}$$

where σ_{ys} is the yield strength of the cell wall material.

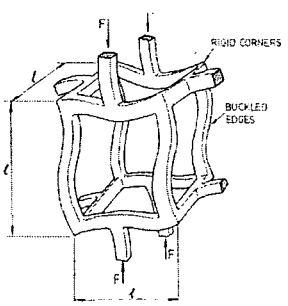

(a)

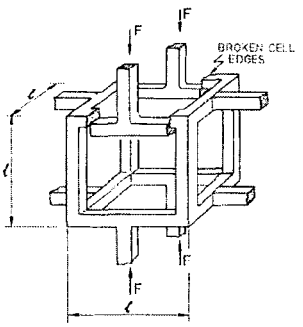

(b)

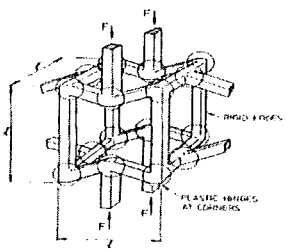

(c)

Figure 1.7 *Deformation modes of foam materials under a compressive load, (a) elastomeric foam, (b) elastic-brittle foam, (c) elastic-plastic foam.*

For brittle foam failing by a mechanism of brittle crushing, the crush strength is again proportional to $(\rho^*/\rho_s)^{3/2}$ and is given **by equation 1.16**

$$\frac{\sigma^*_{cr}}{\sigma_{fs}} = C_6\left(\frac{\rho^*}{\rho_s}\right)^{3/2} \qquad \textbf{Equation 1.16}$$

where σ_{fs} is the modulus of rupture of the cell wall material. The modulus of rupture of an elastic beam is defined as the maximum tensile stress in the beam at the moment of failure.

Most structural foams used for cores in sandwich structures are subjected to tension as well as compression. **Figure 1.8** shows the behaviour of the same three different types of foam under a tensile stress. As with compressive strain, cell wall bending causes the linear region in the stress-strain graph.

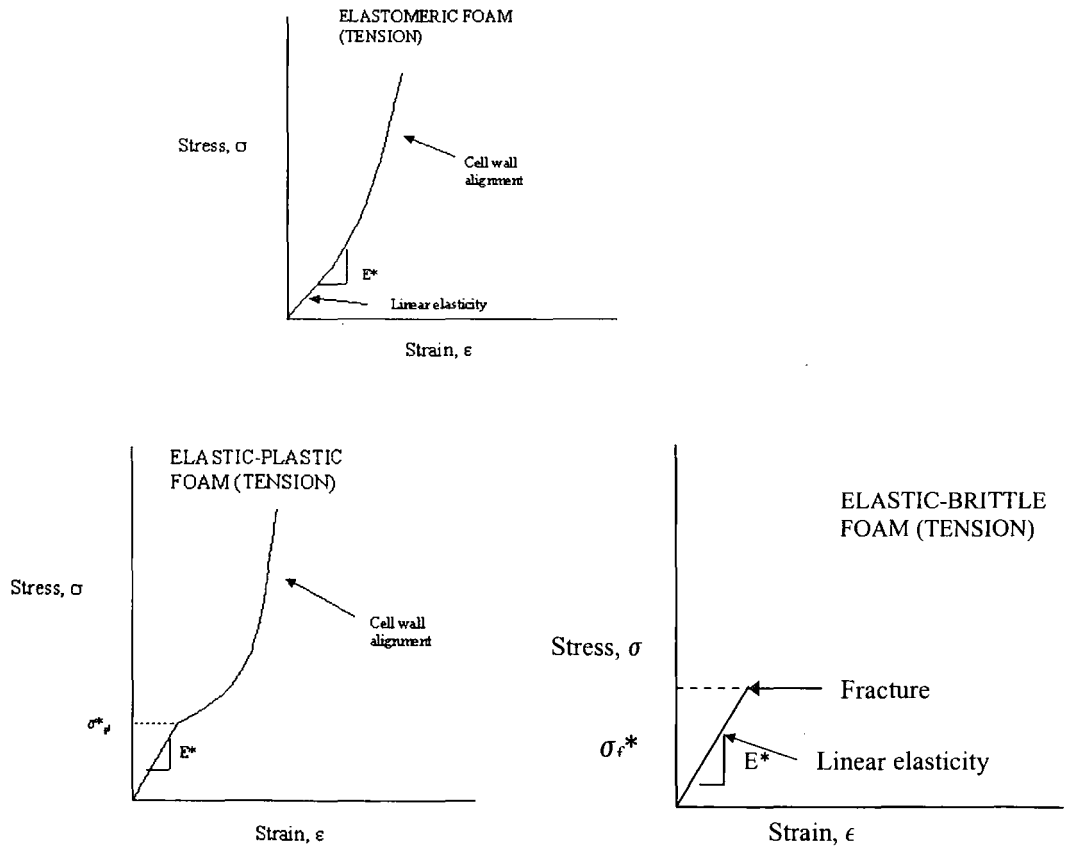

Figure 1.8 *Tensile stress-strain curves for foams a) elastomeric; b) elastic- plastic; c) elastic- brittle.*

The linear-elastic modulus of a foam under tension is the same as that in compression (**equation 1.13**). The moduli of open cell foams are determined by cell edge bending as discussed, but closed cell foams are more complex. Buckling of cell walls causes the

non-linear elastic region for elastomeric foams under compression. This is not possible in tension. Initially the elastic response is dominated by cell edge bending giving the initial value of E* (**equation 1.13**), but as the cell walls rotate towards the tensile axis the stiffness rises causing the increase in stress, over this strain period the value of E* increases.

An elastic-plastic foam essentially behaves according to the same mechanism in tension as in compression in the elastic region. Then, beyond this region, the rotation of the cell walls in tension reduces the bending moment so that after a certain amount of strain the cell walls are aligned with the tensile axis, then any further strain causes plastic extension of the walls themselves. The stress, σ^*, rises over this strain period from the value, σ^*_{pl} shown earlier.

The brittle fracture mechanism in tension is far different from that in compression. In compression the foam displays progressive crushing, in tension it fails by crack propagation through the mid point of the cells (**see figure 1.9**).

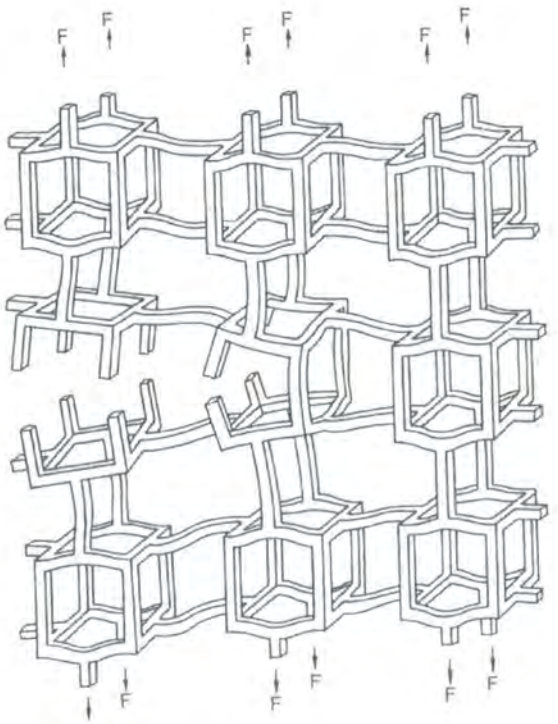

Figure 1.9 *Propagation of crack through a brittle open cell foam.*

Brittle foams respond in the linear-elastic region until fracture. Linear-elastic fracture mechanics are then used to obtain an expression for fracture toughness.

In the case of closed cell foam materials the work done during deformation of the membrane spanning the cell walls can lead to a contribution to the modulus of the material but can also result in failure of the material. This can be shown for the behaviour of an elastic-plastic closed cell material during plastic collapse on the application of a compressive strain. The membranes crumple in the compression direction, but the force required to crumple them is small. At right angles to this direction the membrane faces are stretched and the work required contributes significantly to the yield strength of the material. The equation for the yield strength of an elastic-plastic closed-cell foam, which includes membrane stresses, is shown below

$$\frac{\sigma^*_{pl}}{\sigma_{ys}} = C_5\left(\phi\frac{\rho^*}{\rho_S}\right)^{3/2} + C_5''(1-\phi)\left(\frac{\rho^*}{\rho_s}\right) \qquad \textbf{Equation 1.17}$$

where Φ is the fraction of solid in the edges and relates the cell edge and face thickness t_e and t_f. For open cell foams Φ is equal to 1 and for closed-cell foams $\Phi = 0$. The equation for the elastic modulus of a closed-cell material including membrane stresses is shown in **equation 1.18**.

$$\frac{E^*}{E_s} = C_1\phi^2\left(\frac{\rho^*}{\rho_s}\right) + C_1'(1-\phi)\frac{\rho^*}{\rho_s} \qquad \textbf{Equation 1.18}$$

After elastic and plastic collapse, large strains in compression cause the cell walls to crush and produce a stress-strain curve that rises steeply to a limiting strain, ϵ_d. Both elastomeric and plastic foams follow the same line and this line is described by **equation 1.19**.

$$\varepsilon_d = 1 - 1.4\left(\frac{\rho^*}{\rho_s}\right) \qquad \textbf{Equation 1.19}$$

From the equations discussed by Gibson and Ashby stress-strain maps for each type of foam were prepared. Each map has axes of normalised compressive stress (σ/E_s) and compressive strain. The stress/strain maps show where each mode of deformation (linear elasticity, elastic buckling and plastic collapse) is dominant for different relative densities. **Figure 1.10** shows the stress-strain map calculated from the equations discussed for an elastomeric foam.

The plateau due to elastic buckling remains flat at low relative densities but with increasing relative density a plateau, which increases with stress, is observed. The plateau increases more rapidly with stress as the relative density increases, until there is no plateau observed at a relative density of 0.3.

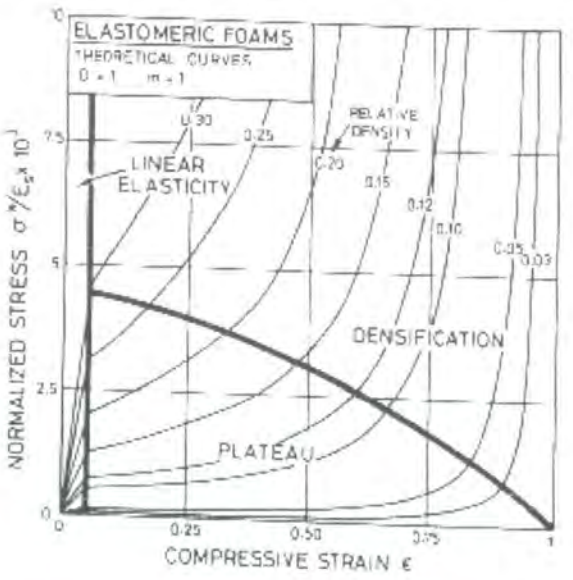

Figure 1.10 *Stress-strain map for an elastomeric foam material constructed from the equations in 1.2.3* [6].

The modulus also increases with increasing relative density and is described by **equation 1.13**. The boundary between the linear elastic region and elastic buckling, is derived by setting the linear elastic stress ($\sigma = E^*\epsilon$, **equation 1.13**), equal to the elastic buckling stress (**equation 1.14**, density corrected) to give, $\epsilon = 0.05$, or a more exact definition in **equation 1.20**.

$$\frac{\sigma}{E_s} = \varepsilon\left[\left(\frac{\varepsilon}{0.03}\right)^{1/2} - 1\right]^4 \qquad \textbf{Equation 1.20}$$

Gibson and Ashby describe a semi-empirical relationship to describe post-buckling behaviour. They found that:

$$\frac{\sigma^*}{\sigma_{el}{}^*} = 1 \text{ when } \varepsilon \le \varepsilon_D\left(1 - \frac{1}{D}\right) \qquad \textbf{Equation 1.21}$$

$$\frac{\sigma^*}{\sigma_{el}{}^*} = \frac{1}{D}\left(\frac{\varepsilon_D}{\varepsilon_D - \varepsilon}\right)^m \text{ when } \varepsilon > \varepsilon_D\left(1 - \frac{1}{D}\right) \qquad \textbf{Equation 1.22}$$

The constants D and m can be calculated by a logarithmic plot of relative stress σ^*/σ_{el}^* against $\epsilon_D/(\epsilon_D-\epsilon)$ where the constant m is the slope of the line and D is the intercept of the line. Once buckling begins the stress is related to the strain by **equation 1.22**.

Foams with a relative density, greater than 0.3, show no plateau and instant densification. **Equations 1.13, 1.19** and **1.22** can be used to provide a criterion for the boundary between buckling and densification. The model shows that during elastic buckling the foam material can exist in two states at almost the same stress, the linear elastic state and the densified state.

The same theory was used to produce stress-strain maps for elastic-plastic foam materials at different relative densities. The elastic region is again described by equating the linear elastic stress equal to the plastic yield stress an equation is derived for the boundary between linear elasticity and plastic yielding and is shown in **equation 1.23**.

$$\frac{\sigma^*}{E_s} = \left(\frac{0.3\sigma_{ys}}{E_s}\right)^4 \frac{1}{\varepsilon^3} \qquad \textbf{Equation 1.23}$$

The post yield behaviour is modelled as for post elastomeric buckling behaviour using **equations 1.21** and **1.22**. The start of densification occurs at a higher relative density of

0.5 compared to elastomeric foams. The foam has to be compressed to a relative density of 0.5 before densification will occur.

There are recent applications of Gibson and Ashby's models in the literature. Ramsteiner et al. [7] compared the tensile and compressive properties of an extruded closed-cell polystyrene and polypropylene foam, an open-cell melamine foam and a polyurethane foam, which they describe as a foam with holes in the lamellae, to the theoretical models of Gibson and Ashby [6]. The morphology of the polyurethane foam is shown in **figure 1.11**. The morphology of the polystyrene and open-cell melamine foams are shown in **figure 1.2 (a)** and **(b)**. The polystyrene foam tested was described as having partly orientated cells. They showed that the tensile modulus and tensile strength for the PS and PP foams fitted the model of Gibson and Ashby for foams with closed-cells when $\Phi = 0.85$ and therefore a 0.15 portion of lamellae. The modulus of the melamine foam fitted the model when $\Phi=0.93$, which was close to the limit for open-cell foams. The tensile strength of the melamine foams were higher than expected compared to the theoretical values. Ramsteiner et al. suggested this increase was due to the orientation of the struts during deformation in the tensile direction.

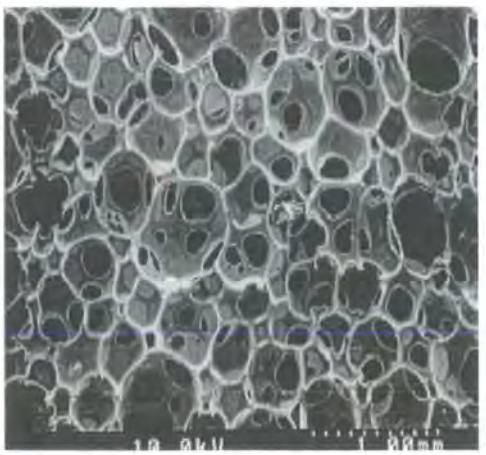

Figure 1.11 *Morphology of the polyurethane foam modelled by Ramsteiner et al.* [7]

Sun et al. [81] compared the compressive and tensile properties of microcellular poly (phenylsulfone) (PPS) and poly (ethersulfone) (PES) foams to the theoretical models of Gibson and Ashby. They found that in compression the experimental values were higher than are predicted by the Gibson and Ashby models especially at high relative densities with discrepancies decreasing at low relative densities. The tensile properties of both the PPS and PES foams show good comparison between the experimentally determined values and the predicted values from the Gibson and Ashby models. There has been no extensive investigation into comparing the behaviour of PolyHIPE materials to the Gibson and Ashby models for open-cell foams. However, Williams et al. [82] produced open-cellular S/DVB PolyHIPE foams via the polymerisation of a HIPE and then filled the open-cellular structure with varying amounts of polymer to prepare what they described as macroporous gel-type and polystyrene-filled foams. The compressive mechanical properties of the differing PolyHIPE materials were also compared to the models already described by Gibson and Ashby. Using **equation 1.13** Williams plotted the compressive modulus of the materials as a logarithmic function of density. They found that the modulus of the polystyrene and gel-filled foam materials compared well with the Gibson and Ashby model. The macroporous-filled foams however did not compare as well as the polystyrene or gel-filled material. They suggested that this was due to the change in microstructure of the material at high relative densities. The yield stress dependency on density was not as straight forward as the modulus dependency. Above 0.4 and below 0.2 gcm^{-3} the behaviour of the macroporous and gel-filled polymer foams is similar to that expected for elastomeric foams, however a problematic discontinuity for foams with a density between 0.2 and 0.4 gcm^{-3} was discovered. The polystyrene-filled materials also followed the model for elastomeric foams above 0.3 gcm^{-3}. From the stress-strain curves, Williams reported

that elastic-plastic and elastomeric as defined by Gibson and Ashby do not adequately represent the foam materials tested, but the terms plastic and elastic-plastic do.

1.5 Core materials and sandwich construction

1.5.1 Introduction

The development of core materials for sandwich applications has progressed steadily from the 1940's till the present, the main effort being to reduce the weight of sandwich panels. Balsa was the first core material to be used and is still in use in applications where weight is not essential such as in cruising yachts [83]. Although heavy, it can offer advantages over other core materials such as excellent compression and stiffness for a relatively low cost. However, apart from being heavy it is also susceptible to water absorption and will eventually rot. Further progress in the 1950's saw the production of honeycomb materials mainly for aerospace applications. Honeycomb materials provide the greatest shear strength and stiffness to weight ratios but adequate bonding to the panel faces can be difficult. As discussed previously honeycomb materials have a hexagonal cross-section but their continued high cost has limited their applications in the aerospace industry. The late 1950's to the early 1960's brought the production of polyvinyl chloride (PVC) and polyurethane (PUR) foam core materials. The more recent developments have come in the shape of cellular thermoplastic cores where the properties can be tailored by orienting the cell structure [83].

The American society for testing and materials (ASTM) defines a sandwich structure as follows:

A structural sandwich is a special form of a laminated composite comprising of a combination of different materials that are bonded to each other so as to utilise the properties of each separate component to the structural advantage of the whole assembly [83].

A sandwich panel usually consists of three main parts shown below;

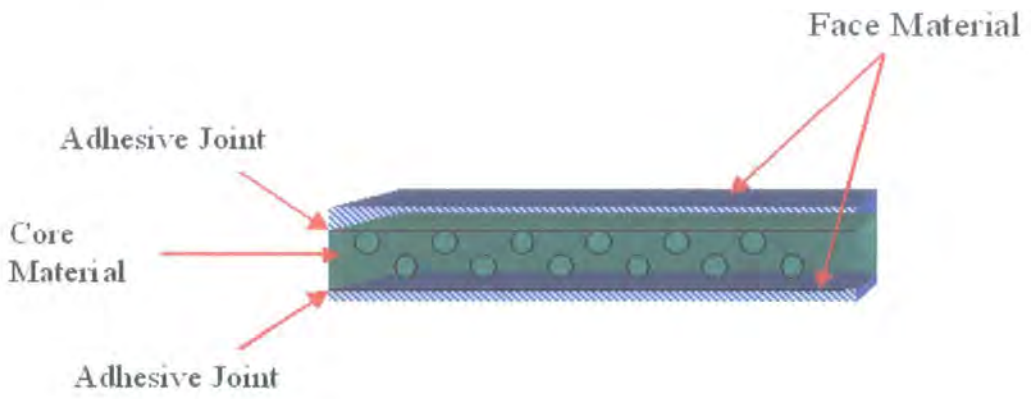

Figure 1.12 *Standard construction of a sandwich panel.*

two thin, strong and stiff faces separated by a thick lighter and weaker core [84]. The face material is adhesively bonded to the core to ensure load transfer between the two components. The bond between the faces and the core must be strong enough to resist shear and tensile stresses between them. Therefore the adhesive that bonds the core to the faces is an important factor in sandwich construction. As discussed previously the choice of core material is now vast with the availability of competitive cellular plastic cores and with the introduction of fibre-reinforced composites (FRC) the choice of face materials has also increased

Practically any structural material that is available in the form of a thin sheet can be used to form the faces of a sandwich panel [83], [84]. The required properties for face materials are

- high stiffness
- high tensile and compressive strength

- impact resistance
- environmental and wear resistance

1.5.2 Face and core materials

Generally, most face materials are classed as either metallic or non-metallic materials. The metallic group contains steel, stainless steel and aluminium alloys. The non-metallic is the larger group, containing plywood, cement, reinforced plastics and fibre composites such as carbon, glass and Kevlar reinforced composites. The latter of the list is the most important face material as they offer greater strength properties but their stiffness is magnitudes lower than their metallic counterparts.

The most important material in sandwich construction is the core material. These are divided into corrugated, honeycomb, balsa wood and cellular foams. The core should have as low a density as possible. Young's modulus perpendicular (compressive modulus) to the core faces should be high to ensure there is no decrease in core thickness. The core material is generally subjected to shear, so good shear strength and stiffness are required. In summary the important properties of a core material are;

- low density
- shear strength and modulus
- compressive stiffness and strength
- thermal insulation

1.5.2.1 PolyHIPE materials versus current core materials

To assess whether PolyHIPE foams are viable as a core material their mechanical properties must be compared to current commercially available core materials, and especially to that of the type of foam materials used in sandwich applications. To compare PolyHIPE materials to current core materials it is necessary to compare to

materials of similar density (50-150 kgm^{-3}). PolyHIPE materials already hold advantages over the commonly used gas blown polymeric foams. Extruded/gas-blown foams are generally closed-cell in nature, as in extruded polystyrene (**see figure 1.2 (b)**) and have void sizes in the 100-500 μm region. This is compared to the interconnecting open cellular network that has already been discussed for a PolyHIPE material (**see figure 1.5**) with a void size of around 10-20 μm and an interconnect size of 2-5 μm. The smaller void size and the increased spherical symmetry have been suggested to lead to enhanced compressive strengths [13]. The ability to absorb large amounts of liquid by capillary action and the porous interconnecting network allows for the PolyHIPE foam materials to be permeable not just to liquids with a high wettability but non-wetting liquids, such as water, also.

The different types of core materials used and the selected properties of commercially available examples were compared and selected core material values are presented in **tables 1-12** in the Appendix at the end of this chapter.

Honeycomb type core materials have been generally used in aerospace applications. They have been produced in a variety of different cell shapes but shape most commonly used is the hexagonal shape as discussed. Shapes such as square, the over-expanded hexagonal and the "flex-core" have also been used.

Euro-composites[85] is the leading manufacturer in lightweight products used as structural materials on land, water and air. They produce three different grades of honeycomb for use in the ship, ferry and train industries. The grades are aerospace grade, the industrial grade and their standard aluminium cores. The properties of their aerospace grade and aluminium honeycombs can be found in **Tables 1** and **2**.

Tubus Bauer [86] produces four grades of honeycomb, which are the polycarbonates, the thermoplastic elastomer, the polyetherimides and the PP grades. They are mainly used

as shock absorbing materials. The properties of polycarbonate and polypropylene grades are shown in **Table 3** in the appendix.

Hexcel [87] is the leading producer of honeycomb materials and manufacture a variety of grades. Their materials are available in a wide range of cell configurations and other products are continually produced in response to new uses for honeycomb sandwich construction. A few examples are listed below;

5052 alloy hexagonal aluminium specification grade **(see Table 4)**

5052 aluminium alloy Rigicell TM aluminium corrugated honeycomb

Aluminium flex-core

5052 aluminium double-flex

HRP fibreglass reinforced phenolic honeycomb`

HRH-327 fibreglass reinforced polyimide honeycomb

HRH-10 aramid fibre/phenolic resin honeycomb

HRH-78 nomex grade aramid fibre/phenolic resin

HRH-49 Kevlar 49 honeycomb

The properties that are required for good structural performance for sandwich structures are those of compressive strength and shear strength. The compressive and shear moduli will also be considered as reasonably high values are required for stiff sandwich structures.

From the mechanical data collected only the compressive modulus values for the Hexcel H5052 range were available. So it was therefore impossible to compare the different honeycomb material grades in this way. From the shear modulus values the Hexcel honeycomb materials came out on top. At a density of 84 kgm^{-3} (5.2 $lbft^{-3}$), the 5.2-1/4-25 Hexcel 5052 has a shear modulus value of 565 MPa in the length direction (245 MPa in the width direction). This is compared to Euro-composites aluminium

honeycomb ECM 6.4-82 (82 kgm^{-3}) which has a shear modulus value of 430 MPa in the length direction (220 MPa in the width direction) and the Tubus Bauer honeycomb PP 8-80 and PP14 (80 kgm^{-3}) which has a shear modulus value of 15 and 13.6 respectively. The names of the Hexcel honeycombs designate the cell size in fractions of an inch i.e. 1/8, the type of aluminium alloy, i.e. 2 and the foil thickness in inches i.e. the 0.006. The published values for the Hexcel honeycombs are greater than the properties of the Euro-composites. Tubus Bauer has a honeycomb with a density of 80 kgm^{-3} but the shear moduli are a lot lower at 15 and 13.6 MPa respectively. We therefore can not compare it to the Hexcel or Euro-composites honeycombs.

From the mechanical information gathered on some commercial honeycombs, it can be observed that Hexcel has the largest range of honeycomb cores with considerably larger compressive moduli than any of the other commercial grades. A density of 80 kgm^{-3} was used to compare the different honeycomb grades but the compressive moduli were not available for all these grades and the shear moduli were therefore used. From the shear moduli it was found that the Hexcel honeycombs had higher values than any of the other grades.

Cellular foams do not offer the same stiffness and strength to weight ratio as honeycomb materials, however they do have other important advantages. They are generally cheaper in cost than honeycombs. In most cases the foam surface is easier to bond to the face material. Foams offer thermal insulation and the closed cell structure of certain foams can ensure the structure will be resistant to water.

A description of some general foams is given below,

Polyurethane (PUR) foams – The urethane polymer is formed through the reaction between isocyanate and polyol with CCl_3F or carbon dioxide as blowing agent. They can be made fire retardent by using additives containing phosphorous. They have low

thermal conductivity and diffusion coefficients, which give them good insulation properties. There mechanical properties are lower than most cellular plastic foams but they are the cheapest of all available core materials. PUR foams can also be foamed in conjunction with the manufacturing of the sandwich structure.

Polystyrene foam is produced by either extrusion or expansion in closed moulds. In both cases the plastic is mixed with the blowing agent, which then expands at elevated temperatures. A major problem is the use of CFC as blowing agent but recently PS foams have been expanded without the use of CFC gases. Producing microcellular polystyrene foams using supercritical carbon dioxide has been studied by Arora et al. (88)

Polystyrene extruded foams have closed cells as shown in **figure 1.2 (b)**. PS extruded foams have good mechanical and insulation properties due to their closed cell nature. They are generally used as a thermal insulation material but can also be used in load carrying structures.

Polyvinylchloride (PVC) foam– PVC foam exists in two different forms, a thermoplastic, called linear PVC foam, and a cross-linked isocyanate version. Linear PVC has great ductility but softens at elevated temperatures. The cross-linked PVC is more rigid, has higher mechanical properties, is less heat sensitive, but is more brittle. The mechanical properties of PVC are higher than any PUR or PS foam but it is also more expensive. It is non-flammable but when burned HCl is released. PVC foams are used in many different sandwich structure applications varying from thermal insulation to aerospace applications and are probably the most widely used core material. They are a 95 % closed-cell at lower densities and completely closed cell at higher densities.

Polymethacrylimide foam (PMI) – The mechanical properties of PMI foams are extremely good perhaps the best of all the commercially available cellular foams, but

the price is the highest. They are generally fairly brittle and also have good temperature resistance. The PMI foams have a closed cell structure as shown below in **figure 1.13**.

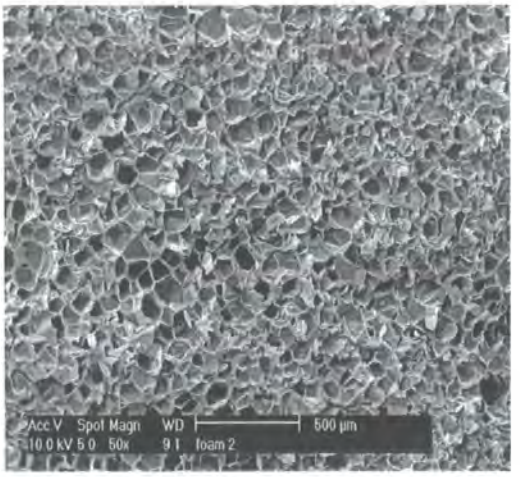

Figure 1.13 *Morphology of a PMI based foam (Rohacell)*[89].

The commercial example of a PMI foam is Rohacell.

Alcan-Airex group [90] produces structural foam cores for road transportation, rail engineering and marine craft. In the road industry the general application is in primary and secondary structures, trucks, lightweight fuel-efficient vehicles and high performance cars. Airex produce five grades of foam: Airex R63 (linear PVC foam); Airex R82 (PEI foam); Kapex; and Herex C70 and C71 ET. The properties of the Airex R63, R82 and Herex C71 ET foams are given in **Tables 5** and **6**.

The DIAB group [91] specialises in sandwich composite structures. The DIAB structures are based on there structural cellular plastic Divinycell. Divinycell is a cross-linked PVC foam and has been used in sandwich construction, advanced insulation and sub-sea use. Examples are pipelines, submarines, wind power generators, aircraft and spacecraft applications. The properties of the Divinycell HT grade are given in **Table 7**.

The ATC Chemical Corporation [92] manufactures the Core-cell linear polymer foam, which is used as a sandwich core in high quality boats. The ATC core-cell material is a styrene/acrylonitrile (SAN)-based foam material. It has a high damage tolerance/ high

impact strength and good thermal resistance, so that the core foam can be used in hulls, decks etc. The foam is produced in seven densities and the properties can be found in **Table 8** in the appendix

Rőhm [93] is a German company that produces the Rohacell PMI cores. As mentioned previously Rohacell is a polymethacrylimide rigid foam. It is isotropic, 100 % closed cell foam. The properties of the Rohacell FX and IG grades are given in **Tables 9** and **10**.

Another range of cellular foams is the metallic foam. A recent industrial survey [94] on metal foams indicated some potential applications from sandwich panels to sound adsorption, impact protection and battery applications (for Nickel foams). There are numerous companies that produce cellular metals worldwide. Alulight [95] (Austria) and Cymat [96] (Canada) produce aluminium foams, while Inco [97] produce nickel foams for batteries and fuel cells. The main type of metal foam used for sandwich applications is the aluminium foam. Companies such as Alulight and Karmann GmbH (Germany), produce sandwich panels consisting of an aluminium core. The major steps in the production of nickel foam are firstly; polyurethane foam of known thickness and porosity is covered with an electrically active material. Nickel is then electroplated on the coated surface, before burning off the polyurethane foam [98]. A final treatment is generally necessary to obtain the wanted mechanical properties. There are two general methods for producing aluminium foams. The first is the powder route. This was developed in 1959 by research staff at the United Aircraft Corporation [99]. The powdered metal is first mixed with a powdered gas-forming material. The gas-forming material has to be carefully chosen so that it releases a large amount of gas at about the melting temperature of the material. This mixture of powders is then compacted and extruded, to give a solid metal material containing a dispersion of powdered foaming

agent. When this solid is heated to the melting point of the metal the "foaming agent" decomposes and releases gas into the molten metal. Metal hydrides, which decompose to metals and hydrogen gas at convenient temperatures, are used as the "foaming agent". The cooling of the foam was a problem and the metal was prone to collapse back to molten metal. Hardy and Peisker [100] presented an alternative route, the liquid route, in a patent four years later, and this process involved by the adding of the foaming agent directly to a semi-molten metal. This process has the advantage of being significantly cheaper than the powder route. A new development in this process was the addition of siliceous materials to the molten aluminium to increase its viscosity and trap the evolved gas in the structure. Also hydrated clays were used as alternative foaming agents. They would release the water molecules trapped in their structure as water vapour when added to the melt. Although some companies produce powder-based foams, the melt-route process remains the main focus of commercial interest.

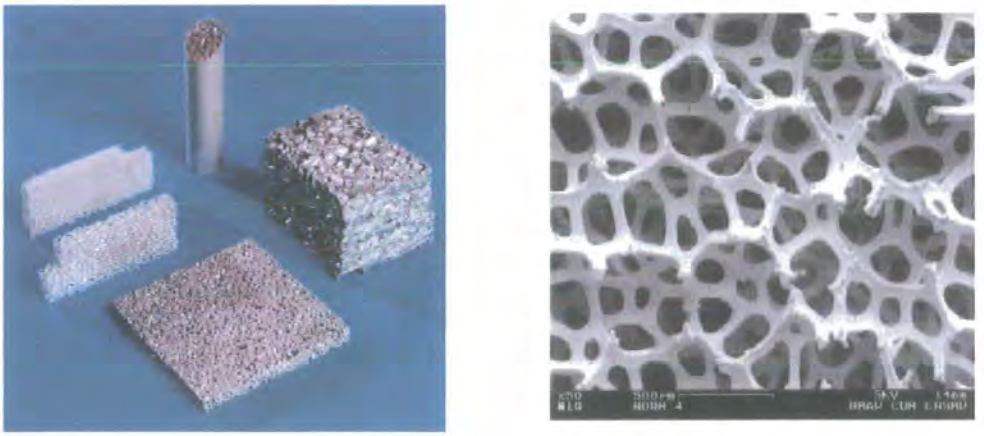

(a) (b)

Figure 1.14 *(a) Photographs of commercially available metal foams [94], (b) open-cellular nickel foam produced by electroplating a polyurethane template [98].*

Although there is no common density between the different ranges of foam materials studied. The range with the best shear and compressive moduli belongs to the Divinycell HT range.

As well as foams and honeycombs being used for core materials in sandwich construction, **balsa wood** also has its place as a commercial core material. The Baltek Corporation [101] produces balsa wood to be used in industry. "End grain" balsa, cut across the grain, has tiny closed cells and high cell wall content. Balsa has a more productive strength-to-cost ratio than synthetic honeycombs and greater strength and cost-effectiveness than synthetic foams. End grain balsa offers high impact resistance and excellent flexural and shear strengths. Balsa has been used in varied sandwich composites in marine, transportation, industrial, architectural and military applications. The two types of balsa studied, were the Baltek balsa standard and the Baltek balsa superlite. The reported mechanical properties are in **tables 11** and **12.**

The two balsa woods with the highest compressive modulus belong to the standard range. D-100 and CK-100 have a compressive modulus of 4070 MPa. In order to compare it is necessary to look at similar densities. Therefore D-57 and CK-57 (100 kgm^{-3}) of the standard balsa range and S47 (108 kgm^{-3}) of the Superlite range will be compared. From these properties, it can be observed that the Superlite S47 has a higher compressive modulus of 2.4 GPa compared to that of 2.2 GPa in the standard range. Similarly, the shear modulus of Superlite S47 (116.17 MPa), is higher than that of the standard D-57 and CK 57 (108 MPa). The data show that even though the standard balsa range has a range of materials at higher densities, the Superlite range has materials with the better compressive and shear moduli. A recent article [102] from workers at the DIAB group compares the compressive and shear properties of the cross-linked and linear PVC foams (Divinycell and Airex R63) to SAN based foams

(Corecell) and PMI-based foams (Rohacell). They also compared the properties of these selected foams and honeycombs to the properties of balsawood at different densities **(see figure 1.15)**. They showed that balsawood has excellent shear and compressive properties compared to foam materials. However, they also highlight the fact balsawood is highly susceptible to water ingress and will eventually rot compared to foam materials, which are lighter and much less susceptible to water.

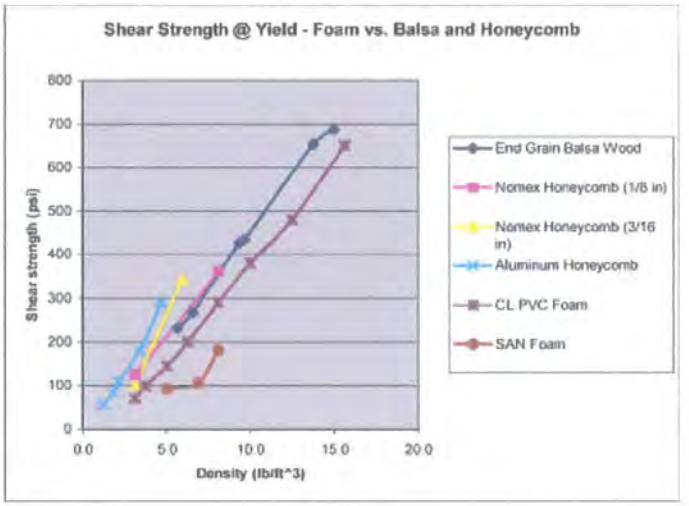

Figure 1.15 *Shear properties of foam materials versus balsa and honeycomb materials*[102].

1.5.3 Modes of failure

Sandwich beams can fail in several ways [103]. The faces can yield plastically; and the compressive face can buckle or wrinkle. The core can also fail too, although this has attracted less attention than face failure. The most common mode of core failure is shear, other possible modes are tensile or compressive yield and, if the core is made of a brittle material, tensile/brittle fracture. The two final modes are delamination of the adhesive and indentation. **Figure 1.16** shows schematically the modes of failure for a sandwich beam construction, where P and L is the applied load and span length respectively.

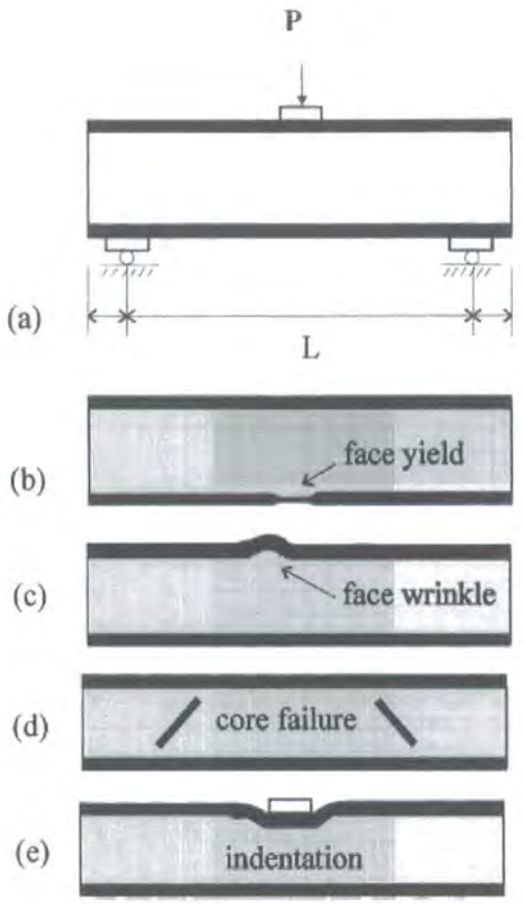

Figure 1.16 *Schematic of the different failure modes of sandwich beams* [103].

1.6 Fibre-reinforced polymer (FRP) composites

1.6.1 Introduction

Engineers in many fields prefer to use fibre-reinforced polymers (FRP) rather than low-density metals or alloys as core materials to produce stiff lightweight structures. An FRP is generally defined as a polymer matrix, either thermoset or thermoplastic that is reinforced with a fibre or another reinforcing material with a sufficient aspect ratio (length to thickness) to provide a reinforcement in one or more direction [104]. FRPs can be anisotropic in nature, where the properties are stronger in the direction of the alligned fibres. The mechanical properties therefore can be tailored for the intended use. The important considerations are:

1) type of fibre

2) fibre-matrix interface

3) orientation of fibre

4) fibre volume

The primary role of the fibre is to carry the load along the length of the fibre to provide strength and stiffness in one direction. The deformation of the matrix is used to transfer stress at the fibre-matrix interface to the high strength fibre. If the fibre length is sufficient the fibre should then take up the same deformation as the polymer matrix and therefore reinforce effectively the polymer material [105]. The fibres also help retard the propagation of cracks by dissipating the energy of the crack and diverting it on a longer propagation path, and therefore producing a material, which is also tough as well as high strength.

1.6.2 Types of reinforcing fibres

Typical fibre materials range from glass, carbon (graphite) to man-made aramid fibres such as Kevlar. Other reinforcing fibres include polyethylene, polypropylene, polyester and cellulose based fibres. Cellulose is also a naturally occurring product in wood.

Glass fibres are based on an alumina-lime-borosilicate composition. They are two types of glass fibre. "E" glasses are the most predominant reinforcing fibres due to their high electrical insulating properties and high mechanical properties. The "S" versions have a higher strength, heat resistance and modulus. Glass is a good impact resistant fibre but weighs more than carbon or aramid fibres. Composites containing glass fibres exhibit extremely good electrical and thermal insulation properties [104].

Carbon fibres are produced by the controlled oxidation, carbonisation or graphitisation of carbon rich organic precursors. The most commonly used precursor is polyacrylonitrile (PAN). These fibres offer excellent compressive strength and modulus values. Carbon fibres are more expensive than glass fibres but offer an excellent

combination of strength, low weight and high modulus. The tensile strength is equal to that of glass fibres were as the modulus is around three to four times higher than glass. The composites produced from these materials are more brittle than glass or aramid fibre based composites [104].

Aramid fibres are aromatic polyamides, the most common example used in reinforcement is Kevlar produced by Dupont. Dupont also produce another widely used aramid fibre with the trade name Nomex, and Akzo Nobel produce an aramid fibre with the trade name Twaron. The structure of the repeat unit of Kevlar is shown in **figure 1.17**.

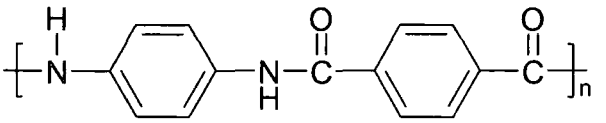

Figure 1.17 *Structure of the repeat unit for Kevlar.*

Aramid fibres have good mechanical properties at low density with the added advantage of excellent toughness and impact resistance. The tensile strength and modulus of aramid fibres are higher than glass fibres. They increase the impact resistance and tensile strength of the composite material in which they are present. Aramid fibres are also insulators of both electricity and heat, and are resistant to organic solvents, fuels and lubricants. Aramid fibre-reinforced composites do not have as good a compressive strength as carbon or glass composites. The compressive strengths of the aramid fibres themselves are slightly lower or very similar to "E" glass fibres. The properties of each fibre may vary with the different grades available so that the properties of the reinforced composite can be tailored for a specific use [104].

1.6.3 Fibre-matrix interface

As discussed previously, the deformation of the polymer matrix transfers stress at the fibre matrix interface to the fibre itself. There are therefore developing methods to

improve this stress transfer across the fibre-matrix interface. To improve fibre resin bonding, the fibres can be surface treated during production to produce a fibre that is more compatible with the polymer matrix. There are a number available for glass fibres. The industrial terms for these treatments are size, binder and finish [106]. A size is a treatment applied after fibres are formed. Temporary sizes are dissolved and washed away and then a permanent finish is applied to improve the resin bonding. Temporary sizes can contain starch gum, hydrogenated vegetable oil or gelatin. Compatible sizes are not removed and can serve the dual function of protecting strands from one another and enhancing bonding with the polymer matrix. Binders are used to hold strands of fibreglass together when woven into a mat or preform. Polyvinylacetate is used due to its good adhesive properties. Finish agents are applied after the fibres are fabricated to make them more compatible with the moulding resin. Generally the binding agents will contain groups; that can react with both the resin during polymerisation and with the OH groups on the surface of the glass.

For fibres that are continuous throughout the whole length of the sample, the load is applied directly to the fibre so that the stress is constant over the whole of its length. Therefore, the matrix transfers no load to the fibre and its main purpose is to bind the fibres together. For discontinuous fibres Cox presented a theory for the longituadal stress distribution along the fibre-matrix interface [105], [106] when the matrix and the fibre are in the elastic state. Cox made two assumptions for his theory:

1) a perfect bond exists between the fibre and the matrix.
2) there is no load transfer through the ends of the fibres.

Cox considered a fibre of length L, embedded in a matrix with strain ϵ. He considered a point distance x from the end of the fibre to obtain the expression for the stress distribution which is shown in **equation 1.24**.

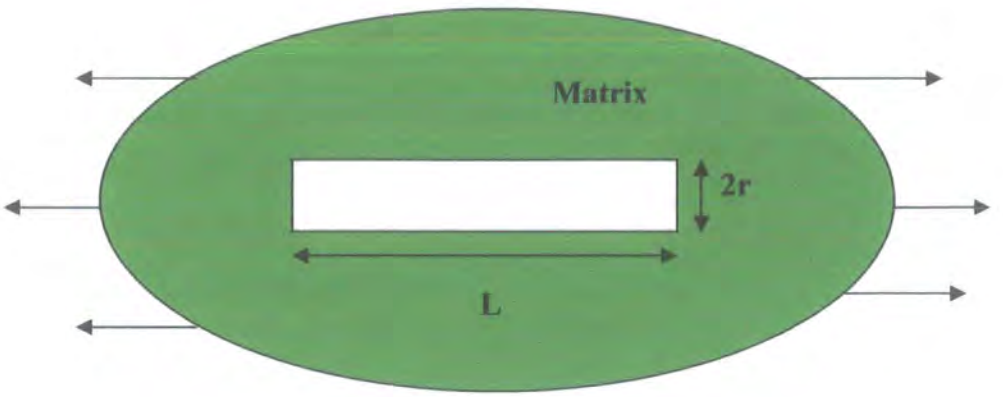

Figure 1.18 *Schematic of the Cox model.*

$$\sigma_f = \frac{(E_f - E_m)\sigma_c}{E_m}\left(\frac{1-\cosh\beta(\frac{L}{2}-x)}{\cosh\beta\frac{L}{2}}\right) \qquad \textbf{Equation 1.24}$$

where the subcripts f and m denote the fibre and the matrix repectively and σ_c is the applied stress. If the maximum possible strain is ε then the maximum possible stress will have a value of εE_f. The critical fibre length, l_c is the length that must be exceeded if the fibre is to be broken. **Figure 1.19** shows the tensile and shear stress distribution across a fibre of length L where $L > l_c$. In order for the composite to have a high tensile strength, generally the length of the fibre used must be greater than the critical length l_c

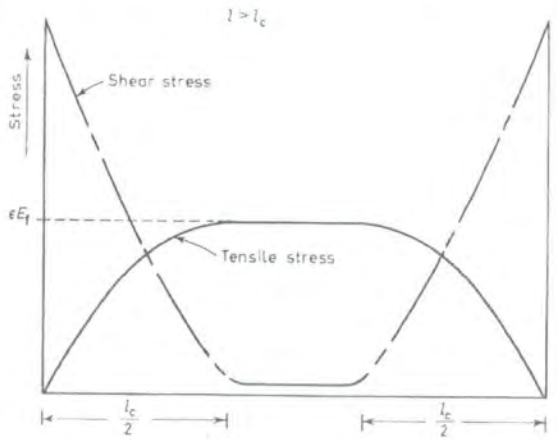

Figure 1.19 *Shear and tensile stress distribution across a fibre length L, where* $L > l_c$ *(105)*

1.6.4 Fibre volume

For the case of discontinuous fibres, the tensile strength of the composite material can be related to the volume fraction of the fibres, V_f, by the use of the Cox model (**equation 1.24**) to produce the relationship shown in **equation 1.25**.

$$\sigma_c = \varepsilon V_f \left[(E_f - E_m) \left(1 - \frac{\tanh \beta \frac{L}{2}}{\beta \frac{L}{2}} \right) - E_m \right] + \varepsilon E_m \qquad \textbf{Equation 1.25}$$

The tensile strength of the composite material varies linearly with the fibre volume.

The fibre volume can also affect the fibre-fibre spacing. With increasing fibre volume the fibre-fibre spacing will decrease. This will increase the stiffness/rigidity of the material, but will restrict the movement or flexibility of the fibre during tensile stretching or flexure.

1.6.5 Fibre orientation

Short fibres are usually randomly orientated and result in isotropic behaviour and the optimum mechanical properties cannot be achieved. In the case of unidirectionally arranged fibres, where the fibres are orientated in one plane, the composite can have excellent strength if the load is parallel to the fibres (**see figure 1.20 (a)**). This type of composite material has anisotropic behaviour. The modulus will depend on the direction of both the applied load and the fibres. When the direction of the load is perpendicular to the fibres the modulus will be low compared to the modulus parallel to the fibres (**see figure 1.20 (b)**). There are three important stresses: σ_c, the stress required for tensile failure of the fibres and the matrix; τ_u, the stress required for shear failure of the matrix or the fibre matrix interface; and σ_u, the stress required for tensile failure normal to the fibres. The tensile stress for the failure of the composite by fibre

fracture [105] is shown in **equation 1.26** and when failure is by shear parallel to the fibres the tensile stress [105] is given by **equation 1.27**.

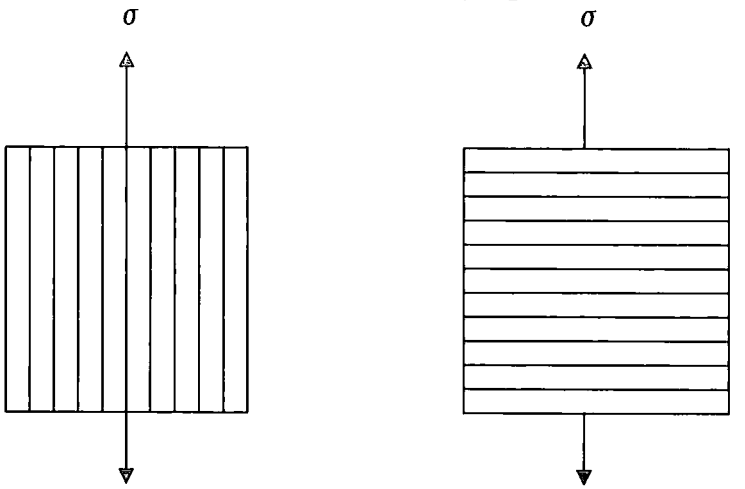

Figure 1.20 *Orientation effect for a single fibre orientation, (a) parallel, (b) perpendicular to stress direction.*

$$\sigma = \sigma_c \sec^2 \phi \qquad \textbf{Equation 1.26}$$

$$\sigma = 2\tau_u \operatorname{cosec} 2\phi \qquad \textbf{Equation 1.27}$$

Equations 1.23 and **1.24** can be used to define a critcal angle Φ_{crit}, above which the strength falls rapidly.

$$\phi_{crit} = \tan^{-1} \frac{\tau_u}{\sigma_c} \qquad \textbf{Equation 1.28}$$

Low values of Φ_{crit} suggest a high degree of anisotropy within the material.

For multiaxial fibre orientation, Kreschnel [105] compared a number of different oriented glass fibre-reinforced composites using a definition for reinforcement efficiency **(equation 1.29)**.

$$\chi = \varepsilon a \cos^4 \phi \qquad \textbf{Equation 1.29}$$

where a is the volume fraction of fibres at angle Φ from the direction of the tensile load.

Table 1.1 shows the values of χ at different glass fibre orientations [106].

Table 1.1 Reinforcement efficiency, χ, for several fibre orientations

Fibre orientation	Stress direction	Reinforcement efficiency, χ
All fibres parallel	1 Parallel to fibres	1
	2 Perpendicular to fibres	0
Fibres in two directions, proportions a_1 and a_2 perpendicular to one another	Angle $\pi/4$ to fibre direction	1/4
Four equal layers of fibres at $\pi/4$ to one another	1 Parallel to any other fibre group or layer	3/8
	2 Angle $\pi/8$ to any other fibre group or layer	3/8
Fibres uniformly distributed in plane	Any (in plane)	3/8
Fibres uniformly distributed in three dimensions in space	Any	1/5

The reinforcement efficiency is a maximum when 100 % of the fibres are aligned in the direction of the tensile stress.

1.6.6 Types of resin/matrix

There are many different resin or matrix types. The most common thermosetting resins are unsaturated polyesters, epoxies and phenolics. There are also recent literature reports of lightweight foam materials being used as the core matrix or to prepare lightweight materials for structural beams, sandwich panels or other applications. Palumbo et al. [107] prepared fibre reinforced syntactic foam composite consisting of a syntactic foam core and a fibre reinforced plastic skin. The syntactic foam material was described as a polymer core consisting of hollow microspheres. The reinforced outer skin consisted of "E" glass fibre reinforced epoxy. The main points described by Palumbo et al. were that they observed no adhesive debonding between the foam core

and the fibre-reinforced skin. The fibre-reinforced skin was determined to be anisotropic compared to the foam core, which was isotropic in nature and the outer skin protected the isotropic core until collapse of the beam. The hybrid material structure collapsed when the glass fibre skin reached its own tensile failure stress.

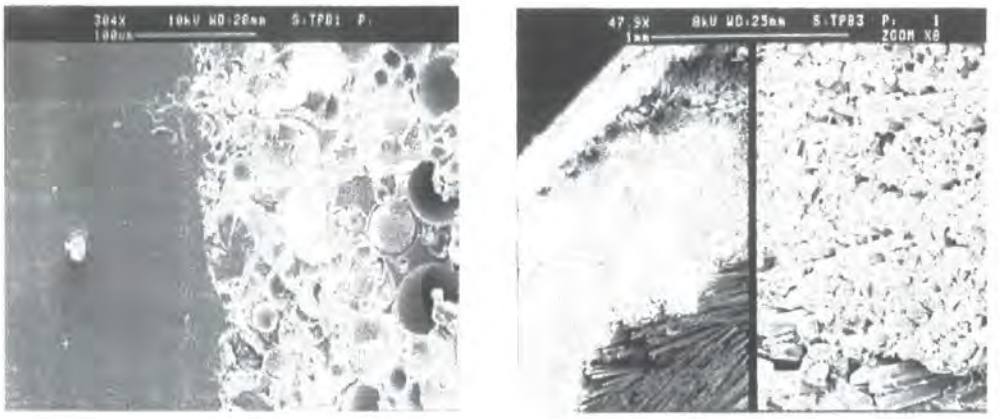

(a) (b)

Figure 1.21 *Images of the fibre-reinforced foam material, (a) failure surface, (b) fibre reinforced skin*[107].

There was also no matrix cracking observed at the mid-span cross-section. Shen et al [108] described a phenolic foam reinforced with short aramid fibres (Nomex) and "E" glass fibres. Phenolic foams are used in structural fields where fire resistance is critical, such as civil, passenger and military aircraft applications. They found that the addition of the aramid fibres enhanced the friability properties of the phenolic foam, with increasing fibre volume. The "E" glass fibre-reinforced material showed no improvement in the friability properties compared to the fibre-free foam. The compressive properties were dependent on the direction of the compressive load. When the compressive load was applied parallel to the direction of the expansion, the modulus values for the Nomex fibres showed a slight decrease but an increase in strength for a fibre volume of 5 wt % compared to the fibre-free foam. With increasing Nomex fibre volume up to 10 wt % there was an increase in modulus value compared

to the 5 wt % materials, but they did not surpass that of the fibre-free phenolic foam. The compressive strength value decreased with increasing fibre volume from 5 to 10 wt % Nomex fibre. The addition of the glass fibres improved both the modulus and compressive strength of the material, with a two-fold increase in the compressive modulus at 10 wt % glass fibre compared to the fibre-free foam. The greater increase in properties of the glass fibre-reinforced material compared to Nomex-reinforced material was said to be due to the greater tensile properties of the glass fibres themselves and greater glass fibre orientation in the foaming direction. This property was enhanced when the compressive load was applied perpendicular to the foaming direction. In this case, the composite foam materials showed an inverse trend where the aramid fibre was more effective than the glass fibre. Both of the fibre-reinforced materials showed greater shear modulus and strength values compared to the fibre-free material, with the glass fibres producing the largest increase. In a further paper, Shen et al. [109] described the enhanced peel resistance of the same fibre-reinforced phenolic foams. The peel process is shown in **figure 1.22**.

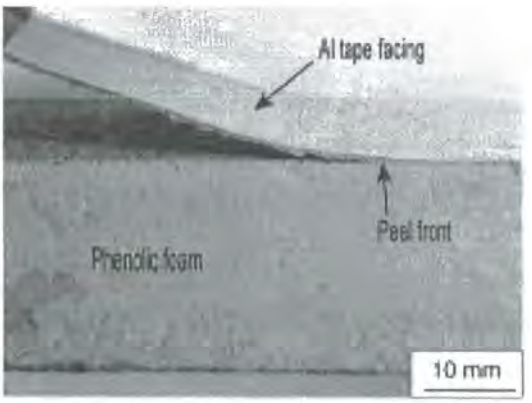

Figure 1.22 *Side view of a peeled specimen* [109].

They showed that the fibre reinforcement greatly increased the peel strength of the material. The aramid fibres in this case were more effective and enhanced the peel strength of the phenolic foam to a greater extent than the glass fibres. This was

suggested to be due to the different fracture behaviour of the two fibre types present within the matrix. Scanning electron microscope images showed the glass fibre surface after fracture was still encased in a phenolic sheath which Shen and co-workers said indicated fibre pull out (**see figure 1.23 (a)**).

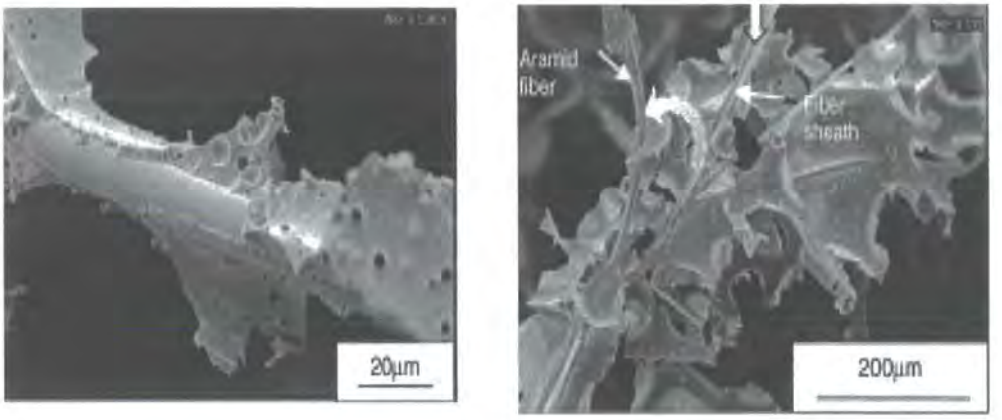

(a) (b)

Figure 1.23 *Microscope images of the glass and aramid fibre-reinforced phenolic foam, (a) glass fibre, (b) aramid fibre* [109].

The aramid fibres showed a micro-peeling behaviour where tiny fibrils (< 0.1 μm) have peeled off from the aramid fibre stem. The micro-peel process was said to be due to the aramid fibres orienting in the direction of the load, resulting in failure of the fibre-matrix bond. This micro-peel process enhanced the peel strength of the aramid fibre-reinforced material due to the presence of the mini-fibrils dissipating the energy of the propagating crack. In the early literature there have also been reports of glass fibre-reinforced closed-cell polyurethane foams. Cotgreave et al. [110] showed that the addition of the glass fibres resulted in a change in the foam morphology of the foam material. They found that glass fibres, which formed in large bundles, gave rise to a stress concentration that weakened the structure. When the fibres formed in a small bundle or a single filament they found that the fibres could divert the crack to give a longer propagation path and generate pullout fragments.

Appendix

Table 1: Euro-composites aerospace grade honeycomb cores

Product Designation		Compression		Shear			
				L Direction		W direction	
	Cell Size (mm)	Density (kg/m^3)	Strength (MPa)	Strength (MPa)	Modulus (MPa)	Strength (MPa)	Modulus (MPa)
ECA	3.2	48	2.1	1.32	48	0.72	30
ECA	3.2	64	4.5	1.78	64	0.97	38
ECA	3.2	64	3.9	1.9	68	1.05	44
ECA	3.2	80	5.5	2.35	80	1.25	48
ECA	3.2	96	7.44	2.8	96	1.68	68
ECA	3.2	123	11.8	3.35	118	1.94	84
ECA	3.2	144	15.2	3.5	128	2.2	94
ECA	4	48	2.68	1.2	42	0.68	28
ECA	4	64	4.65	1.7	58	0.9	40
ECA	4	80	5.7	2.5	78	1.26	44
ECA	4	123	11.5	3.85	125	2.2	70
ECA	4	144	16	4	135	2.4	82
ECA-R	4.8	48	2.8	0.74	24	0.82	44
ECA-R	6.4	48	2.8	0.74	22	0.78	42
ECA-R	4.8	64	4.6	0.84	26	1.04	56
ECA-R	6.4	64	4.5	0.92	26	1.02	56

Table 2: Euro-composites aluminium honeycomb cores

Honeycomb Type		Compression (stabilised)	Shear				Crush Strength
			L Direction		W direction		
	Density (kg/m^3)	Strength (MPa)	Strength (MPa)	Modulus (MPa)	Strength (MPa)	Modulus (MPa)	(MPa)
ECM 6.4- 82	82	4.50	2.40	430	1.40	220	1.7
ECM 9.6- 55	55+/- 15 %	2.75	1.48	253	0.88	170	0.891
ECP 6.4-42	42	not given	0.97	94	0.51	55	not given

Table 3: Tubus-bauer honeycomb core materials

Poly Carbonate		Compression		Shear		Tensile	
	Density (kg/m^3)	Strength (MPa)	Modulus (MPa)	Strength (MPa)	Modulus (MPa)	Strength (MPa)	Modulus (MPa)
PC3.5-90	90	3	not given	0.8	24.5	not given	not given
PC6-70	70	1.9	not given	0.6	21	not given	not given
PC8-70	70	1.8	not given	0.6	20	not given	not given

Poly Ether imide		Compression		Shear		Tensile	
	Density (kg/m^3)	Strength (MPa)	Modulus (MPa)	Strength (MPa)	Modulus (MPa)	Strength (MPa)	Modulus (MPa)
PEI3.5-70	70	2	not given	not given	28.5	not given	not given
PEI6-70	70	1.8	not given	not given	30	not given	not given
PEI8-70	70	1.7	not given	not given	30	not given	not given

Poly Propylene		Compression		Shear		Tensile	
	Density (kg/m^3)	Strength (MPa)	Modulus (MPa)	Strength (MPa)	Modulus (MPa)	Strength (MPa)	Modulus (MPa)
PP 8-80	80	2	not given	0.5	15	not given	not given
PP14	80	2	not given	0.4	13.6	not given	not given

Table 4: Hexcel H5052 honeycomb core materials

Product Designation	Compression (stabilised)		Plate Shear			
			L direction (MPa)		W direction (MPa)	
	Strength (MPa)	Modulus (MPa)	Strength (MPa)	Modulus (MPa)	Strength (MPa)	Modulus (MPa)
1.8-3/4-25	0.95	215	0.74	182	0.46	96
2.3-1/4-10	1.35	310	0.96	220	0.58	112
3.0-3/8-20	2.1	485	1.35	295	0.85	145
3.1-3/16-10	2.3	517	1.45	310	0.9	152
3.4-1/4-15	2.6	620	1.6	345	1.1	166
3.7-3/8-25	2.95	725	1.8	380	1.17	180
3.9-1/2-40	3.3	820	1.94	405	1.25	190
4.3-1/4-20	3.75	965	2.2	455	1.45	205
4.4-3/16-15	4.1	1000	2.25	470	1.48	210
4.5-1/8-10	4.2	1034	2.3	483	1.5	214
5.2-1/4-25	5.2	1310	2.8	565	1.8	245
5.4-3/8-40	5.35	1380	2.9	590	1.95	250
5.7-3/16-25	5.8	1520	3.15	620	2.05	265

Table 5: Airex R82

		Compression		Shear		Tensile	
	Density (kg/m^3)	Strength (MPa)	Modulus (MPa)	Strength (MPa)	Modulus (MPa)	Strength (MPa)	Modulus (MPa)
R82.60	60	0.6	33	0.7	14	1.2	34
R82.80	80	1	54	1.1	22	1.8	52
R82.110	110	1.7	94	1.7	35	2.7	78

Table 6: Airex R63 and Herex C71 ET

		Compression		Shear		Tensile	
	Density (kg/m^3)	Strength (MPa)	Modulus (MPa)	Strength (MPa)	Modulus (MPa)	Strength (MPa)	Modulus (MPa)
R63.50	60	0.38	30	0.5	11	0.9	30
R63.80	90	0.9	56	1	21	1.4	50
R63.140	140	1.6	110	1.85	37	2.4	90
C71	80	1.5	90	1.3	30	2	60

Table 7: Divinycell HT

		Compression		Shear		Tensile	
	Density (kg/m^3)	Strength (MPa)	Modulus (MPa)	Strength (MPa)	Modulus (MPa)	Strength (MPa)	Modulus (MPa)
HT 50	50	0.7	75	0.55	19	1.5	95
HT 70	70	1.15	100	0.9	26	2.1	125
HT 90	90	1.6	125	1.25	33	2.7	150
HT 110	110	2.1	150	1.6	40	3	175

Table 8: ATC Core-cell linear structural foam

		Compression		Shear		Tensile	
	Density (kg/m^3)	Strength (MPa)	Modulus (MPa)	Strength (MPa)	Modulus (MPa)	Strength (MPa)	Modulus (MPa)
A300	50	0.4	22.88	0.66	11.71	1.03	not given
A400	60	0.55	34.46	0.86	17.06	1.26	not given
A450	70	0.66	44.82	93	17.83	1.33	not given
A500	80	0.79	58.23	0.97	21.48	1.64	not given
A550	90	0.98	60.69	1.14	23.02	1.78	not given
A600	100	1.13	63.57	1.31	28.86	2.06	not given

Table 9: Rohacell-FX

		Compression		Shear		Tensile	
	Density (kg/m^3)	Strength (MPa)	Modulus (MPa)	Strength (MPa)	Modulus (MPa)	Strength (MPa)	Modulus (MPa)
51 FX	52	0.4	not given	0.4	14	0.8	35
71 FX	75	0.8	not given	0.7	26	1.5	65

Table 10: Rohacell-IG

		Compression		Shear		Tensile	
	Density (kg/m^3)	Strength (MPa)	Modulus (MPa)	Strength (MPa)	Modulus (MPa)	Strength (MPa)	Modulus (MPa)
31 IG	32	0.4	not given	0.4	13	1	36
51 IG	52	0.9	not given	0.8	19	1.9	70
71 IG	75	1.5	not given	1.3	29	2.8	92
110 IG	110	3	not given	2.4	50	3.5	160

Table 11: Baltek balsa standard

		Compression		Shear		Tensile	
	Density (kg/m3)	Strength (MPa)	Modulus (MPa)	Strength (MPa)	Modulus (MPa)	Strength (MPa)	Modulus (MPa)
D-57	100	6.52	2240	1.85	108	6.9	not given
CK-57	100	6.52	2240	1.85	108	6.9	not given
D-100	150	12.9	4070	2.98	159	13.1	not given
CK-100	150	12.9	4070	2.98	159	13.1	not given

Table 12 Baltek balsa-Superlite

		Compression		Shear		Tensile	
	Density (kg/m3)	Strength (MPa)	Modulus (MPa)	Strength (MPa)	Modulus (MPa)	Strength (MPa)	Modulus (MPa)
S45	78	4.83	1532.45	1.5	94.87	5.94	not given
S46	93	6.2	1954.27	1.78	104.98	7.27	not given
S47	108	7.67	2406.15	2.07	116.17	8.65	not given
S48	119	8.98	2803.96	2.31	126.4	9.83	not given

Chapter 2

Preparation and morphology of styrene/DVB PolyHIPE materials in different mould substrates.

2.1 Introduction

To produce PolyHIPE materials on a relatively large scale, we must ensure our moulding and preparation techniques can produce materials of a suitable quality and uniformity to put forward for testing. This section details the effect of small-scale production of PolyHIPE materials within mould substrates such as glass, PVC, PP, PE and PTFE. It will look at the effect on material uniformity and quality for each mould substrate. This will then give an idea on the type of mould substrate to take forward into large-scale production of the PolyHIPE materials. The effect of the combination of different mould release agents with the different mould substrates will also be detailed.

2.2 Experimental

2.2.1 Materials

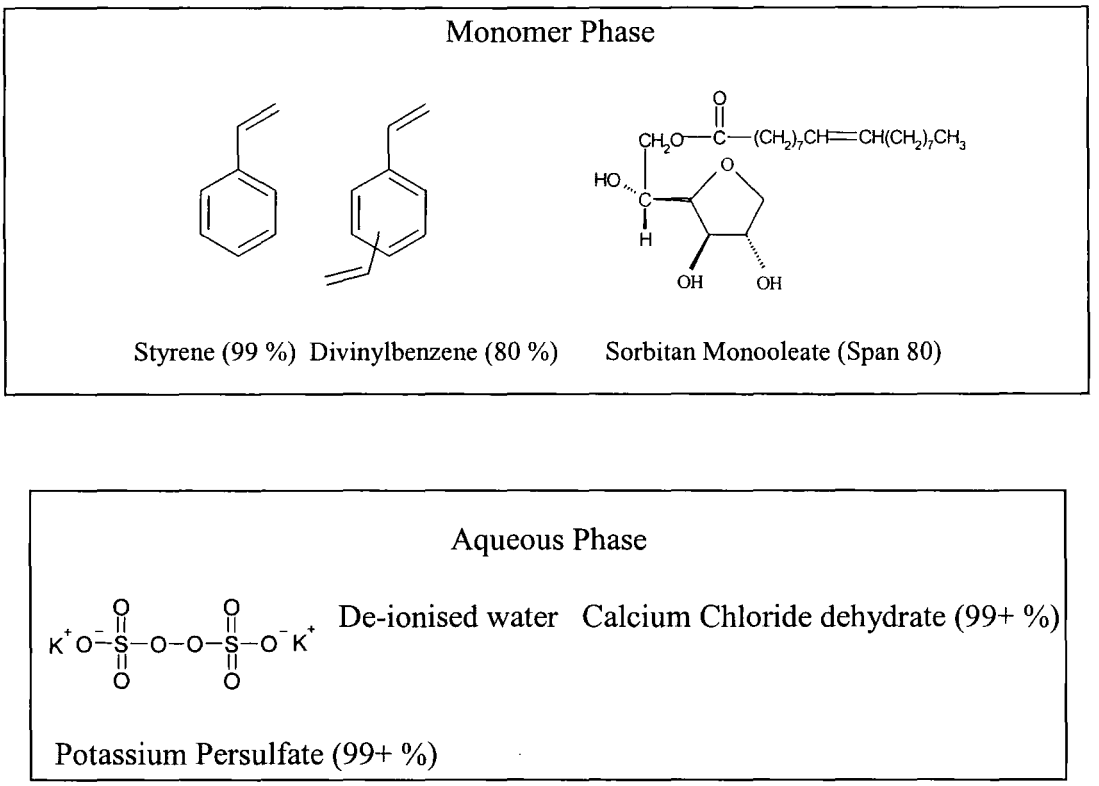

Figure 2.1 *Materials used for HIPE preparation.*

All of the monomers used were purified prior to HIPE preparation, by passing through a column of basic activated aluminum oxide. All of the chemicals used were obtained from Aldrich chemicals with the exception of the de-ionised water.

2.2.2 Instrumentation and characterisation

The morphologies of the PolyHIPE materials produced in this chapter were characterised using an Hitachi S2400 Scanning Electron Microscope fitted with an Oxford instruments Isis 200 Ultra thin X-ray detector and the FEI Philips XL30 Environmental Scanning Electron Microscope.

2.2.3 HIPE preparation and polymerisation

The monomer phase (5 g) was made up of styrene (4.38 g, 42.07 mmol) and divinylbenzene 80 % (0.63 g, 4.80 mmol) and to this was added Span 80 (1 g, 2.33 mmol). The aqueous phase (45 ml) contained potassium persulfate (0.10 g, 0.37 mmol) and calcium chloride dihydrate (0.5 g, 3.40 mmol). This is called a HIPE of 90 % internal phase volume. The monomer phase was placed in a three-necked 100 ml round-bottomed flask and was stirred with a D-shaped PTFE paddle driven by an overhead motor (300 rpm). The aqueous phase was then added drop-wise for 1 hour under a nitrogen atmosphere throughout. A high internal phase emulsion slowly formed. After all the aqueous phase was added the HIPE was left to stir for another 30 min. The HIPE was then transferred to various moulds, **(see figure 2.2)** and left to crosslink at varying times and temperatures. The PolyHIPE, which had formed, was then extracted with water and then propan-2-ol for 2 days each in a Soxhlet apparatus. The PolyHIPE was then dried *in vacuo* at room temperature (2-3 days). Each experiment was carried out only once, unless complete separation of the HIPE occurred and in this case the experiment was carried out until a PolyHIPE material was obtained.

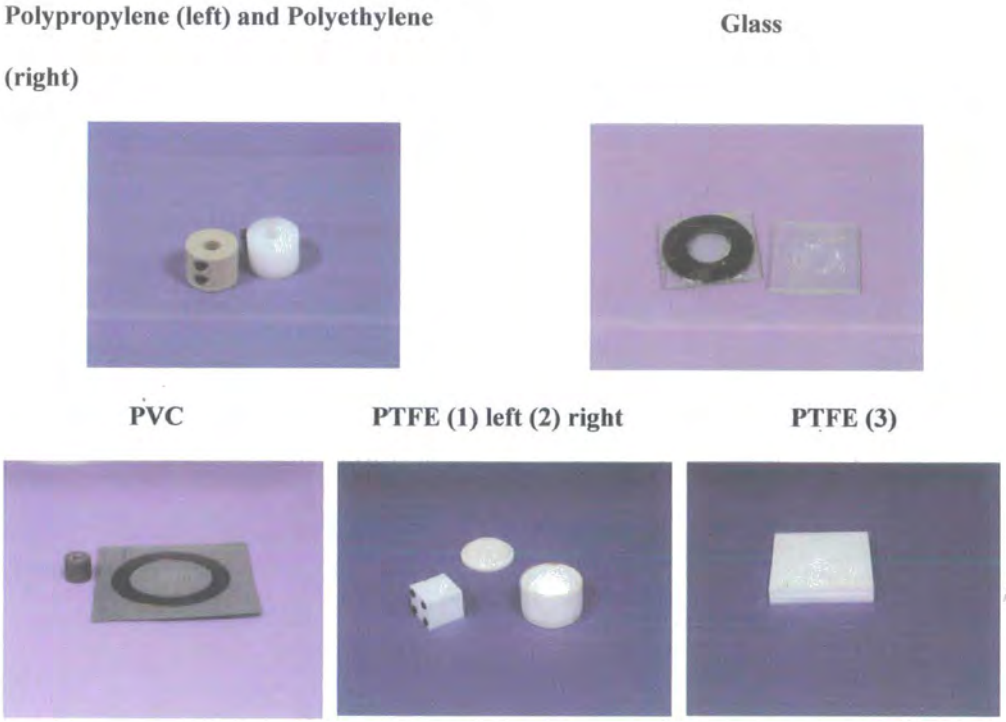

Figure 2.2 *Moulds used for PolyHIPE preparation.*

Mould Dimensions – PVC plate (thickness –2 mm, diameter – 80 mm), Glass (thickness -2 mm, diameter – 29 mm), PTFE (1) (10 mm x 25 mm), PTFE (2) (45 mm x 50 mm), PTFE (3) (110 mm x 10 mm), PVC, PP, PE cylindrical (10 mm x 20 mm).

2.3 Results and discussion

2.3.1 Sample uniformity

The PolyHIPE materials produced from each mould were given a number between 0 and 10 (0 = no PolyHIPE formed, 10 = perfectly homogenous material) based on their sample quality and uniformity. **Table 2.1** gives an overview of the results and observations of the materials produced from the glass mould.

Table 2.1 Results and observations from the glass mould

Mould release agent	Curing Time and Temperature	Sample Quality	Comments
None	60 °C for 24 hours	4	Adherence to surface Patchy formation. Glossy surface.
Vacuum Grease	60 °C for 24 hours	5	No adherence Granular texture to surface
Vacuum grease	100 °C for 24 hours	3	Adherence to surface Yellow colouring
Span 80	40 ° C for 72 hours	2	Gel like paste which is clear around the edges
Tygflor	Room temperature for 24 hours 60 °C for 24 hours	3	Shrinking in from the sides of the mould
PTFE spray	60 °C for 24 hours	6	No adherence

When there was no mould release agent used on the glass plate mould, the PolyHIPE material adhered firmly to the surface of the mould. When removed the PolyHIPE materials produced were glossier on the surface than the materials produced from any other mould substrate suggesting a closed-cell structure. The hydrophilic nature of the glass may cause a layer of separated aqueous phase to form and consequently a separated layer of monomer and surfactant. This could lead to a partially open or closed-cell structure. The polymer formed in patches, the largest being 11 mm in diameter. To help prevent adherence to the mould surface, different mould release agents were placed on to both the top and bottom plate. Coating the glass plates with PTFE spray (**figure 2.3 (b)**) and vacuum grease (**figure 2.3 (a)**) improved sample uniformity and quality. The plates coated with vacuum grease produced a PolyHIPE material with a granular texture on the surface. The plates coated with the PTFE spray

produced a material with a smoother surface, which was less granular in nature. When the polymerisation temperature was increased there were adherence problems with the glass surface. The PolyHIPE material that was produced was also yellow in colour on the surface. This could possibly be due to surfactant oxidation at the higher curing temperature. **Figure 2.3 (a-d)** shows photographs of some of the PolyHIPE materials produced from the glass plate mould.

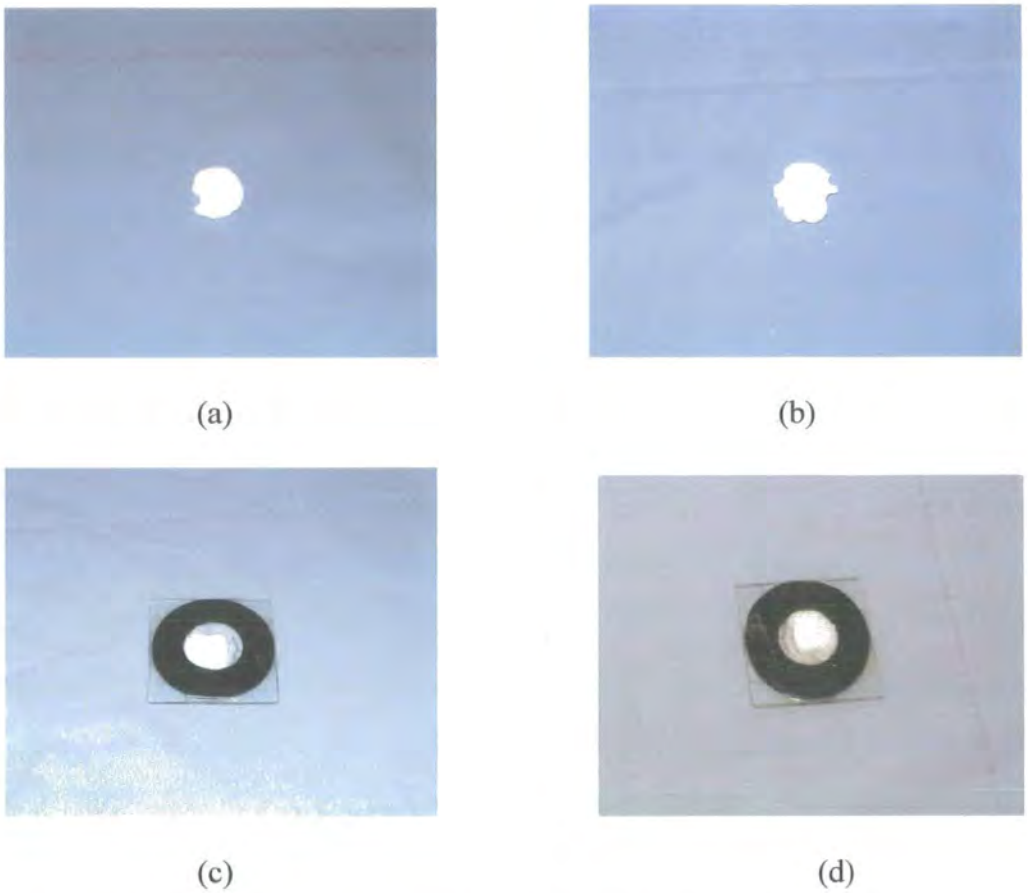

(a) (b)

(c) (d)

Figure 2.3 *PolyHIPE materials produced from the glass mould, (a) vacuum grease, (b) PTFE spray, (c) and (d) cured at 40 °C with Span 80 as a mould release agent.*

Table 2.2 shows the results and observations obtained for the PVC plate and cylindrical moulds.

Table 2.2 Results and observations for PVC plate and PVC cylindrical mould (bold)

Mould release agent	Curing Time and Temperature	Sample Quality	Comments
None	60 °C for 24 hours	0	Possible evaporation of monomer or aqueous phase
None	Room temperature for 24 hours, then 60 °C for 24 hours	0	Possible evaporation of monomer or aqueous phase
None	60 °C for 24 hours	2	Heavy weight on top of plates, small sample formed
Span 80	40 °C for 72 hours	0	No foam formed, gel like paste present
Span 80	100 °C for 6 hours	0	No foam formed, gel like paste present
Tygflor	60 °C for 24 hours	8	PolyHIPE disc produced some holes on surface
PTFE spray	60 °C for 24 hours	7	Holes penetrating sample, fragile
None	**60 °C for 24 hours**	**4**	**Shrinking and large holes on surface of material**

There was no formation of PolyHIPE material when there was no mould release agent present on the PVC plates. When the PVC plates were coated with the PTFE spray (**figure 2.4 (a)**) and the PTFE substrate Tygflor, a PolyHIPE material was produced, with the Tygflor coated PVC plates (**figure 2.4 (b)**) producing the greater quality sample. Possible evaporation of both the monomer and the aqueous phase could provide an explanation to the disappearance of the HIPE and non-production of a PolyHIPE material. Placing a heavy weight upon the PVC plates during polymerisation prevented complete evaporation but only a small amount of PolyHIPE (30

mm diameter) material was produced.

The same problems also occurred with the PVC cylindrical mould. Severe shrinking of the sample occurred. There were also large holes present on the surface of the PolyHIPE produced. Plasticisers, which are used in PVC production to give the material flexibility, can slowly escape from the PVC over a given period of time. This could be a possible factor in HIPE stability and the quality of the foam produced. When the polymerisation temperature is decreased a gel like paste remained (**figure**

2.4 (c)). Decreasing the polymerisation temperature therefore increasing polymerisation time can lead to greater coalescence and emulsion instability reducing sample uniformity and quality.

Table 2.3 Results and observations for the PE cylindrical mould

Mould release agent	Curing Time and Temperature	Sample Quality	Comments
None	60 °C for 24 hours	4	Adherence to mould surface
None	Room temperature for 24 hours 60 °C for 24 hours	5	Shrinking of PolyHIPE material
None	100 °C for 6 hours	5	Pinholes present on PolyHIPE surface

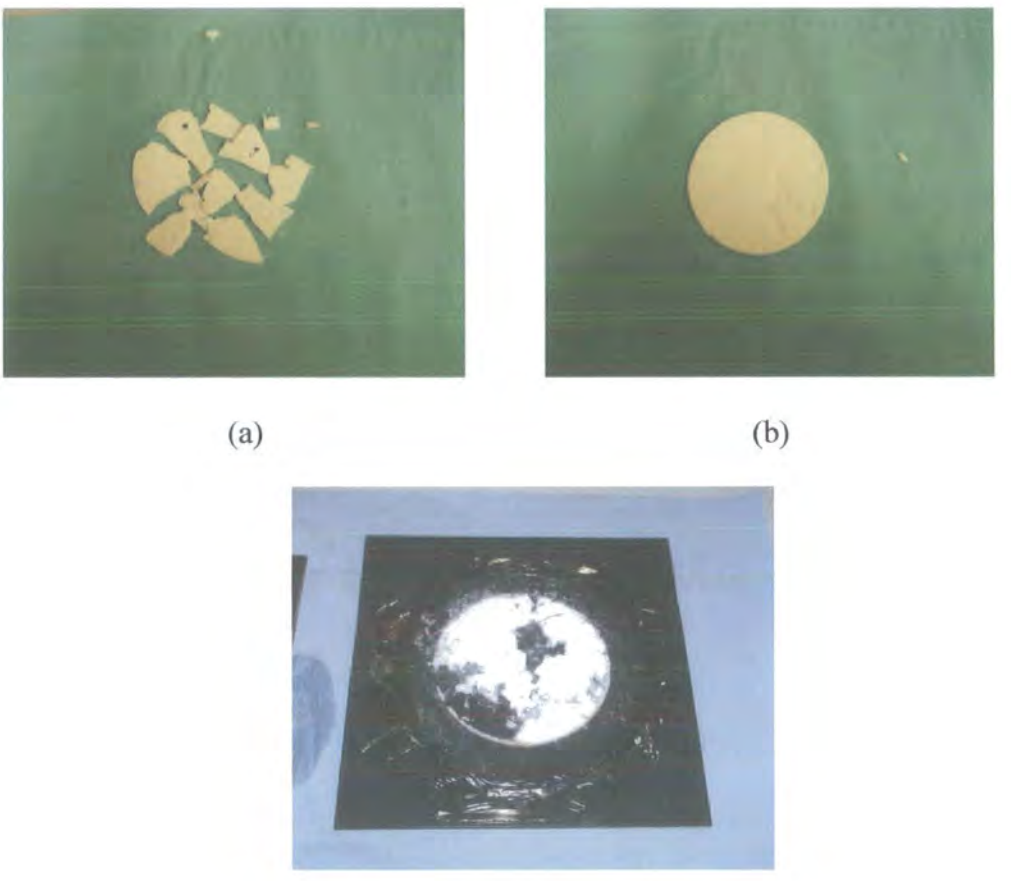

(a) (b)

(c)

Figure 2.4 *PolyHIPE materials produced from the PVC plate mould with different mould release agents, (a) PTFE spray, (b) Tygflor, (c) Span 80 wipe over.*

Table 2.3 provides the results and observations for the PE cylindrical mould.

The monolith formed using the original PE cylindrical mould was difficult to remove and shrinking of the PolyHIPE material also occurred. Increasing the polymerisation temperature had no considerable effect on the sample quality. Increasing the polymerisation temperature decreases the curing time and can allow less time for evaporation to occur. However there were pinholes present on the surface of the PolyHIPE material at a polymerisation temperature of 100 °C. This could be due to localised collapse of the emulsion caused by perturbation of the HIPE at elevated temperatures. The mould design was also causing problems during sample extraction. All of the cylindrical moulds were redesigned to allow easier sample extraction. The cylindrical moulds were all reproduced in two parts, which could be pulled apart after the HIPE had been cured.

Table 2.4 provides the results and observations for the PP cylindrical mould.

Table 2.4 Results and observations for the PP cylindrical mould

Mould release agent	Curing Time and Temperature	Sample Quality	Comments
None	60 °C for 24 hours	6	No shrinking and easily extracted
None	Room temperature for 24 hours 60 °C for 24 hours	4	Shrinking of PolyHIPE material
None	100 °C for 24 hours	3	Adherence to surface

The PolyHIPE material did not show any adherence problems with the PP surface except at higher curing temperatures. Noticeable shrinking of the PolyHIPE occurred, when the HIPE was left covered in the mould at room temperature for 24 hours prior to curing at 60 °C. Leaving more time for possible evaporation to occur produces a sample, smaller than the volume the HIPE occupied, in the mould.

Table 2.5-2.6 provide the results and observations that were recorded for all of the PTFE moulds.

Table 2.5 Results and observations for the PTFE 1 mould.

Lubricant	Curing time and temperature	Covered/uncovered	Sample Quality	Sample Height (mm)
None	60 °C for 24 hours	covered	9	22
None	60 °C for 24 hours	uncovered	9	18
None	Room temperature for 24 hours 60 °C for 24 hours	covered	8	17
None	Room temperature for 24 hours 60 °C for 24 hours	uncovered	8	8

Table 2.5 provides greater evidence for the possible evaporation of both the aqueous phase and the oil phase present in the HIPE. When PTFE 1 is not covered and the HIPE is left exposed to air, there is a reduction in size of PolyHIPE material obtained. There is also a reduction in height when the HIPE is left at room temperature for 24 hours and then cured at 60 °C for 24 hours compared to the HIPE, which is not left at room temperature beforehand. This is apparent for both the exposed and unexposed HIPE to air. There are then two factors to account for, the exposure of the HIPE to air and length of period taken for the HIPE to cure. The photographs in **figure 2.5 (a-c)** shows the different types of sample produced from PTFE 1.

Table 2.6 Results and observations for the PTFE 2 (bold) and PTFE 3 moulds.

Lubricant	Curing Time and Temperature	Sample Quality	Comments
None	**60 °C for 24 hours**	**10**	**No adherence, no holes on foam surface**
None	60 °C for 24 hours	10	No adherence, no holes on foam surface
None	Room temperature for 24 hours 60 °C for 24 hours	7	Solid foam, soft and gel like around edges
None	100 °C for 24 hours	8	Slight shrinking, yellow colouring observed on foam surface. Pin holes on surface

The results and observations for PTFE 2 (in bold) and PTFE 3 are shown in **table 2.6** above.

Both PTFE moulds produce uniform PolyHIPE materials at the standard curing temperature. At higher curing temperatures evaporation may still be a problem even though both of these moulds are sealed with a lid top, before they are placed in the oven. The yellow colouring on the PolyHIPE surface could possibly be due to surfactant oxidation at higher temperatures. The yellow colouring is not present at normal curing temperatures. At higher curing temperatures the stability of the emulsion may be adversely affected causing localised collapse of the emulsion and the presence of the pinholes on the surface of the PolyHIPE material.

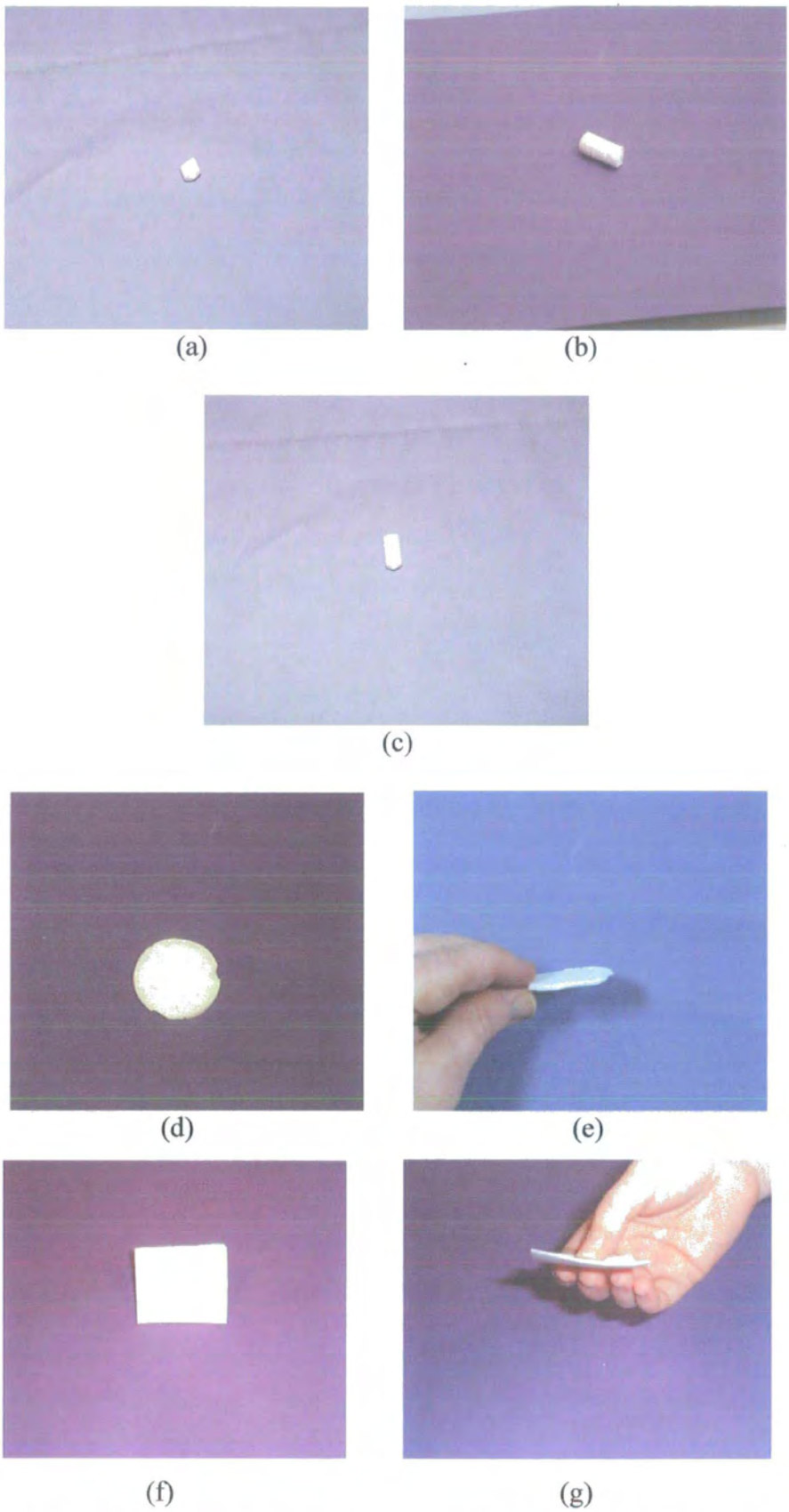

Figure 2.5 *Photographs of PolyHIPE materials from PTFE moulds: (a), (b) and (c) PTFE 1, (d) and (e) PTFE 2, (f) and (g) PTFE 3.*

When the HIPE is left at room temperature for 24 hours prior to curing, a PolyHIPE material of lesser quality is produced. Leaving the HIPE for this period of time before curing may give more time for coalescence and may account for the softer areas present on the PolyHIPE produced. **Figure 2.5 (d-e)** show photographs of materials produced from PTFE 2 and **figure 2.5 (f-g)** show photographs of the materials produced from PTFE 3.

2.3.2 Morphology of PolyHIPEs produced with different mould substrates

The images in **figure 2.6** represent the morphology of the PolyHIPE material prepared with the cylindrical PP mould.

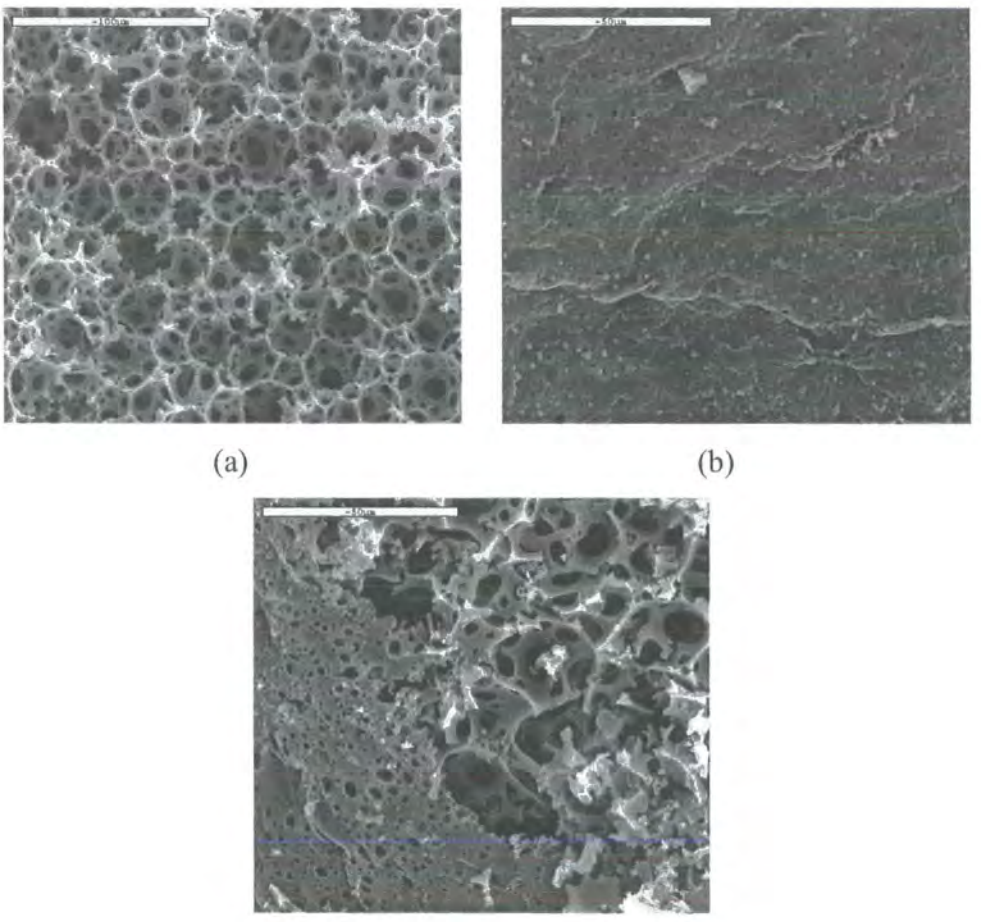

Figure 2.6 *SEM images of sample obtained from PP cylindrical mould: (a) fractured surface, (b) and (c) surface in contact with mould substrate.*

Figure 2.6 (a) shows the fractured surface of the PolyHIPE material. The morphology represents the normal porous, open-cellular structure of a PolyHIPE (**see figure 1.5**). **Figures 2.6 (b)** and **(c)** show the polymer surface in contact with the mould substrate. **Figure 2.6 (b)** shows a region of very low porosity (almost closed-cell) of the polymer surface in contact with the mould. This area may be representative of the sample surface, which is in contact with the mould surface. **Figure 2.6 (c)** shows an extension of this low porous area into a more porous region of the polymer. This region may be due to the small holes on the surface of the polymer, which may not have been in contact with the mould surface and therefore the structure has not been affected to the same extent. The porous region may represent a hole or indentation present on the PolyHIPE surface, which may have been due to trapped air pockets during polymerisation or localised collapse of the emulsion. The closed- cell region is presumably due to the presence of a surface film caused by localised collapse of the emulsion. Preferential wetting of the mould surface by either phase of the emulsion could cause phase separation; the resulting monomer film becomes a surface skin on polymerisation.

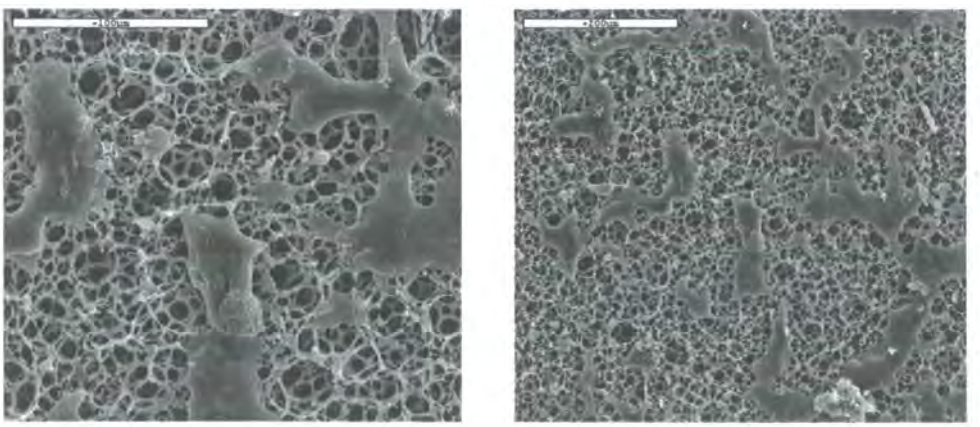

(a) (b)

Figure 2.7 *SEM images of PolyHIPE prepared with PTFE mould (3): (a) and (b) surface in contact with the mould substrate.*

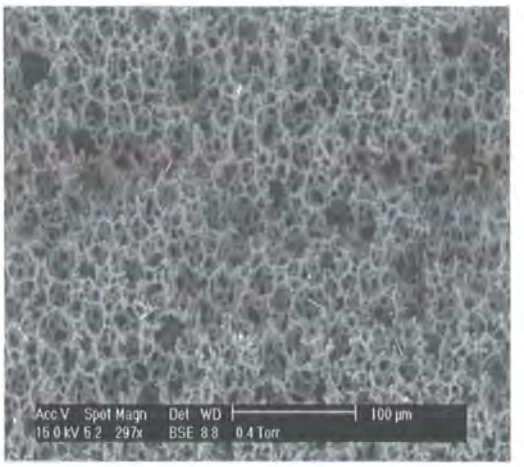

Figure 2.8 *ESEM image of the fractured surface of the PolyHIPE prepared with PTFE 3.*

Both SEMs in **figure 2.7** show the structure of the polymer surface in contact with the PTFE 3 mould. The images are of the same area of polymer but at two different magnifications. From the SEM images we can observe that the majority of the material has the normal porous open-cellular structure but again patches of non-porous structure are evident, due to the formation of a thin film forming over the normal porous structure. This film could be caused again by phase separation and the formation of a layer of separated monomer and surfactant caused by the stability of the HIPE rather than the hydrophobic/hydrophilic nature of the mould surface itself. **Figure 2.8** represents the fractured surface morphology of the material. The ESEM image in **figure 2.8** shows no evidence of the presence of non-porous regions in the fractured surface. The fractured surface of the material has a completely open-cell structure.

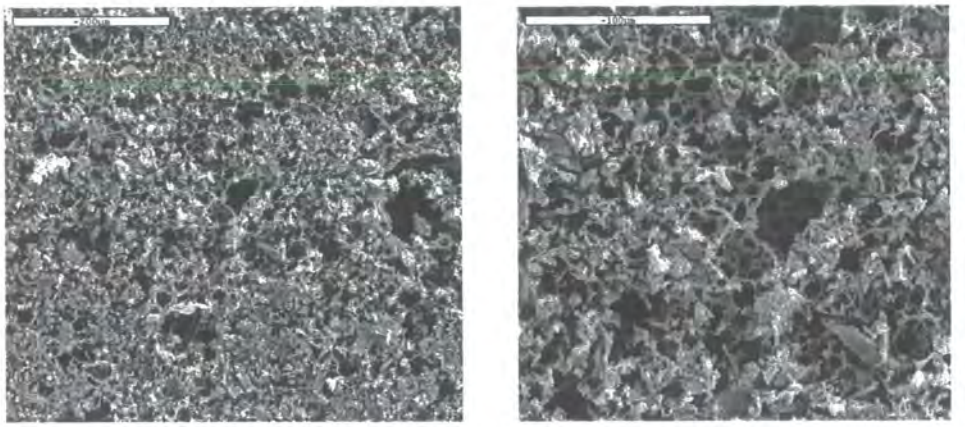

(a) (b)

Figure 2.9 *SEM images of the PolyHIPE obtained from glass mould with vacuum grease as release agent: (a) and (b) surface in contact with mould substrate.*

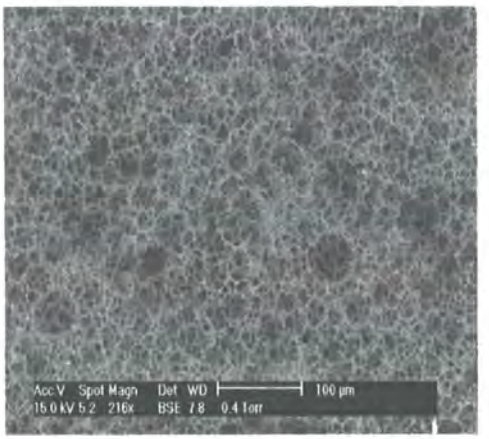

Figure 2.10 *ESEM image of the fractured surface of the PolyHIPE material prepared with the glass mould with vacuum grease as release agent.*

Figure 2.9 (a) and (b) shows SEM images of the polymer surface in contact with the glass surface coated with vacuum grease. Both are of the same area of polymer surface but again at different magnifications. From **Figure 2.9 (a)** it looks as if the porosity and the normal open-cellular structure has been altered at the surface in contact with the mould. At a higher magnification (**Figure 2.9 (b)**) the porous nature of the polymer at the surface and the open-cellular network which exists beyond the surface can be observed.

Figure 2.10 represents the morphology of the surface not in contact with the mould substrate (fractured surface). The ESEM image shows that the morphology of the fractured surface represents the normal open-cellular structure (**see figure 1.5**).

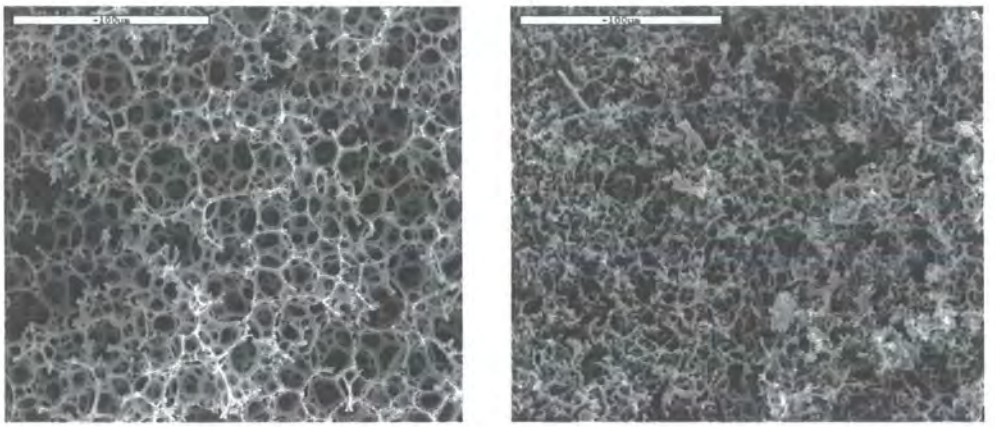

(a) (b)

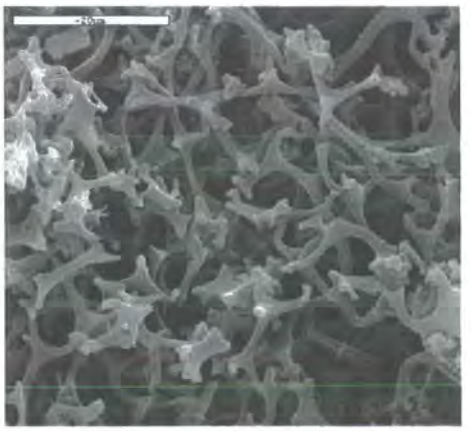

(c)

Figure 2.11 *SEM's of PolyHIPE obtained from PVC cylindrical mould; (a) fractured surface, (b) and (c) surface in contact with mould substrate.*

Figure 2.11 (a) shows the structure of the fractured surface of the polymer. This shows that the normal open cellular PolyHIPE structure is present at the fractured surface. **Figure 2.11 (b)** shows the polymer surface in contact with the PVC mould. This shows that the open-cellular network at the polymer surface has been altered, although there does still seem to be a porous structure to the surface. **Figure 2.11 (c)**

shows a higher magnification image of **figure 2.11 (b)**. This again shows the open cellular network at the polymer surface has been changed.

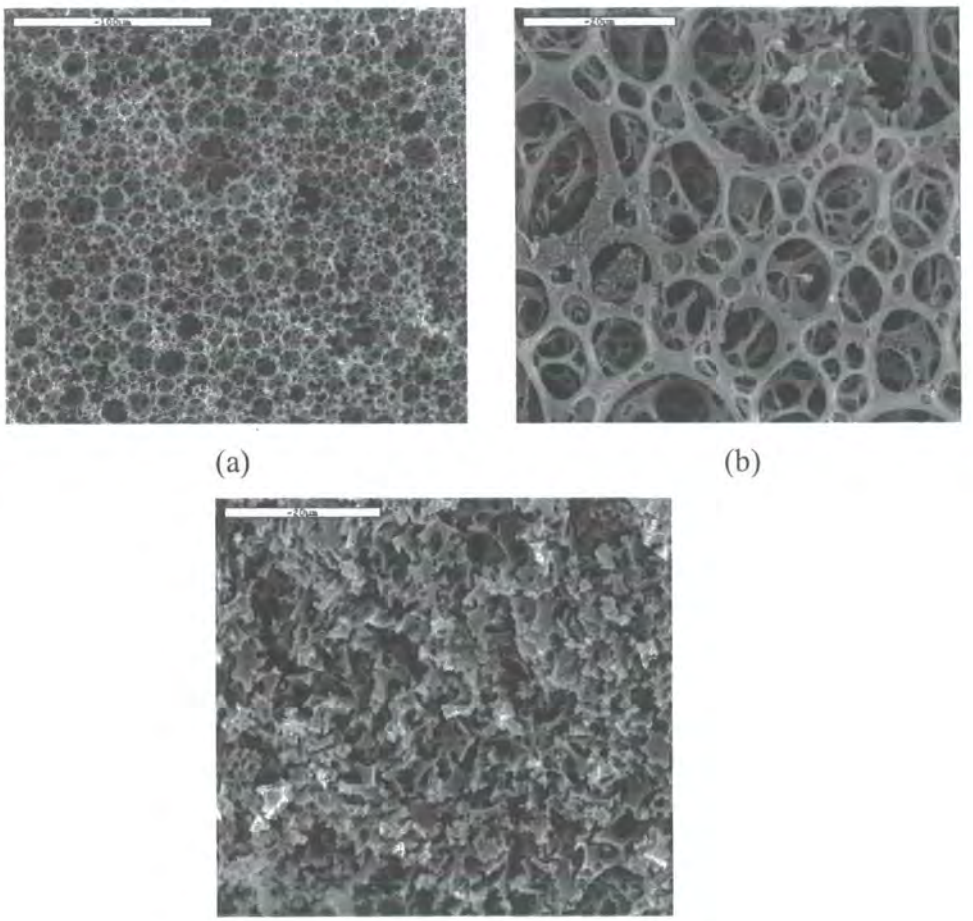

Figure 2.12 *SEM images of the PolyHIPE obtained from the PE cylindrical mould; (a) fractured surface, (b) and (c) surface in contact with mould substrate.*

Figure 2.12 (a) is a SEM image of the fractured surface of the PolyHIPE material prepared with the PE cylindrical mould. Again, as with the other cylindrical moulds, the fractured surface shows the normal porous, open-cellular structure of the PolyHIPE material. The other two SEM images show the structure of the polymer surface in contact with the PE mould. Two different areas were found on the polymer surface. **Figure 2.12 (c)** shows an area were the porosity and open-cellular structure has been altered at the surface. **Figure 2.12 (b)** shows an area on the surface where the open-cellular structure is still intact. **Figure 2.12 (b)** may correspond to the holes

that were present on the surface of the sample and may not have been in contact with the mould substrate during polymerisation.

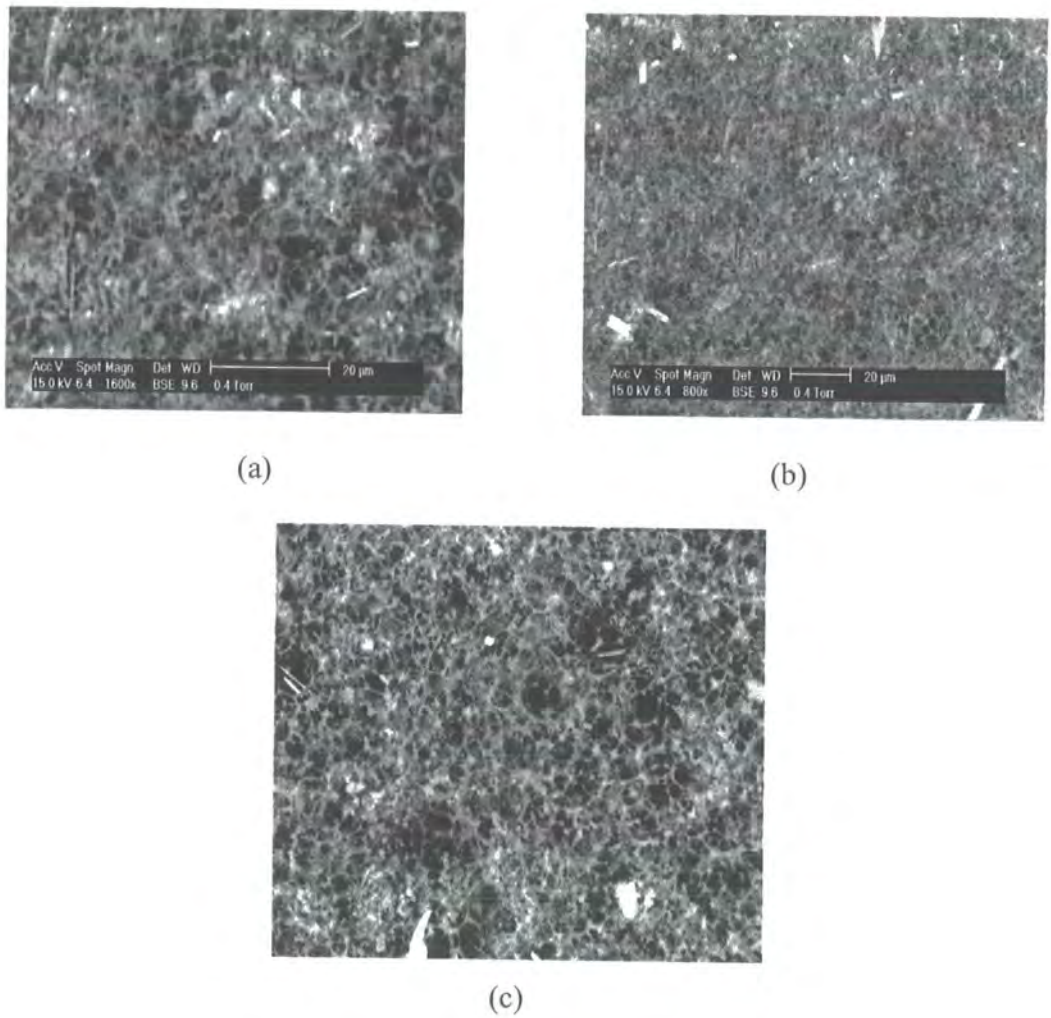

(a) (b)

(c)

Figure 2.13 *ESEM images of PolyHIPE material form PVC plate mould coated in Tygflor: (a) and (b) surface in contact with mould substrate, (c) fractured surface.*

Figure 2.13 (a) and **(b)** show the surface of the PolyHIPE in contact with the Tygflor substrate present on the plate PVC mould. The surface in contact with the Tygflor substrate is less open cell/porous than would normally be expected of normal PolyHIPE morphology. The morphology of the surface not in contact with the Tygflor (fractured surface) is shown in **figure 2.13 (c)**. This represents the normal morphology that is expected of a PolyHIPE material (**see figure 1.5**).

The results described so far are only partially in accord of those described by Akay et al. [155], who related the structure of the PolyHIPE foam materials to the solubility

parameter difference ($\Delta\delta$) between monomer and substrate. In their work it was found that polyethylene (which is similar to polypropylene) resulted in a closed-cell surface. They also found that the foam material adhered to the PE surface which was similar to our observations. They also found that a PVC mould surface lead to adhesion. In the case of glass ($\Delta\delta > 180$) gave rise to an open-cell structure, whereas PTFE ($\Delta\delta = -6.5$) resulted in a closed-cell surface whereas in the work discussed in this chapter the opposite was found. However there were patches of closed-cell structure observed when the PTFE mould was used. This discrepancy could be due the differences in composition or preparation of the emulsions used by Akay et al.

2.4 Conclusions

Based on the observations and the results from the materials produced from each mould substrate, it is clear that the PTFE substrate produces the PolyHIPE material with the greatest quality and uniformity. The PP, PE and glass substrates still produce materials but have a lower quality than is required. Evaporation and adherence also seem to pose problems to sample production. The recorded results from the mould PTFE 1 showed that when the mould was covered and the HIPE was not exposed to air, evaporation and sample reduction could be prevented. Therefore the airtight nature of the mould must also be taken into account when considering a design for large-scale production. Adherence of the PolyHIPE proved a problem at higher curing temperatures with the flat glass mould. Coating the plates with vacuum grease and PTFE spray reduced the adherence to the glass mould. During the SEM and ESEM study the images showed that the porosity and open-cell nature of the surface in contact with the mould is reduced compared to the fractured surfaces. This does not cause a problem for the sample uniformity or quality but may affect the fluid transport properties of the material. PVC is the cheapest mould material available and cost must also be taken into account when moulding the PolyHIPE materials on a

larger scale. It proved difficult to produce suitable PolyHIPE materials from the PVC substrate alone, but when the PVC was coated with a PTFE spray or the PTFE substrate Tygflor, good quality materials could be produced, with the Tygflor coated PVC producing the better of the two. PTFE is one of the most expensive materials and the cost proved too high to produce a mould of suitable size for large-scale production from PTFE alone. A possible mould made from PVC which is coated with PTFE spray or Tygflor to reduce the affect of the PVC on sample quality was deemed to be the best way forward for the next section of the work.

Chapter 3

The reinforcement of PolyHIPE materials by the addition of active fillers to the monomer phase

3.1 Introduction

Active fillers (reinforcing materials) improve certain, but generally not all mechanical properties. A considerable reinforcement requires compatibility between the filler and the polymer matrix. Conventional fillers for polymers can range from fibres, which have already been discussed in **chapter 1**, to the widely used inorganic materials such as clays, micas and kaolins. The dispersion of clay layers in a polymer can optimise the reinforcing modes for carrying applied loads and also deflecting cracks [111]. The combination of the high surface area of the clay and the polymer matrix facilitates transfer to the reinforcement phase allowing for tensile and toughening improvements. Clay nanolayers are generally used as reinforcers in epoxy resins to produce epoxy-clay nanocomposites [112], [113]. To achieve exfoliation, the clay gallery

is first loaded with onium ions and then the layers are expanded by diffusing in the epoxide and then curing. Lan et al [112] showed by the addition of 7.5 vol % of exfoliated silicate layers the strength of the elastomeric epoxy matrix increased by more than 10-fold. More recent work on a glassy epoxy matrix [113] showed that the clay nanolayers reinforce the glassy epoxy matrix under a compressive strain (**see figure 3.1**).

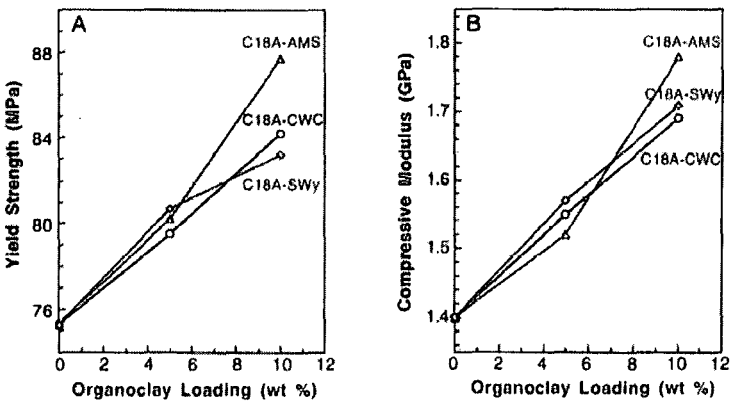

Figure 3.1 *Compressive (A) yield strength and (B) moduli for the epoxy polymer and the exfoliated epoxy-clay nanocomposites with three different kinds of organmontmorillonites* [111], [113].

They have also been used to produce polyurethane composites, polypropylene and polyimide hybrids. Wang et al. [114] reported that in situ polymerisation of a polyol-isocyanate precursor with the clay nanolayers produced a nanocomposite with greater strength and toughness compared to the homopolymer (**see figure 3.2**).

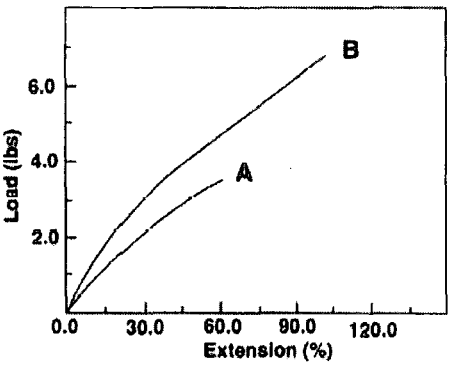

Figure 3.2 *Stress-strain curves for (A) a pristine polyurethane polymer and (B) a polyurethane-clay nanocomposite* [111], [114].

The addition of rubber to a polymer matrix can also be an effective way to mechanically toughen a polymer. Kinloch et al. [115], [116], [117] have carried out studies on the mechanical behaviour of rubber toughened epoxy resins. They showed that a two phase microstructure existed, consisting of small rubber particles (0.5-3 μm) dispersed in and bonded to the epoxy matrix. They discussed several previously proposed toughening mechanisms. They suggested that as the crack advances around the rubber particles, the crack opens and the rubber particles are stretched and must eventually tear before the crack can progress. The energy required to stretch these particles is responsible for the higher fracture toughness. The formation of crazes at stress concentrations around the rubber particle was also reported to act as a toughening mechanism; however during their work they did not find any evidence of crazing or any other void formation within the unmodified epoxy matrix. They also suggest that plastic flow in the epoxy matrix during yielding may produce deformations, which might contribute significantly to the toughening mechanism. Their proposed mechanisms [116] concluded that yielding and plastic flow of the matrix was the primary source of energy dissipation during fracture. A secondary source of energy dissipation was the initiation and growth of voids within the rubber particles or at the particle matrix interface.

High Impact Polystyrene (HIPS) also has structure characterised by rubber particles embedded in a PS matrix [118]. HIPS production is via the polymerisation of styrene containing dissolved polybutadiene (PB). It is a blend of polystyrene (PS) and a graft copolymer of butadiene and styrene, and displays a characteristic "salami" morphology of graft copolymer embedded in a matrix of polystyrene (**see figure 3.3**). These elastomeric domains account for the high impact strength of the material, by nucleating a large number of crazes, leading to a large volume of plastic deformation being formed before failure [119].

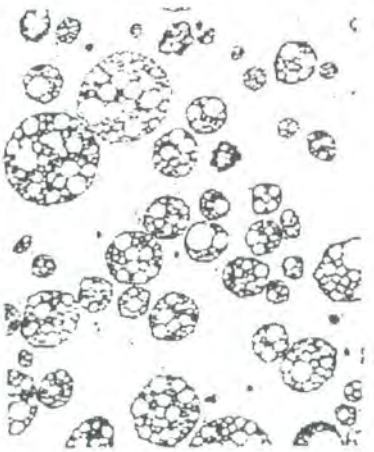

Figure 3.3 *"Salami" phase structures of commercial HIPS* [118].

This section of the work will detail both the small-scale and large-scale preparation of styrene/DVB based PolyHIPE materials containing active fillers, which have been dissolved or dispersed in the monomer phase prior to HIPE formation. The small-scale preparation will provide information on compatibility of the filler material with the polymer matrix. The problems of large-scale sample preparation for mechanical testing will also be detailed.

3.2 Experimental

3.2.1 Materials

Oil Phase

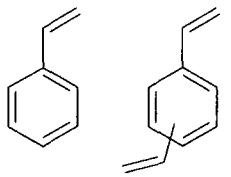

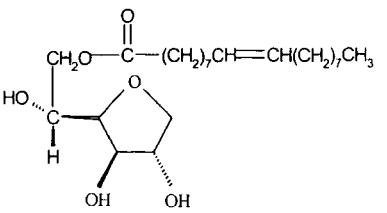

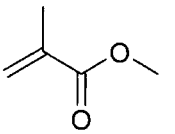

Styrene (99 %) Divinylbenzene (80 %) Sorbitan Monooleate (Span 80) Methyl Methacrylate (99 %)

Aqueous Phase

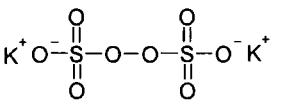

De ionised water Calcium Chloride dehydrate (99 + %)

Potassium Persulfate (99 + %)

Figure 3.4 *Materials used for HIPE preparation.*

All of the monomers used were purified prior to HIPE preparation, by passing through a column of base activated aluminium oxide. Aldrich chemicals supplied all of the chemicals used in **figure 3.4** excluding the de-ionised water. The fibres were obtained from Wrigley's fibres. Nanoclay and Prolabo supplied the clay (Cloisite ®Na^+) and silica gel particles (particle size 35-75 μm). The aluminium particles (size distribution unknown) were obtained from Qinetiq. The polybutadiene (M_w = 420, 000) and polyethylene oxide (M_w = 100,000) used were obtained from Aldrich Chemicals.

3.2.2 Instrumentation and characterisation

The morphologies of the PolyHIPE materials produced in this chapter were characterised using the instrumentation described in **2.2.2**. The thermo-gravimetric

analyses traces were performed with a Perkin-Elmer Pyris 1 TGA. The X-ray diffraction data were obtained from a Siemens D5000 Diffractometer.

3.2.3 Preparation of fibre-reinforced styrene/DVB PolyHIPE materials

3.2.3.1 Small-scale preparation

Table 3.1 provides the length and thickness of each fibre used.

Table 3.1 Fibre length and thickness

Fibre	Length (mm)	Thickness (μm)
Kevlar	1	15
PP	1	15
Viscose	1	12

The monomer phase (5 g) was made up of styrene (4.38 g, 42.07 mmol) and divinylbenzene 80 % (0.63 g, 4.08 mmol) and to this was added 5 % w/w of fibre and Span 80 (1g, 2.33 mmol). The HIPE was then prepared as in **2.2.3**. The HIPE was then transferred into a 100 ml Polyethylene bottle and left to cross-link in the oven at 60 °C for 24-48 hours. The PolyHIPE, which had formed, was then cut away from the Polyethylene bottle and extracted and dried as in **2.2.3**. Each experiment was carried out only once, unless complete separation of the HIPE occurred and in this case the experiment was carried out until a PolyHIPE material was obtained.

3.2.3.2 Large-scale preparation (90 % internal phase volume)

The monomer phase (300 g) was made up of styrene (262.5 g, 2.52 mol) and divinylbenzene 80 % (37.5 g, 0.29 mol) and to this were added Span 80 (60 g, 0.14 mol) and 2.5 % - 10 % w/w fibre. This mixture was then placed in a 3000-ml beaker. The aqueous phase (2700 ml) contained 2700 g de-ionised water, potassium persulfate (5.99 g, 22.18 mmol) and calcium chloride dihydrate (30.02 g, 0.20 mol). Both the monomer and aqueous phase were purged with nitrogen for ten minutes. The

aqueous phase was then added over a one-hour period using a separating funnel. The HIPE was continuously stirred using a metal stirrer with two impellers connected to an overhead stirrer motor for four hours. The HIPE was then transferred into a large PVC mould (height- 100 mm, length- 350 mm, breadth – 250 mm), which had previously been coated with PTFE spray. The HIPE was polymerised in the oven at 60°C for 48 hours. After polymerisation, the polymer block was cut into five separate bars for three point bend tests (350 mm x 25 mm x 50 mm). The five PolyHIPE bars were then dried in a convection oven until constant weight was obtained. **Figure 3.5** shows photographs of experimental set-up and mould used. Each experiment was carried out only once, unless complete separation of the HIPE occurred and in this case the experiment was carried out until a PolyHIPE material was obtained.

Figure 3.5 *Photographs of experimental set-up and mould used in the preparation of samples for mechanical testing.*

3.2.4 Addition of aluminium particles to monomer phase

The monomer phase (5 g) was made up of styrene (4.38 g, 42.07 mmol) and divinylbenzene 80 % (0.63 g, 4.08 mmol) and to this mixture were added 5 % w/w aluminium particles and varying amounts of Span 80 (1g, 2.33 mmol). The HIPE was then prepared as in **2.2.3**. The HIPE was then transferred into a 100 ml polyethylene bottle and cured in an oven at 60 °C for 24-48 hours. The PolyHIPE, which had

formed, was then cut away from the polyethylene bottle and extracted, cleaned and dried as in **2.2.3**. Each experiment was carried out only once, unless complete separation of the HIPE occurred and in this case the experiment was carried out until a PolyHIPE material was obtained.

3.2.5 Addition of silica gel particles to monomer phase

The monomer phase (5 g) was made up of styrene (4.38 g, 42.07 mmol) and divinylbenzene (0.63 g, 4.08 mmol) and to this mixture were added 5 % (w/w) silica gel particles (particle size 35-75 μm) and the surfactant Span 80 (1g, 2.33 mmol). The HIPE was then prepared as in **2.2.3.** The HIPE was then transferred into a 100 ml polyethylene bottle and cured in an oven at 60 °C for 24-48 hours. The PolyHIPE, which had formed, was then cut away from the polyethylene bottle and extracted, cleaned and dried as in **2.2.3**. Each experiment was carried out only once, unless complete separation of the HIPE occurred and in this case the experiment was carried out until a PolyHIPE material was obtained.

3.2.6 Addition of polybutadiene to monomer phase

The monomer phase (5 g) was made up of styrene (4.38 g, 42.07 mmol) and divinylbenzene (0.625 g, 4.08 mmol) and to this was added 2.5 % - 7.5 w/w of polybutadiene (PB) (M_w 420, 000) and varying amounts of Span 80. The PB/styrene mix was left for a period of time under stirring to allow time until the PB had dissolved. Once this time had elapsed, the Span 80 and the divinylbenzene were added. The HIPE was then formed as in **2.2.3**. The HIPE was then transferred into a 100 ml polyethylene bottle and left to cross link in the oven at 60°C for 24-48 hours. The PolyHIPE, which had formed, was then cut away from the Polyethylene bottle and extracted and dried as in **2.2.3**. Each experiment was carried out only once, unless complete separation of the HIPE occurred and in this case the experiment was carried out until a PolyHIPE material was obtained.

3.2.7 Addition of clay/intercalated clay to monomer phase

The clay/ Na montmorillonite melt intercalation with polyethylene oxide (PEO) was carried out as described by Vaia et al. [120]. The intercalation of the PEO with layered silicate material is achieved by heating the polymer with the host at 80 °C. The PEO (M_w = 100,000) (0.28 g) and Na^+-montmorillonite (0.72 g) were thoroughly mixed together in a mortar dish and heated to 80 °C. The intercalated clay (1 g, 5 % w/w) was added to a mixture of styrene (9 g, 86.41 mmol), divinylbenzene (1 g, 7.68 mmol) and the surfactant Span 80 (2 g, 4.66 mmol). The aqueous phase consisted of de-ionised water (90 g), potassium persulfate (0.2 g, 0.74 mmol) and calcium chloride dihydrate (1 g, 6.80 mmol). The HIPE was then prepared as in **2.2.3**. The PolyHIPE material that was produced was cleaned and dried as previously described in **2.2.3**.

The non-intercalated clay (0.1 g) was dispersed into a mixture of styrene (5 g, 48 mmol), divinylbenzene 80 % (1 g, 7.68 mmol), methyl methacrylate (4 g, 39.96 mmol) and Span 80 (2 g, 4.66 mmol). The aqueous phase consisted of de-ionised water (90 g), potassium persulfate (0.2 g, 0.74 mmol) and calcium chloride dihydrate (1 g, 6.8 mmol). The HIPE was then prepared as in **2.2.3**. After placing the HIPE into a polyethylene bottle, the HIPE was then cured at 80 °C in a convection oven for 24 hours. The PolyHIPE material was then cleaned and dried as in **2.2.3**. Each experiment was carried out only once, unless complete separation of the HIPE occurred and in this case the experiment was carried out until a PolyHIPE material was obtained.

3.3 Results and discussion

3.3.1 Addition of fibres to monomer phase

3.3.1.1 Stability and morphology

The small-scale production of the fibre reinforced PolyHIPE materials provided information on both the stability of the HIPE with the fibres present and the morphology of the fibre-reinforced PolyHIPE material. With a loading of 5 % w/w of monomer phase of each fibre, it was possible to form a stable HIPE that produced a uniform fibre-reinforced material after curing. The morphology of the fractured surface of the Kevlar-reinforced material is shown in **figure 3.6**.

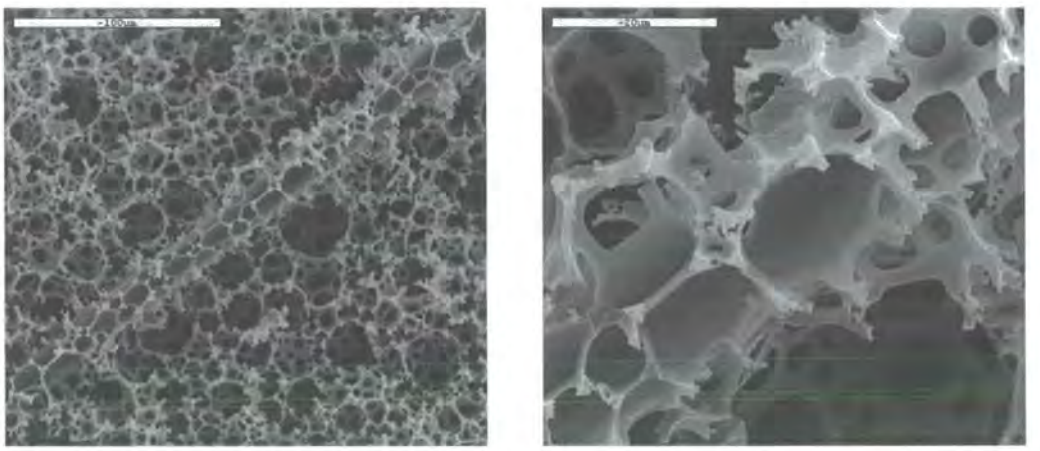

(a) (b)

Figure 3.6 *Morphology of Kevlar-reinforced PolyHIPE material.*

From **figure 3.6** it is shown that the presence of the Kevlar fibre at a loading of 5 % w/w has no effect on the stability or the morphology of the PolyHIPE material produced. The morphology of the fibre-free S/DVB PolyHIPE material is shown in **figure 1.5**. **Figure 3.6 (b)** provides a higher magnification image, which shows the compatibility of the Kevlar fibre with the polymer matrix. After fracture the cellular matrix has remained attached to the fibre surface. For a fibre or any filler material present to provide any significant mechanical enhancement to the material, the filler

must bond strongly with the polymer matrix. The morphology of the fractured surface of the PP-reinforced material is shown in **figure 3.5**.

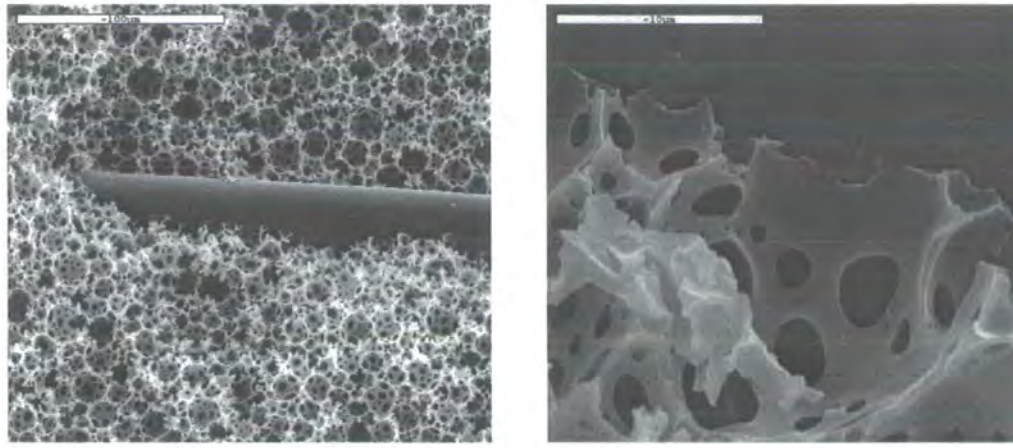

(a) (b)

Figure 3.7 *Morphology of the PP- reinforced PolyHIPE material.*

The morphology of the PolyHIPE material has not been affected by the presence of the PP fibre. **Figure 3.7 (b)** provides a higher magnification image and shows that the PP fibre is not bonded as strongly to the PolyHIPE matrix as in the case for the Kevlar fibre. The cellular structure is easily removed from the surface of the PP fibre. The morphology of the viscose reinforced PolyHIPE material is shown in **figure 3.8**.

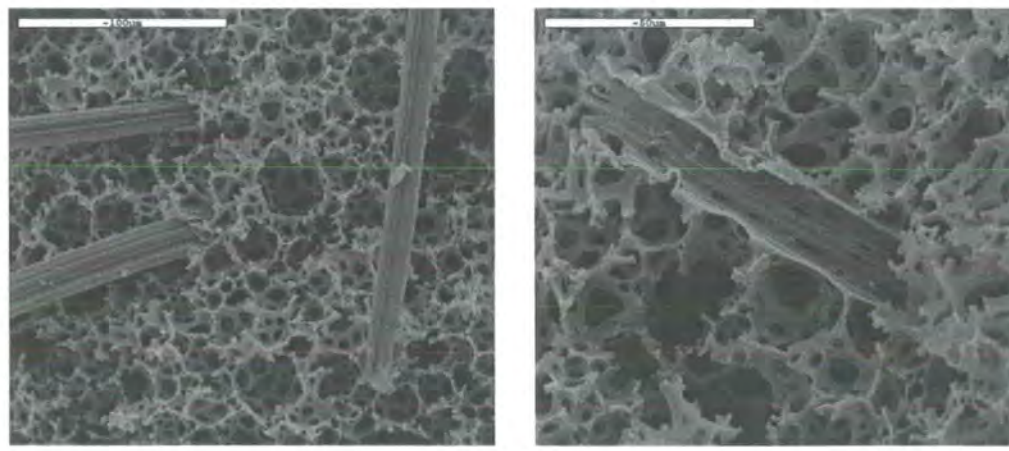

(a) (b)

Figure 3.8 *Morphology of viscose-reinforced PolyHIPE material*

From **figure 3.8** it can be shown that the viscose fibres do not bond strongly with the PolyHIPE matrix. The SEM image on the right shows an area of PolyHIPE, where a

fibre was present but was then ripped away from the PolyHIPE structure during fracture. Dyer et al. [80] explained that fibres of a hydrophilic nature, such as those that contain polar groups, would induce coalescence in the HIPE in the region around the fibre resulting in poor adhesion between the foam and the fibre. Phase separation may occur at the interface between the hydrophilic surface of the fibre and the HIPE. This would result in a layer of water forming at the fibre surface and therefore poor interconnectivity between the fibre and the PolyHIPE structure. In the patent, they claim that fibres which are compatible with the HIPE will lack polar groups and have a critical surface tension between about 15 and 50 dynes/cm, more preferably between 20 and 40 dynes/cm. They list polypropylene and aramid fibres as HIPE compatible, but fibres comprising of cellulose and polyacrylates as non-compatible fibres.

3.3.1.2 Production and processing problems

Although the observations and results from the small-scale preparation experiments provided enough conclusive information to proceed with the large-scale preparation, the scale up of production did encounter problems. The fibre loading levels within the sample are important but are difficult to assess due to fibre movement caused by buoyant forces during curing. This results in a fibre rich outer layer of PolyHIPE material. An example of this is shown in **figure 3.9**. Some areas of the PolyHIPE may also be more fibre-dense than others due to clumping together of fibres or inefficient mixing (**see figure 3.9 (b)**). The dispersion of a high loading of viscose fibres (10 % w/w) did not result in HIPE formation. This was probably due to the hydrophilic nature of the fibre affecting HIPE stability. Therefore no 10 % w/w viscose-reinforced PolyHIPE material could be produced.

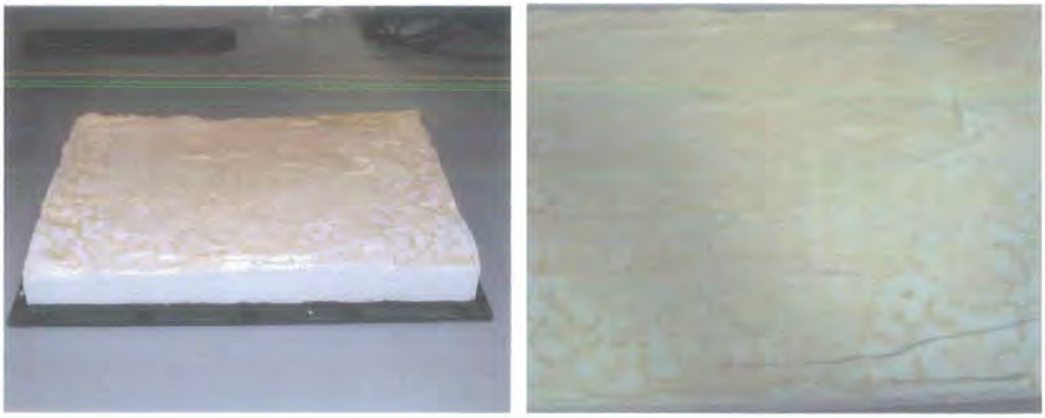

(a) (b)

Figure 3.9 *Pictures of large-scale PolyHIPE material showing Kevlar fibre rich outer layer.*

After the work carried out in **chapter 2**, it had been decided to proceed with a PTFE spray coated PVC mould for the large-scale production. After repeated production of material, sample reproducibility and uniformity started to become a problem. The PolyHIPE materials were found to be soft on the surface in contact with the mould and shrinking from the sides of the mould was becoming apparent. The continued use of the PVC mould could possibly allow time for the plasticisers present in the material to leach out form the PVC affecting the sample uniformity after continued use.

Due to the problems obtained with sample reproducibility, it was decided to change the large-scale set-up for production by replacing the glass beaker with a 4L PE container and the PVC mould with a PP container of similar size **(see figure 3.10)**.

Figure 3.10 *Picture of new large-scale set-up.*

The new large-scale set-up removed most of the processing and production problems that had occurred previously, but did not eradicate the formation of the fibre rich layer present at the outer layer of the PolyHIPE.

3.3.1.3 Sample drying problems

After small-scale preparation, the fibre-reinforced PolyHIPE materials were dried *in vacuo* after cleaning. This was not the case for the large-scale samples, due to the size of the beams produced. The beams were placed in the convection oven, without cleaning, to remove the water present. This in itself produced its own problems due to the large amount of water present within the five sample beams produced. The evaporation and condensation of water vapour on the thermocouple present inside the oven caused overheating, resulting in a fire hazard and sample destruction. The result was to dry each of the five sample beams separately, decreasing the amount of water vapour present within the oven. Even though this reduced the fire hazard and sample destruction, it proved time consuming and increased production time drastically.

3.3.1.4 Determination of fibre loading

As mentioned previously the top surface of the PolyHIPE is inclined to be fibre rich, compared to the centre of the foam due to buoyancy forces. Therefore, the actual weight percent of fibre added to the monomer phase may be an overestimation of the

actual amount in the middle of the foam. As the fibre volume within the polymer is an important factor in optimising the properties of the fibre-reinforced material (**see chapter 1**), it was desirable that an analytical method could be devised to determine a more accurate amount of fibre within the middle of the foam.

3.3.1.4.1 Thermo-gravimetric analyis (TGA)

The samples were heated from 30 °C to 800 °C (10 °Cmin^{-1}) under nitrogen, and the weight loss as the temperature was increased was recorded. The three fibre-reinforced samples as well as PolyHIPE without added fibres as a baseline, were analysed to try and evaluate the weight fraction of fibre incorporated into the PolyHIPE. **Figure 3.11** provides the TGA traces for the three fibre-reinforced samples and the PolyHIPE with no fibres present (Normal).

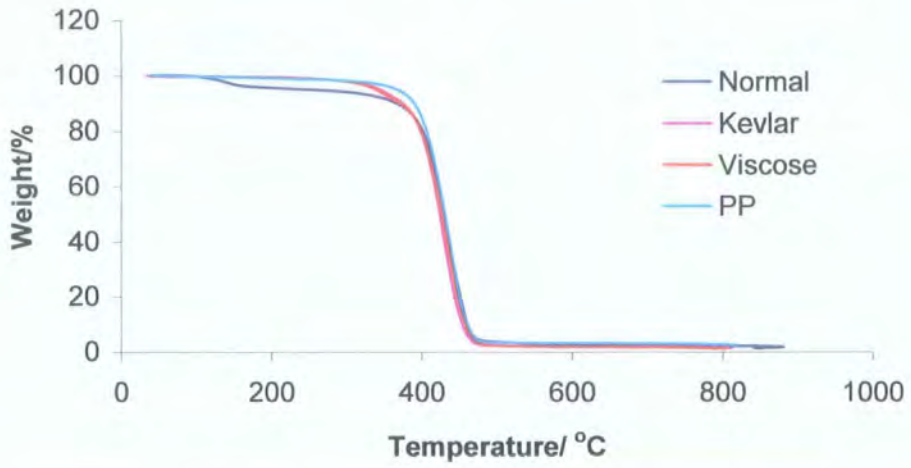

Figure 3.11 *TGA traces of fibre-reinforced and normal PolyHIPE material.*

The TGA traces show no significant differences between the PolyHIPE without fibres and the fibre-reinforced materials. Some of the fibre-reinforced materials have a lower residual weight compared to the fibre-free (normal) PolyHIPE material where it would expected to be higher. The presence of the fibres does not seem to have a

significant effect on the thermal properties of the composite also. There is no drastic change in the decomposition temperature with the addition of the fibres.

3.3.1.4.2 Elemental analysis

Due to the lack of success with the TGA results, elemental analysis was performed on the PolyHIPE samples and the fibres themselves to produce a reliable calculation for the weight percent of fibres present within the foam. Originally it looked as if this would work best for the Kevlar-toughened sample due to the significant difference in nitrogen content between the normal PolyHIPE and the Kevlar-reinforced PolyHIPE. **Table 3.2** shows the elemental analysis results for the Kevlar fibres themselves.

Table 3.2 Elemental analysis results for the Kevlar fibres

Element	Theoretical (%)	Experimental (%)
C	70.6	66.71
H	4.2	4.17
N	11.8	11.19

There is a considerable deviation from the theoretical and the experimental results. The biggest difference is found with to the % C result. This difference could be due to moisture adsorbed by the Kevlar fibres. **Table 3.3** shows the theoretical and experimental results for the S/DVB PolyHIPE

Table 3.3 Elemental analysis results for the S/DVB PolyHIPE

Element	Theoretical (%)	Experimental (%)
C	92.3	88.97
H	7.7	7.8
N	/	/

There is a deviation between the theoretical and the experimental % C results. This again could to be due to moisture or residual salt content within the material.

Table 3.4 shows the calculated and theoretical results for the S/DVB PolyHIPE material reinforced with 5 % w/w Kevlar fibres.

Table 3.4 Elemental analysis results for the S/DVB PolyHIPE reinforced with 5 % w/w Kevlar fibres

Element	Theoretical (%)	Experimental (%)
C	91.2	89.85
H	7.5	7.71
N	0.6	0.38

From the elemental analysis results the percentage of Kevlar fibres added to the HIPE that were present in the PolyHIPE sample could be approximated. The value is calculated as shown in **equation 3.1**.

$$\% \, Kevlar = \frac{\% \, theoretical \, N - \% \, experimental \, N}{\% \, theoretical \, N} \qquad \textbf{Equation 3.1}$$

The percentage of Kevlar fibres added to the monomer phase that were incorporated into the PolyHIPE was calculated to be 63 %. Thus, the value of Kevlar fibres existing in the fibre rich outer can be approximately said to be 37 % of the total fibre weight added.

This same method was used to determine the percent loading of PP fibres in the PolyHIPE material.

Table 3.5 Elemental analysis results for the S/DVB PolyHIPE reinforced with 5 % w/w PP fibres

Element	Theoretical (%)	Experimental (%)
C	91.97	88.72
H	8.03	7.73
N	\	\

The differences in the theoretical and experimental % C and % H values, for both the normal PolyHIPE and the fibre reinforced PolyHIPE, made the calculation for the % PP fibre loading difficult and inaccurate. From the theoretical calculations, the addition of 5 % w/w PP fibres should result in a decrease in % C and an increase % H. The actual experimental results obtained do show a decrease in % C but no increase in the % H. Therefore it was not possible to obtain a value for the % PP fibre loading using the % H values. The use of the decrease in % C provided a value for the % fibre loading, but the accuracy of the value was questioned due to the discrepancies in the theoretical and experimental % C and % H values. The value for the % PP fibre loading is calculated from the % H as shown in **equation 3.2**.

$$\%\ PP = \frac{(\%\ T\ (PP) - \%\ T\ (normal)) - (\%\ E\ (PP) - \%\ E\ (normal))}{(\%\ T\ (PP) - \%\ T\ (normal))}$$ **Equation 3.2**

Where T = theoretical % H and E = experimental % H

The value calculated for the percent loading of PP fibre added was 76 %, with the other 24 % possibly remaining in the fibre-rich outer layer or in the HIPE not removed from container. This value is higher than the percent Kevlar fibre loading, but is subject to considerable uncertainty due to the factors mentioned earlier.

3.3.2 Addition of aluminium particles to monomer phase

The addition of the aluminium particles (5 % w/w of monomer phase) did not have any detrimental effect on the production of a solid polymer monolith, which was silver in colour. **Figure 3.12** provides a picture of the PolyHIPE material produced with the aluminium particles.

Figure 3.12 *Photograph of the aluminium PolyHIPE composite.*

Figure 3.13 provides SEM/ESEM pictures of the fractured surface of the aluminium composite.

Figure 3.13 (a) and (b) are SEM images taken at the Materials Science Unit at Newcastle University, using the BSED (Back Scattering Emission Detector). The BSED allows the aluminium particles present within the structure to become visible. The area circled in blue underwent X-ray analysis to confirm the presence of aluminium particles. The X-ray data are shown in **figure 3.14**.

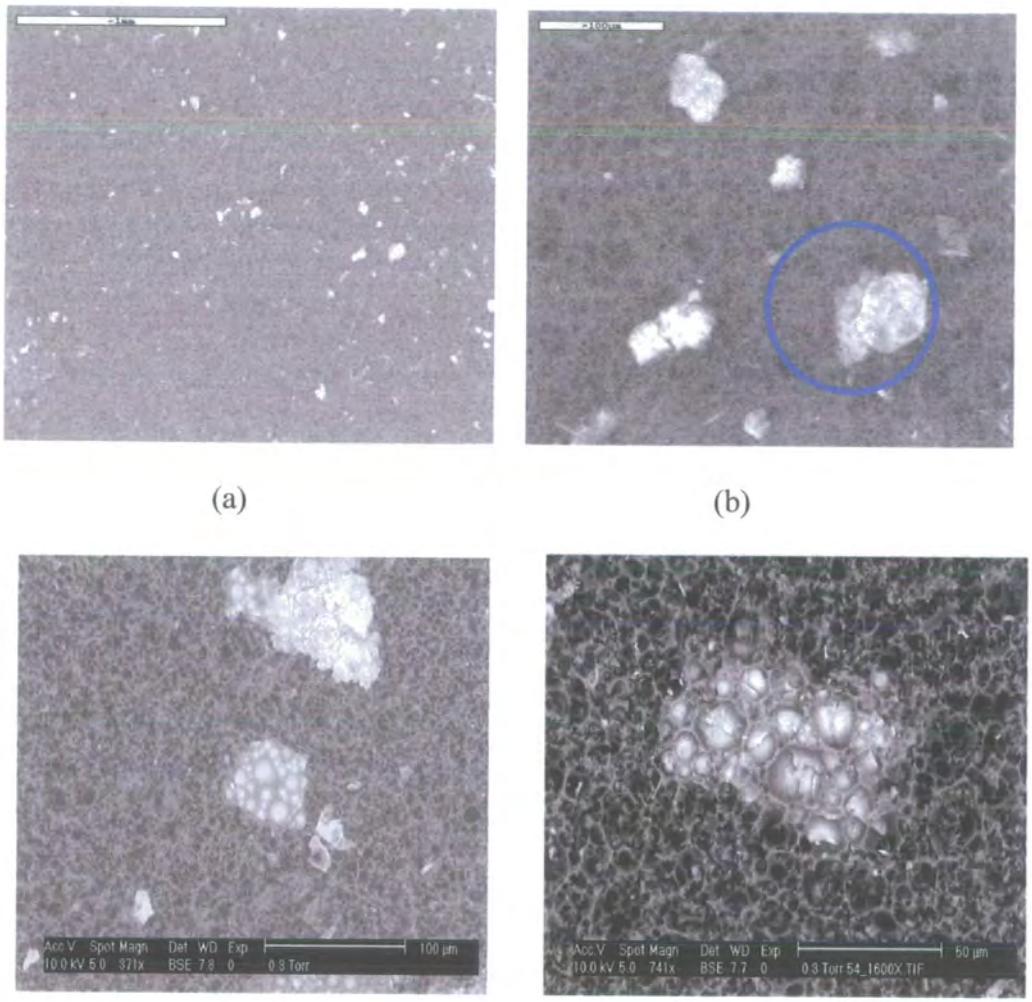

Figure 3.13 *SEM/ESEM images of the fractured surface of the aluminium PolyHIPE material: (a) and (b) SEM images, (c) and (d) ESEM images.*

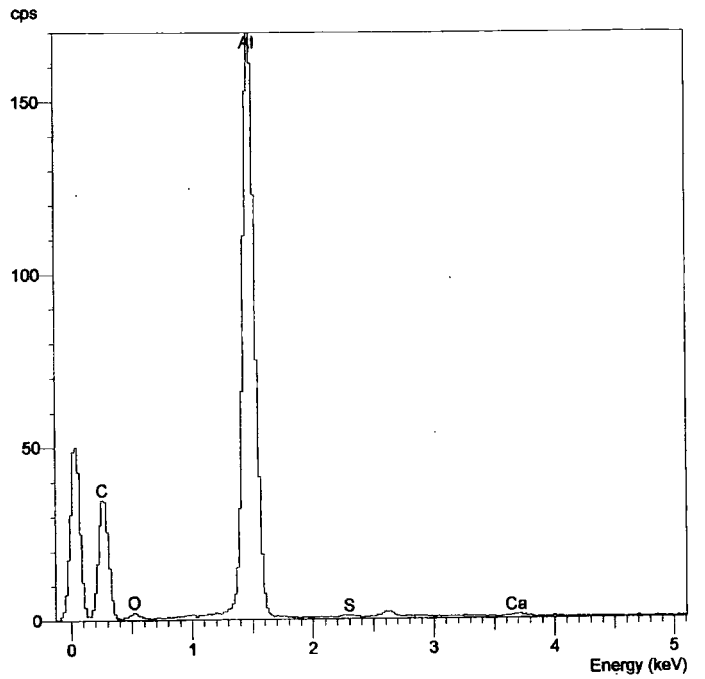

Figure 3.14 *X- ray analysis of the aluminium PolyHIPE composite.*

The X-ray data confirmed the presence of aluminium in the area circled. In **figure 3.13 (c)** and **(d)** the bonding of the aluminium surface to the PolyHIPE structure can be observed. **Figure 3.13(d)** is a higher magnification image of an aluminium particle present in the PolyHIPE material. This shows that the aluminium particle has bonded strongly to the PolyHIPE structure. After fracture, the cellular structure of the PolyHIPE is still present on the aluminium surface.

3.3.3 Addition of silica gel particles to monomer phase

The addition of the silica gel particles at a loading of 5 % w/w of monomer phase did not have any detrimental effect on HIPE stability or on the formation of a solid polymer monolith. **Figure 3.15 and 3.16** shows ESEM images of the fractured surface of the silica gel composite.

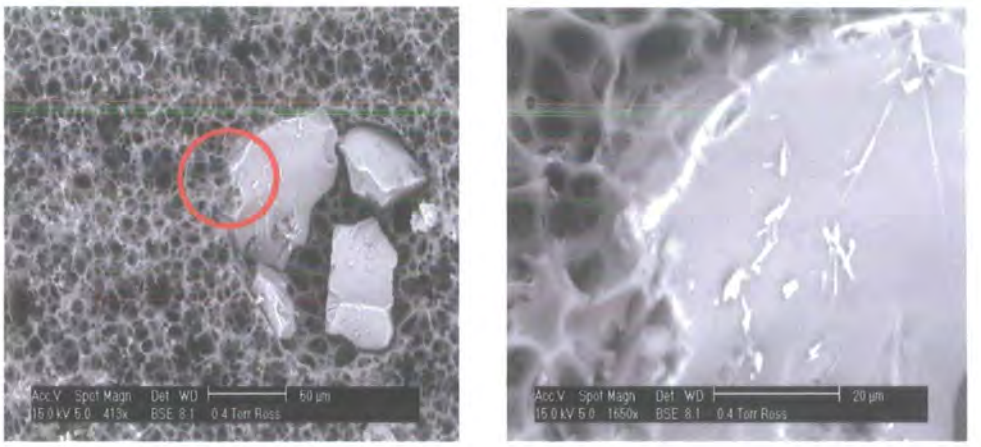

(a) (b)

Figure 3.15 *ESEM images of the fractured surface of the silica gel PolyHIPE.*

Figure 3.15 shows the strength of bonding between the silica gel particle and the PolyHIPE cellular matrix. The particles, rather than being completely bonded to the cellular matrix, are sitting within a large void present in the structure. The silica particles are hydrophilic in nature, and, as in the case of the viscose fibre, the hydrophilic nature of the particle could cause destabilisation of the HIPE in the area surrounding the particle, causing coalescence, therefore producing this large void surrounding the particle. **Figure 3.15 (b)** provides a higher magnification picture of the area circled in red. Although the cellular structure has become detached from the majority of the silica particle surface, there is some bonding/adherence observed at the side of the silica particle. However, this is not the case with the majority of the particles present.

(a) (b)

Figure 3.16 *ESEM images of the fractured surface of the silica gel PolyHIPE.*

Figure 3.16 shows two ESEM images, which provide evidence of coalescence around the area in which the HIPE is in contact with the silica particles. **Figure 3.16 (b)** shows a cluster of particles sitting within a large void present in the PolyHIPE structure. Unlike the case with Kevlar fibres or aluminium particles, the silica particles do not bond completely with the cellular matrix of the PolyHIPE. Therefore, they will be expected to provide little mechanical reinforcement. It is however possible that not only the chemical interaction between the filler and the matrix may affect the mechanical performance but also the filler particle size may affect the mechanical performance. Bose et al. [156] showed that there was a decrease in the flexural properties of mica-filled nylon-6 composites as the particle size increased from 37 to 75 µm. For glass bead-filled LDPE, Yang et al. [157] showed that the elastic modulus of the composite increased with increasing glass bead diameter with an exception for the 2 µm diameter beads at filler content of 15 wt %. The impact strength showed a similar correlation to the yield strength showing a maximum at a bead size of 3 µm. The influence of fibre length has previously been discussed in **chapter 1**. However there have been no extensive literature reports relating

PolyHIPE void size, filler size and the overall mechanical performance of the composite material. **Figure 3.17** shows the X-ray data of the area containing the particles.

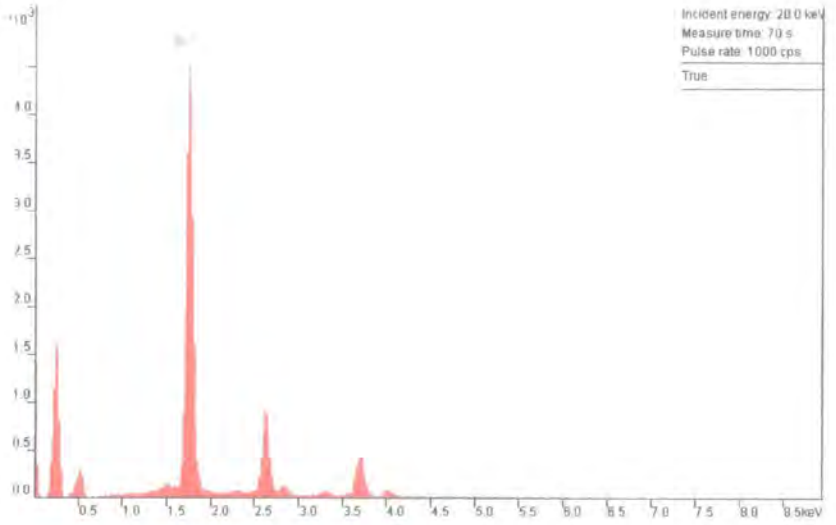

Figure 3.17 *X-ray analysis of the silica gel/ PolyHIPE composite.*

The X-ray data confirm that the particles present within the PolyHIPE structure contain silicon. Other elements present are calcium and chlorine, which would be present due to residual salt particles left after cleaning.

3.3.4 Addition of polybutadiene to monomer phase

An advantage of rubber introduction into the monomer phase is that radical polymerisation in the presence of dissolved rubber potentially yields either a toughened structure or a rubber network structure. There were no problems encountered with dissolving the solid PB in styrene. However, there was a noticeable increase in viscosity of the monomer phase with addition of the PB. The ratio of

styrene to DVB was kept at 90/10 throughout. **Table 3.6** shows the experiments conducted to provide PB PolyHIPE materials.

Table 3.6 Experimental conditions used in S/DVB HIPE formation

Amount of PB (%) [a]	Surfactant Level (%)	Stirrer speed (rpm)	HIPE formed
2.5	20	300	Yes
2.5	20	500	Yes
5	20	300	No
5	10	500	Yes
7.5	10	300	No

a- relative to monomer phase

At a PB loading of 2.5 % w/w, there were no difficulties encountered in HIPE formation. The HIPE produced was more viscous in nature due to the addition of the PB. **Figures 3.18 (a)** and **(b)** show the morphology of the fractured surface of the PB composite material produced using a stirrer speed of 300 rpm. From the ESEM images the presence of voids (50-150 μm) can be observed. These larger voids could be due to the greater viscosity of the monomer phase, which inhibits efficient mixing of the HIPE. To reduce the number of larger voids present, a higher shear/stirrer rate (500 rpm) was used to prepare the HIPE (**see figure 3.18 (c)** and **(d)**).

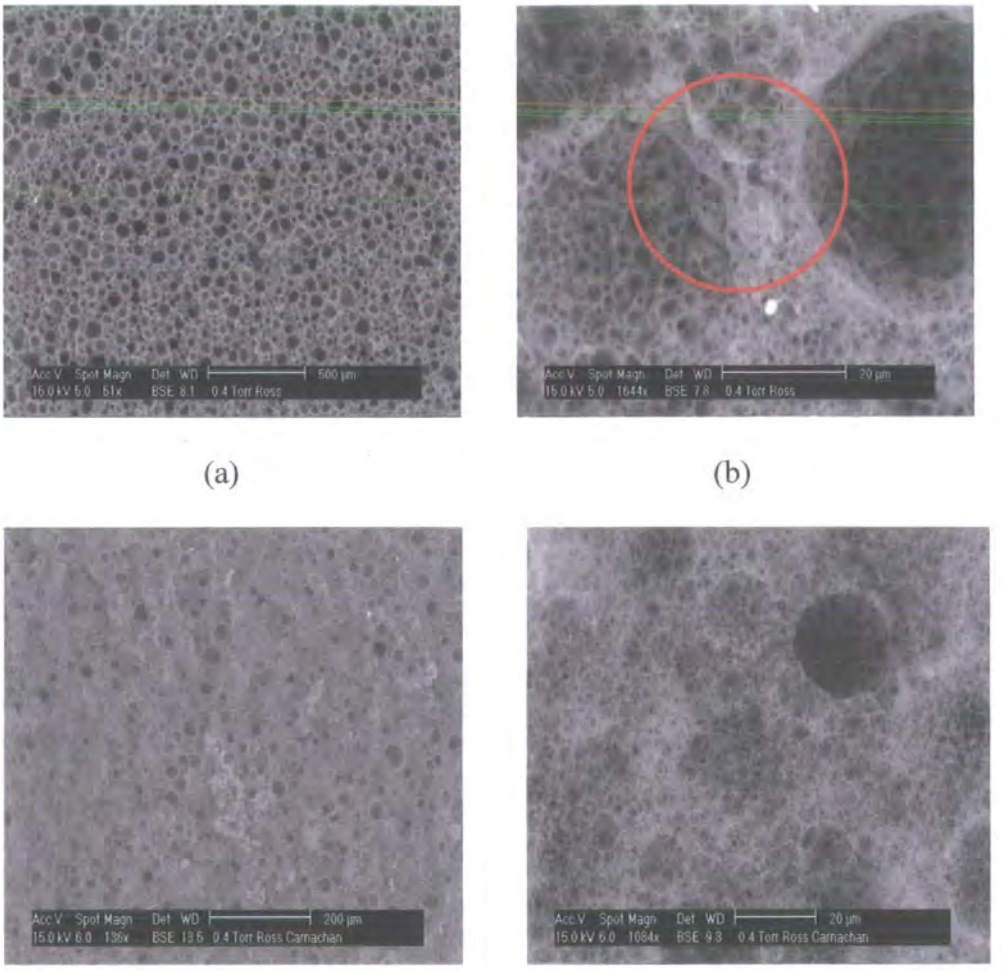

Figure 3.18 *Morphology of the 2.5% PB/styrene PolyHIPE materials: (a) and (b) stirrer speed 300 rpm, (c) and (d) stirrer speed 500 rpm. (Area in red circles represents possible areas of rubber-like domains due to phase separation).*

The increase in stirring rate to 500 rpm resulted in a reduction in content of the larger voids and an overall decrease in void size compared to the material produced with a stirring rate of 300 rpm. This material also has a smaller void size than normal styrene/DVB materials (**see figure 1.5**).

When the PB level is increased to 5 % w/w there is a further increase in monomer phase viscosity. Under a stirring speed of 300 rpm, no HIPE could be formed. The surfactant level was decreased to 10 % w/w and the stirring speed was increased to 500 rpm. A HIPE was formed under these conditions and the morphology of the resulting material is shown in **figure 3.19**.

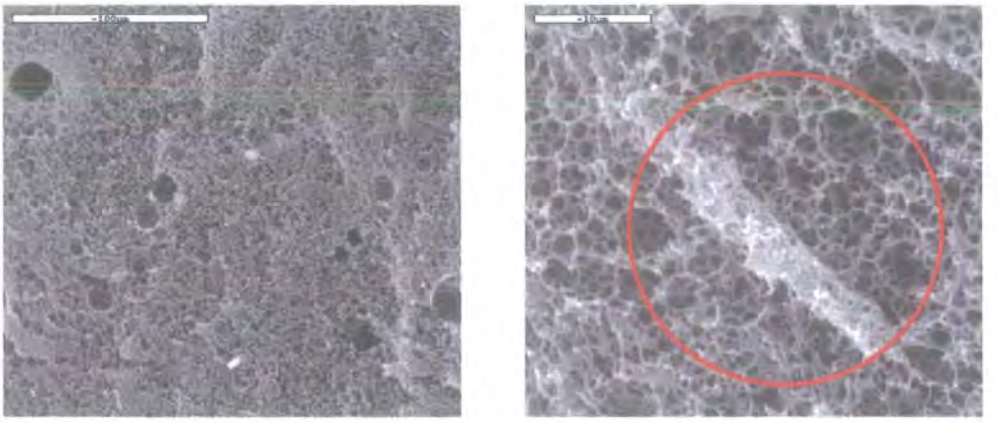

Figure 3.19 *Morphology of the 5 % PB/ styrene PolyHIPE material (Stirrer speed-500 rpm). (Area in red circles represents possible areas of rubber-like domains due to phase separation).*

The PolyHIPE material produced has an open-cell morphology. There are a few large voids present (30 –50 μm), but there is again an overall decrease in void size with the addition of the PB. There is no significant change in void size between the 2.5 % and the 5 % w/w PB PolyHIPE material. The areas present within the red circles show ridge/edges of very low porosity. This could represent possible phase separation of rubber like domains.

Recently Choi et al. [121] related the viscosity of the continuous phase and the shear rate (stirrer speed) to a dimensionless factor called the capillary number. This is given by **equation 3.3**

$$Ca = \frac{\mu_c \dot{\gamma} R}{\sigma} \qquad \textbf{Equation 3.3}$$

where μ_c is the viscosity of the continuous phase, γ is the shear rate, R is the radius of the droplet and σ is the interfacial tension between the two phases.

They suggested that the decreasing cell size could be explained by a relationship between the viscosity ratio and the critical capillary number. The critical capillary number is the capillary number above which the break-up of droplets can take place. As rubber is introduced to the monomer phase the viscosity of the continuous phase

increases, and the viscosity ratio decreases. From **equation 3.3**, droplet size is inversely proportional to the viscosity of the continuous phase. They showed that as the rubber concentration increases, the average void size decreases. However they found there was no significant change in void size when the rubber concentration increased from 2.5 % w/w to 5 % w/w.

They also showed that the average void size decreased with increasing agitation speed.

3.3.5 Addition of clay/intercalated clay to monomer phase

The initial dispersion of non-intercalated clay (2.5 % and 5 % w/w of monomer phase) did not result in HIPE formation due to the hydrophilic nature of the clay material. The decrease to 1 % w/w clay using a monomer phase consisting of styrene, MMA and DVB (50/40/10 %) provided a PolyHIPE material with the morphology represented in **figure 3.20**.

The morphology consists of an open-cell network, containing large voids which are most likely due to coalescence. Even though an open-cell network does exist, the incorporation of the MMA as a co-monomer produces a less porous open-cell structure than would normally be expected for a PolyHIPE material. The interconnecting strut size of the material also seems to have visibly increased in size due to the addition of the MMA monomer. This morphology of MMA-based materials will be discussed in later chapters. The inclusion of the MMA to the monomer phase was as a result of the reported greater interaction of clay with the more polar MMA compared to the less polar styrene [122].

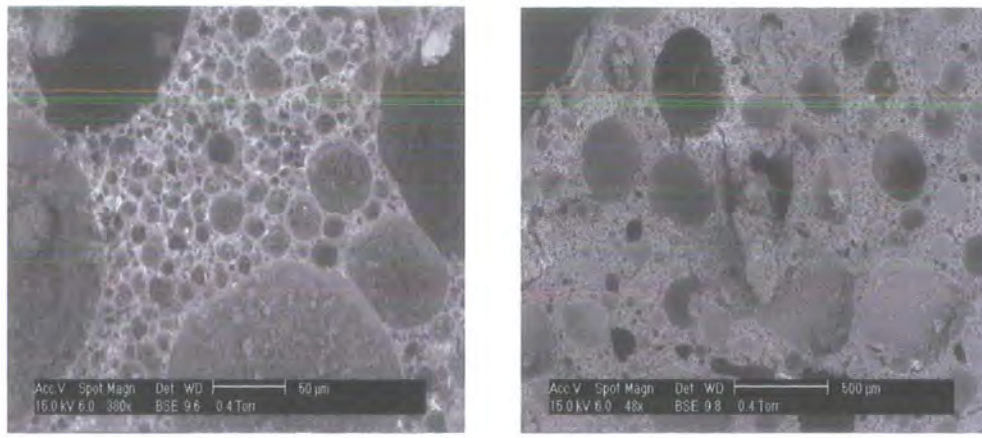

Figure 3.20 *ESEM images of the styrene/MMA/DVB PolyHIPE material containing 1 % w/w clay.*

Due to the hydrophilic nature of clay, dispersion of a high amount within the monomer phase inhibited HIPE formation. **Figure 3.21** provides X-ray data of the non-intercalated clay/PolyHIPE composite.

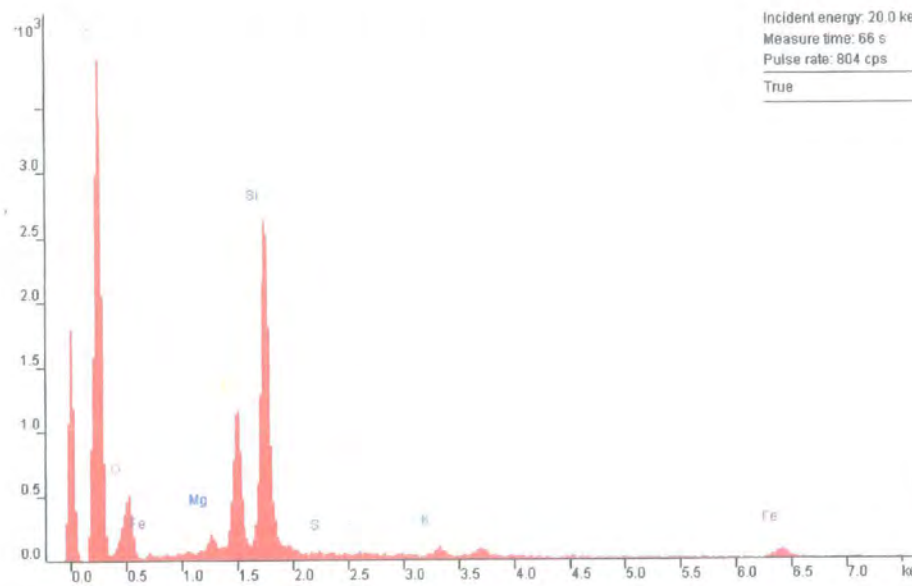

Figure 3.21 *X-ray analysis of the non-intercalated clay/PolyHIPE composite material.*

Even though there are no particles visible from the ESEM images, the X-ray data confirms the presence of silicon, aluminium, magnesium and oxygen elements within the structure. This is consistent for clays/layered silicate materials.

To reduce the water content and increase the compatibility with the HIPE, the clay was intercalated with a suitable polymer, in this case PEO, prior to dispersion into the monomer phase. During intercalation the interlayer water molecules are replaced by the polymer (PEO). In the case of NH_4^+-montmorillonite an initial water content of around 10 % w/w was reduced to 1 % w/w when the clay was intercalated with PEO [122].

In PEO/Na^+-smectite nanocomposites, the polymer preserves more or less distorted the normal helical structure of PEO, as discussed by Aranda and Ruiz-Hitzky [122], [123]. However, after intercalation, NH_4^+- exchanged smectites show evidence suggesting distortion of the helical structure. **Figure 3.22** shows schematically the two different types of structure obtained when intercalating PEO with Na^+-montmorillonite and NH_4^+- montmorillonite.

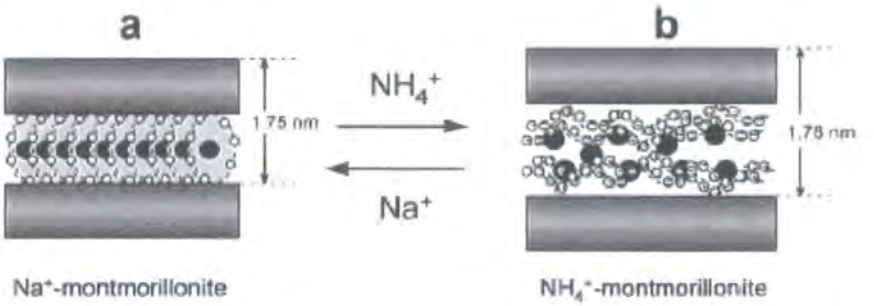

Figure 3.22 *Schematic representation of polymer conformations in PEO/M^+-montmorillonite nanocomposites. (a) $M^+ = Na^+$ (PEO in helical conformation) and (b) $M^+ = NH_4^+$ (PEO chain in double layer arrangement)* [123].

Figure 3.23 provides X-ray diffraction (XRD) patterns for both the PEO/Na^+-montmorillonite before and after intercalation at 80°C. The X-ray pattern shows peaks characteristic of pristine silicate (Peak 1, d=11.61 Å) and crystalline PEO (Peaks 2, 3 and 4, d= 4.63 Å, 3.81 Å and 3.14 Å). After heating to 80°C for 24 hours the PEO peaks have reduced while there is new peaks (6, 7 and 8) relating to the

intercalated silicate. The d spacing of the silicate peak has increased from the 11.61 Å (Peak 1) to 17.76 Å (Peak 5). This is line with what was reported by Vaia et al [120], and similar observations have also been reported for the solution assisted intercalation of Na^+ -montmorillonite and PEO [124].

A PolyHIPE material was produced when the intercalated hybrid was added to the monomer phase. **Figure 3.24** shows ESEM images of the morphology of the fractured surface of the PolyHIPE/intercalated clay composite.

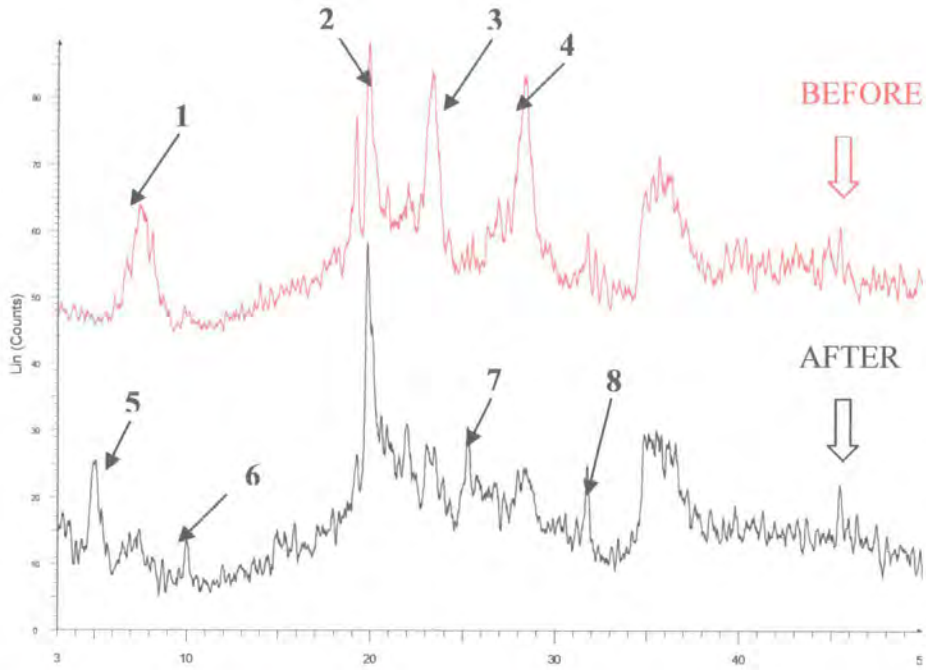

Figure 3.23 *X-ray diffraction traces of PEO/Na^+-montmorillonite hybrid heated to 80°C for 24 hours.*

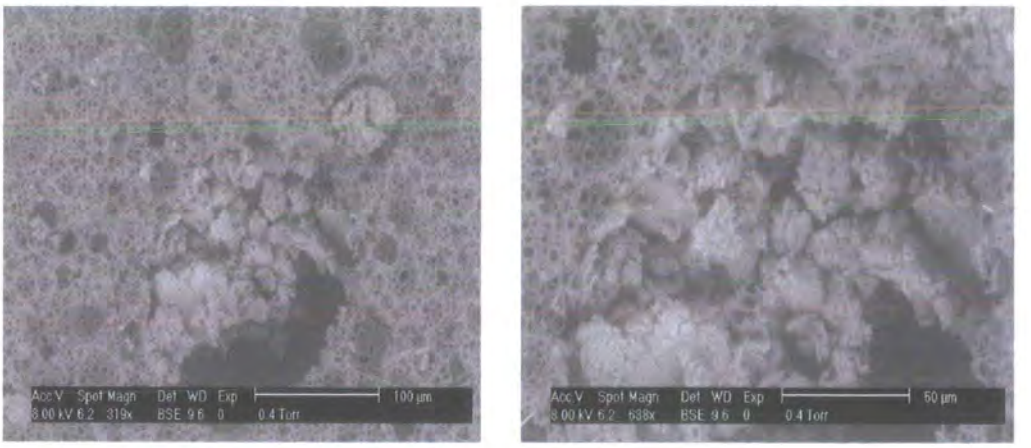

Figure 3.24 *ESEM images of the morphology of the PolyHIPE/intercalated clay composite material.*

The ESEM pictures show that the intercalated clay particles do not bond strongly to the cellular matrix of the PolyHIPE material. As was the case with hydrophilic silica gel particles, there is evidence of coalescence around the areas in contact with the intercalated particles. Therefore little mechanical reinforcement is expected. **Figure 3.25** shows the X-ray data taken from the intercalated clay particles present within the PolyHIPE structure.

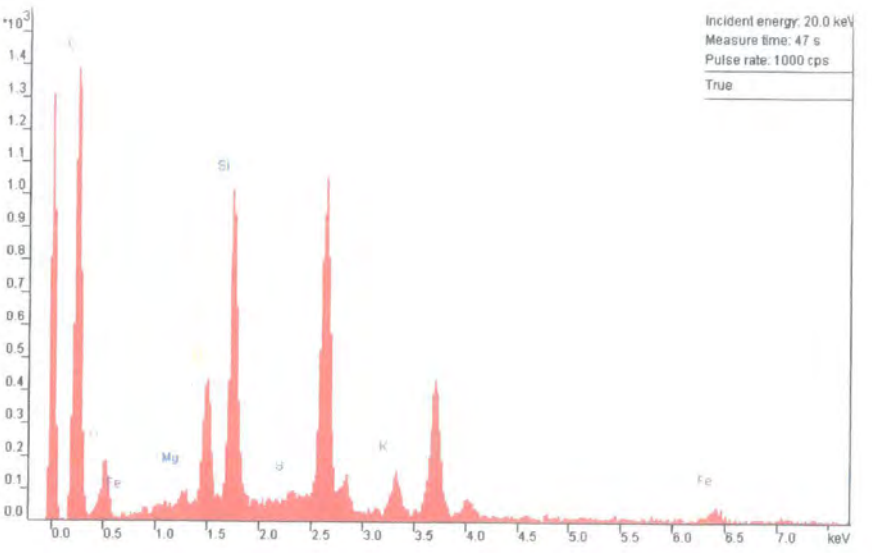

Figure 3.25 *X-ray analysis of the intercalated clay/PolyHIPE composite material.*

The X-ray data confirm that the particles present within the PolyHIPE structure contain silicon, magnesium, oxygen and aluminium, and is consistent with the data found for the non-intercalated clay material.

3.4 Conclusions

From the results and observations in this chapter, it has been shown that it is possible to disperse fillers within the monomer phase prior to HIPE formation and thus prepare a number of different PolyHIPE materials.

The addition of certain fibres allowed material of up to 10 % w/w (monomer phase) loading of fibre to be prepared. The SEM images provided evidence that the Kevlar fibres bonded more strongly to PolyHIPE matrix compared to both the PP and viscose fibres. Scale-up of production of the fibre-reinforced materials resulted in problems, such as mould influence on sample uniformity and drying of the materials within the convection oven. At a high loading of viscose fibres (10 % w/w) it was not possible to prepare a HIPE, due to the hydrophilic nature of fibre material affecting HIPE stability. The value for the weight percentage of fibre present within the centre of the foam was evaluated using elemental analysis. This worked best for the Kevlar-reinforced material compared to the PP and viscose composites.

PolyHIPE composite materials containing aluminium or silica gel particles have also been prepared. SEM and ESEM images provide evidence that the aluminium particles interact strongly with the PolyHIPE matrix compared to the silica gel particles, which cause coalescence of the HIPE in the areas surrounding the particles. X-ray analysis confirmed the particles present in each sample type contained either aluminium or silicon.

This chapter also showed that it was possible to prepare composite PolyHIPE materials containing non-intercalated and intercalated clay material. The non-intercalated clay was dispersed and polymerised within a MMA-based monomer

phase, due to the reported greater interaction of the clay with the polar MMA. The clay was also intercalated prior to HIPE preparation with PEO to reduce the water content of the clay to increase the compatibility for HIPE preparation. The intercalation was observed by the X-ray powder diffraction traces, showing the disappearance of the three PEO peaks and the emergence of new intercalated silicate peaks. The ESEM images showed that the intercalated clay particles do not bond strongly to the PolyHIPE matrix and that coalescence occurs in areas around the particles. X-ray analysis confirmed the presence of silicon, aluminium, magnesium and oxygen in both composites, which is consistent with the structure of layered silicate materials.

The addition of PB to a styrene/DVB monomer phase produced a PB based PolyHIPE composite material. Dissolution of PB also resulted in an increase in viscosity of the monomer phase. The viscosity increased with increasing PB content and made HIPE preparation difficult. The void size of the PolyHIPE material is dependent on the viscosity and shear rate (stirring speed). With increasing viscosity and stirrer speed there was a decrease in void size of the material.

Chapter 4

The preparation and morphology of acrylate- and methacrylate-based PolyHIPE materials

4.1 Introduction

The method of adding active fillers to alter the physical properties of styrene/DVB PolyHIPE materials has been discussed in **chapter 3**. Another method to alter the physical properties is to change the chemical nature of the PolyHIPE material. Glassy monomers such as styrene, chloromethylstyrene and methyl methacrylate provide the PolyHIPE material with structural integrity. Elastomeric monomers such as 2-ethylhexyl acrylate and n-butyl acrylate provide the foam with flexibility and can be used in a sufficient amount to allow compression, bending and twisting during shipping and storage. This section of the work will detail the preparation and morphology of different acrylate- and methacrylate-based PolyHIPE materials. This will include the use of multifunctional methacrylate comonomers as alternative crosslinkers to DVB.

4.2 Experimental

4.2.1 The preparation of acrylate- and methacrylate- based PolyHIPEs

4.2.1.1 Materials

Monomer Phase

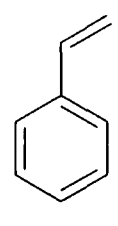

styrene (99 %)

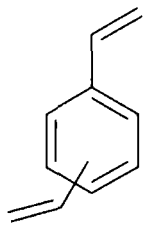

divinylbenzene (80 %)

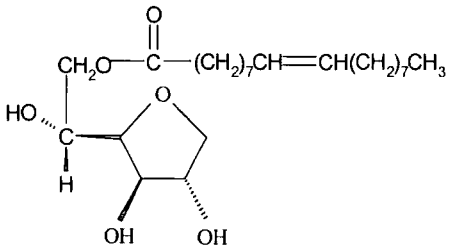

Span 80

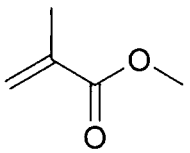

methyl methacrylate (99 %)

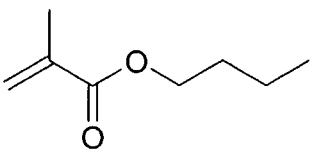

butyl methacrylate (99 %)

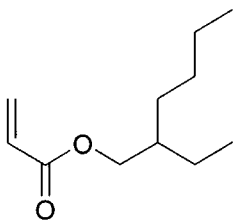

2-ethylhexyl acrylate (98 %)

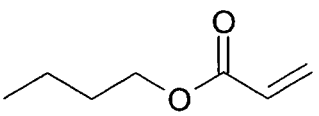

n-butyl acrylate (99 + %)

Aqueous Phase

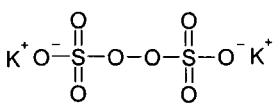

Potassium Persulfate (99 + %)

De ionised water

Calcium Chloride dehydrate (99 + %)

Figure 4.1 *Materials used for HIPE preparation.*

Aldrich chemicals supplied all of the materials, excluding the de-ionised water. The monomers were purified prior to HIPE preparation by passing them through a column of basic activated aluminium oxide.

4.2.1.2 HIPE preparation and polymerisation

The concentrations of each monomer in the oil phase are shown in **table 4.1**. The monomer phase also contained the surfactant Span 80 (2 g, 4.7 mmol). The aqueous phase consisted of de-ionised water (90 g), calcium chloride dihydrate (1.0 g, 6.8 mmol) and potassium persulfate (0.2 g, 0.74 mmol). The HIPE was prepared and cured as in **2.2.3**. The resulting PolyHIPE material was cleaned and dried as in **2.2.3**. Each experiment was carried out only once, unless complete separation of the HIPE occurred and in this case the experiment was carried out until a PolyHIPE material was obtained.

4.2.1.3 Instrumentation and characterisation

The morphologies of the materials were characterised using the instrumentation detailed in **2.2.2**.

4.2.2 The use of alternative multifunctional cross-linkers

4.2.2.1 Materials

The two cross-linkers present with styrene and Span 80 in the monomer phase are shown below in **figure 4.3**.

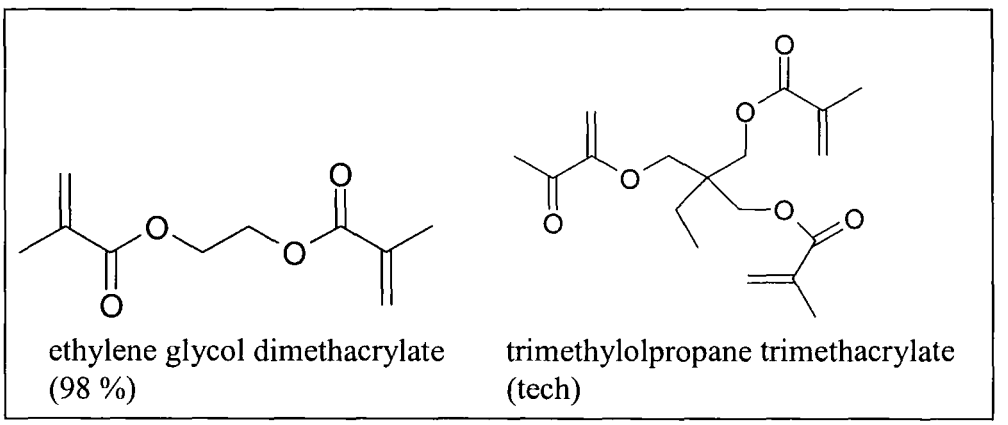

Figure 4.2 *Alternative cross-linkers for PolyHIPE preparation.*

The styrene, Span 80 and EGDMA were obtained from Aldrich chemicals. Avocado Research Chemicals supplied the TMPTM monomer.

The monomers styrene and EGDMA were purified prior to HIPE preparation by passing through a column of base activated aluminium oxide. The TMPTM monomer was not purified prior to HIPE preparation due to its high viscosity.

4.2.2.2 HIPE preparation and polymerisation

The amounts of alternative crosslinker present in the monomer phase are shown in **table 4.1**. The aqueous phase added was the same as in **4.2.1.2**. The HIPE was prepared and cured as in **2.2.3**. The PolyHIPE material was then cleaned and dried as in **2.2.3**. Each experiment was carried out only once, unless complete separation of the HIPE occurred and in this case the experiment was carried out until a PolyHIPE material was obtained.

4.2.2.3 Instrumentation and characterisation

The morphologies of the materials were characterised using the instrumentation detailed in **2.2.2**.

Table 4.1 Monomer phase composition for HIPE preparation

S (g)	DVB (g)	EHA (g)	BA (g)	BMA (g)	MMA (g)	EGDMA (g)	TMPTM (g)
1.0	1	8.0	/	/	/	/	/
3.0	1	6.0	/	/	/	/	/
5.0	1	4.0	/	/	/	/	/
7.0	1	2.0	/	/	/	/	/
1.0	1	/	8.0	/	/	/	/
3.0	1	/	6.0	/	/	/	/
5.0	1	/	4.0	/	/	/	/
7.0	1	/	2.0	/	/	/	/
1.0	1	/	/	8.0	/	/	/
3.0	1	/	/	6.0	/	/	/
5.0	1	/	/	4.0	/	/	/
7.0	1	/	/	2.0	/	/	/
5.0	1	/	/	/	4.0	/	/
7.0	1	/	/	/	2.0	/	/
9.0	/	/	/	/	/	1.0	/
8.0	/	/	/	/	/	2.0	/
7.0	/	/	/	/	/	3.0	/
9.0	/	/	/	/	/	/	1.0
8.0	/	/	/	/	/	/	2.0
7.0	/	/	/	/	/	/	3.0

4.3 Results and discussion

4.3.1 Acrylate- and methacrylate- based PolyHIPEs

4.3.1.1 Stability and morphology

When the monomer composition comprised of 20 % styrene, 10 % DVB and either 80 % w/w, EHA or BA, PolyHIPE materials were produced that were elastomeric in nature, with the EHA-based material showing the greater elastomeric nature. The elastomeric nature of the materials was measured by observation and handling only. **Figure 4.3** provides ESEM images of both the 80 % EHA and 80 % BA material.

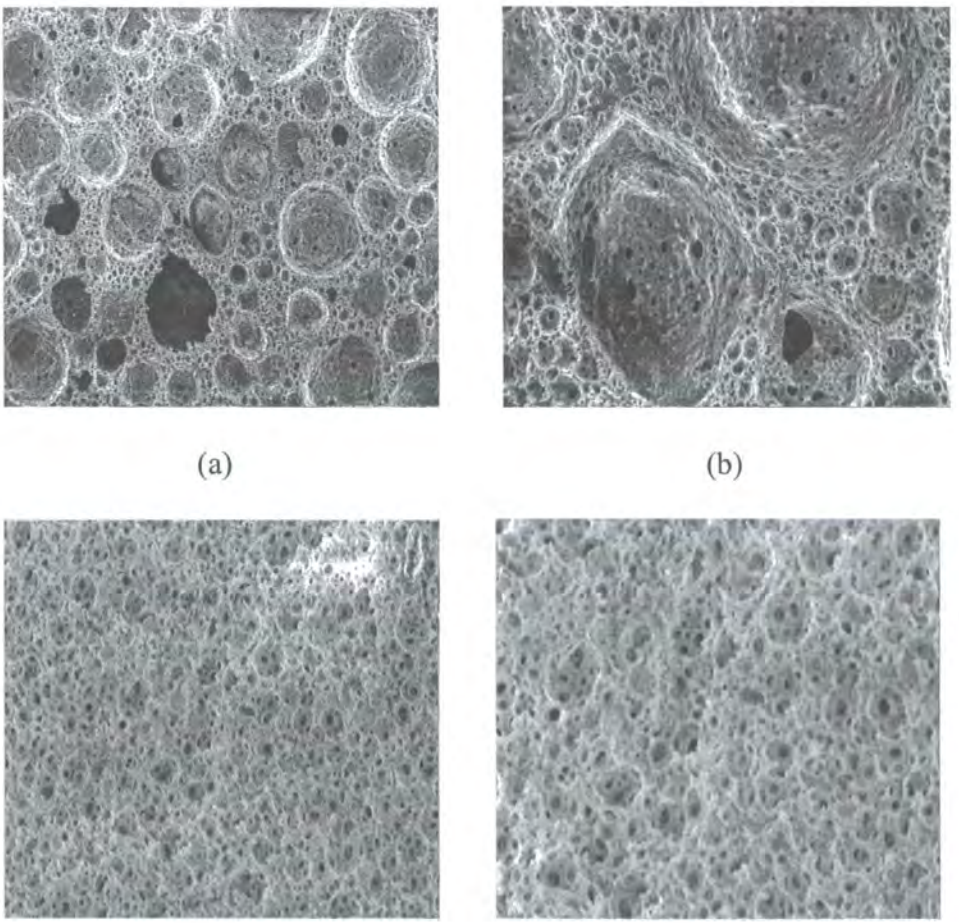

(a) (b)

(c) (d)

Figure 4.3 *ESEM images of the acrylate-based PolyHIPE materials: (a) and (b) 80 % BA, (c) and (d) 80 % EHA.*

The morphologies of both materials are distinctly different. The BA PolyHIPE consists of larger voids surrounded by a smaller open-cell structure. The larger voids

would most likely have been caused by coalescence and HIPE instability due to the presence of the BA. The morphology of the EHA material represents the morphology that normally would be expected of the standard S/DVB PolyHIPE material (**see figure 1.5**). The EHA has no drastic effect on HIPE stability. EHA is a more hydrophobic acrylate compared to BA and therefore will produce a more stable HIPE. **Figure 4.4** shows ESEM images of both the 60 % w/w EHA and BA materials.

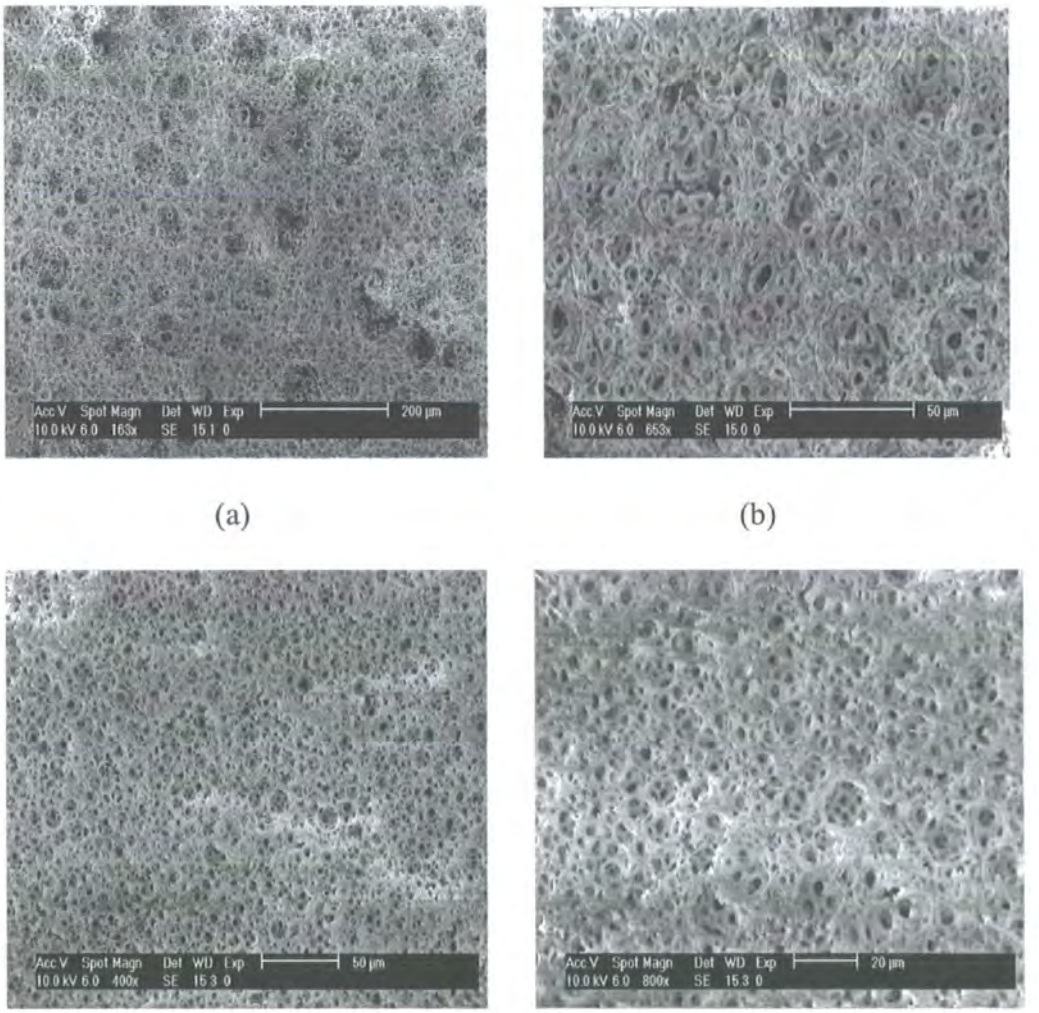

Figure 4.4 *ESEM images of acrylate-based PolyHIPE materials: (a) and (b) 60 % BA, (c) and (d) 60 % EHA.*

The morphology of the BA-based material has been altered with the reduction in BA composition to 60 % w/w. The presence of larger voids has reduced and the morphology of the material is now beginning to resemble the normal open-cell

morphology. There is still an effect on emulsion stability caused by the presence of the BA, as the PolyHIPE material exhibits a more distorted open-cellular structure than would be expected.

The 80 % EHA material shows no drastic change in morphology compared to the 60 % EHA material. The 60 % EHA material has a smaller void size than that of the 60 % BA material, again suggesting that the HIPE containing the EHA is more stable than that of the latter. Both materials were elastomeric in nature, but to a lesser degree due to the reduction in elastomer present in both materials.

Figure 4.5 provides ESEM images of the 40 % w/w acrylate-based materials. With the further decrease in BA content we observe a further decrease in void size (10-20 μm), suggesting a more stable emulsion. The morphology now represents what would be expected of a normal styrene/DVB PolyHIPE material **(see figure 1.5)**. The 40 % BA based PolyHIPE material was now more rigid in nature and had no noticeable elastomeric behaviour. There is no drastic affect on the morphology of the EHA-based PolyHIPE material when the EHA content was decreased to 40 % w/w. The morphology represents the open-cellular structure of the standard styrene/DVB PolyHIPE material. The rigid nature of the 40 % EHA material had increased with the decreasing amount of EHA, but some elastomeric behaviour was still observed.

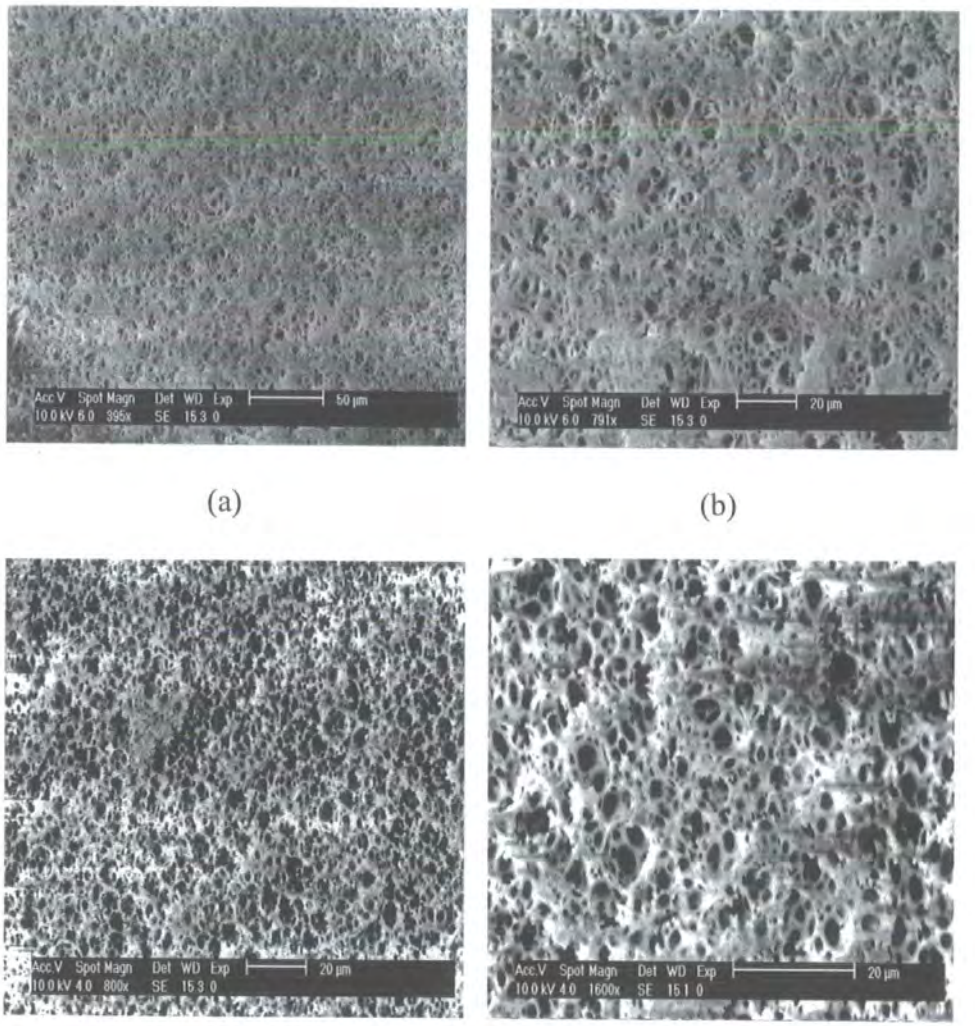

Figure 4.5 *ESEM images of the 40 % w/w acrylate-based PolyHIPE materials: (a) and (b) 40 % BA, (c) and (d) 40 % EHA.*

Figure 4.6 provides ESEM images of the morphology of the 20 % w/w acrylate-based materials.

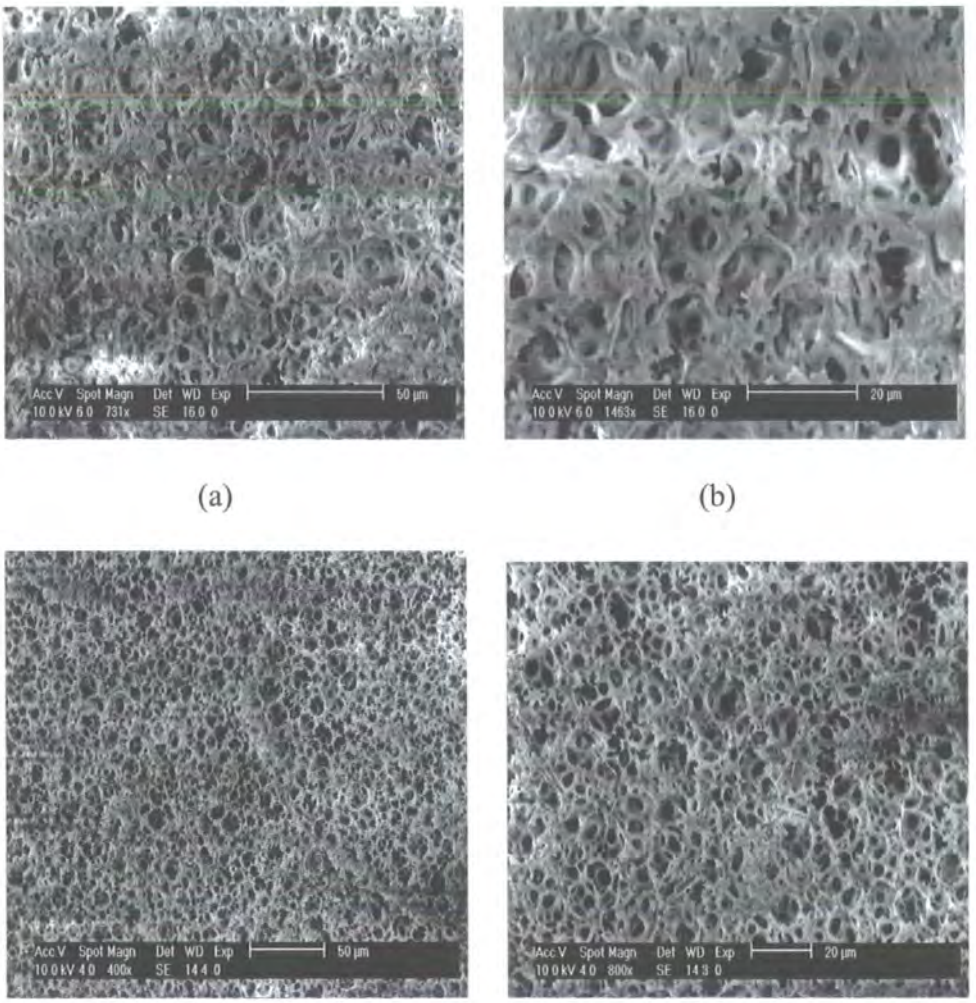

Figure 4.6 *ESEM images of the 20 % w/w acrylate-based PolyHIPE materials: (a) and (b) 20 % w/w BA, (c) and (d) 20 % w/w EHA.*

With the decrease in the amount of acrylate present to 20 % w/w, there is no detrimental change in morphology observed for either the 20 % BA or the 20 % EHA PolyHIPE materials. From the ESEM images, it is observed that the EHA- based material has a smaller void size compared to BA material. This again suggests that the HIPE formed with the presence of EHA is more stable than the HIPE with the BA present. Both of the acrylate materials were rigid in nature and elastomeric behaviour was not observed.

PolyHIPE materials were also prepared using two different methacrylate monomers, butyl methacrylate (BMA) and methyl methacrylate (MMA).

At 80 % w/w methacrylate content, a solid foam could only be obtained from BMA. At 80 % MMA level no PolyHIPE material could be produced due to phase separation of the HIPE. **Figure 4.7** provides ESEM images of the 80 % w/w BMA PolyHIPE material.

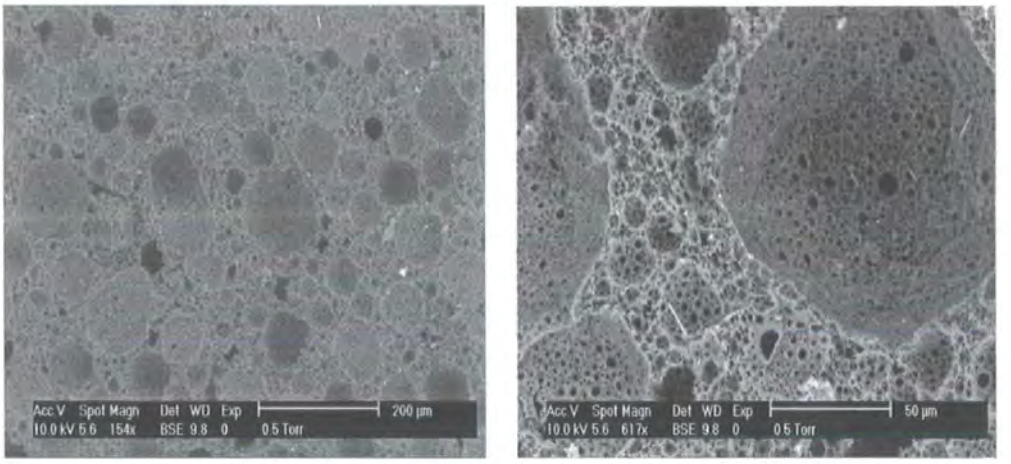

(a) (b)

Figure 4.7 *ESEM images of the 80 % w/w BMA PolyHIPE material.*

As was observed with the high weight content of BA, the ESEM images show the presence of large voids (100-200 µm) within the 80 % BMA material. This again is caused by coalescence due to the hydrophilic nature of the methacrylate monomer. The PolyHIPE material produced was rigid and brittle in nature.

A PolyHIPE material was produced when the MMA content was reduced to 60 %. The material produced was difficult to dry after cleaning, suggesting the material was of very low porosity or of a closed-cell nature. **Figure 4.8** shows ESEM images of the 60 % BMA PolyHIPE material.

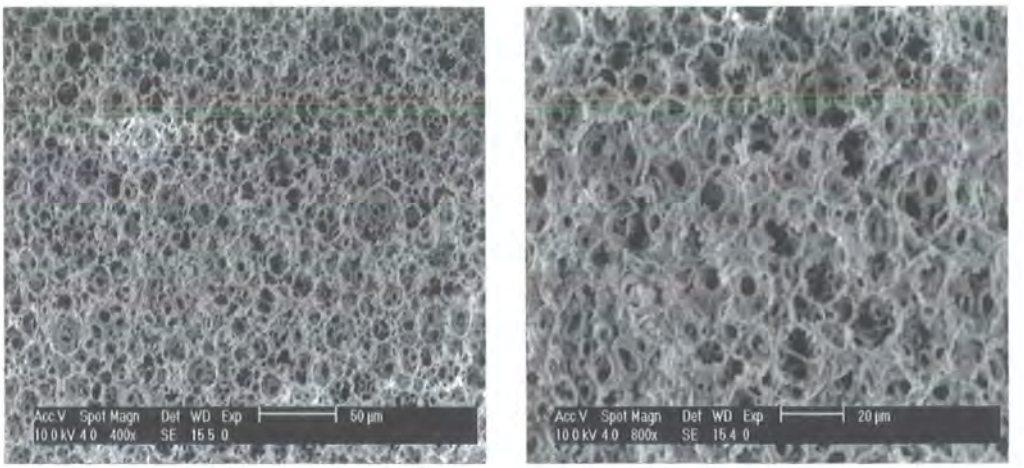

(a) (b)

Figure 4.8 *ESEM images of the 60 % BMA PolyHIPE material.*

The reduction of the BMA content has resulted in a change in morphology. The large voids present have disappeared and the morphology now represents the morphology that would be expected of a PolyHIPE material. With the 60 % BA material there were still signs of HIPE stability being affected. The presence of the methyl group in the methacrylate monomer decreases its hydrophilicity compared to BA; therefore BMA will produce the HIPE with the greater stability.

Figure 4.9 shows ESEM images of the 40 % w/w methacrylate based PolyHIPE materials. There is no detrimental change in morphology with the 40 % BMA material. It is the expected normal open-cellular morphology. The morphology of the 40 % MMA is distinctly different. There are larger voids present, caused by coalescence, but the morphology is one of low porosity and the open-cell nature of the material is less obvious than of what would be expected. The interconnecting strut size is also greater than expected. This could be due to lower HIPE stability producing thicker surfactant films between droplets and therefore smaller interconnects and thicker strut size. This could lead to greater mechanical performance. This low porosity structure for high content MMA materials was also noticed in **chapter 3**. Due to the greater hydrophobicity of BMA compared to MMA,

the HIPE produced containing BMA will be greater in stability compared to a HIPE containing MMA. This could account for the ability to produce high content BMA materials compared to MMA where it was not possible.

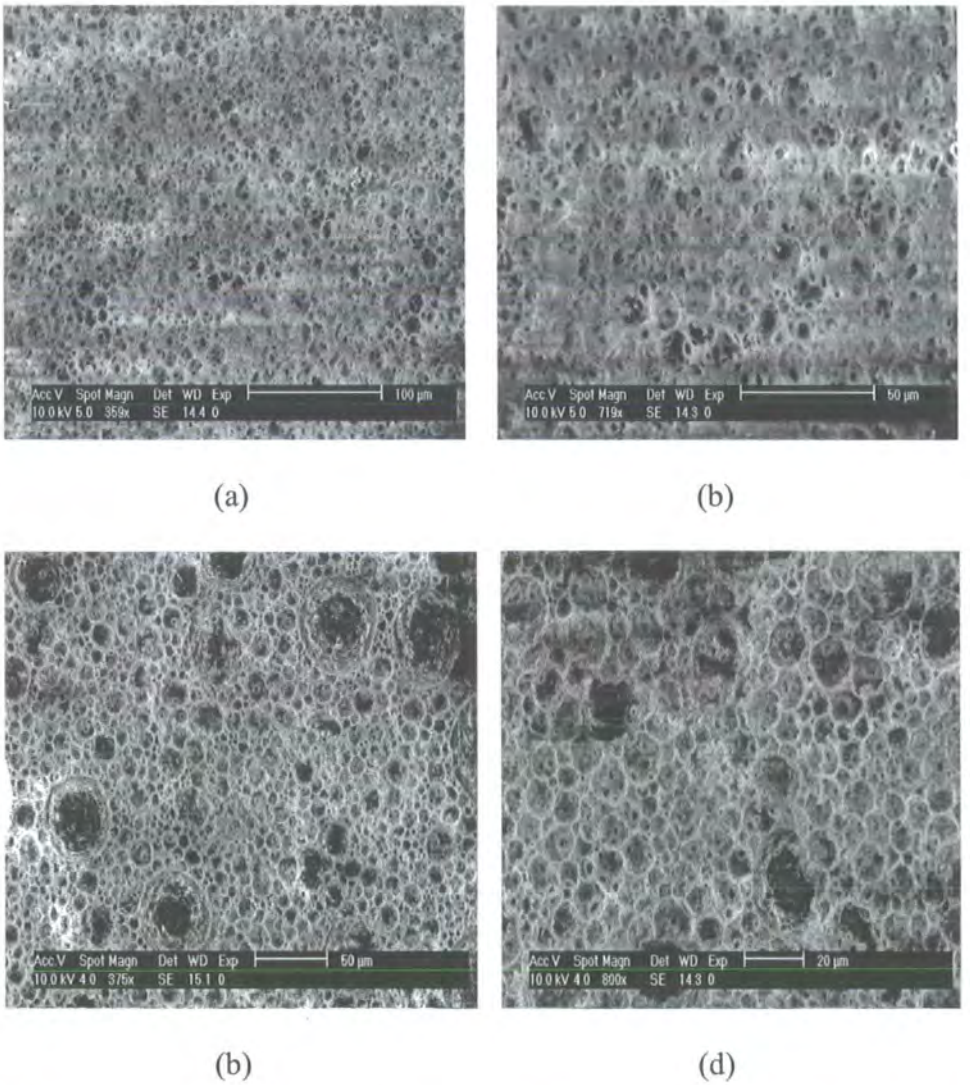

Figure 4.9 *ESEM images of the 40 % w/w methacrylate-based PolyHIPE materials: (a) and (b) 40 % BMA, (c) and (d) 40 % MMA.*

Figure 4.10 shows the ESEM images of the 20 % w/w methacrylate-based PolyHIPE materials. The 20 % BMA PolyHIPE material has an open-cell structure, which is slightly distorted compared to what would be expected of a normal PolyHIPE morphology. Due to the presence of the BMA, even at 20 % w/w, there is still an effect on HIPE stability.

The reduction of MMA content to 20 % w/w resulted in a change in morphology compared to the 40 % w/w PolyHIPE material. There are no large voids present, and the 20 % material has an open-cell structure with greater porosity compared to the 40 % MMA material. The morphology of the 20 % MMA material now represents the morphology that would normally be expected of a PolyHIPE material.

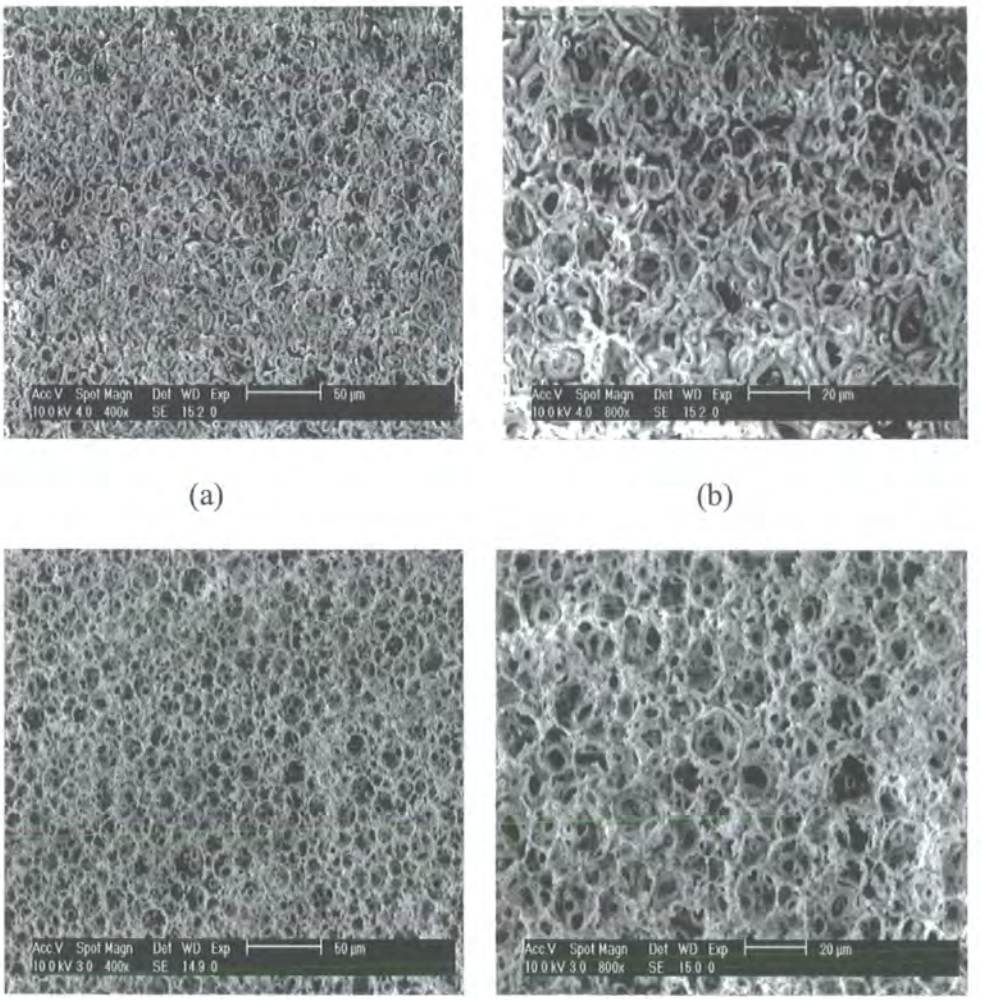

Figure 4.10 *ESEM images of the 20 % w/w methacrylate-based PolyHIPE materials: (a) and (b) 20 % BMA, (c) and (d) 20 % MMA.*

4.3.2 The use of alternative multifunctional cross-linkers

4.3.2.1 Stability and morphology

The standard cross-linker used in PolyHIPE production is DVB. As discussed in **chapter 1**, Williams et al. [70] have investigated the microstructure and mechanical properties of PolyHIPE materials with 0 –100 % DVB. In this section, the use of two different methacrylates as cross-linkers, shown in **figure 4.2**, and their effect on the morphology of the PolyHIPE materials produced will be discussed.

Figure 4.11 shows an ESEM image of the 90/10 styrene/EGDMA PolyHIPE material.

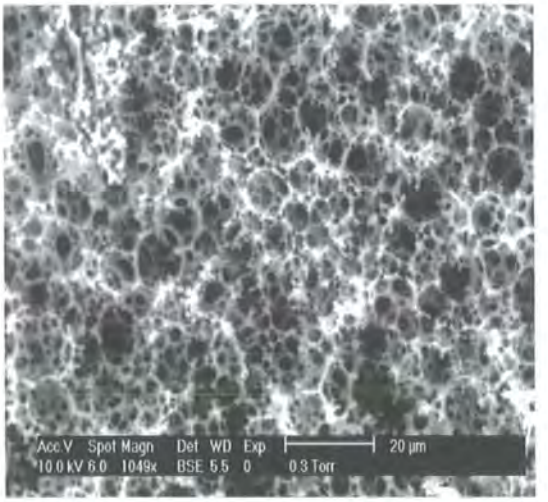

Figure 4.11 *ESEM image of the 90/10 styrene/EGDMA PolyHIPE material.*

The replacement of DVB with EGDMA as cross-linker resulted in no detrimental effect on the morphology of the PolyHIPE material. The ESEM image shows the open-cell morphology that would normally be expected of a PolyHIPE material. The void size of the material is approximately 10- 20 µm, which is what is expected for the standard S/DVB PolyHIPE material (**see figure 1.5**). **Figure 4.12** shows ESEM images of the 80/20 % styrene/EGDMA material.

The increase in EGDMA content has had no detrimental effect on the morphology of the material.

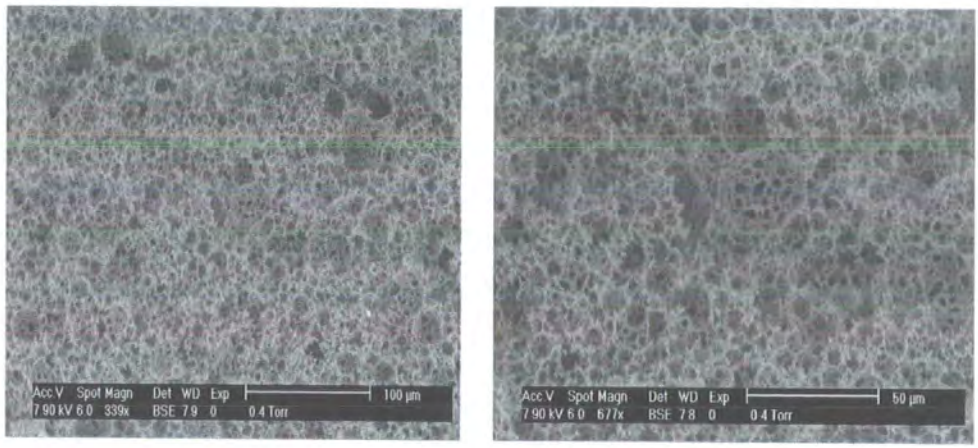

(a) (b)

Figure 4.12 *ESEM images of the 80/20 % styrene/EGDMA PolyHIPE material.*

The morphology is an open-cell interconnecting structure, which represents the structure that normally would be expected from a PolyHIPE material. The void size is around 10-20 µm although there is a presence of larger voids, which suggests some signs of HIPE stability being affected.

Figure 4.13 shows ESEM images of the 70/30 % styrene/EGDMA PolyHIPE material.

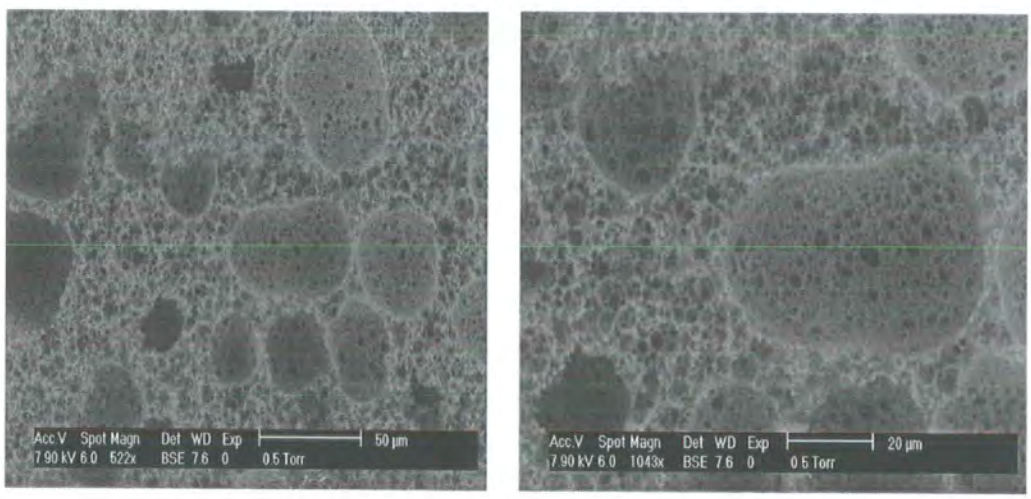

(a) (b)

Figure 4.13 *ESEM images of the 70 /30 % styrene/EGDMA PolyHIPE material.*

With a further increase in EGDMA content, a change in morphology is observed. An open-cellular structure does exist but there are large voids of around 100 µm in

diameter present. The increase in the hydrophilicity of the monomer phase due to the increasing content of EGDMA has adversely affected HIPE stability, causing coalescence and producing the larger voids present in the structure.

A composite material containing styrene, MMA and EGDMA was also produced. **Figure 4.14** shows ESEM images of the 60/20/20 % styrene/MMA/EGDMA PolyHIPE material.

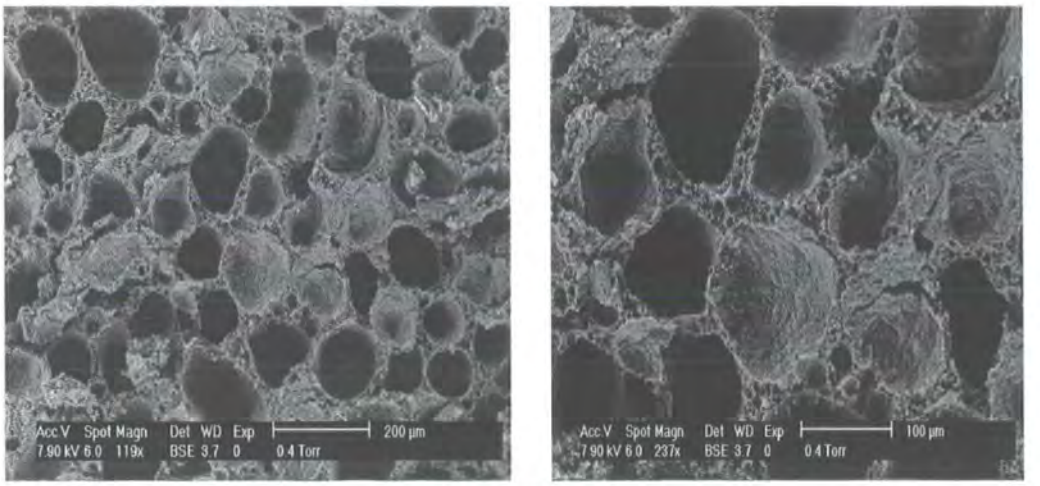

Figure 4.14 *ESEM images of the 60/20/20 % styrene/MMA/EGDMA PolyHIPE material.*

The morphology of the PolyHIPE material consists of large non-porous voids. The presence of the hydrophilic MMA as well as the EGDMA leads to greater HIPE instability and a non open-cell morphology. The low porosity, closed-cell nature is a common aspect observed so far for methacrylate-based PolyHIPE foam materials.

Figure 4.15 shows ESEM images of 90/10 styrene/TMPTM PolyHIPE material.

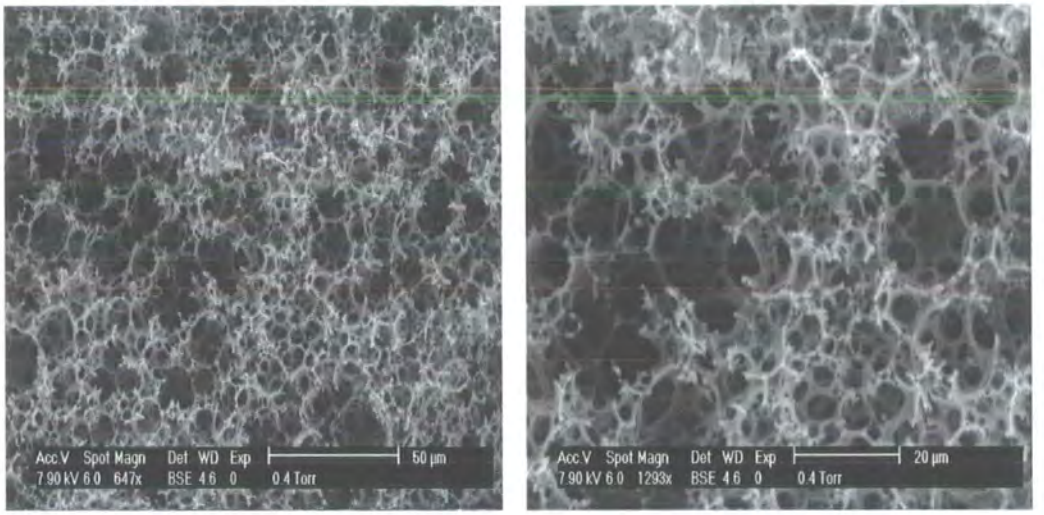

(a) (b)

Figure 4.15 *ESEM images of the 90/10 % styrene/TMPTM PolyHIPE material.*

The morphology of the 90/10 styrene/TMPTM PolyHIPE material consists of a normal open-cell structure, with a cell size of around 20 µm that would normally be expected from a PolyHIPE material

Figure 4.16 shows ESEM images of the 80/20 styrene/TMPTM PolyHIPE material.

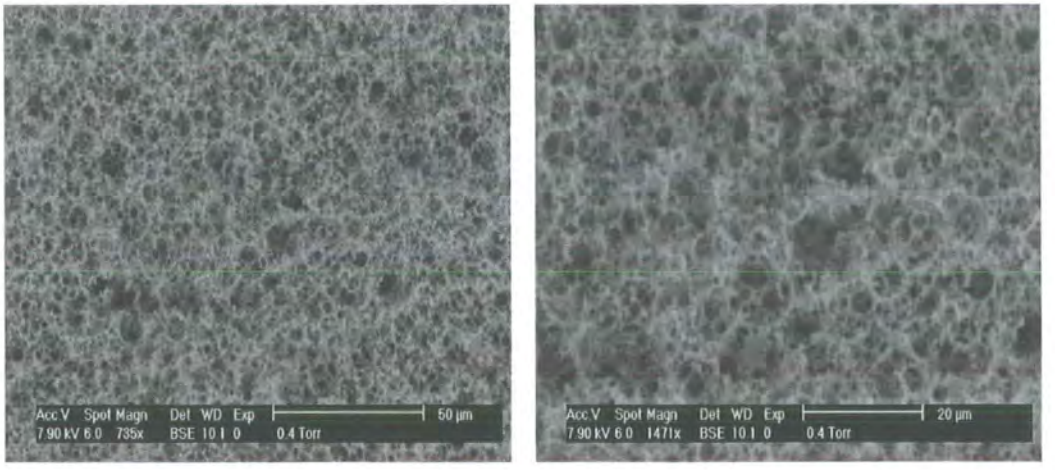

(a) (b)

Figure 4.16 *ESEM images of the 80/20 styrene/TMPTM PolyHIPE material.*

The morphology of the PolyHIPE is the normal open cellular structure that would normally be expected of a PolyHIPE material. There is a decrease in void size, to approximately 10 µm, compared to the 10 % w/w TMPTM material. This could be due to the increase in viscosity of the monomer phase with increasing TMPTM

concentration. This increase in viscosity can lead to a reduction in void size as already mentioned in **3.3.4**.

4.4 Conclusions

The results and observations in this section of the work indicate that it is possible to prepare open-cellular PolyHIPE materials with different physical characteristics by the addition of different acrylates and methacrylates to the monomer phase of HIPEs. The addition of EHA and BA produced elastomeric type foam materials. The elastomeric nature of both materials decreased with decreasing acrylate content and increasing styrene content. At high concentrations of EHA, there was no noticeable effect on the morphology of the foam material. At high concentrations of BA (80 % w/w), however, there were large voids present within the morphology of the material. This was suggested to be due to the presence of the relatively hydrophilic BA decreasing HIPE stability and causing coalescence. This effect on HIPE stability decreased with decreasing BA content, and at low concentrations (below 60 % w/w) the morphology of the material represented the open-cellular structure of PolyHIPE material.

The addition of BMA and MMA produced a more rigid PolyHIPE material. At a concentration of 80 % w/w MMA, it was not possible to prepare a PolyHIPE material due to HIPE phase separation. At 60 % w/w, a PolyHIPE material was produced that was difficult to dry and remained dense in nature; this suggested a material of a closed-cell nature or of very low porosity. At 40 and 20 % w/w MMA, PolyHIPE materials were produced. The morphology of the 40 % MMA material contained an open-cell structure of low porosity and small interconnect size. The decrease in MMA concentration increased HIPE stability and produced a PolyHIPE material with greater porosity and an open-cellular structure that represented what would normally be expected of a PolyHIPE material. At high concentrations of BMA (80 % w/w)

there were large voids present, due to the decrease in HIPE stability with the presence of the hydrophilic BMA. With decreasing BMA content, HIPE stability increased and a material with a more uniform morphology was produced.

PolyHIPE materials containing two different methacrylate based cross-linkers have also been produced. Both EGDMA and TMPTM produced materials that were open-cell in nature. The structures represented the morphology expected of a PolyHIPE material. With increasing EGDMA content there were signs of HIPE stability decreasing and coalescence occurring. With an increase in TMPTM content from 10 to 20 % w/w there was a decrease in void size possibly due to the increase in viscosity of the monomer phase.

Chapter 5

Optimising processing conditions

5.1 Introduction

In **chapter 1** the plasticisation effect of the surfactant Span 80 was discussed. This effect can result in a weakening of the mechanical properties of the PolyHIPE. Span 80 is also present at an amount of 20 % w/w of the monomer phase and is generally removed from the PolyHIPE material by washing with water and a lower alcohol after polymerisation. From an industrial point of view this would greatly increase production time and the overall cost of processing the material. In this chapter, the production and morphology of PolyHIPE materials, prepared with an optimised surfactant system (OSS) [36], at a lower weight percent level of monomer phase (7 % w/w), will be discussed. To reduce production time the preparation of PolyHIPE materials using a redox initiator [42] to reduce the curing time of the material will be discussed. The effect of temperature on the curing time of both the thermally and redox-initiated PolyHIPE materials will also be discussed.

5.2 Experimental

5.2.1 Materials and instrumentation

5.2.1.1 Materials

The ionic and non-ionic surfactants Span 80, Span 20, dodecylbenzenesulfonic acid, sodium salt (tech) and cetyltrimethylammonium bromide were supplied by Aldrich Chemicals. The monomers used were supplied by Aldrich Chemicals and were purified prior to HIPE preparation by passing through a column of basic activated aluminium oxide. Potassium persulfate (99 + %), iron (II) sulfate heptahydrate (98 + %),$_{L}$- ascorbic acid (99 %), hydrogen peroxide (27.5 % w/w solution in water), cobalt (II) ethylhexanoate (65 wt. % solution in mineral spirits), ammonium persulfate (98 + %), sodium metabisulfite (97 %) and t-butyl peroxide (98 %) were supplied by Aldrich Chemicals.

5.2.1.2 Instrumentation

The morphologies of the materials were characterised using the instrumentation described in **2.2.2**.

5.2.2 Optimisation of surfactant system

5.2.2.1 S/DVB based PolyHIPE materials

Figure 5.1 shows the structures of the three components of the co-surfactant system.

The monomer phase consisted of styrene (9 g, 86.4 mmol), divinylbenzene (1 g, 7.68 mmol) (80 %) and the OSS system: Span 20 (0.63 g, 1.81 mmol), CTAB (0.04 g, 0.11 mmol) and DDBSS (0.03 g, 0.09 mmol). The aqueous phase consisted of 90 g de-ionised water, calcium chloride dihydrate (1 g, 6.8 mmol) and the initiator potassium persulfate (0.2 g, 0.74 mmol). The HIPE was then prepared and cured as described in **2.2.3**. The PolyHIPE material produced was then cleaned and dried as described in **2.2.3.** Each

experiment was carried out only once, unless complete separation of the HIPE occurred and in this case the experiment was carried out until a PolyHIPE material was obtained.

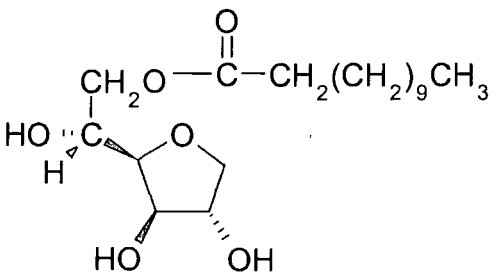

6.3 % w/w sorbitan monolaureate (Span 20)

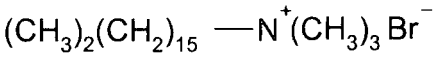

0.4 % w/w cetyltrimethylammoniumbromide (CTAB)

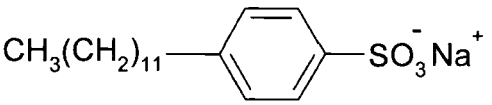

0.3 % w/w dodecylbenzenesulfonic acid, sodium salt (DDBSS)

Figure 5.1 *Surfactants used in the OSS system.*

5.2.2.2 Acrylate and methacrylate-based PolyHIPE materials

Table 5.1 shows the experiments carried out with acrylate and methacrylate based monomers using the OSS and differing co-surfactant compositions. The aqueous phase composition in all cases was identical to that discussed in **5.2.2.1**. The HIPE was prepared and cured as described in **2.2.3**. The PolyHIPE material produced was then cleaned and dried as described in **2.2.3**. Each experiment was carried out only once, unless complete separation of the HIPE occurred and in this case the experiment was carried out until a PolyHIPE material was obtained.

Table 5.1 Experiments carried out with the OSS system and (meth) acrylate - based monomers

Monomers	Amount (g)	Surfactant	Amount (g)	Observations
MMA Styrene DVB	2.0 7.0 1.0	S20 CTAB DDBSS	0.63 0.04 0.03 Total = 7 %w/w	No HIPE formed
EHA Styrene DVB	8.0 1.0 1.0	S20 CTAB DDBSS	0.63 0.04 0.03 Total = 7 %w/w	No HIPE formed
EHA Styrene DVB	8.0 1.0 1.0	S80 CTAB DDBSS	0.63 0.04 0.03 Total = 7 %w/w	HIPE phase separated in oven during curing
EHA Styrene DVB	8.0 1.0 1.0	S80 CTAB DDBSS	0.83 0.04 0.03 Total = 9 %w/w	HIPE more viscous. PolyHIPE formed
MMA Styrene DVB	4.0 5.0 1.0	S80 CTAB DDBSS	0.83 0.04 0.03 Total = 9 %w/w	HIPE formed. 2.23 g water on surface of PolyHIPE after curing
MMA Styrene DVB	6.0 3.0 1.0	S80 CTAB DDBSS	0.83 0.04 0.03 Total = 9 %w/w	HIPE phase separated in oven during curing
MMA Styrene DVB	4.0 5.0 1.0	S80 CTAB DDBSS	0.93 0.04 0.03 Total = 10 %w/w	3.58 g of free water on PolyHIPE surface
MMA Styrene DVB	6.0 3.0 1.0	S80 CTAB DDBSS	0.93 0.08 0.06 Total = 10.7 %w/w	HIPE phase separated before all of the water could be added
MMA Styrene DVB	6.0 3.0 1.0	S80 CTAB DDBSS	1.03 0.04 0.03 Total = 11 %w/w	HIPE phase separated before all of the water could be added
Styrene EGDMA	9.0 1.0	S80 CTAB DDBSS	0.83 0.04 0.03 Total = 9 %w/w	HIPE formed. PolyHIPE materials produced

5.2.3 Preparation of PolyHIPE materials using a redox initiator

The monomer phase consisted of styrene (9 g, 86.4 mmol) and divinylbenzene (1 g, 7.68 mmol). To this was added an aqueous phase, which consisted of de-ionised water (90 g), calcium chloride dihydrate (1 g, 6.8 mmol), ascorbic acid (0.18 g, 1.02 mmol) and iron (II) sulfate heptahydrate (0.036 g, 0.13 mmol). The HIPE was then prepared as in **2.2.3**. After HIPE preparation, hydrogen peroxide (27.5 % w/w solution in water (1 g, 8.1 mmol) was added to the HIPE. The HIPE was then left under constant agitation for a further five minutes to allow for efficient mixing of the hydrogen peroxide within the emulsion. The HIPE was then cured at varying temperatures (**see table 5.2**). The PolyHIPE material produced was cleaned and dried as described in **2.2.3**.

Table 5.2 Redox initiator conditions for the preparation of S/DVB PolyHIPE materials

Sample code	Initiators	Amount (g)	Curing temperature (°C)
162RJC	Ascorbic acid Iron (II) sulfate Hydrogen peroxide	0.18 0.036 1	60
163RJC	Ascorbic acid Iron (II) sulfate Hydrogen peroxide	0.18 0.036 1	Room temperature
164RJC	Potassium persulfate Sodium metabisulfite	0.2 0.2	60
165RJC	Cobalt (II) (before HIPE preparation) Iron (II) sulfate Hydrogen peroxide	0.18 0.036 1	60
166RJC	Cobalt (II) (after HIPE preparation) t-butyl peroxide	0.2 0.67	60
201RJC	Ascorbic acid Iron (II) sulfate Hydrogen peroxide	0.18 0.036 1	80
203RJC	Ascorbic acid Iron (II) sulfate Hydrogen peroxide	0.18 0.036 1	100
204RJC	Iron (II) sulfate Hydrogen peroxide	0.036 1	60

5.3 Results and discussion

5.3.1 Optimisation of surfactant system

Figure 5.2 shows an ESEM image of the morphology of the S/DVB PolyHIPE material prepared with the OSS described in **5.2.2.1**.

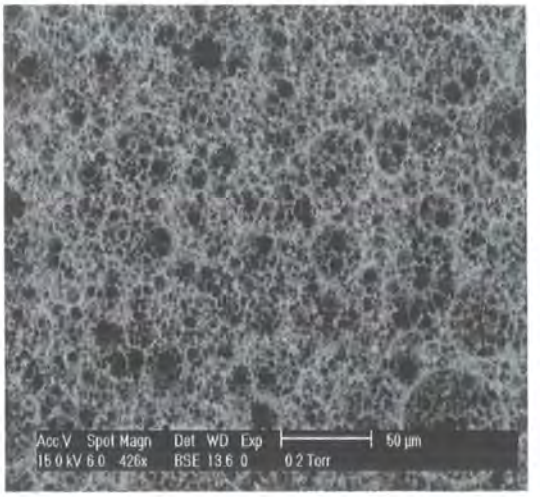

Figure 5.2 *ESEM of a S/DVB PolyHIPE material prepared using the OSS system.*

The morphology is the open-cellular structure expected for a S/DVB PolyHIPE material as shown in **figure 1.5**. However the S/DVB PolyHIPE material prepared using the OSS shows a greater void/interconnect size distribution compared to the S/DVB material prepared using Span 80. This effect could possibly be due to the presence of coalescence by rupture of the thin surfactant films between the droplets. There is also a presence of larger interconnecting windows, producing a more open network PolyHIPE material, compared to the standard S/DVB material. As discussed in **chapter 1** more stable emulsions will have thinner surfactant films separating the droplets and therefore larger interconnects. It cannot be determined conclusively whether the OSS system is producing a more stable emulsion compared to Span 80. The presence of a small number of larger voids (~ 50 µm) establishes some doubts, but the increase in open-cell nature and larger interconnect size suggests heavily that it is. The S/DVB material prepared with the OSS felt tougher, especially when dry compared to the S/DVB material

prepared with Span 80 only. By observation and handling only the physical properties of the OSS material had improved compared to the S/DVB material prepared with Span 80. Although producing a S/DVB-based PolyHIPE material using the OSS was straight-forward, this was not the case when acrylate or methacrylate-based monomers were added to the monomer phase. When EHA and MMA were used no HIPE could be formed employing the OSS surfactant formulation used to prepare the S/DVB material. When Span 80 replaced the surfactant Span 20 at the same weight percent, a HIPE could be formed, but this phase separated on curing. Increasing the Span 80 concentration to 8.3 % w/w, both EHA and MMA-based materials could be produced. **Figure 5.3** shows ESEM images of the 80 % w/w EHA-based PolyHIPE material using a co-surfactant ratio of 8.3 % S80, 0.4 % CTAB and 0.3 % DDBSS.

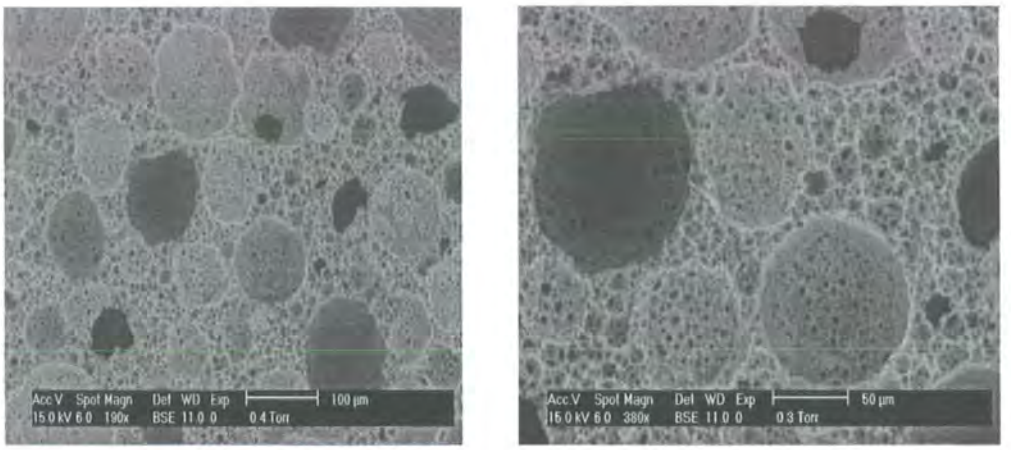

Figure 5.3 *Morphology of the 80/20 % EHA/styrene PolyHIPE material prepared with S80, CTAB and DDBSS.*

The ESEM images show a significant presence of larger voids (> 50 µm) compared to the 80 % EHA-based material prepared with only Span 80 (**see figure 4.3**). This suggests that coalescence is occurring and the HIPE produced with this co-surfactant mixture (9 % w/w monomer phase) produces a HIPE with greater instability compared to the HIPE prepared with just Span 80 (20 % w/w monomer phase). The EHA-based PolyHIPE monolith produced with this co-surfactant mixture had the presence of pimple

like holes on the surface of the material in contact with the PE bottle surface, which is also an indication of emulsion instability. As was the case with the S/DVB material prepared with the OSS, the EHA-based material felt tougher compared to the material prepared with Span 80. However, the EHA-based material prepared with the co-surfactant mixture still showed elastomeric behaviour, where the degree to which it could be deformed was significantly less compared to the material prepared with Span 80.

Figure 5.4 shows the morphology of the 40 % w/w MMA-based PolyHIPE material prepared with a co-surfactant system containing 8.3 % Span 20, 0.4 % CTAB and 0.3 % DDBSS.

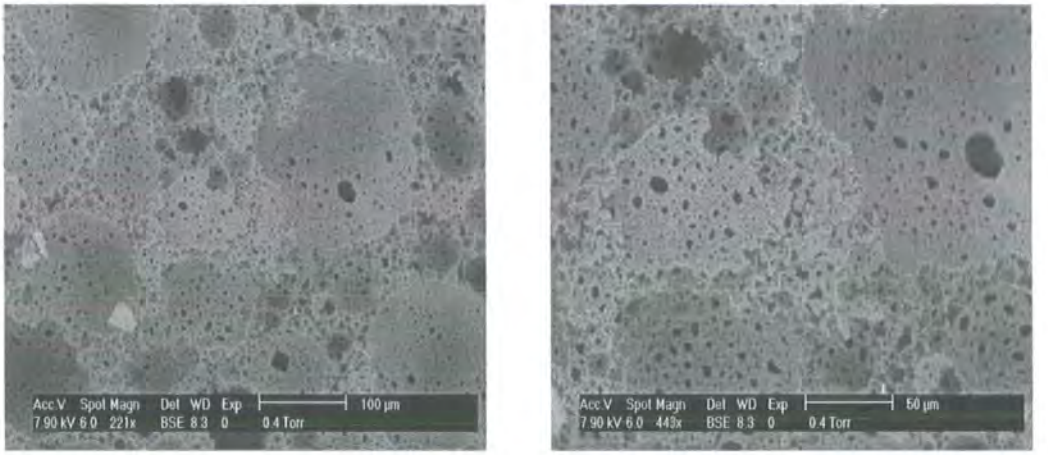

Figure 5.4 *MMA-based PolyHIPE material prepared with a co-surfactant composition of 8.3 % Span 80, 0.4 % CTAB and 0.3 % DDBSS.*

The PolyHIPE material produced was of low porosity/small interconnect size and open-cell nature compared to the standard morphology of the S/DVB PolyHIPE material (**see figure 1.5**). The large voids present (50-125 µm) indicate coalescence and emulsion instability. When Span 80 was used as the sole surfactant a low porous MMA-based PolyHIPE material was also produced (**see chapter 4, figure 4.9**). There was also a presence of large voids (~ 30-50 µm) when Span 80 was used as the sole surfactant, although the void size was less than that prepared with the co-surfactant mixture,

indicating that even though the HIPE prepared with 20 % w/w Span 80 showed signs of instability, it produced a more stable emulsion than that prepared with the co-surfactant system.

Increasing the Span 80 concentration in the co-surfactant mixture had a detrimental effect on the HIPE stability effect and the morphology of the material. **Figure 5.5** shows the morphology of the 40 % MMA-based PolyHIPE material prepared with a co-surfactant concentration of 9.3 % Span 80, 0.4 % CTAB and 0.3 % DDBSS.

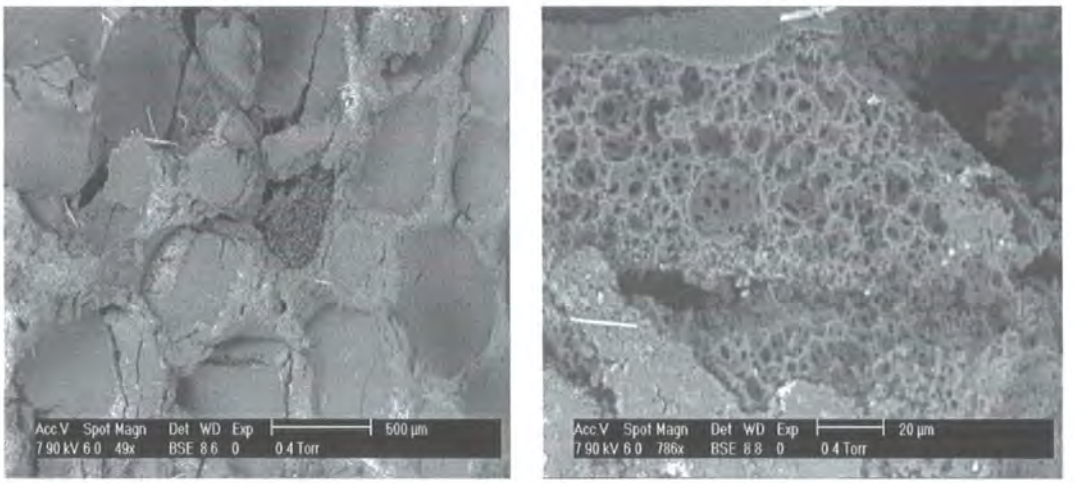

(a) (b)

Figure 5.5 *Morphology of the MMA-based PolyHIPE material prepared with a co-surfactant composition of 9.3 % Span 80, 0.4 % CTAB and 0.3 % DDBSS.*

The PolyHIPE material is now almost 100 % closed cell material with only small areas of open-cell structure existing as shown by the ESEM image in **figure 5.5 (b)**. This is similar to the closed-cell morphology obtained for S/DVB PolyHIPE materials at low Span 80 concentrations as reported by Williams et al. [67]. Further increases in both the non-ionic and ionic surfactant concentration within the co-surfactant mixture and the salt concentration in the aqueous phase showed no improvement in the homogeneity of both the morphology and the PolyHIPE monolith itself.

The co-surfactant mixture was also used to prepare a PolyHIPE material consisting of 90 % styrene with 10 % EGDMA as cross-linker. The morphology of the S/EGDMA material prepared using a co-surfactant composition of 8.3 % Span 80, 0.4 % CTAB and 0.3 % DDBSS is shown in **figure 5.6**.

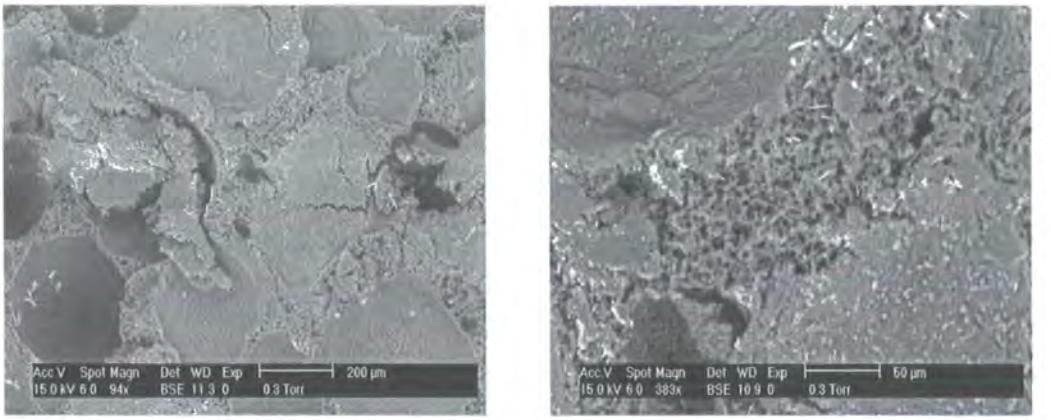

(a) (b)

Figure 5.6 The *morphology of the 90/10 S/EGDMA PolyHIPE material, prepared using a co-surfactant composition of 8.3 % Span 80, 0.4 % CTAB and 0.3 % DDBSS.*

The 90/10 styrene/EGDMA material is almost completely closed-cell with only a small degree of open-cellular structure present as shown **in figure 5.6 (b)**. This is compared to the 90/10 styrene/EGDMA material prepared from 20 % Span 80 which had an open-cellular interconnected structure (**see figure 4.11**). In the case of both the MMA- and EGDMA-based PolyHIPE materials prepared with the co-surfactant system, the surface hardness had noticeably increased compared to the materials prepared with Span 80. This suggests that either completely removing or decreasing the amount of Span 80 present as surfactant or co-surfactant can lead to a possible improvement in the mechanical properties of the material.

5.3.2 Preparation of PolyHIPE materials using a redox initiator

The advantage of using a redox initiator is that it does not require thermal energy to produce a solid PolyHIPE monolith and can produce radicals that will cure a HIPE at

room temperature. This is compared to potassium persulfate initiator, which needs a certain amount of thermal energy to dissociate the O-O bond to produce radicals that will propagate and start polymerisation. A redox couple consisting of reducing agents iron (II) sulfate heptahydrate and ascorbic acid with an oxidising agent hydrogen peroxide was compared at different temperatures to the standard water-soluble initiator potassium persulfate.

Table 5.3 shows a comparison of the polymerisation times for both initiators at different temperatures.

Table 5.3 Polymerisation time at different polymerisation temperatures for the redox and potassium persulfate initiated PolyHIPE materials.

Redox initiator (iron (II), ascorbic acid and hydrogen peroxide		Potassium persulfate	
Temperature (°C)	Polymerisation time (hours)	Temperature (°C)	Polymerisation time (hours)
Room temperature	72	Room temperature	Left for 72 hours, no PolyHIPE formed
60	4	60	24
80	2.5	80	5
100	1.75	100	4

From **table 5.3** it can be observed that the redox initiator has a more rapid polymerisation time at all temperatures used compared to the potassium persulfate initiator. The extent of the difference decreases with increasing temperature. At higher temperatures there is a greater effect on the polymerisation time of the potassium persulfate initiated material. However at elevated temperatures (80-100 °C) the homogeneity of both the redox and potassium persulfate initiated PolyHIPE material produced was affected. There was a presence of pin holes/defects on the surface of the monliths caused by possible localised collapse of the emulsion. The fractured surface also contained large holes/defects within the material possibly due to trapped water vapour at polymerisation temperatures near or at 100 °C. This was similar to the observations discussed in **chapter 2** where sample homogeneity decreased with

increasing temperature. Therefore, although the polymerisation time for the potassium persulfate is rapid at high temperatures (80-100 °C), the quality of the sample produced decreases at these temperatures. The redox initiator produces a more homogenous/uniform material more rapidly at the standard curing temperature of 60 °C compared to the potassium persulfate initiator.

The morphology of the PolyHIPE materials produced with the redox couple containing iron (II) sulfate, ascorbic acid and hydrogen peroxide and the potassium persulfate initiated material produced at different temperatures are shown in **figures 5.7** and **5.8**.

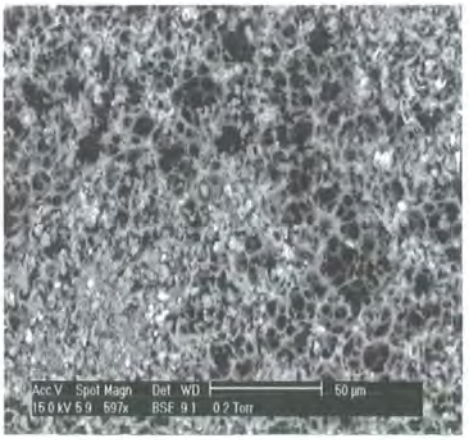

(a)

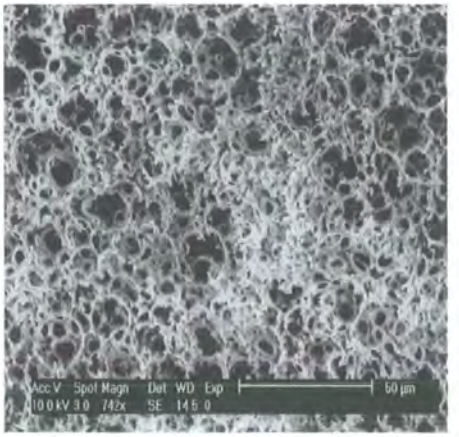

(b)

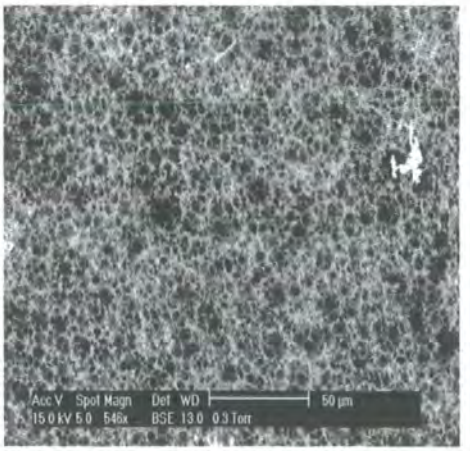

(c)

Figure 5.7 *ESEM images of the S/DVB PolyHIPE material prepared with a redox initiator: (a) room temperature, (b) 60 °C, (c) 80 °C*

The morphology of each redox-initiated material produced at different temperatures represents the normal open-cellular structure that would be expected for a PolyHIPE material. There is no significant difference in the void or interconnect size between the redox-initiated PolyHIPE materials cured at room temperature or 60 °C. Increasing the temperature from 60 to 80 °C resulted in a decrease in void size from around 20 to around 10 μm.

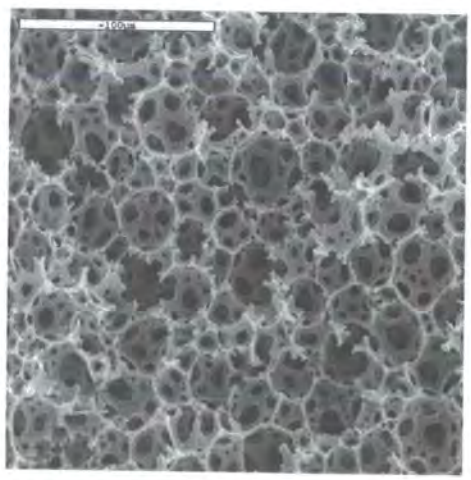

(a)

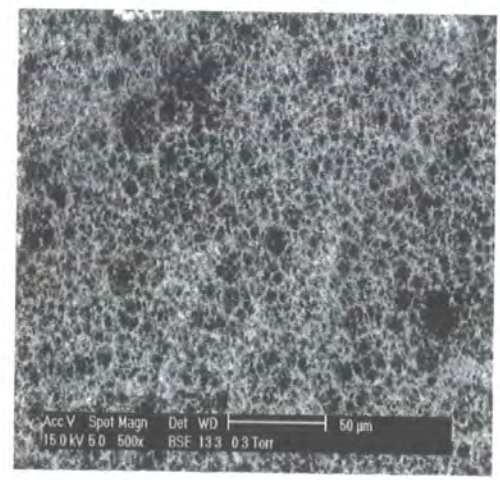

(b)

(c)

Figure 5.8 *Morphology of the S/DVB PolyHIPE material prepared with potassium persulfate as initiator, (a) 60 °C, (b) 80 °C, (c) 100 °C.*

In the case of the potassium persulfate initiated material, when the polymerisation temperature was increased from 60 to 80 °C there was a decrease in void size obtained from 25-30 to 10-15 μm. A further increase in temperature to 100 °C resulted in a further decrease in void size to around 5-10 μm. This effect is possibly due to the decrease in polymerisation time with increasing polymerisation temperature reducing the time available for coalescence of the emulsion droplets resulting in the reduction in void size. The redox-initiated PolyHIPE material cured at the standard temperature of 60 °C has a smaller void size compared to the potassium persulfate initiated material. This is due again to the decrease in polymerisation time compared to the persulfate initiated material, allowing less time for coalescence. At higher temperatures (80 °C) there is no significant difference in the void size between the two different initiated materials. This is due to a reduction of the polymerisation time of the potassium persulfate initiated material towards the polymerisation time of the redox-initiated material at that temperature.

It was thought the role of the ascorbic acid within the redox couple was to act as a catalyst re-producing Fe (II) from Fe (III) after oxidation of the Fe (II) with hydrogen peroxide. When the ascorbic acid was removed from the redox couple there was no change in the polymerisation time at 60 °C. The role of the ascorbic acid is therefore unclear. This redox system was discovered in the patent literature to produce EHA-based PolyHIPE materials [46]. The reaction scheme for the production of hydroxyl radicals that will initiate vinyl polymerisation [125] is shown in **figure 5.9**.

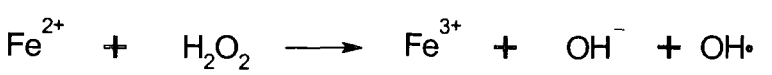

Figure 5.10 *Reaction for the production of hydroxyl radicals from a ferrous salt and hydrogen peroxide* [125].

The ascorbic acid present in the initiator was replaced with a cobalt (II) complex, another possible redox component. There was no significant difference in polymerisation time achieved with this blend compared to the potassium persulfate at 60 °C (24 hours). In addition replacing the ascorbic acid with the cobalt (II) complex reduced the effect of the redox initiator by increasing the polymerisation time. It is unclear how the three-component redox system is working, as the complete removal of the ascorbic acid resulted in no effect on the polymerisation time, but the replacement of the ascorbic acid with a different reducing agent such as a cobalt (II) complex had an adverse effect on the polymerisation time. **Figure 5.10** shows the morphology of the S/DVB material produced with the cobalt (II), iron (II) and hydrogen peroxide redox initiator. It is possible that the cobalt (II) complex is not as effective a reducing agent as either the ascorbic acid or the iron (II) salt due the cobalt (II) complex sterically hindering the attack of the O-O bond on the hydrogen peroxide that produces the hydroxyl radicals.

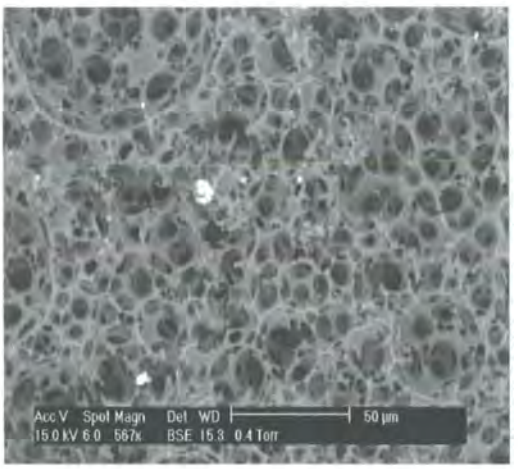

Figure 5.10 *ESEM image of the S/DVB PolyHIPE material prepared with a redox initiator containing 0.18 g cobalt (II) ethylhexanoate, 0.036 g iron (II) sulfate heptahydrate and 1 g hydrogen peroxide.*

The presence of the cobalt (II) complex has no adverse affect on the morphology of the PolyHIPE material. There is a decrease in void size compared to the potassium

persulfate initiated material at the same temperature. The cobalt (II) reducing agent was also used in combination with t-butyl peroxide as a redox couple. Again there was no significant difference in polymerisation time compared to the potassium persulfate initiated material (~ 24 hours), indicating that it was not as efficient an initiator as the iron (II), ascorbic acid and hydrogen peroxide combination. The morphology of the PolyHIPE material produced using cobalt (II) ethylhexanoate and t-butyl peroxide as initiator is shown in **figure 5.11**.

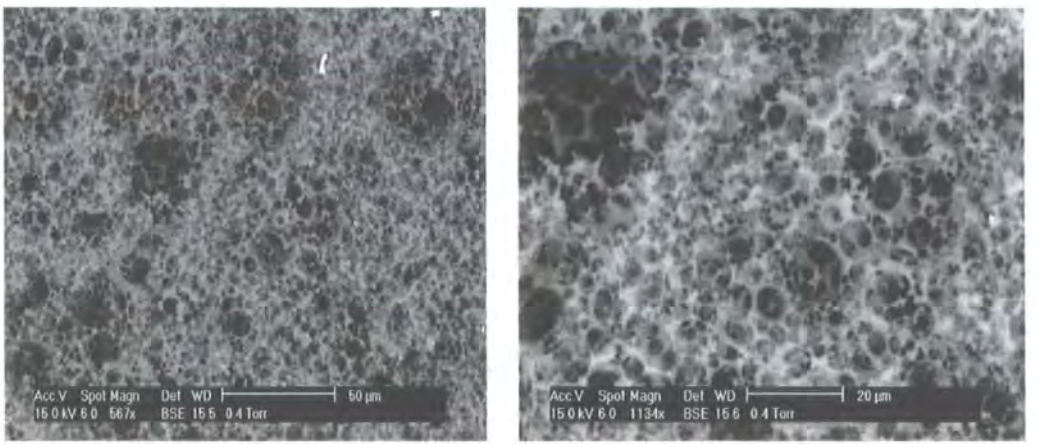

Figure 5.11 *Morphology of the S/DVB PolyHIPE material prepared with, cobalt (II) ethylhexanoate and t-butyl peroxide as initiator.*

The presence of the cobalt (II) complex and t-butyl peroxide as initiator resulted in a decrease in void size compared to the potassium persulfate initiated material although there was an increase in the polymerisation time compared to the iron (II) system. The formation of the open-cellular structure of a PolyHIPE material generally coincides with the gel-point of the emulsion where interconnects between adjacent droplets generally start to appear as discussed in **chapter 1**. It is possible that, even though the polymerisation times are significantly different, the gel points of the emulsions may not differ significantly. This was not investigated as decreasing the production or polymerisation time was the main aim of the investigation.

Another redox couple consisting of potassium persulfate and sodium metabisulfite was also used. The addition of metabisulfite had no effect on the polymerisation time compared to the S/DVB material prepared only with potassium persulfate. The morphology of the S/DVB PolyHIPE material prepared with the potassium persulfate/sodium metabisulfite redox couple is shown in **figure 5.13**.

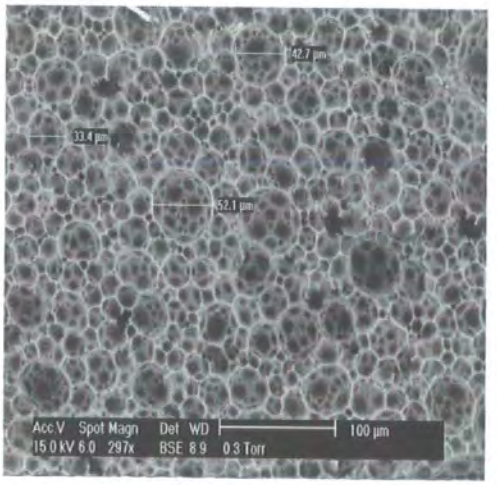

(a)

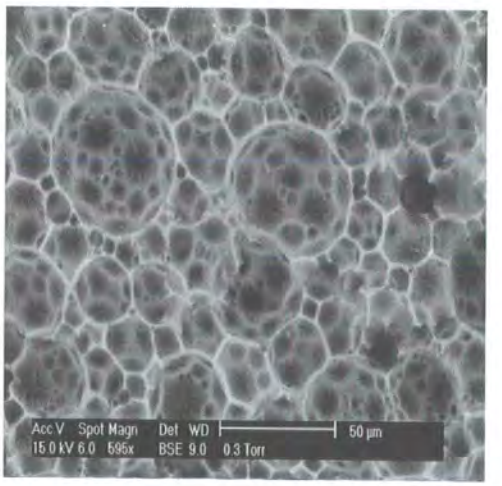

(b)

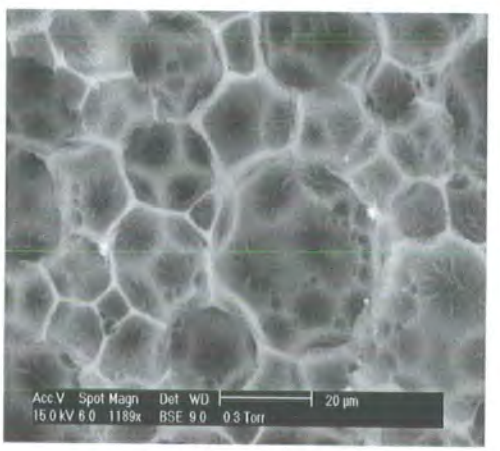

(c)

Figure 5.12 *ESEM images of the S/DVB PolyHIPE material prepared with a redox couple containing 0.2 g potassium persulfate and 0.2 g sodium metabisulfite.*

A presence of larger voids (~50 μm) was observed when the redox couple of potassium persulfate/sodium metabisulfite was used as initiator. **Figure 5.13 (c)** shows a higher magnification image of the same material. From the higher magnification image the

closed-cell nature of the material can be observed. A thin layer of material covers the cell walls of PolyHIPE material and no interconnecting holes are visible from the ESEM images. It is shown from the ESEM images that the addition of the sodium metabisulfite has adversely affected emulsion stability. The presence of larger voids of ~ 50 μm in size due to coalescence and the closed cell nature of the material are all indications of emulsion instability.

5.4 Conclusions

From the observations and results in this chapter it has been shown that it is possible to prepare S/DVB PolyHIPE materials with a so-called optimised surfactant system (OSS) containing Span 20, cetyltrimetylamoniumbromide and dodecylbenzenesulfonic acid, sodium salt. This surfactant system was present at a lower weight percent of the monomer phase (7 % w/w) compared to the standard emulsification conditions where Span 80 is present at 20 % w/w. It was unclear whether the OSS system gave rise to a more stable emulsion. From ESEM images it was suggested that the PolyHIPE material prepared with the OSS had a greater degree of open cell nature and a larger interconnecting window size compared to the standard S/DVB PolyHIPE material prepared with Span 80. The OSS sample qualitatively was found to have a greater surface hardness compared to the S/DVB material prepared from Span 80 only.

It was not possible to prepare methacrylate or acrylate based-PolyHIPE materials using this co-surfactant system. Exchanging the surfactant Span 20 for Span 80 at Span 80 amounts of 8.3 and 9.3 % w/w produced PolyHIPE materials from EHA, MMA and EGDMA. The methacrylate- and acrylate- based materials produced, as with the S/DVB material, were qualitatively found to have a greater surface hardness compared to their counterparts prepared with Span 80 only. This suggested that by either completely removing or decreasing the concentration of Span 80 in the surfactant system the

mechanical and physical properties of either the S/DVB or the (meth)acrylate based materials could be improved.

It was shown that it was possible to decrease the polymerisation time of a S/DVB HIPE by replacing the standard thermal initiator potassium persulfate with a redox initiator. The redox couple that provided the most rapid polymerisation time consisted of iron (II) sulfate heptahydrate, ascorbic acid and hydrogen peroxide. Increasing the polymerisation temperature resulted in a decrease in polymerisation time for both the redox and potassium persulfate initiated materials. From ESEM images it was also shown that there was a continuing decrease in void size of both the redox and potassium persulfate initiated material with increasing polymerisation temperature.

It was suggested that the role of the ascorbic acid was to act as a catalyst reproducing iron (II) by the reduction of iron (III) produced from the reduction of hydrogen peroxide. The removal of the ascorbic acid from the redox couple had no affect on the polymerisation time of the S/DVB PolyHIPE material at 60 °C. The replacement of the ascorbic acid with the reducing agent cobalt (II) ethylhexanoate resulted in a polymerisation time of 24 hours at 60 °C.

Other redox systems such as cobalt (II) ethylhexanoate and t-butyl peroxide produced open-cell S/DVB PolyHIPE materials but within the same time as the standard initiator potassium persulfate and not as rapidly as the ascorbic acid, iron (II) and hydrogen peroxide redox initiator. A redox couple of potassium persulfate and sodium metabisulfite produced a closed-cell S/DVB material within the same polymerisation time as potassium persulfate on its own.

Therefore for the production of uniform S/DVB PolyHIPE materials it was decided that the possible optimum conditions for production contained the OSS and the ascorbic acid,

iron (II) salt and hydrogen peroxide initiator system at a polymerisation temperature of between 60 and 80 °C.

Chapter 6

Flexural and compressive mechanical testing

6.1 Introduction

This chapter will detail the results obtained from the mechanical tests performed on selected 90 % void (0.1 gcm^{-3}) PolyHIPE materials. This will include the three-point bend tests on the fibre-reinforced PolyHIPE materials and the compressive tests performed on the acrylate and methacrylate-based PolyHIPE materials. The flexural and compressive properties of the PolyHIPE material prepared with the optimised surfactant system (OSS) will also be detailed.

** This is a nominal porosity and is calculated from the water/oil ratio e.g. 90/10 water/oil is a 90 % void material.*

6.2 Experimental

6.2.1 Flexural (three point bend) tests

The flexural modulus of elasticity and the flexural strength of the PolyHIPE materials tested were determined following the method described in BS 4370 [126].

6.2.1.1 Materials

The PolyHIPE materials were prepared and dried as described in **3.2.3.2**.

6.2.1.2 Measurement of dimensions and density

The materials were cut into five bars as outlined in **3.2.3.2**. The dimensions are as follows,

350 mm –length

50 mm –width

25 mm –thickness

The dimensions were measured with a rule accurate to +/- 0.5 mm. The mass of each bar was measured with a balance, which had an accuracy of at least +/- 0.5 mg. The densities were then calculated using mass/volume measurements and were expressed in gcm^{-3}.

6.2.1.3 Instrumentation

The three-point bend tests were carried out on an Instron 4302, with a 2kN load cell and a crosshead speed of 20 $mmmin^{-1}$. The span length (L) was 300 mm.

6.2.1.4 Procedure

The test specimens were placed symmetrically on the supports as shown in **figure 6.1.**

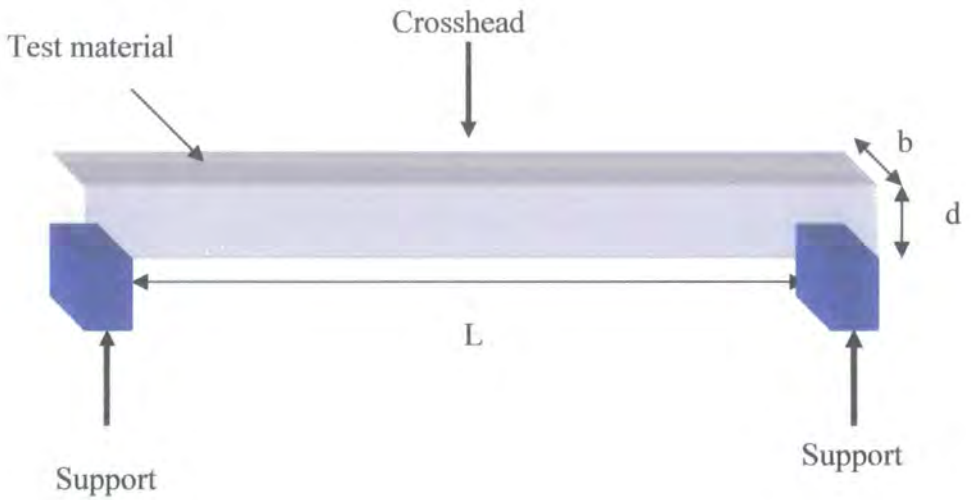

Figure 6.1 *Three-point bend test set-up.*

The force/deformation curve is then obtained and is shown in **figure 6.2**. The testing is then stopped once fracture has been obtained.

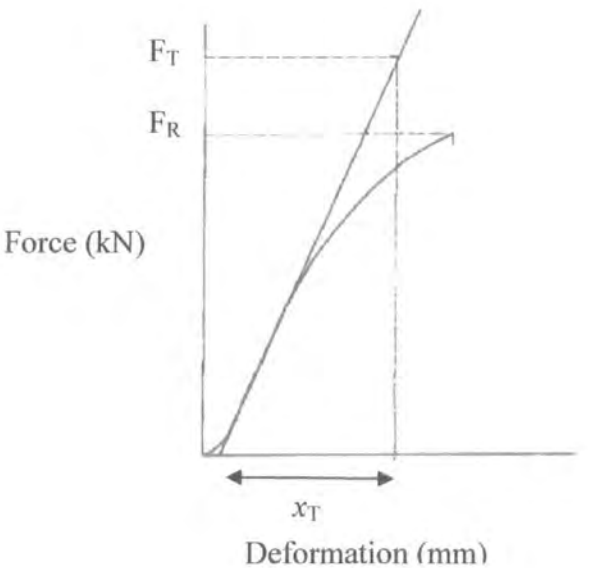

Figure 6.2 *Typical force/deformation curve for 0.1 gcm^{-3} PolyHIPE material.*

The flexural modulus, E is then calculated using **equation 6.1**,

$$E = \frac{L^3 F_T \times 10^6}{4bd^3 x_T} \qquad \textbf{Equation 6.1}$$

where

F_T = Force (kN)

x_T = corresponding deformation (mm)

L = span (mm)

b = specimen width (mm)

d = specimen thickness (mm)

The flexural strength, is then calculated using **equation 6.2**.

$$R = \frac{1.5 F_R L \times 10^6}{bd^2} \qquad \textbf{Equation 6.2}$$

where

F_R = maximum force applied (kN)

L = span (mm)

b = specimen width (mm)

d = specimen thickness (mm)

6.2.2 Compression tests

To determine the compressive strength and modulus of the core materials the method outlined in ASTM C365-00 [127] was used.

6.2.2.1 Materials

The PolyHIPE materials tested were prepared and dried as outlined in **4.2.1.2, 4.2.2.2**.

6.2.2.2 Measurements of dimensions and density

The samples were cut into cubes of 10 mm x 10 mm x 10 mm. The dimensions were measured to the nearest 0.25 mm using vernier calipers. The weight of each test sample was measured to the nearest 0.1 g and the density calculated using mass/volume measurements and was expressed in gcm^{-3}.

6.2.2.3 Instrumentation

The samples were tested on an Instron 4302 with a 1 kN load cell and a crosshead speed of 2 $mmmin^{-1}$.

6.2.2.4 Procedure

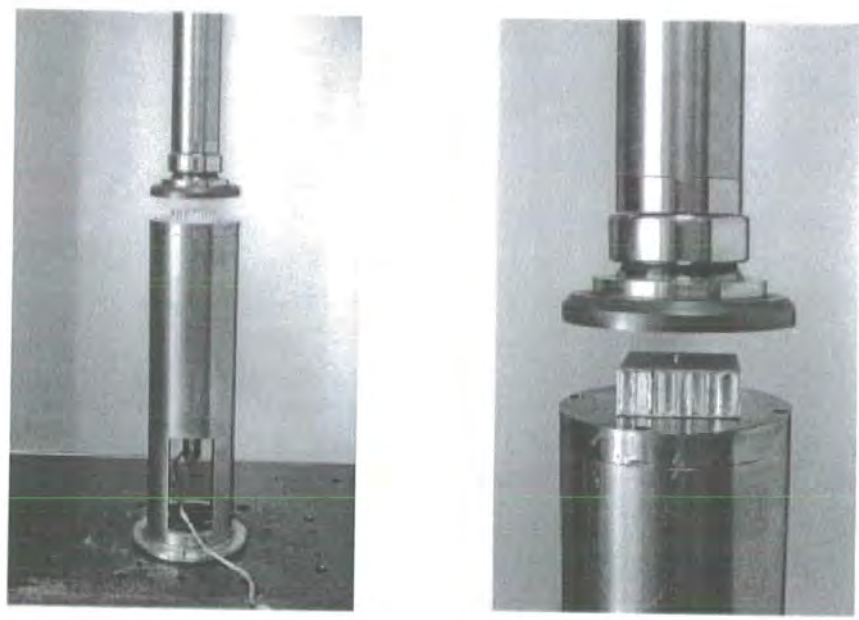

Figure 6.3 *Compressive test set-up.*

Figure 6.4 shows a typical load/extension curve for compression testing.

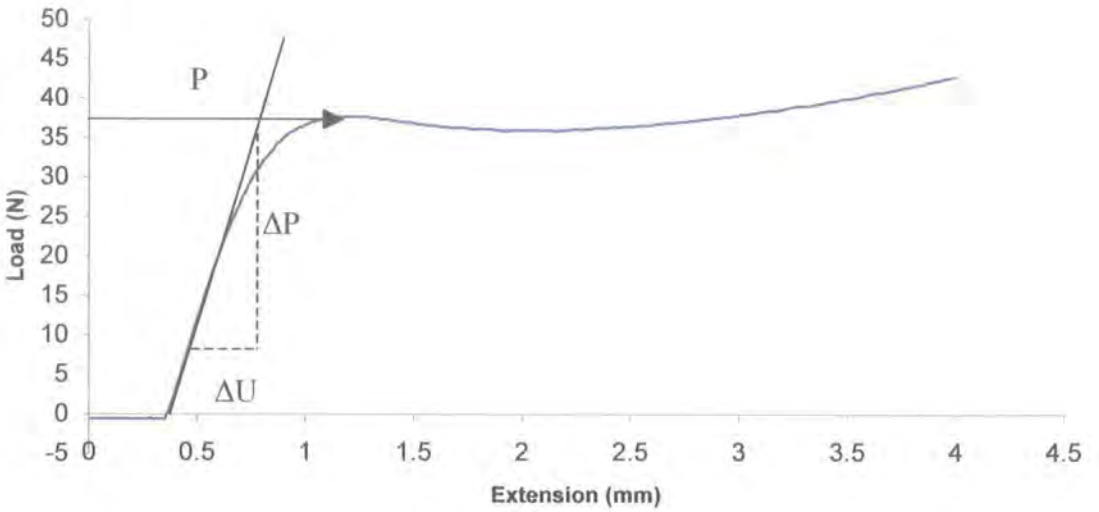

Figure 6.4 *A typical load/extension curve for compression testing of 0.1 gcm^{-3} PolyHIPE material.*

The flatwise compressive strength and modulus are calculated from **equations 6.3 and 6.4** .

$$\sigma = \frac{P}{A}$$ **Equation 6.3**

where:

σ = core compressive strength (MPa)

P = ultimate load (N)

A = cross sectional area (mm ^{2})

$$E = \frac{St}{A}$$ **Equation 6.4**

where:

E = core compressive modulus (MPa)

S = (ΔP/ΔU) slope of initial linear portion of load/extension curve

t = core thickness (mm)

6.3 Results and discussion

6.3.1 Flexural (three point bend) tests

Table 6.1 shows the results from the flexural tests on the PolyHIPE materials.

Table 6.1 Flexural tests results on the PolyHIPE materials

Sample name [a]	Mean density (gcm^{-3})	Mean Flexural Modulus, E [b] (MPa)	Mean Flexural strength, R [b] (MPa)
N	0.126	48.9 +/- 3.0	0.77 +/- 0.15
2.5 % V	0.139	46 +/- 7.6	0.84 +/- 0.14
5 % V	0.138	44.1 +/- 3.8	0.75 +/- 0.20
2.5 % PP	0.136	60 +/- 8.1	1.02 +/- 0.21
5 % PP	0.143	62.5 +/- 2.5	1.02 +/- 0.10
2.5 % K	0.143	62.7 +/ 6.2	1.0 +/- 0.13
5 % K	0.149	55.5 +/- 2.3	0.92 +/- 0.09
10 % K	0.155	69.8 +/- 12.6	0.81 +/- 0.21
OSS	0.128	68.8 +/- 6.3	1.51 +/- 0.20

a: N = normal 90/10 S/DVB PolyHIPE with 20 % Span 80, V = viscose reinforced-PolyHIPE, PP = polypropylene-reinforced PolyHIPE, K = Kevlar-reinforced PolyHIPE, OSS = PolyHIPE prepared with optimised surfactant system.

b: expressed as +/- standard deviation

6.3.1.1 Fibre-reinforced PolyHIPE materials

Figure 6.5 shows the force-deformation (extension) curves obtained for the normal 90/10 S/DVB PolyHIPE materials during the three-point bend tests.

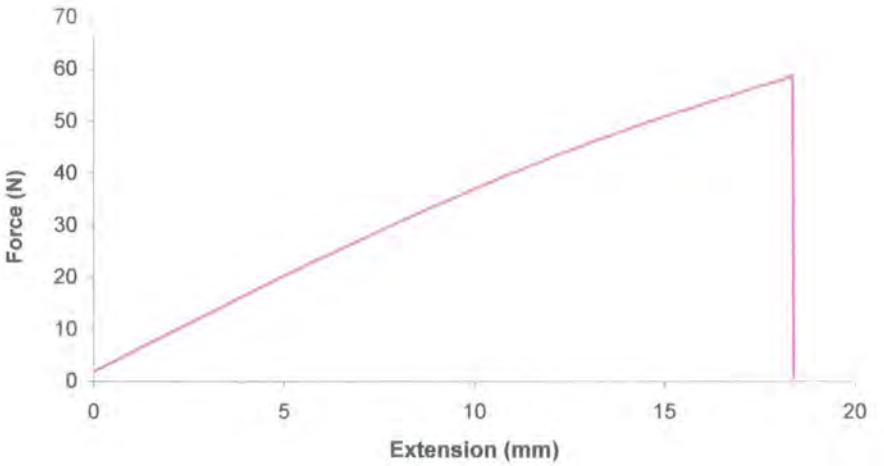

Figure 6.5 *Force-deformation (extension) graph for the normal S/DVB PolyHIPE material.*

The PolyHIPE material shows the behaviour of an elastic-brittle foam as described by Gibson and Ashby [6]. The material shows linear elastic behaviour up to the point where catastrophic brittle fracture by crack propagation occurs.

Figure 6.6 shows a graph comparing the flexural modulus of all the fibre-reinforced materials tested. From the bar chart, it is shown that the addition of fibres, with exception to the viscose, has resulted in an increase in the flexural modulus compared to the standard S/DVB PolyHIPE material. There is no significant difference between the values obtained for the PP and the Kevlar fibres at the 2.5 and 5 % w/w concentration loadings. The greatest increase is obtained when the Kevlar fibre concentration is at 10 % w/w.

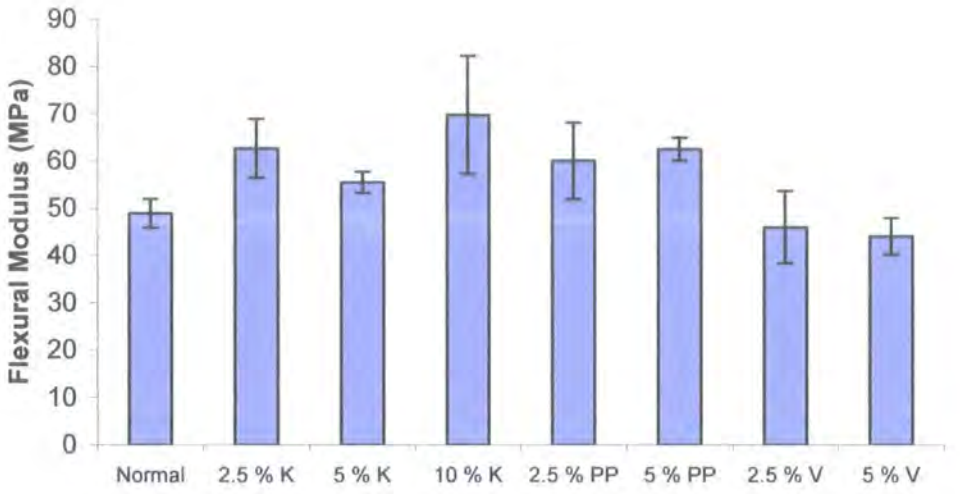

Figure 6.6 *Comparison of the flexural modulus of the fibre-reinforced PolyHIPE materials.*

The SEM images in **chapter 3** (**figures 3.6, 3.7 and 3.8**) showed that the Kevlar and PP fibres bonded more strongly to the cellular matrix than the viscose fibres, which showed the weakest interaction. This is reflected in the results obtained for the flexural modulus. The addition of the viscose fibres has no effect on the modulus values of the S/DVB PolyHIPE material, due to the weak interaction with the cellular matrix. The addition of the Kevlar and PP fibres results in an increase in modulus value due to the stronger interaction with the matrix. There is no significant difference in the modulus values for the Kevlar and PP fibres at the same concentration. The Kevlar fibre was expected to produce a material with a greater modulus value than the PP due to stronger bonding with PolyHIPE material as observed in the SEM images.

The increase in fibre concentration/volume was discussed in **chapter 1** and should also have an effect on the modulus value. The increase in fibre concentration should produce a material that is more rigid and brittle in nature, resulting in an increase in modulus. The Kevlar reinforced materials do show an increase in modulus from 2.5 % to 10 %

w/w concentration, but with an unexpected decrease for the 5 % w/w material. The PP reinforced material shows a slight increase in modulus when increasing the fibre concentration from 2.5 % to 5 %. With the viscose reinforced material there is no significant change when the concentration of fibres is increased from 2.5 % to 5 %.

Figure 6.7 shows a graph comparing the flexural strength of the fibre-reinforced materials

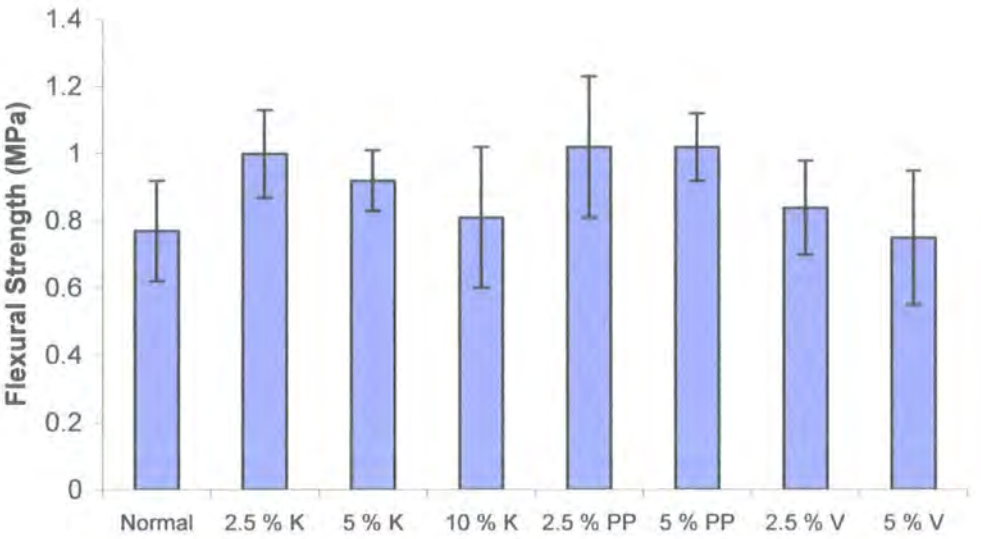

Figure 6.7 *Comparison of the flexural strengths of the fibre-reinforced PolyHIPE materials.*

Generally with the addition of fibres to the PolyHIPE material there is an increase in flexural strength compared to the fibre-free material. The Kevlar- and PP-reinforced materials show the greatest increase in flexural strength while the viscose-reinforced material, as with the modulus, shows no significant increase. With increasing Kevlar and viscose fibre concentration, there is a noticeable decrease in flexural strength. This could be due to the increasingly brittle nature of the material with increasing fibre volume, making the material more prone to crack propagation. The modulus is calculated from the linear elastic region of the force-deformation graphs. This region is dependent on the cell wall bending of the material where as the flexural strength is

determined from the stress at fracture. The more rigid the material with increasing fibre volume, the less deformation due to cell wall bending will occur and therefore there will be an increase in modulus value but fracture at a lower ultimate force.

6.3.1.2 Optimised surfactant system

Figure 6.8 shows a graph comparing the flexural modulus of the PolyHIPE material prepared with the optimised surfactant system, with the normal S/DVB PolyHIPE material prepared with Span 80 and the fibre-reinforced PolyHIPE materials

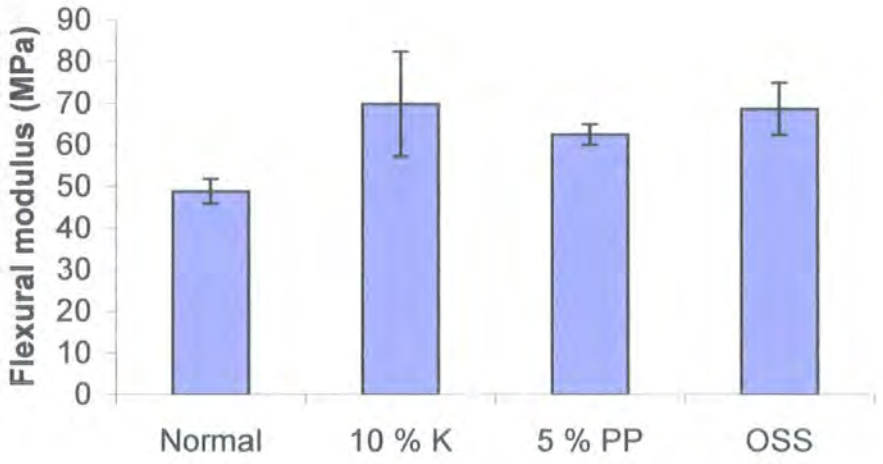

Figure 6.8 *Comparison of the flexural moduli of the PolyHIPE materials prepared using the surfactants Span 80 and the optimised surfactant system, with the fibre-reinforced PolyHIPE materials.*

The bar chart shows that replacing the surfactant Span 80 with the optimised surfactant system produces an increase in the flexural modulus of the material. This modulus value is roughly equal to the highest value obtained from the fibre-reinforced materials. **Figure 6.9** shows a graph the comparison of the flexural strengths of the same range of PolyHIPE materials.

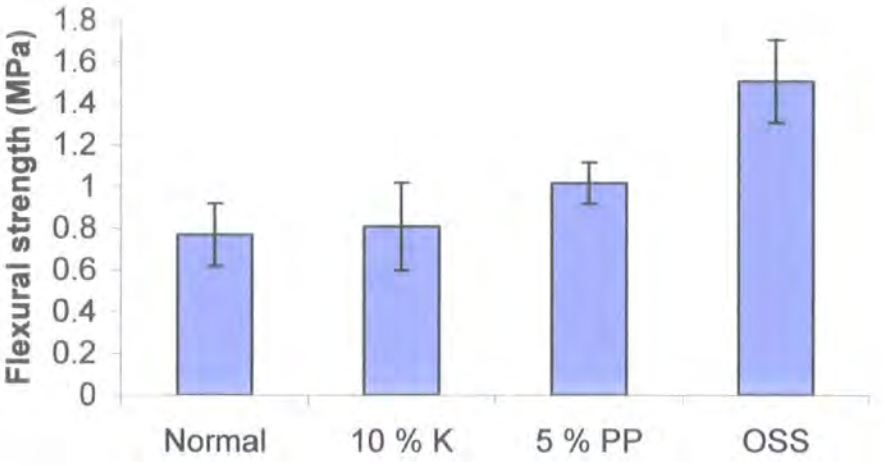

Figure 6.9 *Comparison of the flexural strengths of the PolyHIPE materials prepared with Span 80 and the optimised surfactant system with the fibre-reinforced PolyHIPE materials.*

The graph shows more than a two-fold increase in flexural strength in the PolyHIPE material when Span 80 is replaced with the optimised surfactant system. Significantly, the value for the OSS material is considerably higher than the values obtained for the best-performing fibre-reinforced materials. These values enhance the already reported observations that the surfactant Span 80 acts as plasticiser, weakening the PolyHIPE structure [67].

6.3.2 Compressive test results

Tables 6.2 and 6.3 show the results obtained from the compressive tests.

Table 6.2 Compressive test results for the PolyHIPE materials

Sample name [a]	Mean density (gcm^{-3})	Mean compressive modulus, E [b] (MPa)	Mean compressive strength, σ [b] (MPa)
Normal	0.116	16.71 +/- 1.95	0.707 +/- 0.074
20 % EHA	0.132	15.69 +/- 0.49	0.610 +/- 0.008
40 % EHA	0.153	0.646 +/- 0.31	0.112 +/- 0.005
60 % EHA	0.153	0.08 +/- 0.02	0.024 +/- 0.001
80 % EHA	0.141	0.018 (only one result)	0.016 (only one result)
20 % BA	0.134	17.92 +/- 2.81	0.780 +/- 0.032
40 % BA	0.128	17.51 +/- 3.08	0.912 +/- 0.013
60 % BA	0.150	0.623 +/- 0.046	0.054 +/- 0.005
80 % BA	0.149	0.141 +/- 0.034	0.024 +/- 0.005
20 % BMA	0.133	17.72 +/- 3.76	0.976 +/- 0.007
40 % BMA	0.128	16.66 +/- 5.01	0.871 +/- 0.003
60 % BMA	0.129	12.33 +/- 1.04	0.546 +/- 0.019
80 % BMA	0.104	16.88 +/- 1.53	0.663 +/- 0.063
20 % MMA	0.130	18.50 +/- 0.24	1.18 +/- 0.038
40 % MMA	0.126	31.50 +/- 4.4	1.71 +/- 0.02
OSS	0.118	24.52 +/- 1.16	1.16 +/- 0.094
5 % w/w silica gel	0.137	19.12 +/- 0.67	0.947 +/- 0.024
5 % w/w aluminium	0.101	13.42 +/- 0.77	0.770 +/- 0.050

a: normal = standard 90/10 S/DVB PolyHIPE material, EHA = 2-ethylhexyl acrylate, BA = n-butyl acrylate, BMA = butyl methacrylate, MMA = methyl methacrylate, OSS = PolyHIPE prepared with optimised surfactant system.

b: values expressed as +/- standard deviation

Table 6.3 Compressive test results for the PolyHIPE materials

Sample name [a]	Mean Density (gcm^{-3})	Mean compressive modulus, E [b] (MPa)	Mean compressive strength, σ [b] (MPa)
10 %EGDMA	0.102	15.00 +/- 0.96	0.753 +/- 0.04
20 % EGDMA	0.130	11.16 +/- 0.90	0.586 +/- 0.02
30 % EGDMA	0.126	14.91 +/- 2.55	0.599 +/- 0.07
10 % TMPTM	0.131	9.91 +/- 0.66	0.372 +/- 0.02
20 % TMPTM	0.133	4.55 +/- 1.57	0.209 +/- 0.02
70 S/ 20 MMA/ 10 EGDMA	0.126	22.29 +/- 2.00	1.20 +/- 0.08
10 % MPS	0.201	8.11 +/- 0.71	0.636 +/- 0.17

a: EGDMA = ethyleneglycol dimethacrylate, TMPTM = trimethylolpropane trimethacrylate, MPS = methacryloxypropyl trimethoxysilane.

b: values expressed as +/- standard deviation.

6.3.2.1 Acrylate- and methacrylate-based PolyHIPE materials

Figures 6.10 and **6.11** show the compressive modulus and strength results for the EHA based PolyHIPE materials.

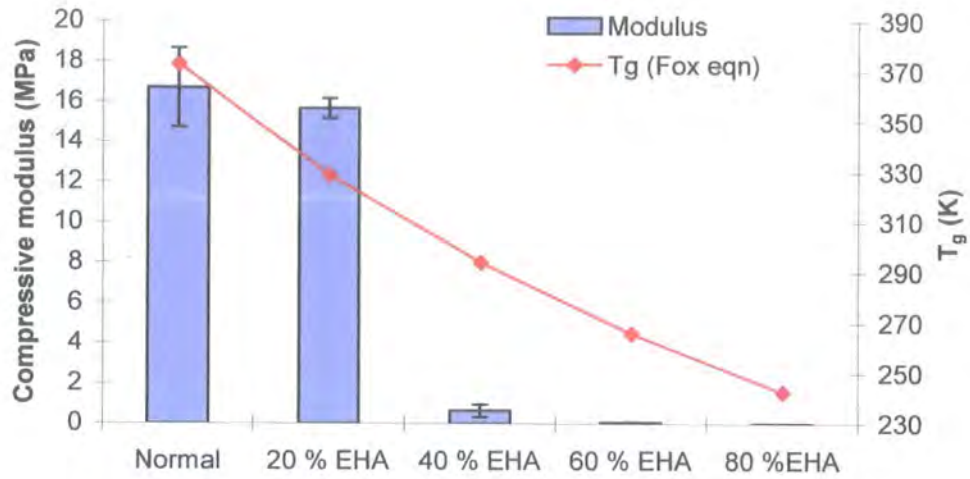

Figure 6.10 *A graph showing the compressive modulus trend for the EHA-based PolyHIPE material.*

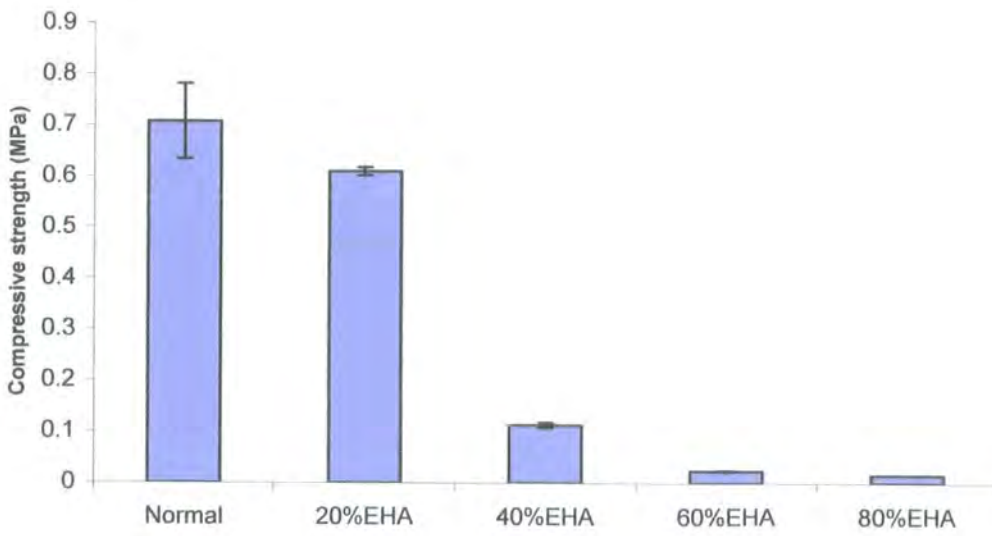

Figure 6.11 *A graph showing the compressive strength results for the EHA-based PolyHIPE materials.*

For the EHA-based material, the expected decrease in modulus and compressive strength is observed with increasing elastomer concentration. The most significant decrease occurs when the EHA concentration is increased from 20 to 40 % w/w. The compressive modulus values have also been compared to the estimated T_g values of the foam materials calculated using the Fox equation (**see chapter 1, equation 1.8**). The T_g values used for the homopolymers of styrene and EHA where 373 and 223 K respectively [128]. From the estimated T_g values calculated from the Fox equation, it can be predicted that the 20 % EHA material will be a glassy/rigid material at room temperature (T_g = 329 K). This is compared to the 40 % EHA material which is predicted to be elastomeric at room temperature (T_g = 294 K) and therefore accounts for large the drop in modulus when the EHA concentration is increased from 20 to 40 % w/w

Figures 6.12 and 6.13 show the compressive modulus and strength trend for the BA - based PolyHIPE materials.

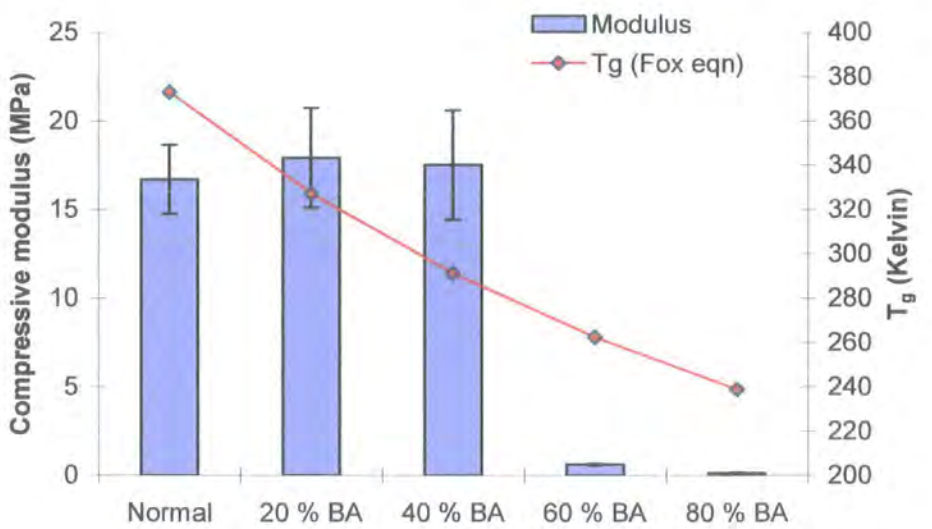

Figure 6.12 *Compressive modulus results for the BA-based PolyHIPE materials.*

For the BA-based PolyHIPE materials, there is no decrease in modulus value as expected from the decreasing T_g trend estimated from the Fox equation, with increasing

BA content. However there is a significant decrease in modulus value when the BA content is increased from 40 % to 60 % w/w. This is compared to the EHA-based materials where the drop in modulus occurred when the increasing the EHA content from 20 to 40 %. One hypothesis is the greater flexibility of the longer hexyl side chain compared to the shorter butyl side chain produces a more flexible material. However the reported T_g values [128] for the homopolymers of poly(n-butylacrylate) (219 K) and poly(2-ethylhexyl acrylate) (223 K) are similar. The addition of the ethyl branch to the hexyl side chain restricts rotation of the side chain bonds [31] and therefore increase the T_g and decrease flexibility compared to poly(n-hexyl acrylate) (216 K) [130] and poly(n-butyl acrylate). The Fox equation estimates that the 40 % BA material will be an elastomeric material at room temperature (T_g = 291 K), similar to the EHA-based materials, and therefore a decrease in modulus value would be expected. However this decrease did not occur until the content of BA used was 60 %. The reported copolymer reactivity ratios of styrene (r_1=0.96), EHA (r_2= 0.31) and styrene (r_1= 0.79) and BA (r_2 = 0.34) [130] are also similar. This suggests that at low concentrations of acrylate it is highly probable that no EHA or BA diads will exist, only styrene-EHA and styrene-BA sequences. At higher concentrations EHA and BA diads are more probable resulting in an enhancement in flexibility of the material. This however does not explain the increased rigidity of the BA-based materials at the same concentration as the EHA-based materials. Another possibility is the differing hydrophilicity of the two different acrylates. In **chapter 4**, it was observed that HIPEs containing BA were less stable, and produced PolyHIPE materials with larger voids, due to coalescence, compared to a HIPE containing EHA. As BA has a higher degree of hydrophilicity than EHA, it is possible that some of the BA may reside in the aqueous phase during polymerisation. This may not occur for EHA due to the greater hydrophobicity of the acrylate. This would result in a BA-based PolyHIPE material with an elastomer content less than that

of the EHA-based materials. Therefore the flexible nature of the EHA-based materials would be greater compared to the BA-based materials at the same acrylate content.

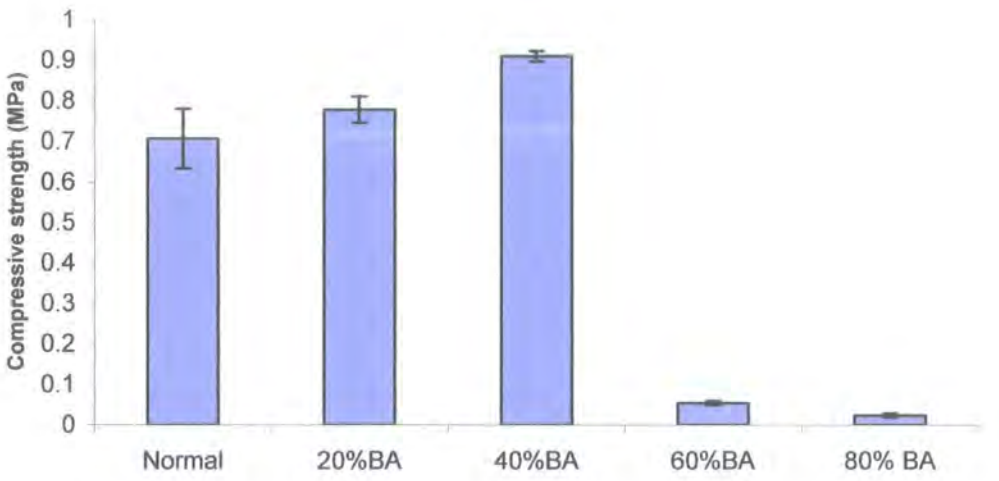

Figure 6.13 *A graph showing the compressive strength trend for the BA-based PolyHIPE materials.*

The trend for the compressive strength differs from that of the modulus. At initial low concentrations of BA (20 –40 % w/w) there is an increase in compressive strength of the normal S/DVB PolyHIPE material. The compressive strength is calculated from the plastic yield stress, σ^*_{pl} or the elastic collapse stress σ^*_{el} depending on whether the material is elastic-plastic or elastomeric in behaviour. The compressive strength trend shows that the presence of the BA at low concentrations reinforces the polymer in yield until the transition from possible elastic-plastic behaviour to more elastomeric behaviour at BA content of 60 % w/w. As discussed for the modulus values, at low acrylate concentrations it is highly probable that only styrene-BA sequences are present. The introduction of a flexible acrylate segment into the styrene chain may dissipate just enough energy to reinforce the polymer during yield at low concentrations until the transition from elastic-plastic to elastomeric occurs at higher concentrations, due to the greater probability of BA-BA diads being present. There is no significant difference

between the modulus values of the 20 and 40 % w/w BA materials compared to the standard material, suggesting that the BA has no effect on the bulk of the material within the elastic region at low concentrations. This reinforcement in strength is not observed with the EHA-based materials again suggesting that the shorter side chain BA is producing a stronger material at these acrylate concentrations.

Figures 6.13 and **6.14** show the compressive modulus and strength results for the BMA based PolyHIPE material.

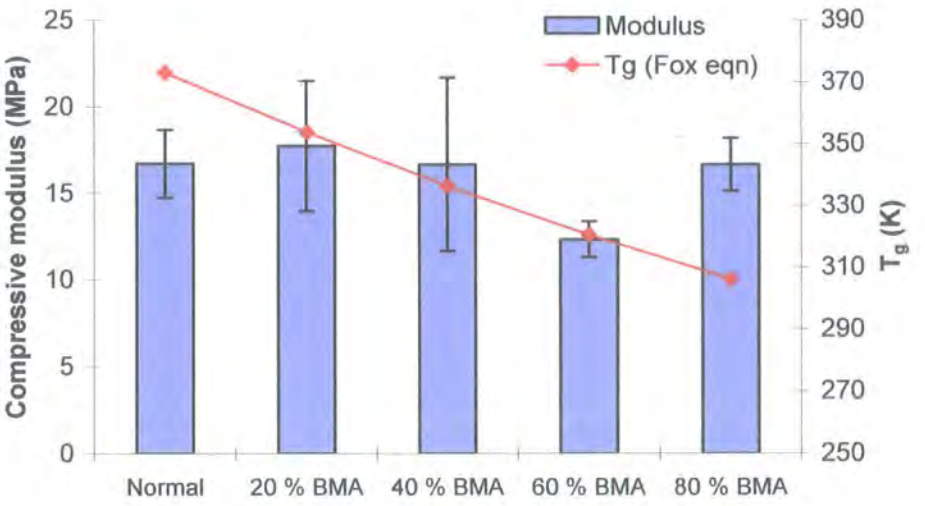

Figure 6.14 *Compressive modulus results for the BMA-based PolyHIPE materials.*

As with the BA- based materials, there is no significant change in modulus value of 20 and 40 % BMA materials compared to the normal PolyHIPE material. At 60 % BMA, the modulus is lower however. There is an unexpected value obtained for the 80 % BMA material that does not follow the expected decreasing trend. The T_g of the BMA-based materials decrease with increasing BMA content as estimated from the Fox equation but all the materials are estimated to be a rigid/glassy material at room temperature. The T_g values used for the homopolymers of styrene and BMA were 373 and 293 K respectively [128].

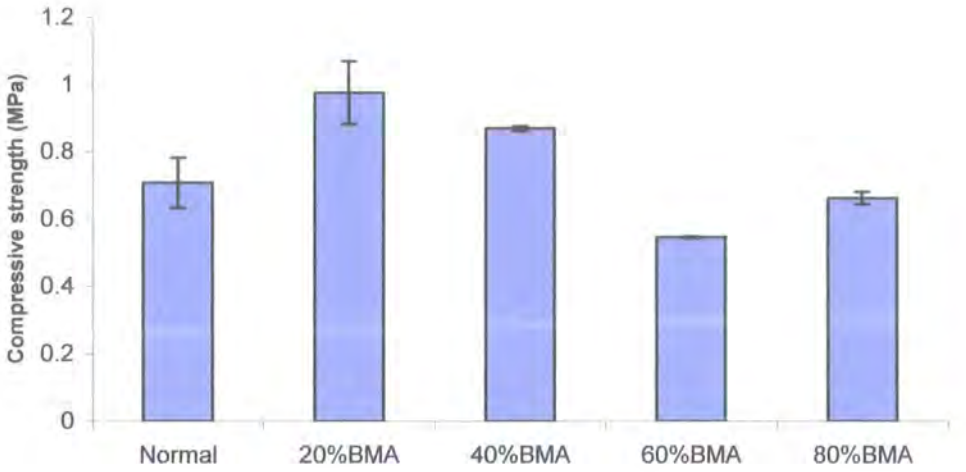

Figure 6.15 *Compressive strength results for the BMA-based PolyHIPE materials.*

Excluding the 80 % w/w BMA material, the expected decreasing trend in compressive strength with BMA concentration is observed. As was the case with the BA-based material, at initial low concentrations of BMA (20 and 40 % w/w) there is an increase in compressive strength compared to the standard S/DVB PolyHIPE material. However the increase obtained for the BMA-based materials is greater than that obtained with BA, due to the increased rigidity of BMA. The addition of the methacrylate at low concentrations initially reinforces the polystyrene material in yield until the majority of the copolymer consists of BMA where the compressive strength falls below that of the standard S/DVB due to the greater flexibility of poly(butyl methacrylate) compared to polystyrene. As occurred with the addition of BA to the system, at low concentrations of BMA the PolyHIPE is reinforced in yield but there is no effect on the bulk of the material within the elastic portion.

Figures 6.16 and **6.17** show the compressive modulus and strength trends for the MMA based PolyHIPE material.

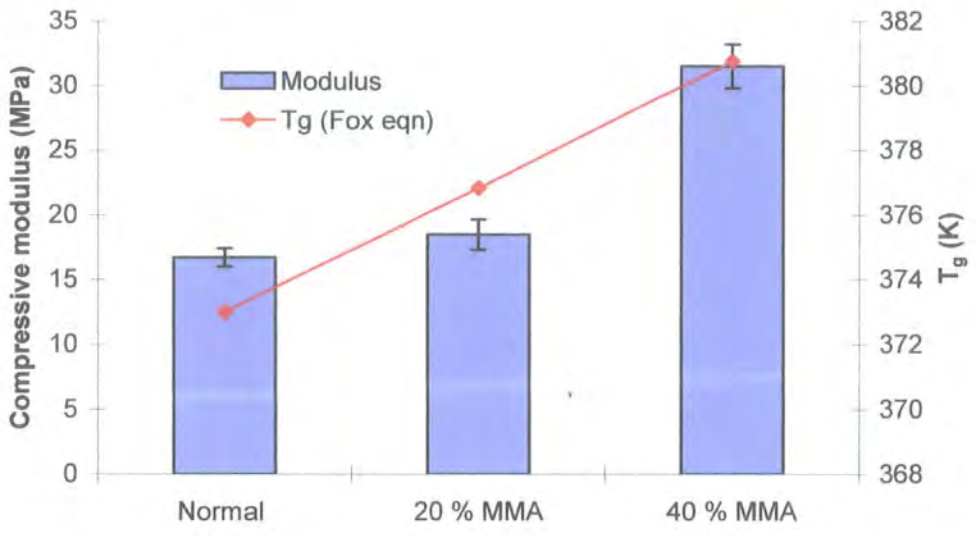

Figure 6.16 *Compressive modulus results for the MMA-based PolyHIPE materials.*

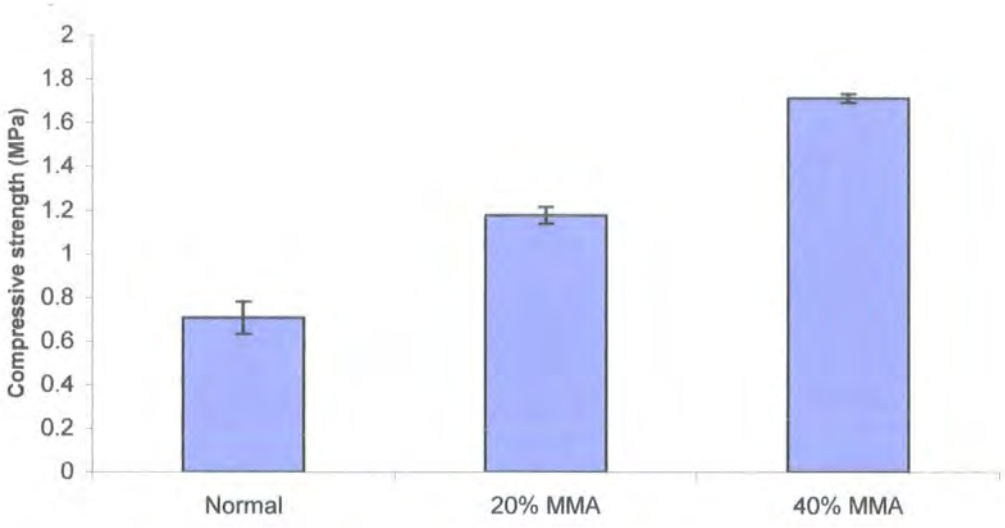

Figure 6.17 *Compressive strength results for the MMA-based PolyHIPE materials.*

The expected increase in modulus with increasing MMA concentration is observed due to the stronger/more rigid nature of the short MMA side group. At 20 % w/w concentration there is no significant difference in modulus value compared to the standard S/DVB PolyHIPE material. As discussed in **chapter 4**, the morphology of the 40 % MMA-based material was an open-cellular structure of low porosity/closed cell nature. This could account for the increase in compressive strength and modulus

compared to the 20 % w/w material, which exhibited the standard open-cellular structure of a S/DVB PolyHIPE material. Gibson and Ashby's work, [6] discussed in **chapter 1**, also described how closed-cell-type foam materials are stronger mechanically compared to open-cellular materials due to the added mechanism of cell face stretching.

As with the modulus, the compressive strength values increase with increasing MMA concentration. At 20 %w/w there is a significant increase in the strength value compared to the standard S/DVB PolyHIPE material. **Figures 6.18** and **6.19** show the compressive modulus and strength results for the different methacrylate- and acrylate- based PolyHIPE materials at 20 % w/w concentration.

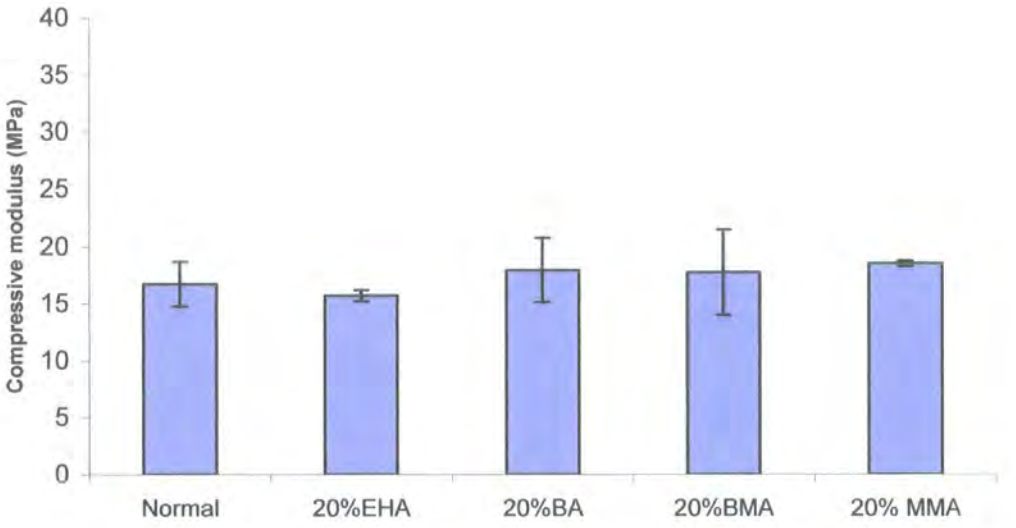

Figure 6.18 *Comparison of the compressive modulus results of the acrylate- and methacrylate-based PolyHIPE materials at 20 % w/w concentration.*

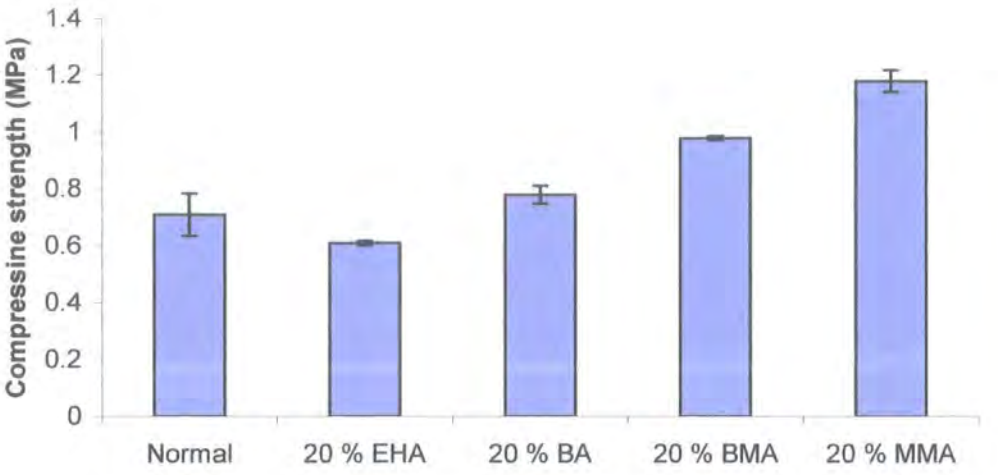

Figure 6.19 *A comparison of the compressive strength results of the methacrylate- and acrylate-based PolyHIPE materials at 20 % w/w concentration.*

At concentrations of 20 % w/w methacrylate and acrylate, there is no effect on the bulk properties of the material in the elastic portion, but from **figure 6.19** it can be observed that the addition of the acrylate and methacrylate monomers reinforces the foam material during yielding with the effect increasing from the longer side chain EHA to the shorter side chain MMA. The methacrylates show an increasing effect compared to the acrylates due to their more rigid, stronger nature caused by the presence of the backbone methyl group reducing chain flexibility.

6.3.2.2 Optimised surfactant system

The flexural properties of the S/DVB PolyHIPE material prepared using the OSS were evaluated in **6.3.1.2**. The compressive modulus and strength values of the OSS material were also compared to the normal S/DVB PolyHIPE material prepared with Span 80 and the 40 % MMA-based PolyHIPE material. These values are shown in **figures 6.20** and **6.21**.

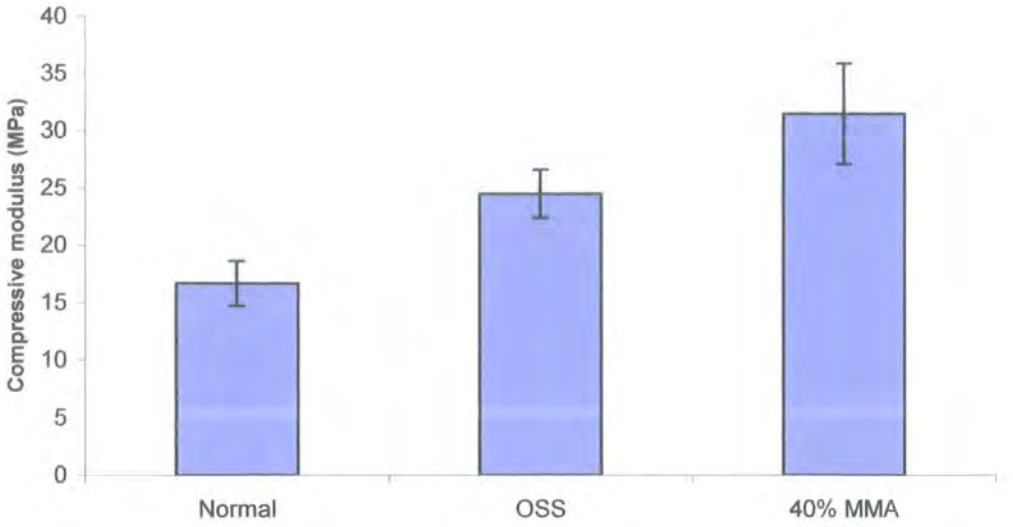

Figure 6.20 *Comparison of the compressive modulus values of the normal S/DVB PolyHIPE material (20 % Span 80), the PolyHIPE material prepared with optimised surfactant system and the 40 % MMA-based PolyHIPE material.*

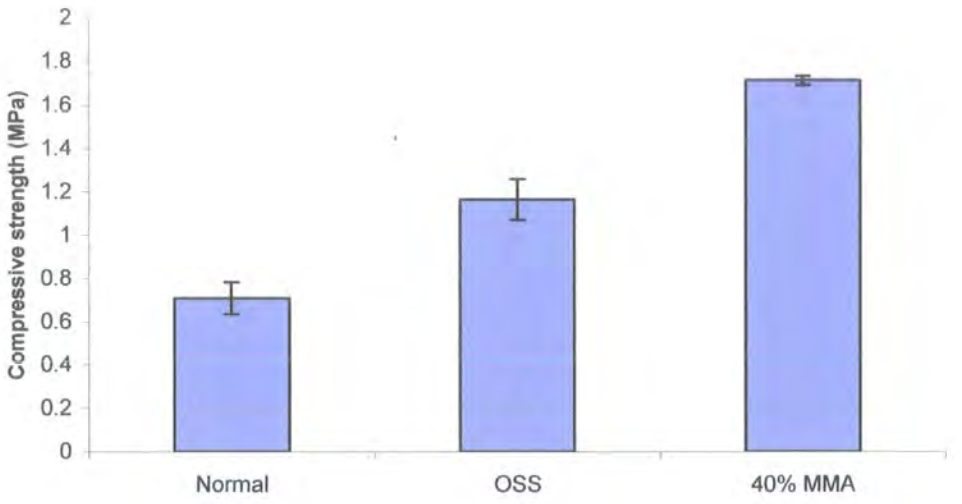

Figure 6.21 *Comparison of the compressive strengths of the normal S/DVB PolyHIPE material (20 % Span 80), the PolyHIPE material prepared with the optimised surfactant system and the 40 % MMA-based PolyHIPE material.*

The replacement of the surfactant Span 80 with the OSS resulted in an increase in modulus and almost a two-fold increase in compressive strength compared to the S/DVB material prepared with 20 % Span 80. The replacement of the Span 80 with the

OSS removes the plasticisation effect of the Span 80 and produces a stronger foam material in both flexure and compression.

6.3.2.3 The use of alternative of multifunctional cross-linkers

Figures 6.22 and **6.23** show the compressive modulus and strength results for the S/EGDMA-based PolyHIPE materials.

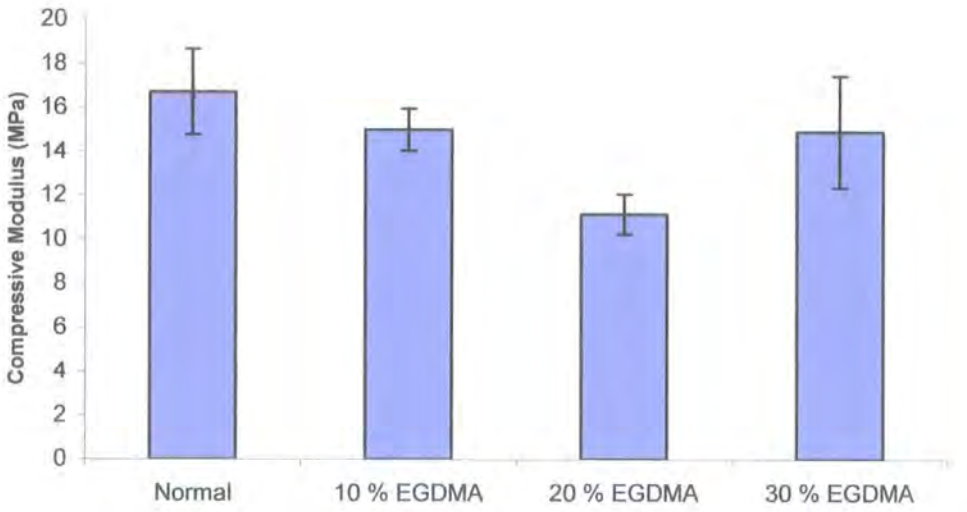

Figure 6.22 *Compressive modulus values of the S/EGDMA PolyHIPE material and the standard S/DVB PolyHIPE material.*

The compressive modulus of the PolyHIPE material decreases slightly when DVB at 10 % w/w is replaced with the monomer EGDMA at the same concentration. This suggests that the presence of the EGDMA instead of DVB is producing a weaker or more flexible material. With increasing EGDMA concentration there is a further decrease in modulus value at 20 % w/w but then an increase in value similar to the 10 % w/w when the EGDMA concentration is increased to 30 % w/w.

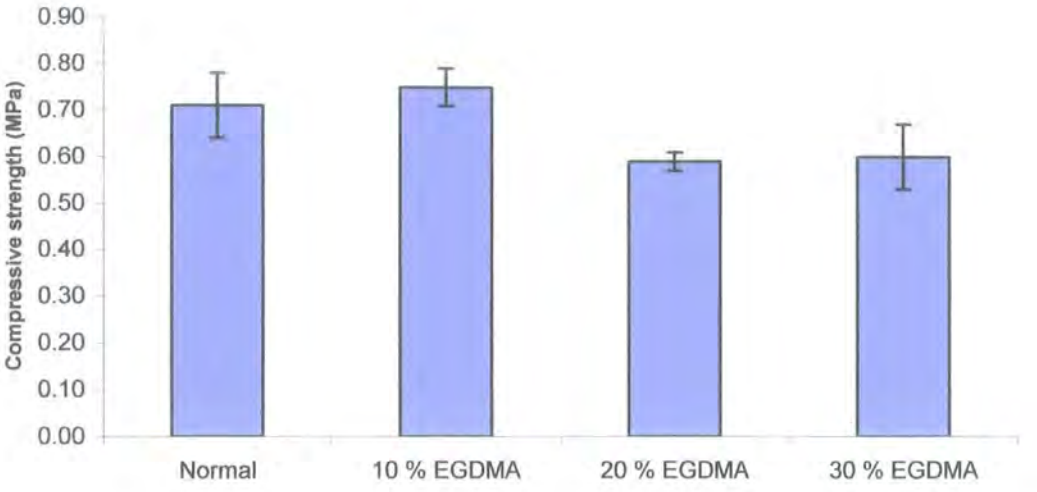

Figure 6.23 *A comparison of the compressive strength values of the S/EGDMA-based PolyHIPE materials and the standard S/DVB PolyHIPE material.*

The compressive strength values show a decrease from the standard 90/10 S/DVB materials at an EGDMA concentration level of 20 % w/w. At 10 and 30 % w/w there is no significant difference in the strength value compared to the standard PolyHIPE material at 10 % w/w DVB concentration. This decrease in the properties of the material can possibly be explained by the copolymer reactivity ratios of styrene, DVB and EGDMA (**see table 6.4**).

Table 6.4 Copolymer reactivity ratios for styrene, EGDMA and DVB [128]

M_1	M_2	r_1	r_2
Styrene	EGDMA	0.39	0.67
Styrene	m-DVB	0.58	0.58
Styrene	p-DVB	0.26	1.18

When the reactivity ratios of M_1 and M_2 are less than one then the M_1 radical will prefer to react with monomer 2 and vice versa. When the reactivity ratios are greater than one, the M_1 radical will react with monomer 1 and vice versa. In each case both divinylbenzene and EGDMA is the reactive monomer. Therefore the cross-linker

concentration will be used rapidly at the start of the polymerisation. For the case of S/DVB, is probable that DVB-DVB segments may occur. This may not affect the overall properties of the material as it is chemically similar to styrene. However for S/EGDMA, it is probable that flexible EGDMA-EGDMA segments may exist, with the number of segments increasing with EGDMA concentration, therefore increasing the flexibility of the material and decreasing the modulus value. Other hypotheses are that i) the cross-linker may be acting as a plasticiser or ii) greater steric hindrance with EGDMA, which will affect the cross-linking reaction. If the latter is the reason, it would be more likely for the tri-functional methacrylate compared to the di-functional EGDMA. As discussed in **chapter 1**, cross-linked foams prepared with divinylbenzene have a high number of residual unreacted double bonds [63]. If this was also the case for EGDMA, then the flexibility of the material would increase due to the greater flexibility of the EGDMA side chain compared to the DVB side chain present on the polymer.

Figures 6.24 and **6.25** show the comparison of the compressive modulus and strength values of the normal S/DVB PolyHIPE material, the 80/20 S/EGDMA PolyHIPE material and the 60/20/20 S/MMA/EGDMA PolyHIPE material.

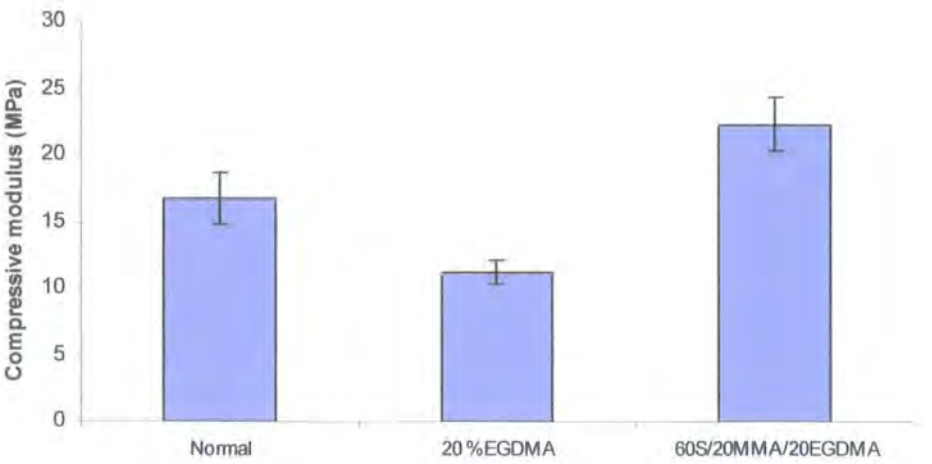

Figure 6.24 *Compressive modulus values of the 90/10 S/DVB PolyHIPE material, 80/20 S/EGDMA material and the 60/20/20 S/MMA/EGDMA PolyHIPE material.*

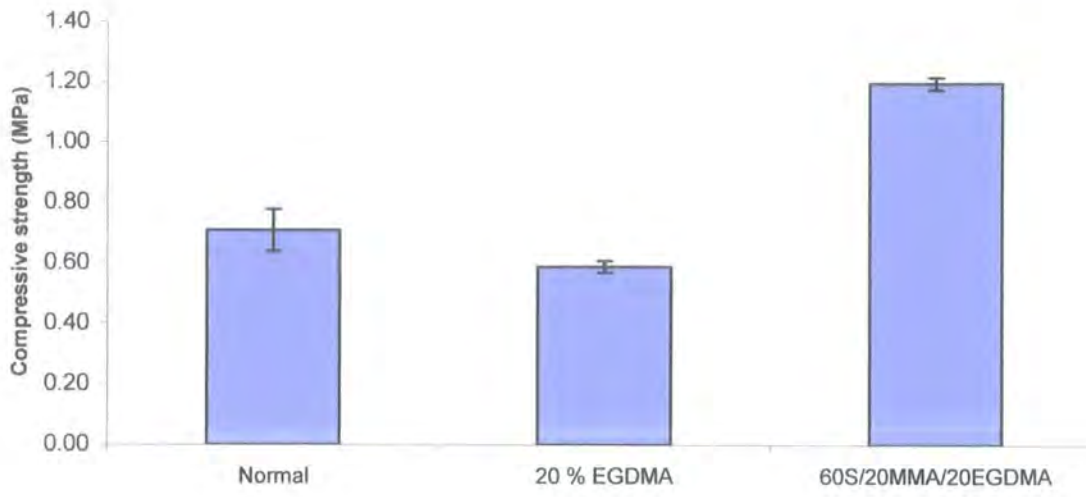

Figure 6.25 *Compressive strength values for the 90/10 S/DVB PolyHIPE material, 80/20 S/EGDMA material and the 80/20/20 S/MMA/EGDMA PolyHIPE material.*

With the addition of MMA there is an increase in both compressive modulus and strength compared to the 90/10 S/DVB material and the 80/20 S/EGDMA PolyHIPE material. This is possibly due to the combination of the MMA monomer producing a PolyHIPE material with a low porosity/closed cell morphology and the more rigid nature of the MMA itself producing a stronger PolyHIPE structure.

Figures 6.26 and **6.27** show the comparison of the compressive modulus and strength values of the S/TMPTM based PolyHIPE materials and the standard S/DVB PolyHIPE material.

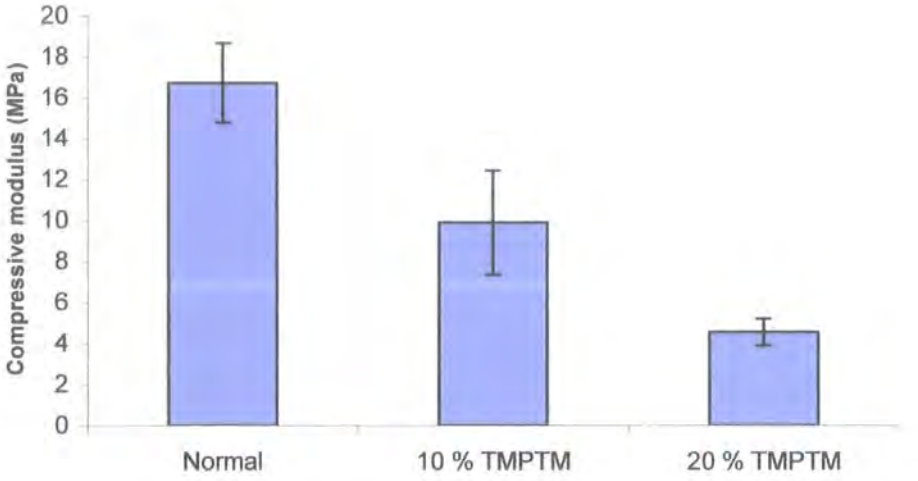

Figure 6.26 *Compressive modulus values of the S/TMPTM-based PolyHIPE materials and the standard S/DVB PolyHIPE material.*

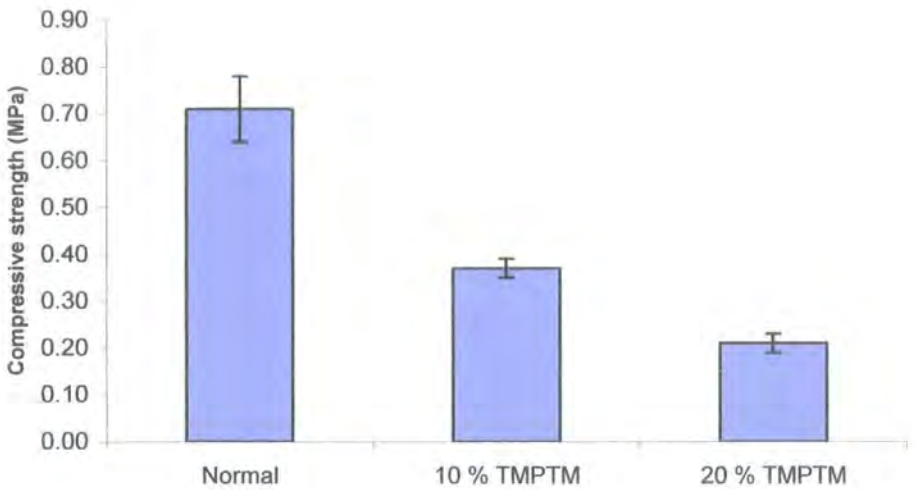

Figure 6.27 *Comparison of the compressive strength results for the 90/10 S/DVB PolyHIPE material and the S/TMPTM-based PolyHIPE materials.*

With increasing TMPTM concentration from 10 to 20 % w/w, there is a steady decrease in the compressive modulus and strength compared to the standard 90/10 S/DVB PolyHIPE material. The decrease in the properties of the S/TMPTM material compared to the S/DVB material could be due to steric effects preventing cross-linking of all the vinyl groups of the TMPTM and possibly acting as plasticiser reducing the properties of

the material. The latter explanation is supported when looking at the load/extension graphs (**figure 6.28**) for materials prepared with TMPTM.

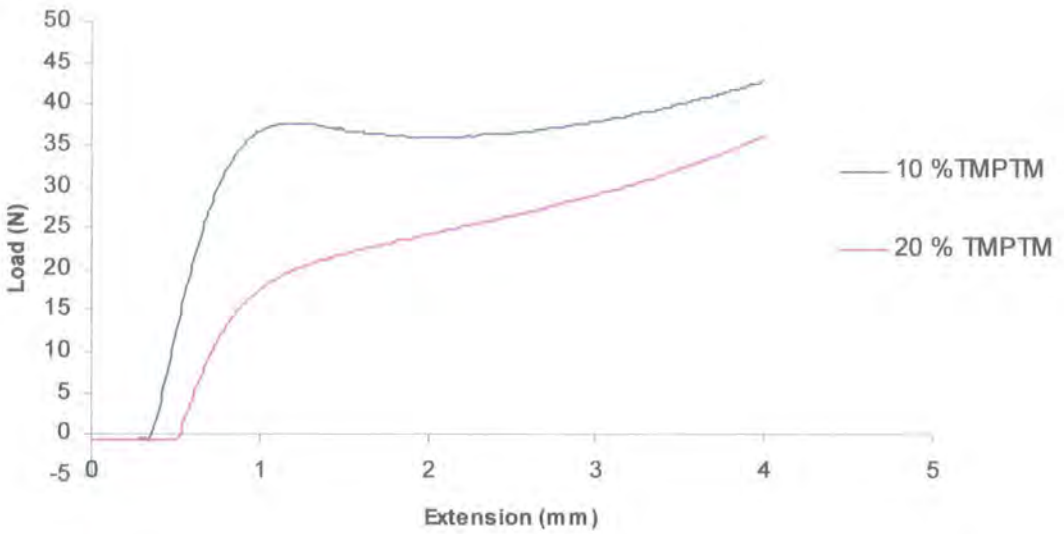

Figure 6.28 *Load/extension curves for the 90/10 S/TMPTM material and the 80/20 S/TMPTM PolyHIPE materials.*

At 10 % w/w TMPTM, there is plastic behaviour observed after yielding, but as the concentration is increased to 20 % w/w there is a plateau region where stress increases with increasing strain. This suggests that the material is either so weak or flexible in nature, due to the factors mentioned previously, that the cellular structure collapses so quickly that densification and the linear-elastic state (elastic buckling) co-exist. This shape of stress/strain curve is common in elastomeric type materials with increasing relative density. Gibson and Ashby [6] showed that by using the equations discussed in **chapter 1**, they can produce stress/strain maps (**see figures 6.29** and **6.30**) for each type of foam material. The curve for the 20 % w/w TMPTM material shows the behaviour for elastomeric foam materials, reinforcing the suggestion that the TMPTM monomer acts as a plasticiser producing a more flexible material. Rigid plastic foams produce a longer, flatter plateau region during plastic collapse.

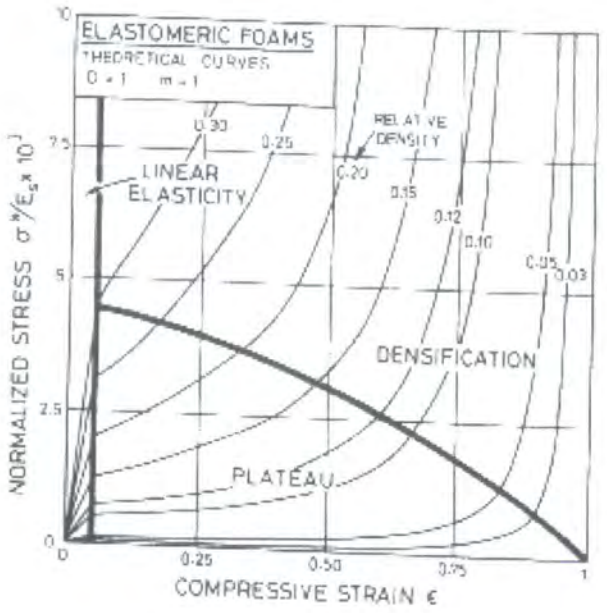

Figure 6.29 *Stress-strain map for an elastomeric foam material constructed from the equations in 1.2.3* [6].

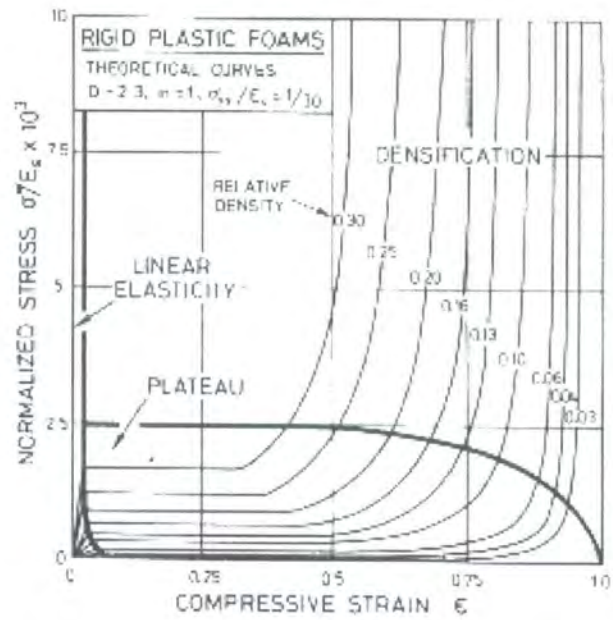

Figure 6.30 *Stress-strain map for a rigid plastic foam material, constructed from the equations in 1.2.3* [6].

6.3.2.4 Addition of active fillers to monomer phase

Figures 6.31 and **6.32** show the comparison of the compressive modulus and strength values for the 90/10 S/DVB PolyHIPE material, the 5 % w/w aluminium/S/DVB PolyHIPE composite and the 5 % w/w silica/S/DVB PolyHIPE composite.

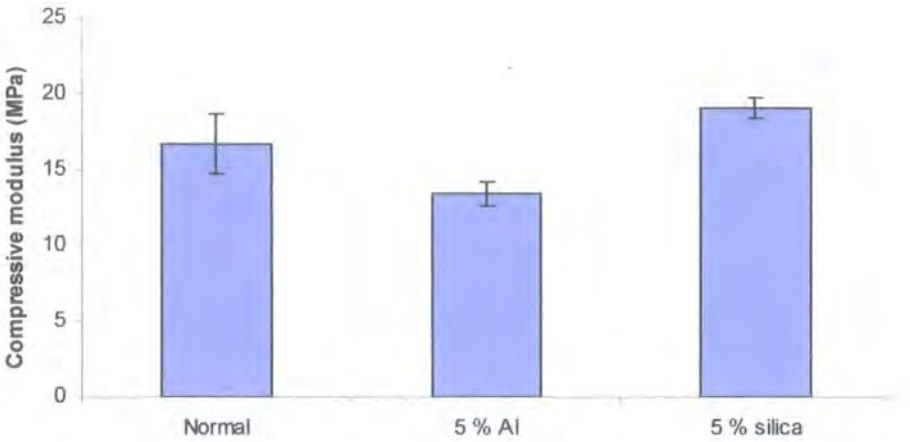

Figure 6.31 *Comparison of the compressive modulus values for the normal 90/10 S/DVB PolyHIPE material, 90/10 S/DVB with 5 % w/w Al material and the 90/10 S/DVB with 5 % w/w silica PolyHIPE materials.*

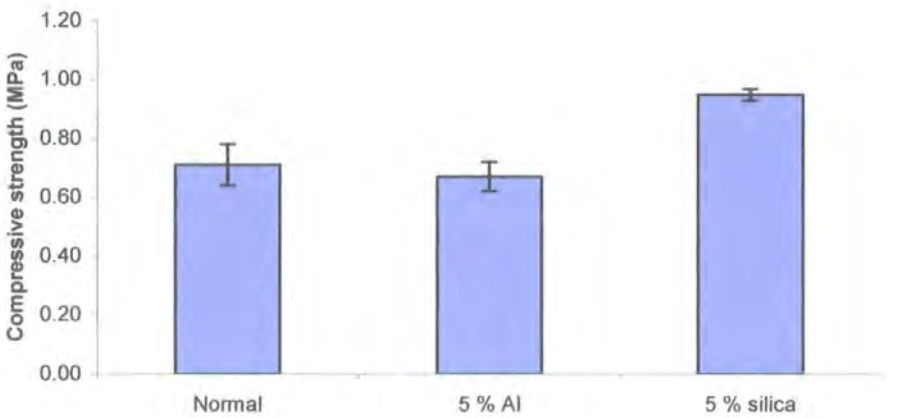

Figure 6.32 *Compressive strength values for the normal 90/10 S/DVB PolyHIPE material, the 90/10 S/DVB with 5 % w/w Al and the 90/10 S/DVB with 5 % w/w silica PolyHIPE materials.*

The addition of aluminium particles to the S/DVB material did not show the mechanical improvement that was expected. The compressive modulus and strength values show no

improvement from the S/DVB material with no filler present. The strong bonding of the aluminium particle with the PolyHIPE matrix (**see figure 3.13**) may produce a more brittle material with weaker mechanical performance.

The addition of the silica particles, on the other hand, resulted in an increase in both compressive modulus and strength of the S/DVB material, with the latter showing the greater improvement.

6.4 Conclusions

From the flexural test results it was shown that the addition of either Kevlar or PP fibres resulted in an increase in both the flexural modulus and strength of the S/DVB PolyHIPE materials. The addition of viscose fibres resulted in no increase in flexural modulus or strength of the S/DVB material, possibly due to poor bonding with the cellular PolyHIPE structure and the viscose fibre. The difference in mechanical performance of the fibre-reinforced materials could also be due to the variation in filler dispersion rather than any difference in chemical interaction between the foam structure and the fibre. The S/DVB PolyHIPE prepared using the OSS showed both an increase in flexural modulus and a two-fold increase in flexural strength, compared to the S/DVB PolyHIPE prepared using Span 80 as surfactant. This supports the literature findings that Span 80 acts as a plasticiser, producing a more flexible material. The use of the OSS also produced an increase in both the compressive modulus and strength compared to the S/DVB material prepared with Span 80.

The compressive properties of the acrylate- and methacrylate-based PolyHIPE materials were also reported. The incorporation of EHA produced a PolyHIPE material that was elastomeric in nature at high concentrations. The elastomeric behaviour of the material decreased with decreasing EHA concentration. This was shown in compressive modulus and strength trends. With increasing EHA concentration, there was a steady decrease in both compressive modulus and strength as expected. This was due to the greater

flexibility of poly (EHA) compared to polystyrene. The incorporation of the shorter side group monomer BA also produced a PolyHIPE material that was elastomeric in nature. At concentration of up to 20 % and 40 % w/w there was no significant change in the modulus values, whereas the incorporation of 40 % EHA caused a dramatic decrease in modulus. EHA produced a more flexible material at lower concentrations than BA. A considerable decrease in modulus was obtained when the majority of the polymer was BA-based (60 % w/w) and the PolyHIPE material showed elastomeric behaviour. At 20 % and 40 % w/w BA the compressive strength of the PolyHIPE material increased, showing that at low concentrations the BA reinforces the foam material in yield until the it changes from a rigid/plastic to an elastomeric material in nature. At higher concentrations, when the foam material was elastomeric in nature and the compressive strength decreased rapidly as expected.

The incorporation of BMA produced a PolyHIPE material that was more rigid in nature compared to that obtained with BA. This greater rigidity of methacrylates compared to acrylates is due to the steric hindrance of the methyl group present in the backbone of the polymethacrylates. The compressive modulus values for BMA-containing materials showed no change compared to the normal S/DVB material at BMA concentrations 20 and 40 % w/w. However there was a decrease in modulus value when the BMA content was 60 % w/w, due to the greater flexibility of polyBMA compared to polystyrene. This was similar to the 60 % BA material, but the decrease in modulus was less with BMA due to it's reduced flexibility compared to BA. The compressive strength values showed an increase at concentration levels of 20 % and 40 % w/w BMA and then the expected decrease at 60 % BMA. As with BA, the BMA reinforces the PolyHIPE in yield at low concentrations until the expected decrease when the majority of the material consists of BMA, which is more flexible than polystyrene.

The incorporation of MMA produced a PolyHIPE material that was rigid in nature. The compressive modulus and strength values increased with increasing MMA concentration as expected due to the more rigid nature of poly(MMA) compared to polystyrene. The compressive modulus and strength values of each acrylate and methacrylate at a concentration level of 20 % w/w were compared. This showed that the addition of the acrylate and methacrylate monomers had no effect on the bulk material properties but reinforced the foam material in yield with the effect increasing with decreasing chain length of the side group from EHA to MMA.

It has also been shown that it is possible to prepare styrene-based PolyHIPE materials by replacing DVB with multifunctional methacrylate-based cross-linkers such as EGDMA and TMPTM. The addition of EGDMA and TMPTM produced a weaker more flexible material compared to the normal S/DVB material. This could be due to steric hindrance affecting the cross-linking reaction or the cross-linker acting as a plasticiser. It was also suggested that the reactivity ratio of EGDMA would result in the formation of possible EGDMA-EGDMA segments producing a material with greater flexibility, compared to the normal S/DVB material. Increasing the TMPTM content also resulted in a decrease in modulus value.

The compressive properties of the PolyHIPE materials containing aluminium- and silica-based filler materials were also evaluated. There was an increase in the compressive modulus and strength with the addition of the silica particles, whereas the addition of the aluminium particles had little effect on the material properties. There was a small decrease in modulus value and no difference in the compressive strength value. This was unexpected due to the stronger interaction of the aluminium particle with the cellular matrix of the material compared to the silica particle.

Chapter 7

Preparation and mechanical compressive and shear testing of PolyHIPE core materials

7.1 Introduction

This chapter will detail the preparation, morphology and mechanical testing of selected 95 % void (0.05 gcm^{-3}) PolyHIPE materials. The combination of the OSS with 10 % w/w Kevlar fibres will be compared to the standard 90/10 S/DVB PolyHIPE material, the OSS material without Kevlar fibres, the 40 % MMA based PolyHIPE material and the PolyHIPE material prepared using the redox initiator.

The chemistry, morphology and preparation of resorcinol/formaldehyde-(RF) and urea/formaldehyde-(UF) based PolyHIPE core materials using a polycondensation reaction will also be discussed. The shear and compressive mechanical properties of these materials will also be compared to commercially based core materials available at the present moment.

7.1.1 Urea/formaldehyde chemistry

More than 70 % of the urea/formaldehyde (UF) resin produced is used by the forests products industry for a range of applications [129]. The resin can be used to bond particleboard, medium density fibreboard, and as a laminating adhesive for bonding furniture goods and interior doors. This type of thermosetting resin is classed as an amino resin. UF resins make up around 80 % of the amino resins produced worldwide, whereas melamine-formaldehyde resins make up the majority of the remainder of this resin class. The use of UF resins as a major adhesive in the forests products industry is due to the low cost, low cure temperatures, water solubility and the resistance to abrasion [129]. Also the excellent thermal properties, and lack of colour of the cured resin. The major disadvantage of these resins compared to other thermosetting adhesives such as phenol-formaldehyde resins, is the lack of resistance to moist conditions, especially in the presence of heat. These conditions can lead to bond reversal and the release of formaldehyde, which is a suspected carcinogen.

Urea/formaldehyde resins are formed by the reaction between urea and formaldehyde [129], which takes place in two stages. Firstly the urea is hydroxymethylated by the addition of formaldehyde to the amino groups (**see figure 7.1**). This reaction leads to the production of mono-, di- and trimethylolureas. The tetrafunctional urea is not produced in detectable quantities. The addition of the formaldehyde takes place over the whole pH range. The reaction rate of the formaldehyde addition is dependent on the pH (**see figure 7.2**)

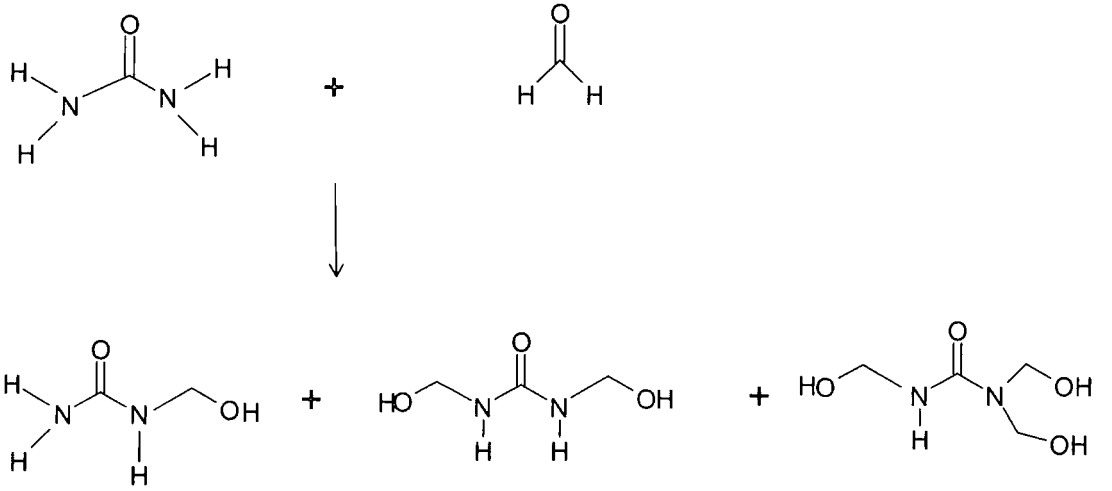

Figure 7.1 *Formation of mono-, di- and trimethylolurea by the addition of formaldehyde to urea.*

The second stage is the intermolecular condensation of methylolureas to low molecular weight polymers/oligomers. The formation of oligomers increases with decreasing pH value.

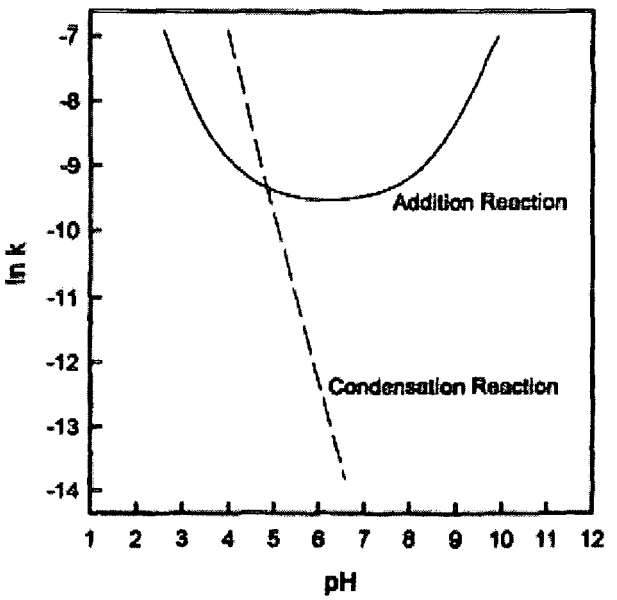

Figure 7.2 *Influence of pH on the rate constant (k) for addition and condensation reactions of urea and formaldehyde* [129].

The increase in molecular weight of the UF resin under acidic conditions is thought to be due to a combination of reactions leading to the formation of:

a) Methylene bridges between amido nitrogens by the reaction between the methylol and amido groups on reacting molecules,

b) Methylene ether linkages by the reaction of two methylol groups,

c) Methylene linkages from methylene ether linkages by the release of formaldehyde,

d) Methylene bridges by reaction of methylol groups by releasing water and formaldehyde.

a)

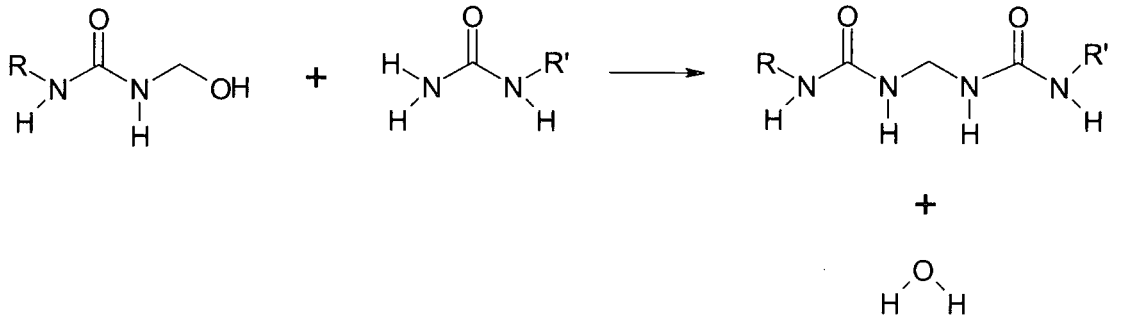

c)

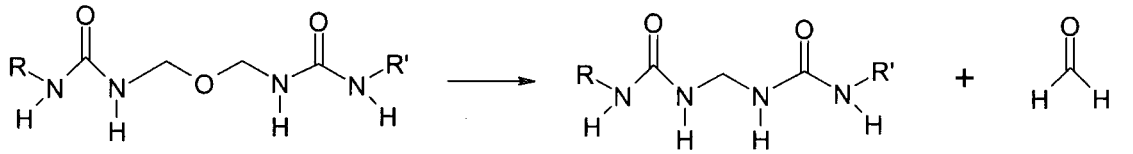

Figure 7.3 *Condensation reactions of methylolureas, which can lead to cross-linking.*

As urea has a functionality to formaldehyde greater than two, theory predicts that resins are able to form three-dimensional networks [130]. **Figure 7.3** shows two examples of reactions described previously, which can lead to cross-linking. Both these networks with only methylene linkages are formed but networks with di-methylene ether linkages can also be formed. The difference between the two pH profiles of the two stages is used to advantage in the commercial production of UF resins. In most cases the reaction is carried out in two stages. The first stage involves

the addition of formaldehyde to form methylolureas under basic conditions. This allows the addition reaction to be carried out in the absence of the condensation reaction of the methylolureas. The second step involves bringing the reaction mixture to the acidic side (~ pH 5) and the condensation reaction proceeds until a desired viscosity is reached. The mixture is then cooled and neutralised and the water is removed by vacuum distillation until a desired solids content is reached (~ 60 – 65 % w/w). The resin is then cured using an acid catalyst. Ammonium chloride and ammonium sulfate are the most widely used catalysts. Resin cure is normally conducted at temperatures ~ 120 °C and a pH < 5. The reactions during the final curing stage are said to be similar to those that occur during the condensation of the methylolureas [129].

7.1.2 Resorcinol/formaldehyde chemistry

Phenolic resins are also prepared by the step growth (condensation) polymerisation of di-functional monomers, in this case resorcinol and formaldehyde. Under standard reaction conditions substitution occurs only in the ortho and para positions relative to the phenolic hydroxyl group. Resorcinol (**see figure 7.4**) as a dihydric phenol (1,3 dihydroxybenzene) exhibits a high reaction rate with formaldehyde.

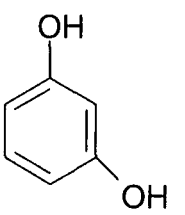

Figure 7.4 *Structure of resorcinol*

The reaction mechanism can be described using phenol (hydroxybenzene) as an example. The three reactions which must be accounted for are: formaldehyde

addition to phenol, chain growth or pre-polymer formation and cross-linking or curing reaction.

Formaldehyde is present in aqueous solution and methanediol is usually observed as the key monomeric species [130]. Novolak resins are obtained by the reaction of phenol and formaldehyde under acidic conditions. These materials are linear or slightly branched condensation products linked by methylene bridges. Resols are obtained by reaction of phenols and formaldehyde under basic conditions. They are made up of polynuclear hydroxymethylphenols, which can be transformed into a three-dimensional network by the application of heat or addition of acid [130].

Catalysts such as oxalic acid or phosphoric acid can be used for the acid catalysed condensation industrially for a more controllable reaction. Stronger acids such as sulphuric and hydrochloric provide a low pH resulting in a highly exothermic reaction. The reaction rate increases with decreasing pH. Under acidic conditions the first reaction is the electrophilic hydroxymethylation of phenol shown in **figure 7.5**. The carbonium ion formed from the methanediol is the reactive species.

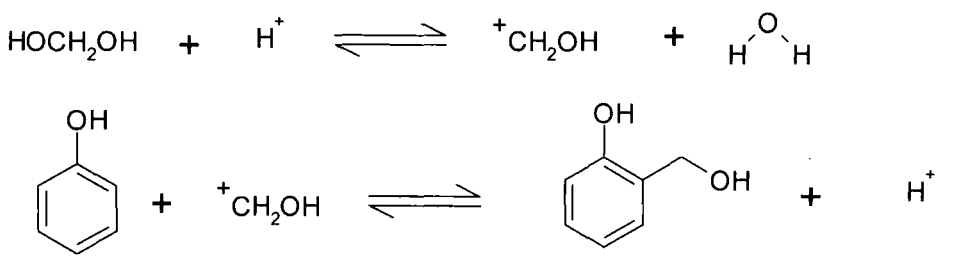

Figure 7.5 *Electrophilic hydroxymethylation of phenol.*

The hydroxymethylated phenols cannot be isolated under acidic conditions. This is due to the formation of the resonance stabilised benzylic carbonium ion, which reacts rapidly to form dihydroxydiphenylmethanes shown in **figure 7.6**. Werstler [131], [132] reported that the most dominant substituent is methylol in the ortho-position. Methylol levels at the para-position also increased but at a slower rate.

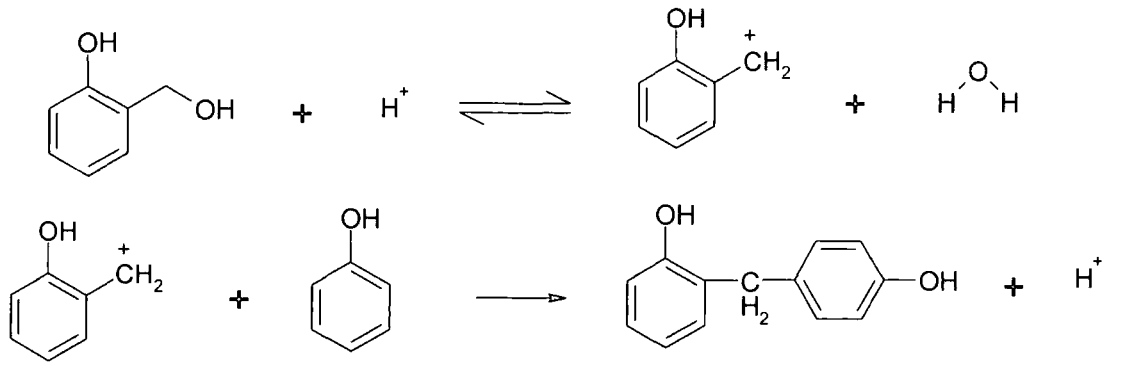

Figure 7.6 *Formation of dihydroxyphenylmethane compounds during the reaction of phenol and formaldehyde.*

They also reported that the para-substituted intermediates are more reactive than the ortho. The para-substituted phenols undergo immediate condensation and the first methylene bridges, which were observed by NMR are para-para bridges [131), (132)] by the ortho-para and then ortho-ortho bridges. The resorcinol/formaldehyde reaction proceeds similarly. Christiansen [(133)] studied the resorcinol-formaldehyde reaction in dilute solution using ^{13}C NMR. In the early stages, the initial set of signals suggested substitution at the C4 and C6 carbons with a small peak due to the C2 carbon. There was also a signal due to the presence of the hemiformal carbon, from the reaction of formaldehyde with the hydroxymethyl group attached to C4 (**see figure 7.7**).

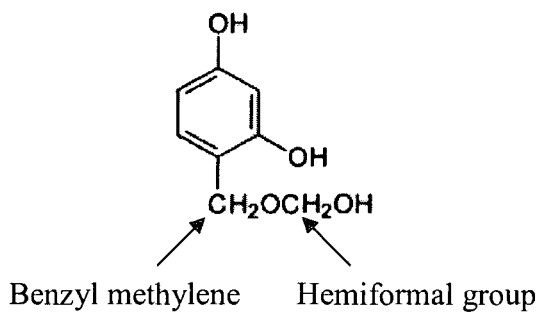

Figure 7.7 *Hemiformal-based compound formed by the reaction of formaldehyde with hydroxymethylated resorcinol.*

After around 60-75 minutes the resorcinol peak intensity had decreased by 90 % and a broad peak existed due to the formation of methylene linkages (diarylmethanes) by condensation of the hydroxymethyl groups at the 4 - and 6 – positions. The 4,4-methylene bridges (para-para) were observed first, followed by the 2,4-methylene bridges (ortho-para) and the 2,2-methylene bridges. **Figure 7.8** shows the plot of changes in distribution of derived species during the resorcinol/formaldehyde reaction.

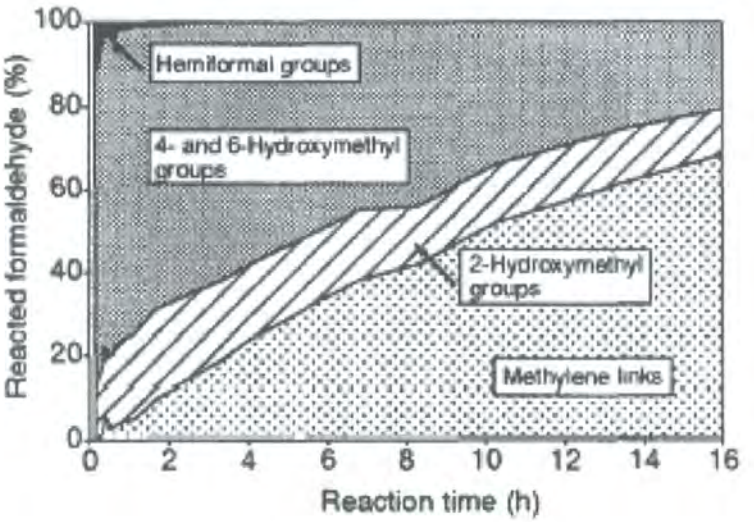

Figure 7.8 *Summary plots of changes in the distribution of derived species during the resorcinol/formaldehyde reaction* [133].

7.2 Experimental

7.2.1 Materials

Aldrich Chemicals supplied the formaldehyde (37 % w/w solution in water), urea (98 %), resorcinol (98 %), ammonium chloride (99.5 + %) and the low odour kerosene. Borden Chemicals supplied the urea/formaldehyde resin UL 177 (61.5 % solids content) and Rhodia Chemicals supplied the surfactant Miranol (Sodium Cocoamphoacetate).

For the preparation of the 95 % void styrene- and MMA- based materials, Aldrich chemicals supplied the monomers styrene (99 %), methyl methacrylate (99 %) and DVB (80 %). Aldrich chemicals also supplied the surfactants Span 80, Span 20, dodecylbenzenesulfonic acid sodium salt (tech) cetyltrimethylammoniumbromide and the initiators potassium persulfate (99 + %), hydrogen peroxide (27.5 % w/w solution in water), $_{L}$-ascorbic acid (99 %) and iron (II) sulfate heptahydrate (98 + %). The monomers styrene, DVB and MMA were purified prior to HIPE preparation by passing them through a column of basic activated aluminium oxide.

7.2.2 Instrumentation and characterisation

The morphologies of the materials were characterised using the instrumentation described in **2.2.2**. The thermo-gravimetric analysis traces for the materials were obtained from the instrumentation described in **3.2.2**. The compressive and shear core tests were carried out on an Instron 4302 with a 1 kN load cell and a crosshead speed of 0.5 $mmmin^{-1}$.

7.2.3 Preparation of urea/formaldehyde-based PolyHIPE materials

7.2.3.1HIPE preparation and polymersiation

Table 7.1 shows the differing compositions of the continuous and oil phases used to prepare urea/formaldehyde based PolyHIPE materials. The continuous phase containing a mixture of urea or UF resin/water, formaldehyde and surfactant, was placed in a PE bottle. The oil phase (cyclohexane or kerosene) was then added drop-wise under constant stirring (300 rpm) until an opaque o/w HIPE had formed. The acid catalyst used (ammonium chloride or 1M HCl) was either added before or after HIPE formation. The HIPE was then placed in the oven at 50 ° C for 30 minutes and then left to cure at room temperature until a white cross-linked monolith had formed. Each experiment was carried out only once, unless complete separation of the HIPE occurred and in this case the experiment was carried out until a PolyHIPE material was obtained.

Table 7.1 Continuous and internal phase compositions for UF-based PolyHIPE preparation

Sample code	Continuous phase composition	Catalyst	Solvent (internal phase)
189 RJC	16.2 g formaldehyde 6 g urea 3.2 g DDBSS	2 g, 37.4 mmol ammonium chloride (after HIPE formation)	197 ml cyclohexane
190RJC	16.2 g formaldehyde 6 g urea 3.2 g DDBSS	2 g, 37.4 mmol ammonium chloride (before HIPE formation)	197 ml cyclohexane
192RJC	16.2 g formaldehyde 6 g urea 2.5 g Miranol	2 g, 37.4 mmol ammonium chloride (before HIPE formation)	197 ml cyclohexane
193 RJC	16.65 g UF resin 5.55 g water 2.5 g Miranol	0.32 g, 6.98 mmol ammonium chloride (before HIPE formation)	197 ml cyclohexane
194RJC	16.65 g UF resin 5.55 g water 2.5 g Miranol	2 g, 37.4 mmol ammonium chloride (before HIPE formation)	197 ml cyclohexane
197RJC	16.65 g UF resin 5.55 g water 2.5 g Miranol	1M HCl added after HIPE formation until pH paper showed pH of around 4-5	197 ml cyclohexane
198RJC	16.65 g UF resin 5.55 g water 2.5 g Miranol	2 g, 37.4 mmol ammonium chloride (before HIPE formation)	157 ml kerosene
206RJC	37 g UF resin 8.4 g water 2.5 g Miranol	1 ml 1M HCl added before HIPE formation. Another 4 ml HCl added after 1 hour	177 ml cyclohexane
209RJC	18.5 g UF resin 4.2 g water 1.2 g Miranol	5 ml 1M HCl added after HIPE formation	177 ml cyclohexane
210RJC	18.5 g UF resin 8.4 g water 2.4 g MiranoL	5 ml 1M HCl added after HIPE formation	177 ml cyclohexane
211RJC	37 g UF resin 8.4 g water 2.5 g Miranol	5 ml 1M HCl added before HIPE formation	177 ml cyclohexane
212RJC	16.65 g UF resin 5.55 g water 2.5 g Miranol	5 ml 1M HCl added after HIPE formation	197 ml cyclohexane
215RJC	78.3 g UF resin 22.73 g water 10 g Miranol	25 ml 1M HCl added after HIPE formation	1900 ml cyclohexane
220RJC	37 g UF resin 8.4 g water 2.5 g Miranol	5.55 g, 102.8 mmol ammonium chloride (before HIPE formation)	177 ml cyclohexane
221RJC	16.65 g UF resin 5.55 g water 2.5 g Miranol	4 g, 74.8 mmol ammonium chloride (before HIPE formation)	197 ml cyclohexane
222RJC	16.65 g UF resin 5.55 g water 2.5 g Miranol	6 g, 112.2 mmol ammonium chloride (before HIPE formation)	197 ml cyclohexane

7.2.4 Preparation of resorcinol/formaldehyde-based PolyHIPE materials

7.2.4.1 HIPE preparation and polymerisation

7.2.4.1.1 Small- scale preparation

A mixture of resorcinol (8.3 g, 75.38 mmol) and formaldehyde (12.2 g, 40 % aq, 150.3 mmol) were mixed together in a polyethylene bottle until all of the resorcinol had dissolved. The amphoteric surfactant Miranol (2.3 g) was then added to the solution. To this mixture cyclohexane (180 ml, 1.75 mol) was then added until a high internal phase emulsion had formed. After HIPE formation the acid catalyst phosphoric acid (3 g, 50 % aq, 15.3 mmol) was added to the emulsion. The emulsion was then placed in the oven at 60 °C for 10 minutes after which a rigid salmon pink coloured monolith had formed. The cyclohexane and remaining water were then removed *in vacuo* at 50 °C. Each experiment was carried out only once, unless complete separation of the HIPE occurred and in this case the experiment was carried out until a PolyHIPE material was obtained.

7.2.4.1.2 Large-scale preparation

To produce samples for mechanical testing, a mixture of resorcinol (83 g, 0.75 mol), formaldehyde (122 g, 1.5 mol) and Miranol (23 g) were placed in a 4l plastic container. To this mixture cyclohexane (1800 ml, 17.5 mol) was added until an opaque HIPE had formed. After emulsion formation phosphoric acid (30 g, 50 % aq, 0.15 mol) was added as catalyst for the reaction. The emulsion was then placed in the oven at 60 °C for 10 minutes after which a rigid salmon pink coloured monolith had formed. Each experiment was carried out only once, unless complete separation of the HIPE occurred and in this case the experiment was carried out until a PolyHIPE material was obtained.

7.2.5 Preparation of 95 % void styrene- and MMA-based PolyHIPE materials

7.2.5.1 HIPE preparation and polymerisation

To produce the following styrene and MMA based PolyHIPE materials for compressive and shear core testing, the following formulations were placed in a 4L plastic beaker:

1) styrene (90 g, 0.86 mol), divinylbenzene 80 % (10 g, 76.8 mmol), surfactant: Span 80 (20 g, 46.7 mmol).

Aqueous phase – de-ionised water (1900 g), calcium chloride dihydrate (21.12 g, 0.14 mol), initiator – potassium persulfate (2.22 g, 8.21mmol)

2) styrene (90 g, 0.86 mol), divinylbenzene 80 % (10 g, 76.8 mmol), surfactant: Span 80 (20 g, 46.7 mmol).

Aqueous phase – de-ionised water (1900 g), calcium chloride dihydrate (21.12 g, 0.14 mol), redox initiator – ascorbic acid (1.8 g, 10.22 mmol), iron (II) sulphate heptahydrate (0.36 g, 1.29 mmol), *hydrogen peroxide (27. 5 % w/w solution in water) (10 g, 80.83 mmol) * - added after HIPE formation.

3) styrene (90 g, 0.86 mol), divinylbenzene 80 % (10 g, 76.8 mmol), surfactant: Span 20 (6.3 g, 18.18 mmol), dodecylbenzenesulfonic acid sodium salt (0.4 g, 1.15 mmol), cetyltrimethylammoniumbromide (0.3 g, 0.82 mmol).

Aqueous phase – de-ionised water (1900 g), calcium chloride dihydrate (21.1 g, 0.14 mol), initiator - potassium persulfate (2.22 g, 8.21 mmol).

4) styrene (90 g, 0.86 mol), divinylbenzene 80 % (10 g, 76.8 mmol), Kevlar fibres (10 g), surfactant: Span 20 (6.3 g, 18.18 mmol), dodecylbenzenesulfonic acid, sodium salt (0.4 g, 1.15 mmol), cetyltrimethylammoniumbromide (0.3 g, 0.82 mmol).

Aqueous phase – 1900 g water, calcium chloride dihydrate (21.12 g, 0.14 mol), initiator – potassium persulfate (2.22 g, 8.21 mmol).

5) styrene (50 g, 0.48 mol), methyl methacrylate (40 g, 0.87 mol), divinylbenzene 80 % (10 g, 76.8 mmol), surfactant: Span 80 (20 g, 46.7 mmol)

Aqueous phase – de-ionised water (1900 g), calcium chloride dihydrate (21.12 g, 0.14 mol), initiator – potassium persulfate (2.22 g, 8.21 mmol).

The aqueous phase was added dropwise to the monomer and surfactant mixture until a high internal phase emulsion had formed. The HIPE was then placed in a plastic container and placed in a convection oven at 60 °C to cure the emulsion. The monolith was removed and samples of specific size were cut from the monolith produced. The water was then removed from the PolyHIPE first by placing in a vacuum oven at 50 °C to remove the majority of the water and then in a convection oven at 60 °C until a constant weight was reached. Each experiment was carried out only once, unless complete separation of the HIPE occurred and in this case the experiment was carried out until a PolyHIPE material was obtained.

7.2.6 Compressive core tests

To determine the compressive strength and modulus of the core materials the method outlined in ASTM C365 [127] was used.

7.2.6.1 Measurements of dimensions and density

The samples prepared and dried in **7.2.4.1.2** and **7.2.5.1** and in were cut into six separate blocks of 50 mm x 50 mm x 10 mm. The dimensions were measured to the nearest 0.25 mm. The weight of each test sample was measured to the nearest 0.1 g and the density calculated using mass/volume measurements and was expressed in gcm^{-3}.

7.2.6.2 Procedure

The tests were carried out and the values calculated as described in **6.2.2.4.**

7.2.7 Shear core tests

The ASTM test method C 273 [134] determines the shear strength of a core material parallel to the plane of the sandwich and the shear modulus associated with strains in a plane normal to the facings.

7.2.7.1 Measurements of dimensions and density

The PolyHIPE materials prepared in **7.2.4.1.2** and **7.2.5.1** were cut into six separate blocks of 120 mm x 50 mm x 10 mm. The thickness of the specimens was measured to the nearest 0.025 mm and the length and width to the nearest 0.25 mm using vernier calipers. The specimens were weighed to the nearest 0.1 g and the densities were calculated using weight volume measurements and expressed in gcm^{-3}.

7.2.7.2 Procedure

Steel plates bonded directly to the sandwich core material support the test specimen. The thickness of the plates is varied with the strength of the core material, but the plate length is determined so that the line of action of the direct tensile or compressive forces, pass through the diagonally opposite corners of the sandwich as shown in **figure 7.9**. The load is applied to the end of the rigid plates in compression or tension (**see figures 7.10 (a)** and **(b)** and **figure 7.11**) through a spherical bearing block or a universal joint so as the load is distributed uniformly across the whole length of the specimen. The tensile shear plates can be attached with either bolts or pins to the loading fixture. The load is applied at a constant rate of movement of the crosshead that the maximum load will occur to within 3-6 min. The failure is desired to be 100 % failure of the core. Failure due to plate or core adhesive failures should be rejected.

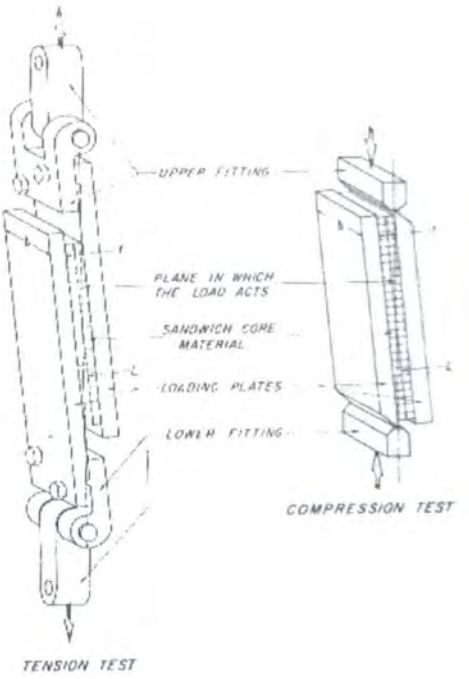

Figure 7.9 *Plate shear specimen, load line of action*

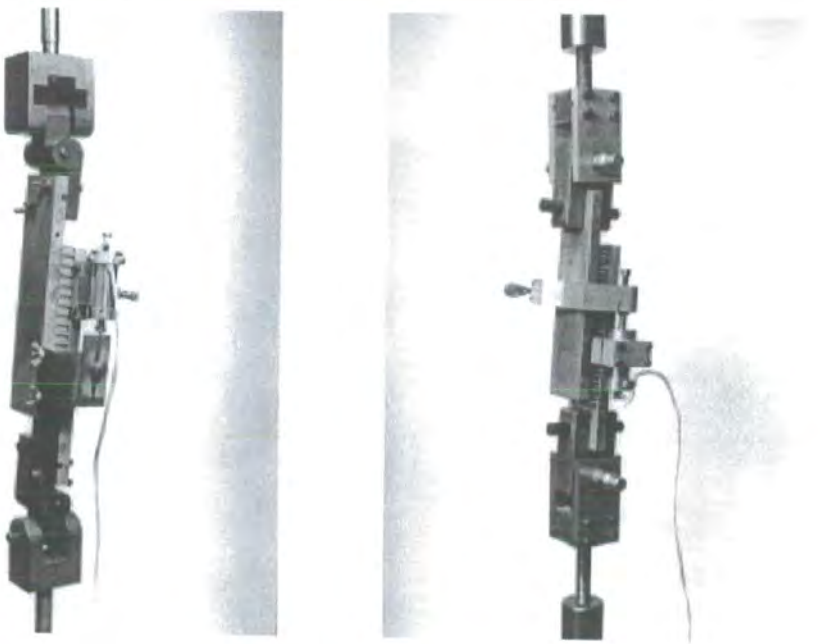

(a) (b)

Figure 7.10 *Tensile plate shear tests, (a) bolted specimen (b) pinned specimen*

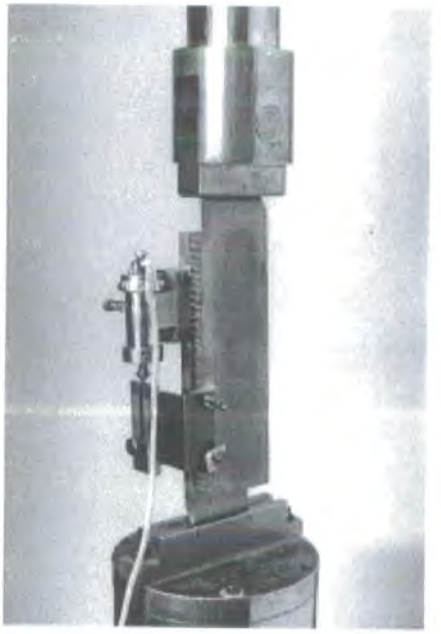

Figure 7.11 *Compressive plate shear test*

Figure 7.12 shows a load/extension chart obtained under a shear stress for a PolyHIPE material. The shear stress, τ, is calculated from **equation 7.1**:

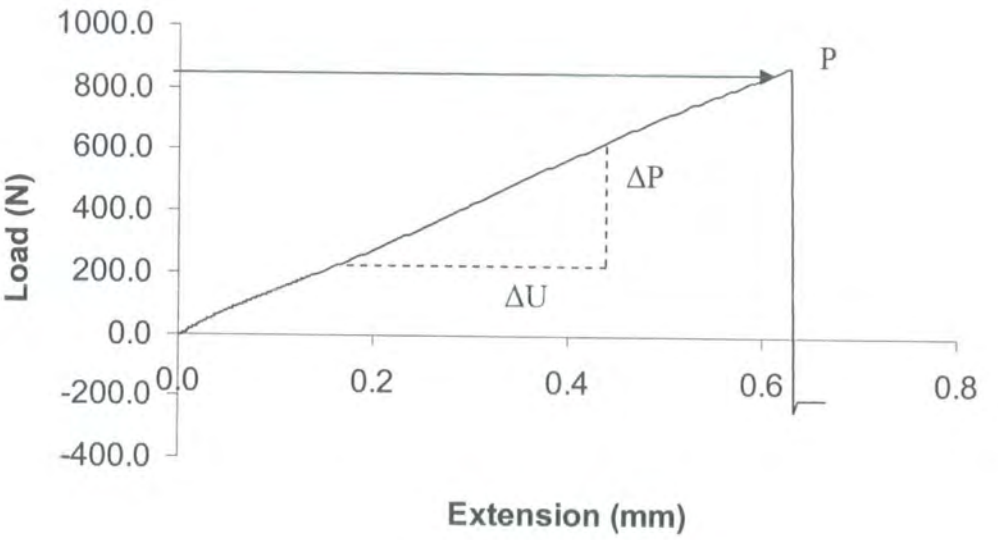

Figure 7.12 *A load/extension curve obtained during shear testing of a PolyHIPE foam material.*

$$\tau = \frac{P}{Lb}$$ **Equation 7.1**

where:

P = load on specimen , (N)

L = length of specimen, (mm)

b = width of specimen, (mm)

The shear modulus, G, is calculated using **equation 7.2**:

$$G = \frac{St}{Lb}$$ **Equation 7.2**

where:

S = $\Delta P/\Delta U$ slope of load /deflection curve, (N/mm)

u = displacement of loading plates; and

t = thickness of core, (mm)

7.3 Results and discussion

7.3.1 Urea/formaldehyde-based PolyHIPE materials

7.3.1.1 Processing conditions and morphology

In initial experiments (189 and 190RJC) when no pre-polymer resin was used, a PolyHIPE monolith could not be produced. After the HIPE had been placed in the oven at 50 °C for 30 minutes, it changed from opaque to white in nature. After leaving the HIPE at room temperature for 48 hours some gelation had occurred but no solid monolith had been produced. In **figure 7.2** is shown the influence of pH on the rate constant for the addition and condensation reactions of urea and formaldehyde during resin formation. It was mentioned in **7.1.1** that this process was carried out in two stages. Firstly the formation of the methylolureas is carried out under basic conditions. This allows the reaction to proceed in the absence of the condensation reactions of the methylolureas. Then the reaction is brought an acidic pH, around pH 5, and the condensation reactions are carried out until a high viscosity is reached. This procedure is only pre-polymer resin formation. The resin is then cured, for adhesive purposes, using an acid catalyst. This is normally conducted at pH < 5 and at 120 °C [129]. In our initial reactions it may only be the pre-polymer formation that is occurring in the HIPE, with no cross-linking or curing occurring. When the pre-polymer resin UL 177 was present and ammonium chloride (2 g) was used as catalyst, a PolyHIPE material was produced that showed elastomeric behaviour. **Figure 7.13** shows ESEM images of the fractured surface of the urea/formaldehyde PolyHIPE material (194RJC)

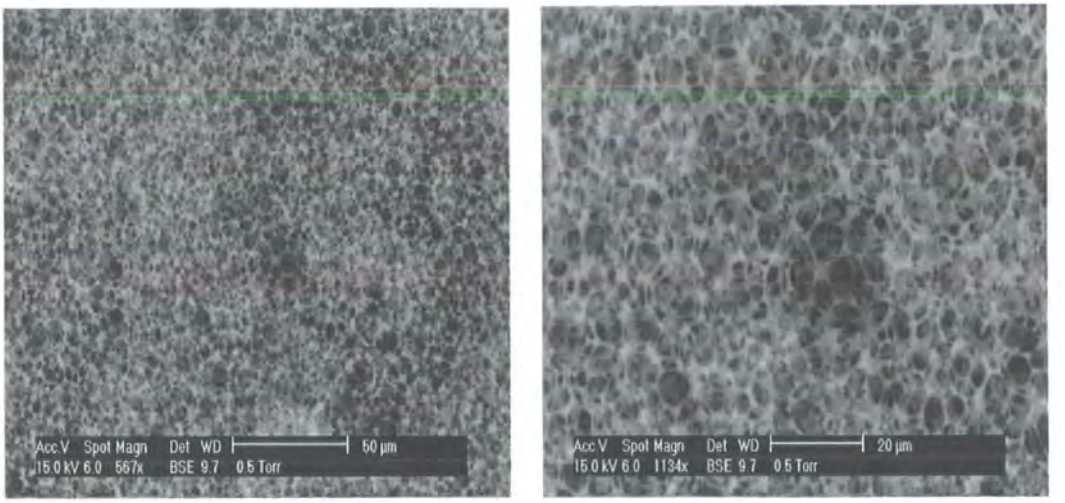

Figure 7.13 *ESEM images of the urea/formaldehyde based PolyHIPE material (194RJC).*

The morphology is an interconnecting open-cellular structure that would normally be expected from a PolyHIPE material. The void size and interconnecting strut size are smaller compared to the standard S/DVB PolyHIPE material (**see figure 1.5**). The density of the material was measured to be 0.08 gcm^{-3}. At a level of 0.32 g ammonium chloride (193RJC) with the same resin/water composition there was no solid monolith formed. The pH of an ammonium chloride (weak acid) solution can be related to its pK_a using **equation 7.3**,

$$pH \approx \frac{1}{2} pK_a - \frac{1}{2} \log[HA] \qquad \textbf{Equation 7.3}$$

where [HA] = [NH_4Cl] and the pKa of ammonium chloride = 9.25.

At a quantity of 0.32 g of ammonium chloride using **equation 7.3**, the pH is equal to 4.79 and at a quantity of 2 g the pH is equal to 4.39. The rate of the cross-linking reactions (condensation of methylolureas to form methylene bridges) increases with increasing acidity (decreasing pH). At a pH of 4.79 the rates of the addition and condensation are practically similar, where as at 4.39 the condensation reaction will proceed more rapidly. With increasing ammonium chloride concentration in 221 and

222RJC (4 and 6 g ammonium chloride) the materials produced, were weaker in nature with 222RJC producing a PolyHIPE material that was easily compressed into a powder. With increasing ammonium chloride concentration there was no significant decrease in polymerisation time (4 and 6 g ammonium chloride). **Figure 7.14** shows ESEM images of the UF-based PolyHIPE material produced with an ammonium chloride quantity of 6 g.

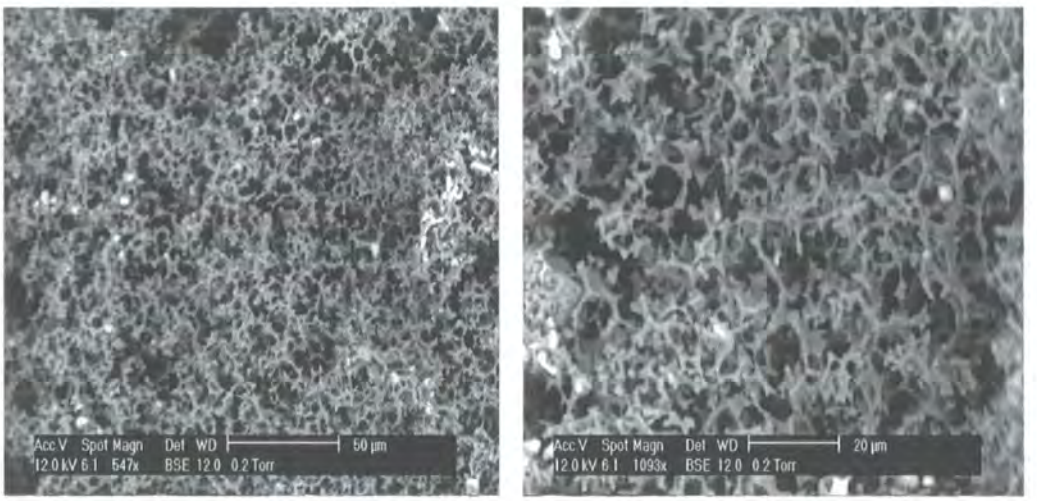

Figure 7.14 *ESEM images of the UF-based PolyHIPE material prepared with an ammonium chloride quantity of 6 g (222RJC.).*

The morphology of the UF based PolyHIPE material has been altered with increasing catalyst concentration. The PolyHIPE is open-cell in nature, but the interconnecting nature of the material has decreased compared to the UF material prepared with 2 g ammonium chloride (194RJC). This change in morphology could account for weaker properties of the material.

Hydrochloric acid (1M) was also used as a catalyst for the reaction. In 197 RJC there was no PolyHIPE material formed, the emulsion turned from opaque to white in nature but no monolith was produced. In 206 RJC, after adding 1 ml of HCL prior to HIPE preparation and curing at 50 °C for 30 minutes, the HIPE was left for one hour at room temperature. After this time no PolyHIPE material had formed, and another

4 ml of HCL was added to the HIPE. After another 24 hours at room temperature, a PolyHIPE material was produced, that was more rigid in nature than the materials of the same UF resin content (220RJC) produced with ammonium chloride as catalyst. The UF resin content was greater and the PolyHIPE material produced had a higher density of 0.19 gcm $^{-3}$ compared to 194RJC, due to the increase in UF resin content. This increase in density could account for the more rigid nature of the material. **Figure 7.15** shows ESEM images of the morphology of the material.

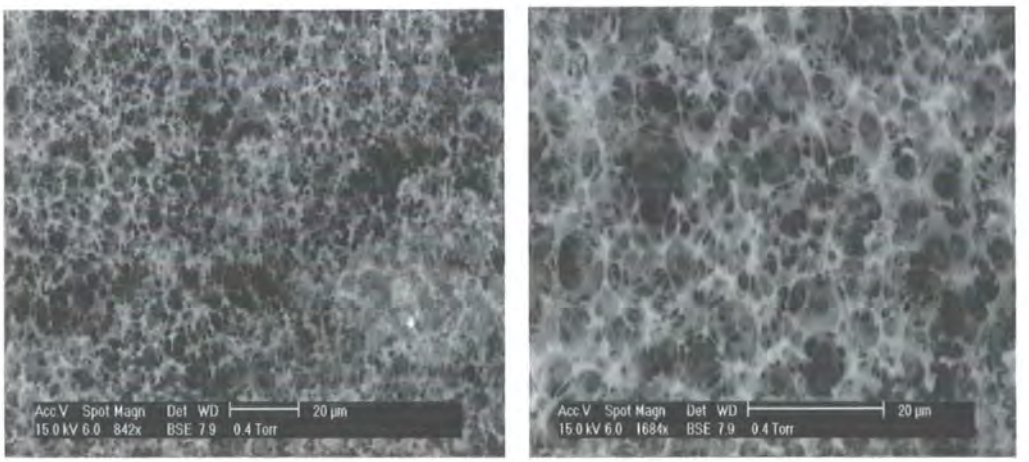

Figure 7.15 *ESEM images of the UF material prepared with 1M HCl as catalyst (206RJC).*

The morphology of the UF PolyHIPE material prepared using 1M HCl as catalyst, is similar to the morphology of the material prepared with ammonium chloride, although the HCl-cured material is more rigid in nature. The final properties of the UF PolyHIPE material are dependent on the pH within the emulsion. When 5 ml of 1M HCl was added before HIPE formation (211RJC) no PolyHIPE material was formed. In 209, 210 and 212RJC the 1M HCl was added after HIPE preparation, again no PolyHIPE material formed after 48 hours. Finding the optimum conditions especially with the use of HCl as catalyst proved difficult. The only HCl cured material produced was made by adding a small amount of acid beforehand, curing at

50 °C for 30 minutes and then adding more acid to the emulsion after 1 hour at room temperature.

The solvent generally used throughout the UF HIPE preparation was cyclohexane. This has a boiling point of 80 °C and therefore can limit the polymerisation temperature used. The higher boiling solvent kerosene was also used for HIPE preparation. Once the monolith had formed the kerosene was extremely difficult to remove from the PolyHIPE material even at a reduced pressure in the vacuum oven. After drying under vacuum for 72 hours the material was weak and crumbly in nature. **Figure 7.16** shows ESEM images of the UF PolyHIPE material produced when kerosene was used as the solvent (198RJC).

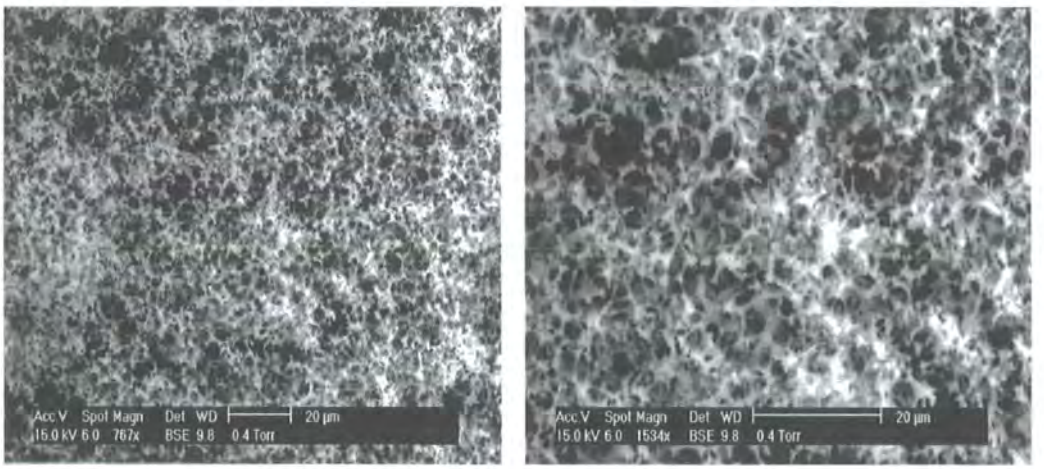

Figure 7.16 *ESEM images of the UF PolyHIPE material prepared using kerosene as the internal phase.*

There was no significant change in the morphology of the material after removal of the majority of the kerosene compared to the materials prepared after removal of the cyclohexane internal phase. The long chained hydrocarbon kerosene may act as a plasticiser during polymerisation, weakening the PolyHIPE structure.

The HIPE preparation was also performed on a larger scale to try and produce materials for mechanical testing. However several problems were encountered. In 215RJC the HIPE viscosity increased extremely quickly, therefore cyclohexane

addition became increasingly more difficult. There was no monolith produced after the acid catalyst (1M HCl) was added to the emulsion. A white powder material was produced after the removal of the cyclohexane and water. Due to the increasing viscosity of the HIPE, a greater concentration of water was used in the UF resin /water mixture in 216RJC. Due to the larger concentration of water present, expansion of the HIPE occurred due to the foaming of the water itself. The addition of the acid catalyst as in 215RJC provided no PolyHIPE monolith, only a granular white powder after removal of the cyclohexane and the water.

7.3.1.2 Thermal analysis

Figure 7.17 shows a TGA trace, in the presence of nitrogen, of the UF based PolyHIPE material and the normal S/DVB PolyHIPE material.

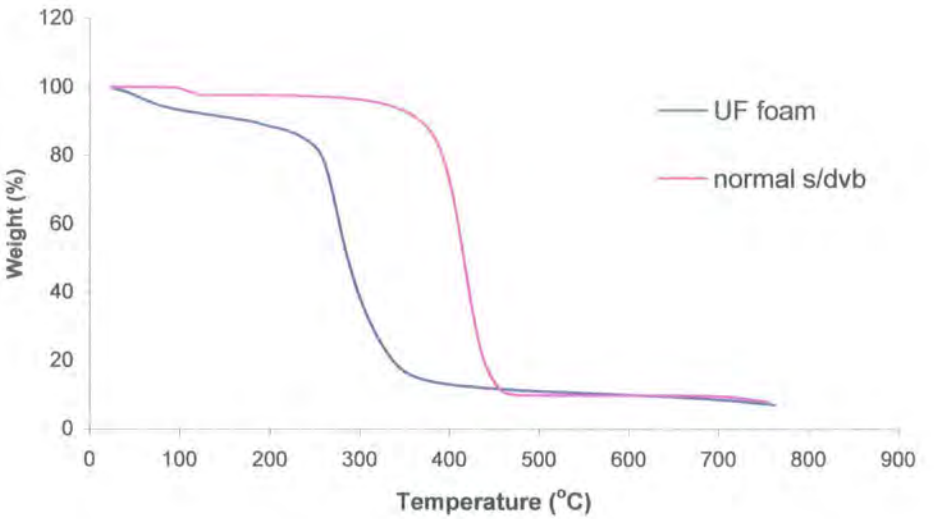

Figure 7.17 *TGA traces (in the presence of nitrogen) for the UF-based PolyHIPE material and the S/DVB PolyHIPE material.*

The TGA trace obtained for the UF-based PolyHIPE material is similar in shape to the S/DVB material. Thermal degradation for polystyrene usually occurs due to an unzipping or chain scission mechanism [135]. Degradation occurs at a lower

temperature for the UF-based PolyHIPE material (250-260 °C) compared to the S/DVB material (~ 400 °C). Conley [135] described the thermal decomposition of butylated UF resins. At 150-200 °C carbon dioxide and butanol products were detected. Above 250 °C complete volatilisation of the polymer occurred producing products such as butane, paraformaldehyde and water. This corresponds to the complete decomposition of the UF material from the TGA trace.

7.3.2 Resorcinol/formaldehyde-based PolyHIPE materials

7.3.2.1 Processing conditions and morphology

7.3.2.1.1 Small-scale preparation

On addition of the phosphoric acid and subsequent curing of the HIPE at 60 °C, a rigid salmon pink coloured PolyHIPE monolith was produced (**see figure 7.18**).

Figure 7.18 *A photograph of the small-scale resorcinol/formaldehyde-based PolyHIPE material.*

The morphology of the RF-based PolyHIPE material is shown in **figure 7.19**.

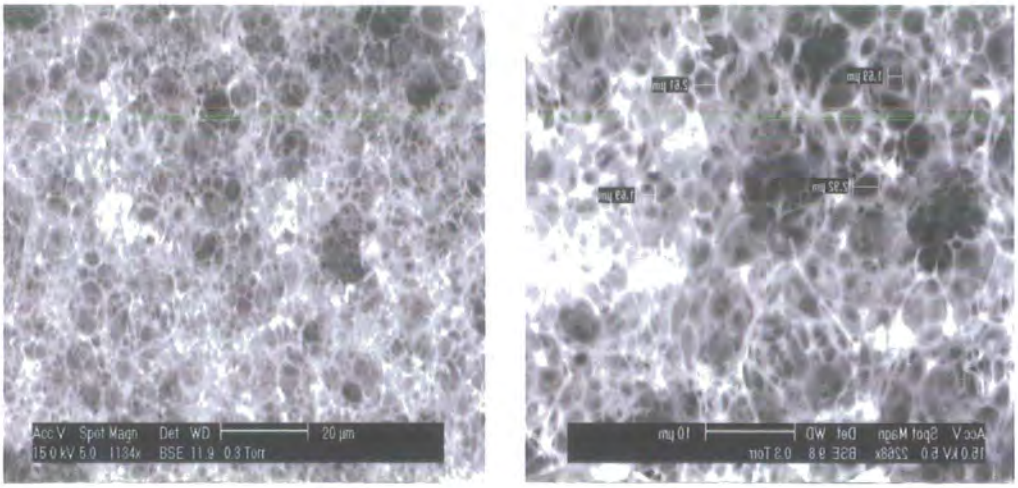

Figure 7.19 *ESEM images of the resorcinol/formaldehyde-based PolyHIPE material.*

The morphology of the RF PolyHIPE material is an interconnecting open-cellular structure that would normally be expected from a PolyHIPE material (**see figure 1.5**). There is a decrease in void and pore/interconnect size compared to the standard S/DVB PolyHIPE material. This is possibly due to the rapid curing time which prevents further coalescence of the emulsion droplets and production of larger void sizes. When the polymerisation temperature is decreased to 40 °C, the PolyHIPE is formed in around 25 minutes. At room temperature the PolyHIPE is formed in 50-60 minutes. **Figure 7.20** shows the ESEM images of the morphology of the RF material cured at room temperature.

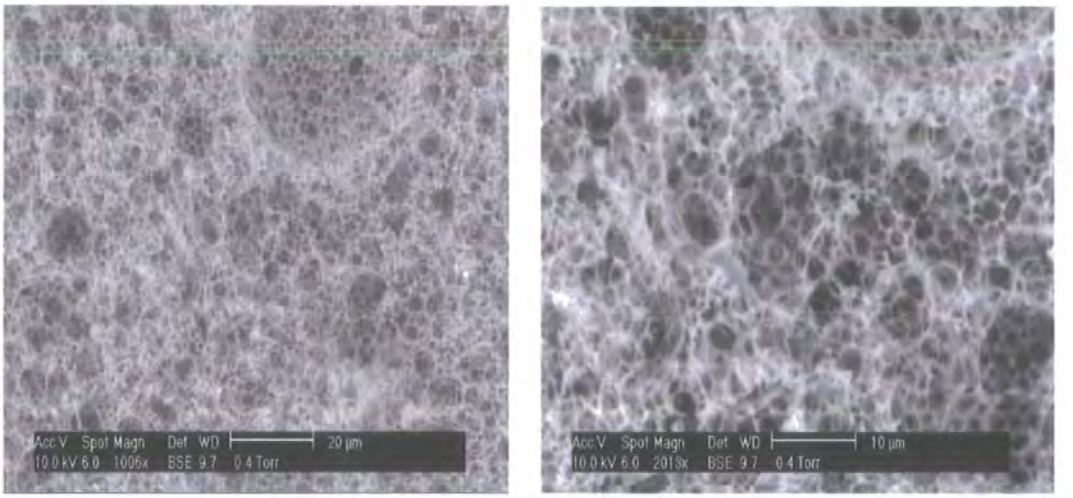

Figure 7.20 *ESEM images of the resorcinol/formaldehyde-based PolyHIPE material cured at room temperature.*

With the decrease in polymerisation temperature and the increase in polymerisation time there is now a presence of larger void sizes within the morphology of the material. The increase in polymerisation time allows more time for coalescence of the emulsion droplets.

7.3.2.1.2 Large-scale preparation

The scale-up of production of the RF-based PolyHIPE material produced minor problems. As discussed in **7.1.2** the reaction between resorcinol and formaldehyde is rapid and exothermic in nature. The scale-up of production increased HIPE preparation time and therefore gave the RF reaction more time to proceed. This caused the HIPE to increase in viscosity during cyclohexane addition, making the incorporation of all of the cyclohexane difficult. Higher shear rates (800-900 rpm) had to be used towards the end of the cyclohexane addition. The increase in HIPE viscosity also produced problems with sample uniformity. There were large voids present in the monolith after polymerisation, caused by air gaps produced between the HIPE layers after pouring into the plastic mould. **Figure 7.21** shows photographs of the RF-based PolyHIPE monolith after polymerisation.

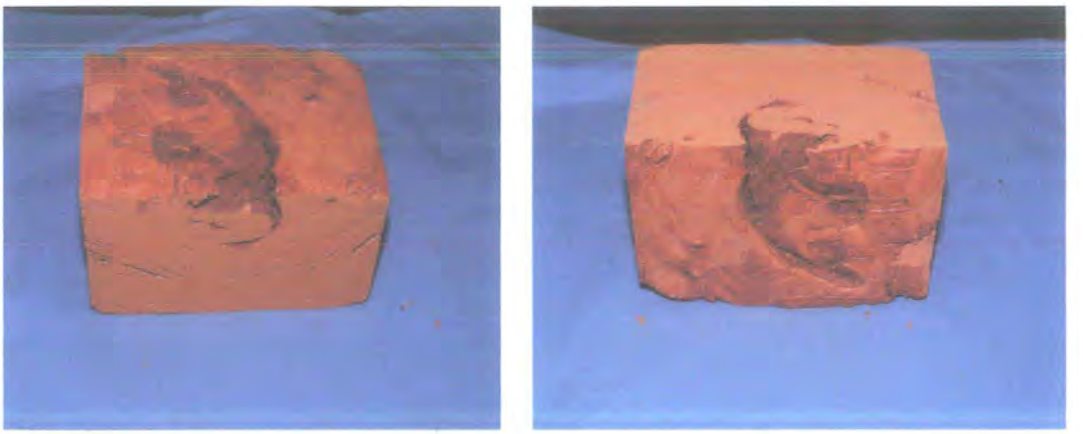

Figure 7.21 *Photographs of the RF-based PolyHIPE monolith produced for mechanical testing.*

To prevent this gelation and increase in HIPE viscosity, the plastic beaker containing the resorcinol/formaldehyde/surfactant mixture was placed in a mixture of ice and water during cyclohexane addition. This helped reduce the HIPE viscosity and improve the uniformity of RF PolyHIPE material. **Figure 7.22** shows ESEM images of the RF material produced for mechanical testing. The ESEM images show the open-cellular structure that was observed with the RF sample produced during small-scale preparation. There is a presence of larger voids (~50 μm) that could possibly be due to coalescence or trapped air pockets within the monolith due to the factors mentioned previously.

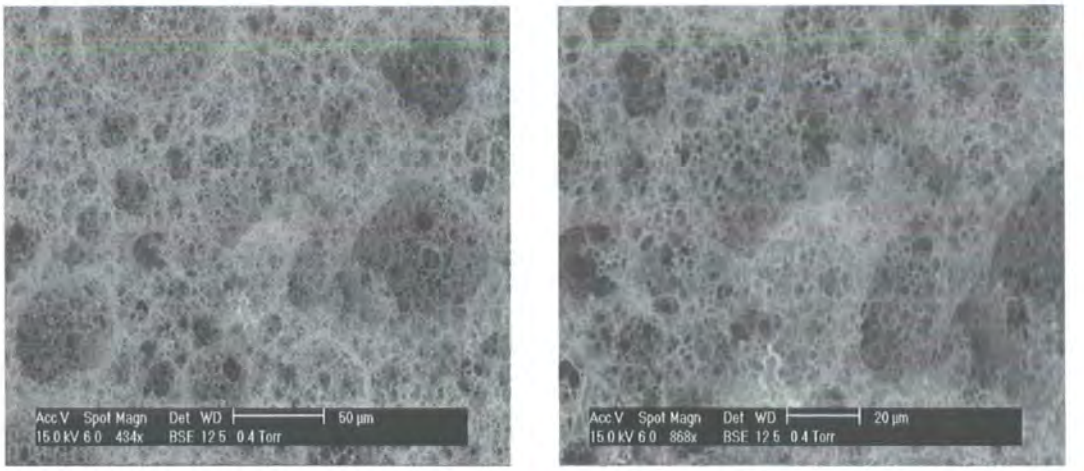

Figure 7.22 *ESEM images of the RF-based PolyHIPE material produced for mechanical testing.*

Kevlar fibres (5 % w/w) were added to the resorcinol/formaldehyde/surfactant mixture prior to HIPE preparation to produce a fibre-reinforced RF PolyHIPE material. The addition of the Kevlar fibres increased the continuous phase viscosity and therefore the HIPE viscosity increased, making cyclohexane addition difficult towards the end of the HIPE preparation. **Figure 7.23** shows ESEM images of the fibre reinforced RF-based PolyHIPE material. From **figure 7.23 (a)** there are large voids and holes observed within the material, due to coalescence or the high viscosity due to the presence of the Kevlar fibres, preventing efficient mixing. **Figures 7.23 (b) and (c)** show the interaction of the Kevlar fibre with the RF based cellular matrix. From the ESEM images it is clear that Kevlar fibre bonds strongly to the RF matrix and that they can inhibit crack propagation by slowing down or deviating the crack as shown in **figure 7.23 (b)**.

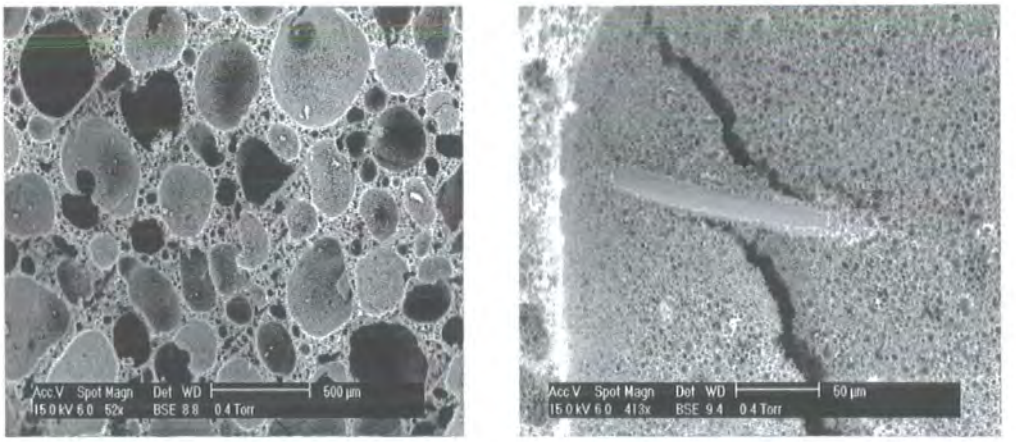

(a) (b)

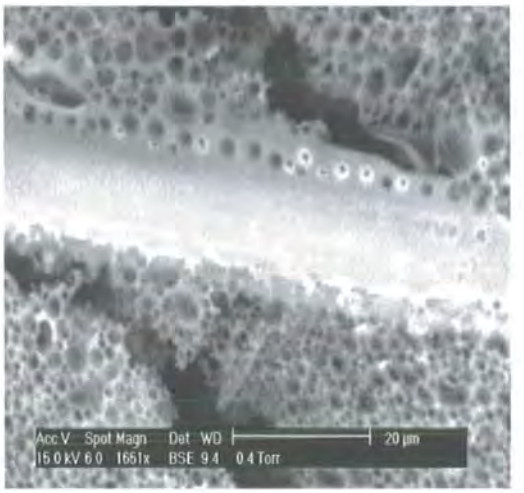

(c)

Figure 7.23 *ESEM images of the Kevlar reinforced RF-based PolyHIPE material.*

7.3.2.2 Thermal analysis

Figure 7.24 shows TGA traces obtained under both nitrogen and air, for the RF and S/DVB based PolyHIPE materials. The shape of the curve obtained for the RF based material is different from that obtained for the S/DVB and other based PolyHIPE materials previously. The curve for the S/DVB PolyHIPE material shows instant decomposition at a certain temperature. This TGA trace is characteristic for polystyrene and other olefin based polymers. As mentioned previously the thermal degradation of polystyrene to a large extent is by a chain scission or unzipping mechanism. In the presence of air the temperature at which this decomposition

occurs, decreases due to the catalytic nature of oxygen reducing the energy activation barrier for degradation, therefore enhancing decomposition. The RF PolyHIPE material shows the typical TGA trace for a phenolic resin [135]. In the presence of nitrogen there is a steady decrease in weight to ~ 60 % at 750 °C. According to Conley [135] the degradation process is accelerated by the phenyl groups adjacent to the methylene bridges, and is dependent on the number of the dihydroxyphenyl methane units present in the material. In the presence of oxygen the decomposition rate of the RF material increases, as expected, at temperatures greater than 400 °C. This is due to the presence of oxidative degradation of the polymer to produce carbon dioxide and carbon monoxide, which are the major products of oxidative degradation at temperatures above 450 °C.

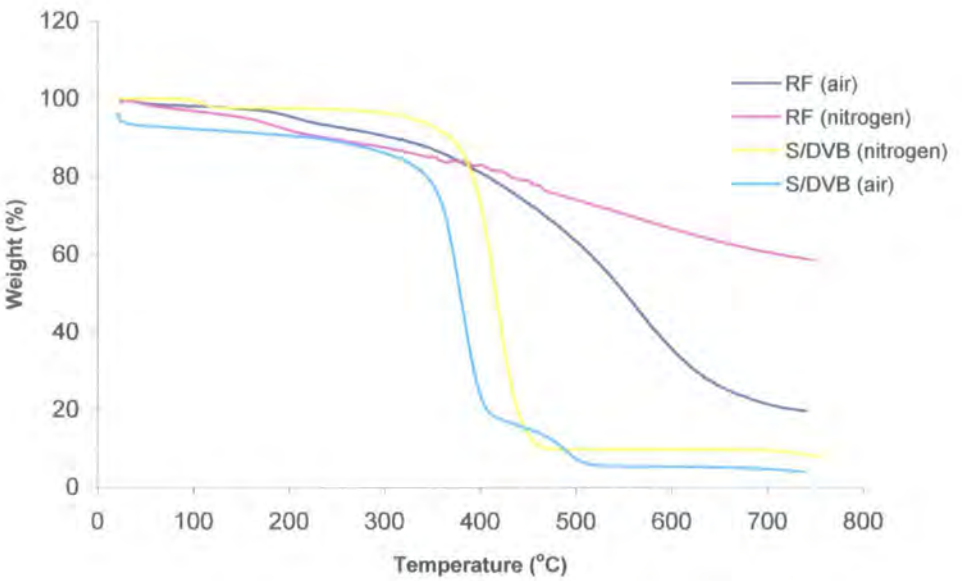

Figure 7.24 *TGA traces of the RF and S/DVB-based PolyHIPE materials obtained under air and nitrogen.*

This could also account for the lower residual mass compared to the RF material exposed to a nitrogen atmosphere. In the presence of an inert atmosphere such as nitrogen there may only be thermal degradation/fragmentation products or a low

concentration of oxidative degradation products. At temperatures up to 400 °C water and paraformadehyde are the major products formed [135]. Products from thermal degradation due to fragmentation or pyrolysis are also present at high temperatures. The residual mass at 750 °C was 20 % w/w. The RF-based PolyHIPE material shows greater thermal and thermo-oxidative stability, than the S/DVB PolyHIPE material in the presence of both air and nitrogen.

7.3.3 95 % void styrene- and MMA-based PolyHIPE materials

7.3.3.1 Stability and morphology

The increase in internal (droplet) phase volume added had no drastic effect on HIPE formation. Towards the end of the HIPE preparation, droplet phase addition became more difficult due to the increase in internal phase volume and HIPE viscosity. **Figure 7.25** shows ESEM images of the 95 % 90/10 S/DVB PolyHIPE material prepared with Span 80 as surfactant.

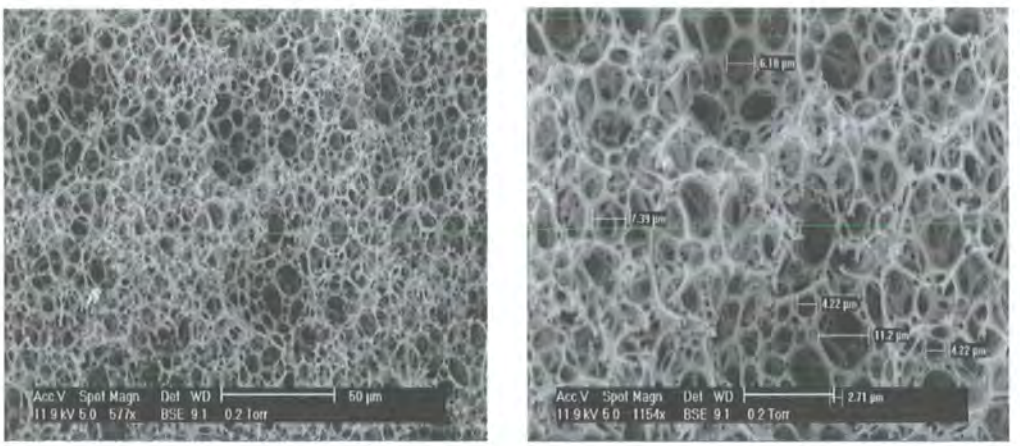

Figure 7.25 *ESEM images of the 95 % void S/DVB based PolyHPE material.*

The ESEM images show that the 95 % S/DVB PolyHIPE material has an interconnecting morphology with a higher degree of porosity and open-cellular nature compared to the 90 % void material, due to the increase in droplet phase volume. The void size from the ESEM images is in the range 15-25 µm.

Figure 7.26 shows ESEM images of the 95 % void S/DVB material prepared with the optimised surfactant system. The ESEM images show the standard open-cellular morphology of a PolyHIPE material (**see figure 1.5**). As was apparent for the 90 % void material (**see chapter 5**), there is a presence of larger than expected voids (70-120 μm) and the presence of larger interconnect sizes when the OSS system is used as surfactant.

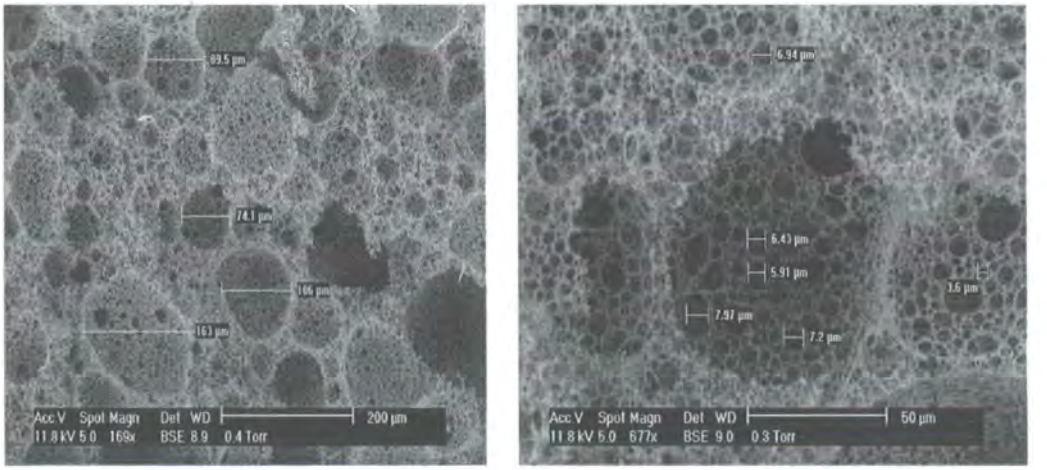

Figure 7.26 *ESEM images of the 95 % void S/DVB PolyHIPE material prepared with the OSS.*

The presence of the larger voids is most likely due to coalescence of the droplet phase. This sign of emulsion instability could be due to the lower concentration of surfactant present in the monomer phase with the OSS (7 % w/w) compared to Span 80 (20 % w/w). Since both the addition of fibres and the use of the OSS resulted in an increase in both the flexural and compressive properties of the PolyHIPE material, the two methods were combined to observe if any added mechanical performance could be obtained. **Figure 7.27** shows ESEM images of the 95 % void S/DVB PolyHIPE material prepared with OSS reinforced with 10 % w/w Kevlar fibres.

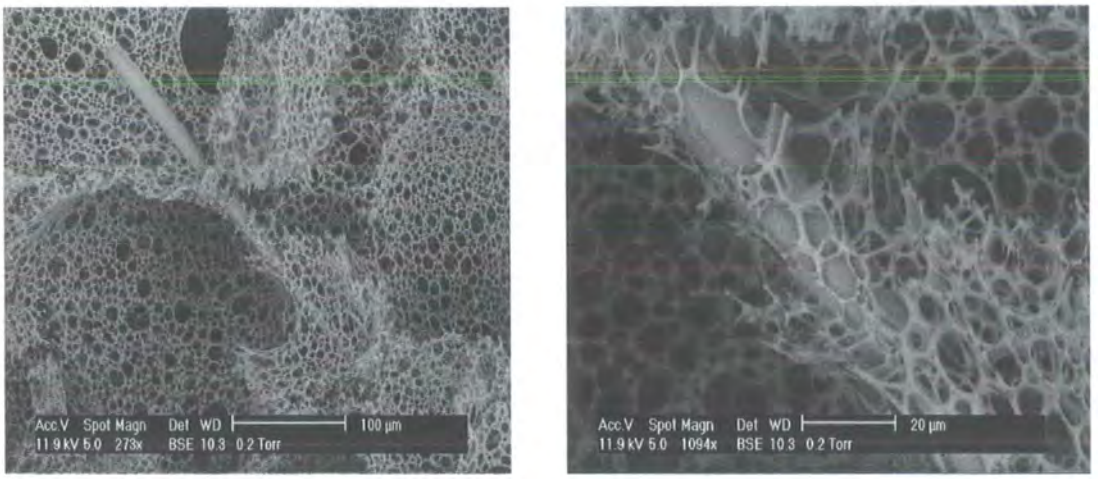

Figure 7.27 *ESEM images of the 95 % void S/DVB PolyHIPE material prepared with the OSS and reinforced with 10 % w/w Kevlar fibres.*

The fibre-reinforced PolyHIPE material has the normal open-cellular structure that would be expected from a PolyHIPE material. The ESEM images also show the interaction of the Kevlar fibre with the S/DVB PolyHIPE matrix. As was shown in **chapter 3**, the Kevlar fibre does bond strongly with the PolyHIPE matrix and therefore an enhancement in mechanical performance is expected.

Figure 7.28 shows ESEM images of the 95 % S/DVB PolyHIPE material prepared with the redox initiator.

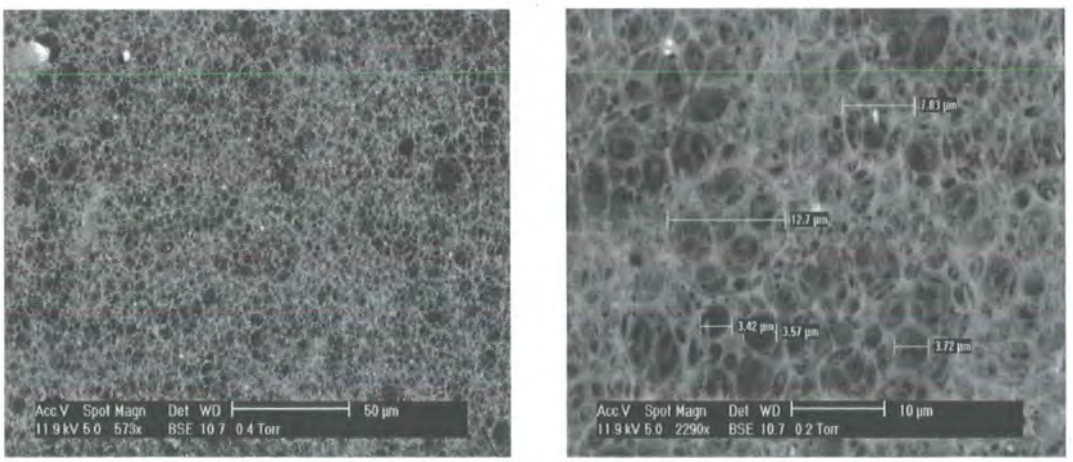

Figure 7.28 *ESEM images of the 95 % void S/DVB PolyHIPE material prepared with a redox initiator.*

The morphology of the redox-initiated material is the normal open cellular morphology that would be expected from a PolyHIPE material. As was already discussed for the 90 % void redox-initiated PolyHIPE material (**see chapter 5**), there is a decrease in the void size compared to the potassium persulfate-initiated material. This is due to the decrease in curing time with the use of the redox initiator allowing less time for coalescence of the droplet phase to occur.

Figure 7.29 shows ESEM images of the 95 % void S/MMA/DVB PolyHIPE material.

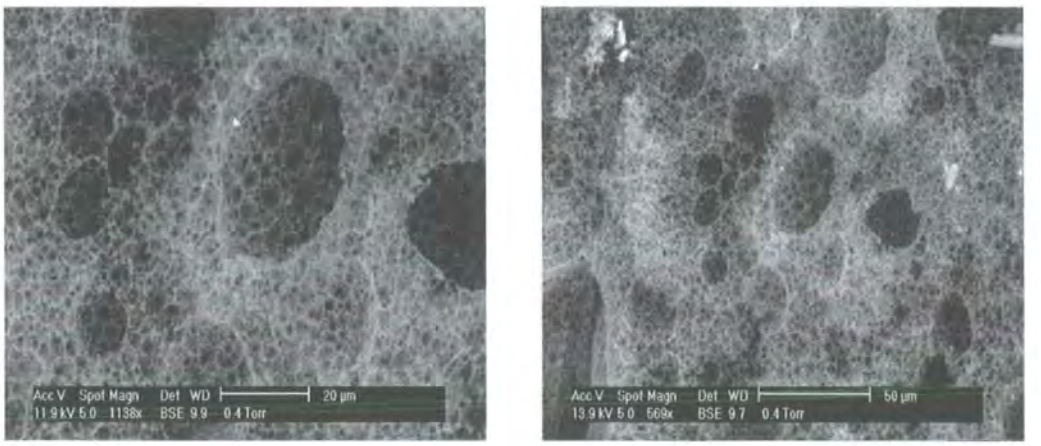

Figure 7.29 *ESEM images of the 95 % void S/MMA/DVB PolyHIPE material.*

The morphology of the 95 % void MMA based material is similar to that observed for the 90 % void material (**see chapter 4**). The morphology is of a structure which is less open-cell in nature. This structure was common for MMA-based PolyHIPE materials. The larger voids present are again due to decreasing emulsion stability and coalescence of the droplet phase due to the presence of the hydrophilic MMA.

7.3.4 Mechanical test results

7.3.4.1 Core shear tests

Table 7.2 shows the results obtained from the core shear tests.

Table 7.2 PolyHIPE core shear tests

Sample name [a]	Mean density (gcm^{-3})	Mean shear modulus, G (MPa) [b]	Mean shear strength, τ (MPa) [b]
OSS 10K	0.069	3.84 +/- 0.87	0.41+/- 0.08
OSS	0.062	4.36 +/- 2.00	0.39 +/-0.09
Normal	0.068	3.06 +/- 1.09	0.20 +/- 0.02
Redox	0.064	2.50 +/- 0.35	0.21+/- 0.05
40 % MMA	0.061	2.54 +/- 0.23	0.17 +/- 0.01
RF	0.064	3.11 +/- 0.52	0.15 +/- 0.03
RF 5K	0.081	4.28 +/- 0.35	0.27 +/- 0.008

a- OSS 10K = 90/10 S/DVB PolyHIPE material prepared with the OSS and containing 10 % w/w Kevlar fibres, OSS = 90/10 S/DVB PolyHIPE material prepared with the OSS, normal = standard 90/10 S/DVB PolyHIPE material prepared with Span 80 (15 % w/w), redox = 90/10 S/DVB PolyHIPE material prepared using a redox initiator, 40 % MMA = 50/40/10 S/MMA/DVB PolyHIPE material, RF = resorcinol/formaldehyde based PolyHIPE material, RF 5K= resorcinol/formaldehyde PolyHIPE material containing 5 % w/w Kevlar fibres.

b- expressed as +/- standard deviation

7.3.4.1.1 Styrene- and MMA-based PolyHIPE materials

Figures 7.30 and 7.31 show a graph comparing the shear modulus and strength values for the styrene- and MMA-based PolyHIPE materials.

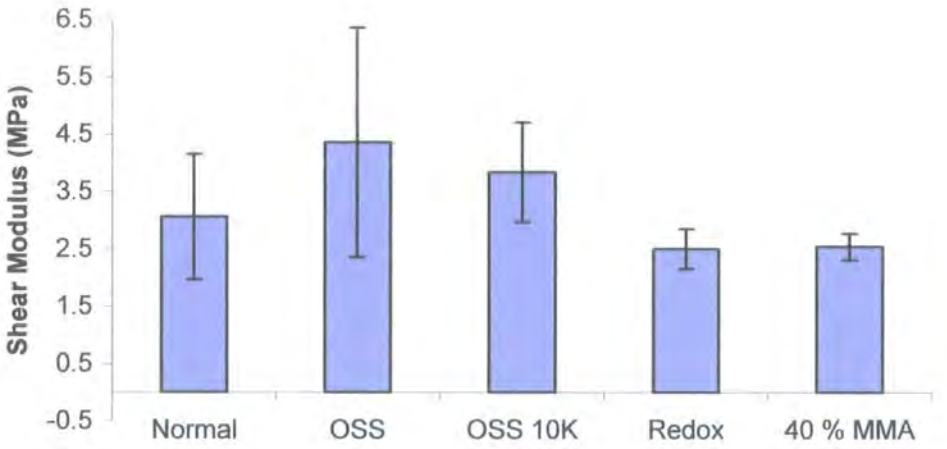

Figure 7.30 *Comparison of the shear modulus values of the styrene- and MMA based-PolyHIPE materials.*

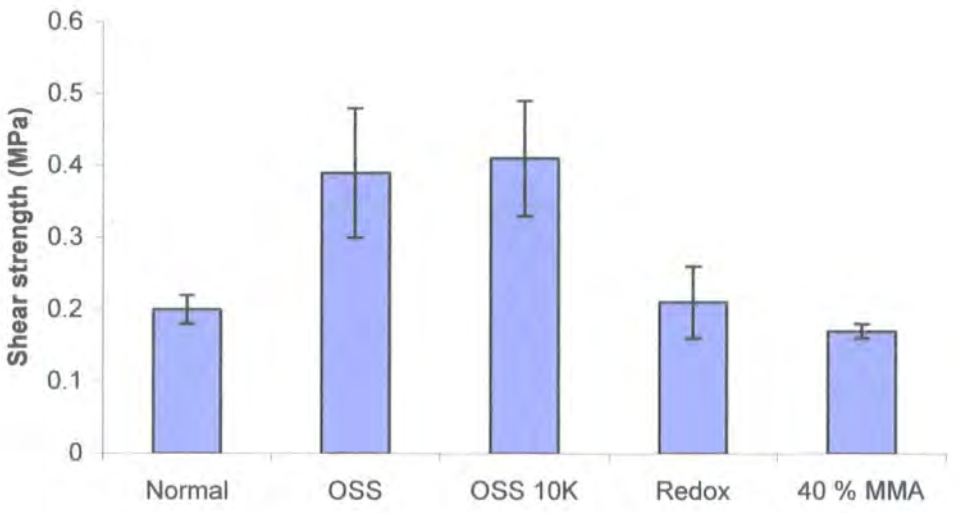

Figure 7.31 *Comparison of the shear strength values for the styrene- and MMA based-PolyHIPE materials.*

The S/DVB PolyHIPE material prepared using the OSS as surfactant instead of Span 80 provided the best enhancement in shear modulus and strength for the S/MMA based materials. The addition of the Kevlar fibres to the PolyHIPE provided no further significant increase in the shear properties of the material. As was discussed in **chapter 6**, replacement of the surfactant Span 80 with the OSS provides a more rigid/stronger PolyHIPE material, due to the absence of the plasticisation effect of Span 80. The redox-initiated and MMA-based materials showed no increase in the shear properties compared to standard S/DVB PolyHIPE material. The result for the MMA-based PolyHIPE material was disappointing after the enhancement in the compressive properties in the material shown in **chapter 6**. At this lower relative density, it may be that the effect of MMA on the properties of the material is not so significant. **Figure 7.32** shows photographs of the PolyHIPE materials after tensile shear core testing and **table 7.3** provides the shear modulus and strength values for the samples specimens present in the photographs. The photographs show the point of failure for each material and where the foams have become detached from the plate materials. There is a correlation between the shear test results and the points of fracture/de-bonding of the materials. From **figure 7.32 (c)** for XA20594, XA20595 and XA20596, when the PolyHIPE material has become detached from the steel plates, a lower than average modulus and strength value is obtained. For XA20594 there was no modulus or strength value obtained due to complete de-bonding of the foam from the face material. The importance of the adhesion between the core and face materials to the strength of the sandwich panel has already been discussed in **chapter 1**. This is also apparent for XA20570 and XA20571, where there is a lower than average modulus and strength value when the majority of the core material has become detached from the face material.

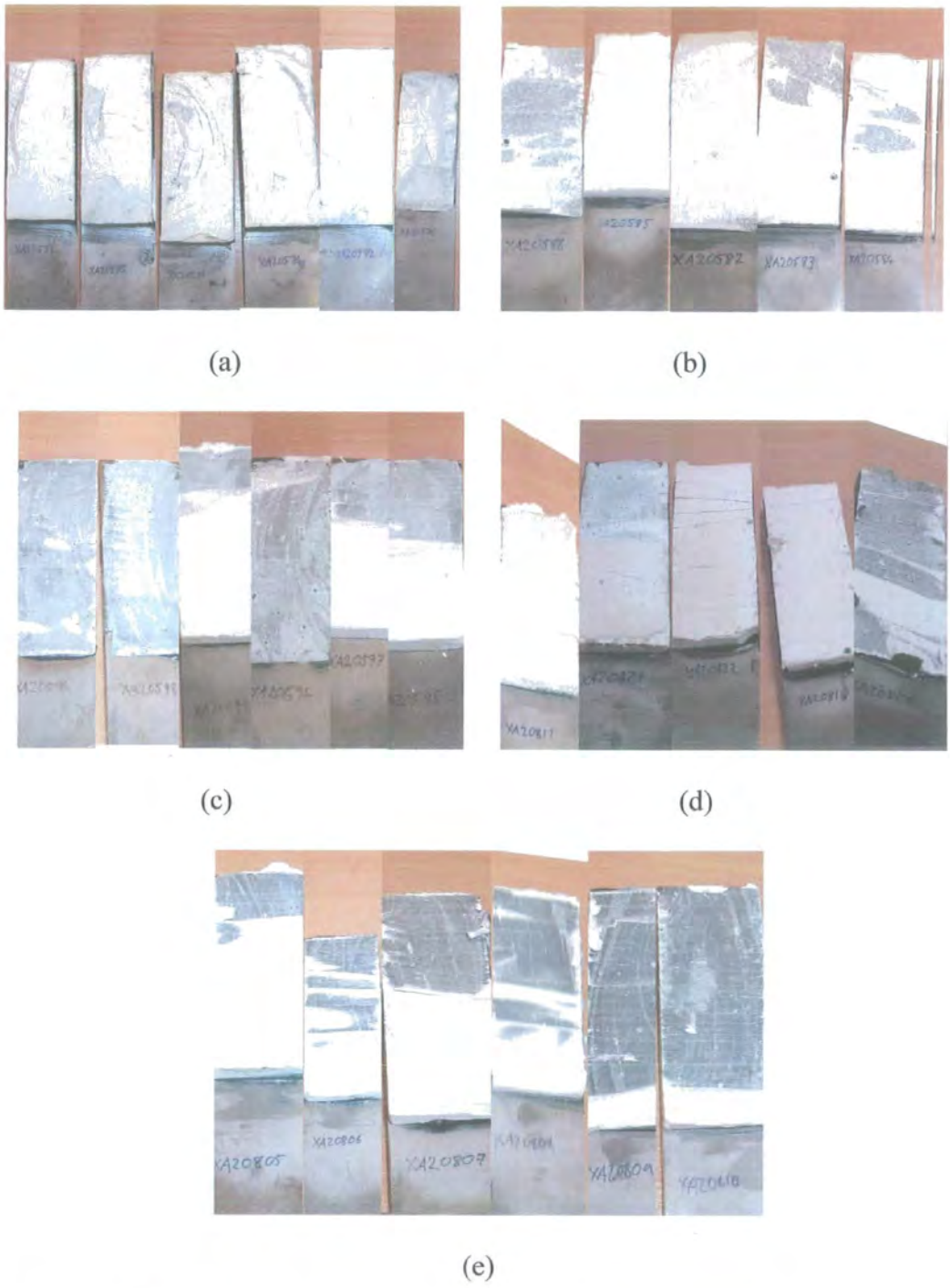

Figure 7.32 *Photographs of the S/MMA based core materials after tensile shear testing, (a) S/DVB material prepared with OSS, (b) S/DVB material prepared with OSS and 10 % w/w Kevlar fibres, (c) standard S/DVB material prepared with Span 80, (d) S/DVB material prepared with redox initiator and (e) S/MMA/DVB material prepared with Span 80.*

Table 7.3 Shear test results of all the PolyHIPE core samples tested

Sample name [a]	Sample Code	Shear Modulus (MPa)	Shear strength (MPa)
OSS 10 K	XA20570	2.96	0.29
	XA20571	2.99	0.38
	XA20572	3.46	0.34
	XA20573	4.26	0.46
	XA20574	4.20	0.47
	XA20575	5.20	0.49
OSS	XA20582	2.8	0.27
	XA20583	3.86	0.49
	XA20584	1.64	0.45
	XA20585	4.8	0.27
	XA20586	6.93	0.43
	XA20587	6.12	0.42
Normal	XA20594	No data	No data
	XA20595	1.99	0.20
	XA20596	1.99	0.17
	XA20597	3.33	0.18
	XA20598	4.54	0.23
	XA20599	3.46	0.22
Redox	XA20817	2.77	0.2
	XA20818	2.36	0.16
	XA20819	0.00	0.29
	XA20820	2.53	0.18
	XA20821	2.82	0.18
	XA20822	1.97	0.22
40 % MMA	XA20805	2.18	0.16
	XA20806	2.76	0.18
	XA20807	2.48	No data
	XA20808	2.59	0.19
	XA20809	2.80	0.19
	XA20810	2.42	0.16

a- see ***table 7.2***.

7.3.4.1.2 Resorcinol/formaldehyde-based PolyHIPE materials

Figures 7.33 and 7.34 show the graphs comparing the shear modulus and strength values for the standard S/DVB PolyHIPE material, the S/DVB PolyHIPE material prepared with the OSS- and the RF-based PolyHIPE materials.

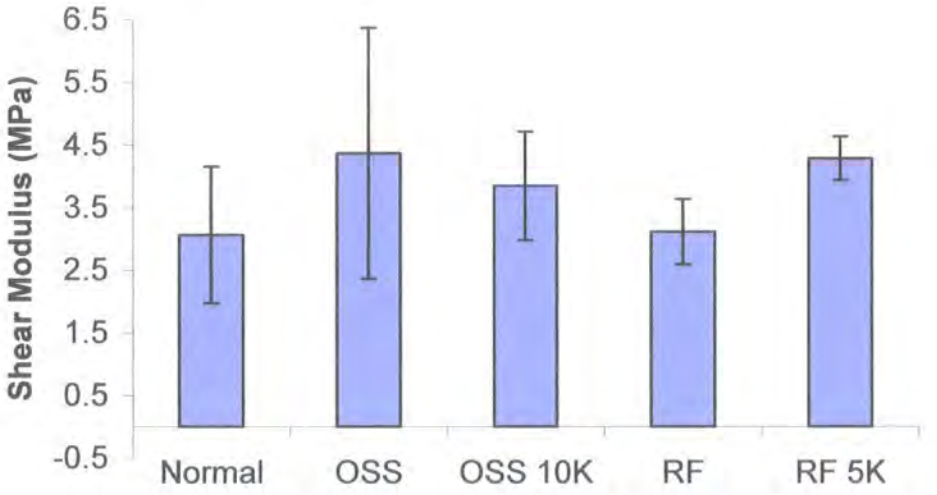

Figure 7.33 *Comparison of the shear modulus values of the standard S/DVB material, the S/DVB materials prepared with the OSS and the RF-based PolyHIPE materials.*

The RF-based PolyHIPE material shows no significant difference in modulus value compared to the S/DVB PolyHIPE material. When the Kevlar fibres are added to the material there is significant increase in modulus, equal to the S/DVB material produced with the OSS. This increase could be due to a combination of the presence of the fibres and the difference in morphology of the two materials. The morphology of the RF-based PolyHIPE materials used for mechanical testing was discussed in **7.3.2.1.2**. The Kevlar-reinforced RF material had a morphology consisting of large voids of low porosity/closed-cell nature surrounded by an open-cellular structure of smaller void size. This was said to be due to the increasing HIPE viscosity making solvent addition difficult towards the end of HIPE preparation.

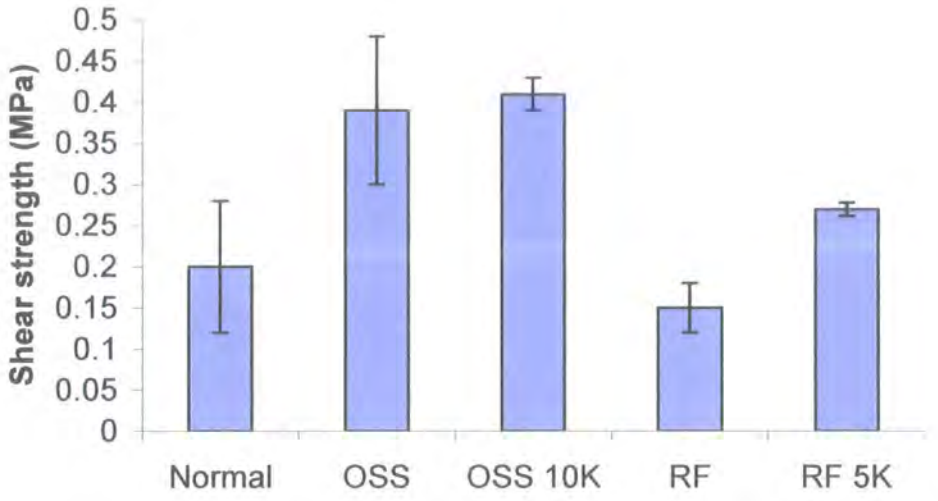

Figure 7.34 *Comparison of the shear strength values of the standard S/DVB material, the S/DVB materials prepared with the OSS and the RF-based PolyHIPE materials.*

The fibre-free material showed an interconnecting structure with a higher degree of open-cellular nature than the fibre-reinforced RF material. The influence of the porosity and closed cell nature on the mechanical performance of a material has of a porous material has already been discussed (**see chapter 1**) and may account for the enhanced modulus value of the fibre-reinforced RF material.

The shear strength values of both fibre-reinforced and fibre-free RF material are significantly lower than that of the S/DVB material prepared with the OSS. However, the fibre-reinforced RF material does have a higher shear strength value than that of the standard S/DVB material prepared with Span 80. This enhancement again could be due to the factors already mentioned for the shear modulus values. The low shear strength values suggest that the RF material is more brittle in nature compared to the S/DVB PolyHIPE materials. The processing problems discussed in **7.3.2.1.2** must also be taken into account. Small holes/defects may still be present

due to these factors and may affect the mechanical performance of the material compared to the S/DVB PolyHIPE materials.

7.3.4.2 Core compression tests

Table 7.4 provides the core compressive modulus and strength values obtained for each PolyHIPE material.

Table 7.4 Results obtained from the PolyHIPE core compression tests

Sample name [a]	Mean density (gcm^{-3})	Mean compressive modulus, E (MPa) [b]	Mean compressive strength, σ (MPa) [b]
OSS 10 K	0.070	10.86 +/- 0.75	0.507 +/- 0.1
OSS	0.068	9.10 +/- 0.75	0.367 +/- 0.002
Normal	0.062	7.67 +/- 0.75	0.357 +/- 0.02
Redox	0.067	7.68 +/- 0.75	0.277 +/- 0.006
40 % MMA	0.069	7.31 +/- 0.75	0.358 +/- 0.017
RF	0.065	5.74 +/- 2.14	0.644 +/- 0.024
RF 5K	0.082	10.05 +/- 0.35	0.667 +/- 0.021

*a- see **table 7.2**.*

b- expressed as +/- standard deviation

7.3.4.2.1 Styrene- and MMA-based PolyHIPE materials

Figures 7.35 and 7.36 show the core compressive modulus and strength results for the styrene and MMA based PolyHIPE materials.

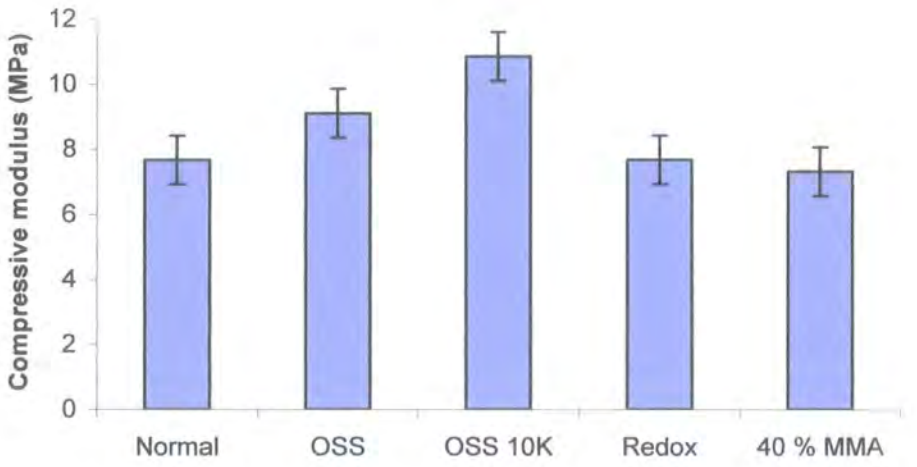

Figure 7.35 *Comparison of the core compressive modulus values for the styrene- and MMA-based PolyHIPE materials.*

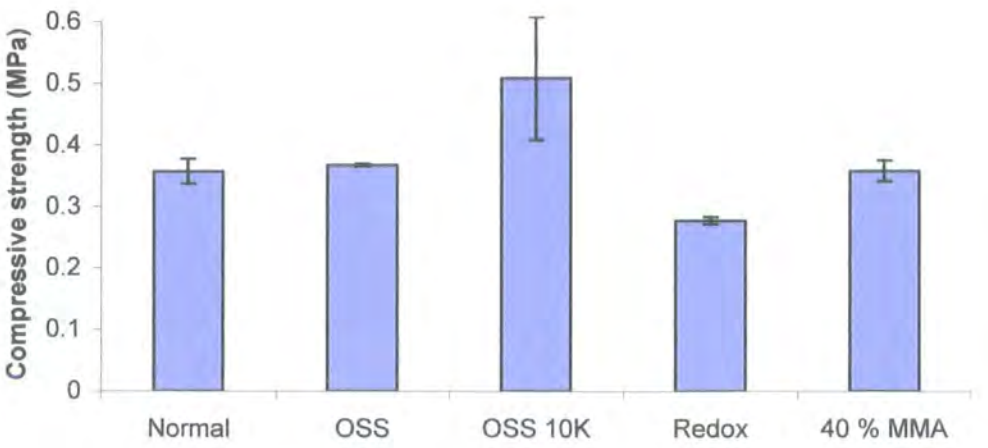

Figure 7.36 *Comparison of the core compressive strength values for the styrene- and MM- based PolyHIPE materials.*

The S/DVB PolyHIPE material prepared with the OSS shows the greatest improvement in the compressive properties compared to the standard S/DVB material. The redox-initiated S/DVB PolyHIPE and the MMA-based PolyHIPE material show no change significant change or improvement. The addition of the Kevlar fibres to the OSS PolyHIPE material provided only a small increase in shear strength. However, the addition of the Kevlar fibres did provide a significant improvement of the PolyHIPE material in both yield and the elastic (modulus) behaviour of the material under a compressive stress. The MMA-based material, as with the shear tests, did not show the expected improvement in performance in compression. The 90 % void (0.1 gcm^{-3}) MMA-based material, as discussed in **chapter 6**, provided a significant improvement in mechanical performance under a compressive stress, at a concentration level of 40 % w/w. At a density of 0.05 – 0.06 gcm^{-3} (95 % void) the MMA has no considerable effect on the mechanical performance of the foam material. There is no change in morphology of either the 95 % material compared to the 90 % MMA (40 % w/w) to suggest a change in mechanical performance, the structures of both materials are very similar. The 90 % void materials were cleaned with water and propan-2-ol prior to testing. The cleaning procedure removes any residual salt or surfactant present within the material. Due to the sample size of the 95 % void materials and the length of time that would be needed to clean and dry these materials, the 95 % void materials were not cleaned prior to drying or testing. This would leave residual surfactant present within the material during the drying process. The effect of Span 80 acting as a plasticiser during polymerisation has already been discussed. Further drying of the material in the presence of Span 80 could lead to further detrimental effects on the MMA-based foam properties.

7.3.4.2.2 Resorcinol/formaldehyde-based PolyHIPE materials

Figure 7.37 and 7.38 show the compressive modulus and strength values of the standard S/DVB PolyHIPE material, the S/DVB PolyHIPE materials prepared with the OSS and the RF-based PolyHIPE materials.

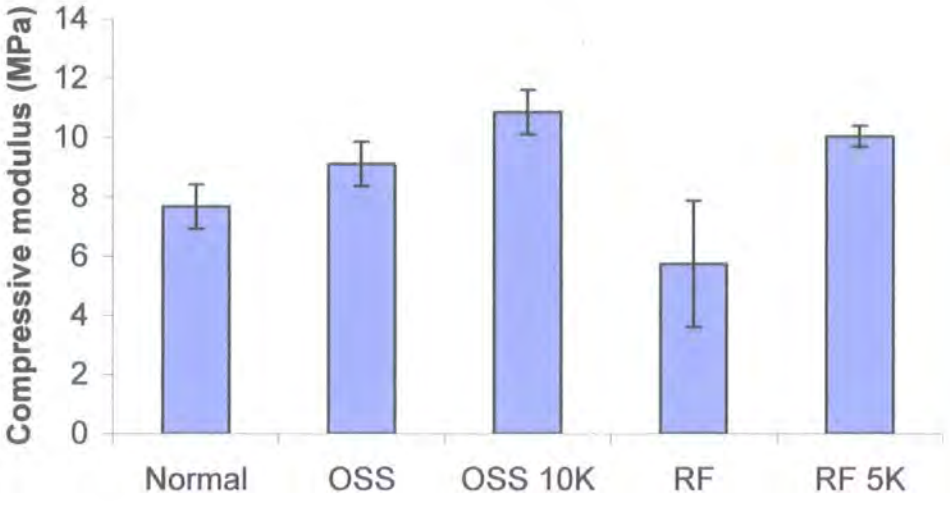

Figure 7.37 *Compressive modulus values for the standard S/DVB PolyHIPE material; the S/DVB PolyHIPE materials prepared with the OSS and the RF-based PolyHIPE materials.*

The fibre-free RF material shows a significant decrease in compressive modulus value compared to the standard S/DVB PolyHIPE material. This again could be due to the processing problems affecting sample uniformity and the mean modulus value as discussed in **7.3.2.1.2**. The large standard deviation obtained for the RF-based material also suggests a problem with sample uniformity. The addition of the Kevlar fibres produces a RF material with improved modulus values compared to the standard S/DVB material in compression. The fibre-reinforced RF material is also similar to or equal in compressive modulus value to the S/DVB PolyHIPE material prepared with the OSS and the fibre-reinforced OSS material.

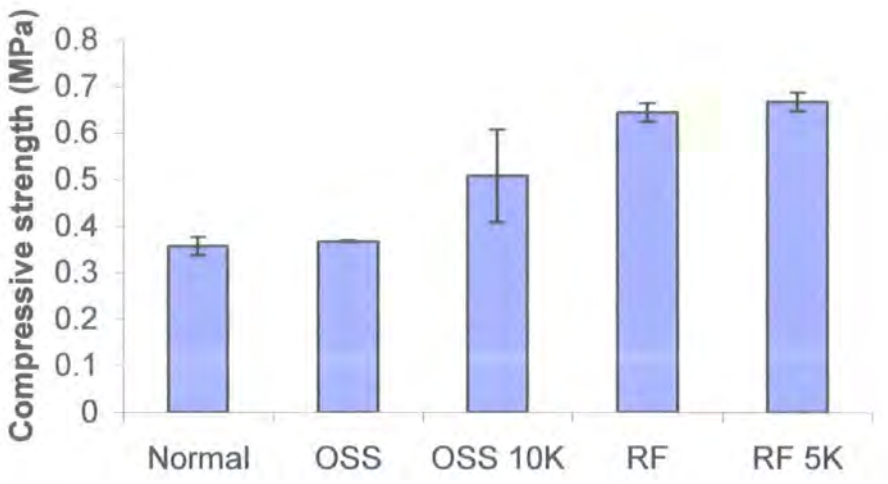

Figure 7.38 *Compressive strength results for the standard S/DVB PolyHIPE material, the S/DVB PolyHIPE materials prepared with the OSS and the RF based PolyHIPE materials.*

The fibre-free and the fibre-reinforced RF materials produce more than a two-fold increase in compressive strength compared to the standard S/DVB material. The RF materials also show a significant increase compared to the S/DVB materials prepared with the OSS. The compressive strength of a foam material, as discussed previously (**see chapter 1**), is measured at the point of collapse of the cellular foam structure. Under a compressive stress the modes of collapse are elastomeric buckling, plastic yielding, or brittle crushing. The increase in the compressive strengths of the RF material compared to the S/DVB materials, suggest that the RF network is a more rigid, highly cross-linked network than the S/DVB network, producing a stronger foam material during the yielding process (plastic collapse). The similarities in the compressive strength values of both the fibre-free and the fibre-reinforced RF material, support the argument that the low compressive modulus value obtained for the non-reinforced RF material is due to the variation in sample uniformity as discussed previously.

7.3.5 Comparison with commercially available core materials

To assess whether PolyHIPEs can viable as core materials, they must be compared to the commercially available core materials. The different types of core material were discussed in **chapter 1** and the mechanical data on selected materials were shown in **tables 1-12** in the appendix.

The shear strengths of our two best materials, the fibre-free and the fibre-reinforced OSS material, compare well with the Divinycell HT material at 50 kgm^{-3} (0.55 MPa) and were also equal to the shear strength of the Rohacell FX at 50 kgm^{-3} (0.4 MPa). This is promising as Rohacell is generally a closed-cell material (**see chapter 1**). The shear strengths of the OSS PolyHIPE materials are also comparable to the Tubus-Bauer honeycomb (polypropylene) materials at 80 kgm^{-3} (0.4-0.5 MPa), but do not come close to the balsa wood materials at the same density values. The shear modulus values for all the tested PolyHIPE materials are far less than those of the commercially available materials examined.

Our best styrene-based PolyHIPE material containing the OSS and 10 % w/w Kevlar fibres (0.51 MPa) and the RF-based PolyHIPE materials (0.64 and 0.67 MPa) compete very well on the compressive strength performance with the commercial foams such as Airex R82 (0.6 MPa), Divinycell HT (0.7 MPa), ATC core (0.4, 0.5 and 0.66 MPa) and Rohacell FX (0.4 MPa) at roughly the same density of material (50 – 60 kgm^{-3}). The modulus on the other hand does not really compete with any of the commercial foam core materials at the present moment. The properties of the PolyHIPE core materials tested do no compete with the commercially available honeycomb or balsa wood materials due to the anisotropic nature of the these materials.

7.4 Conclusions

In this chapter it has been shown it is possible to prepare cellular UF-based PolyHIPE materials by the curing of a UF resin within a HIPE by the addition of an acid catalyst. When ammonium chloride was used as a catalyst, an elastomeric PolyHIPE material was produced within 48-72 hours. The PolyHIPE material, which was produced, had an interconnecting open-cell morphology. When 1M HCl was used as catalyst a UF-based PolyHIPE material was produced within 24 hours. The material produced was more rigid in nature than the material produced when ammonium chloride was used as catalyst. The TGA trace for the UF-based PolyHIPE material was similar in shape to the S/DVB material, but the temperature at which the majority of thermal degradation begins is lower than that for S/DVB.

It was also shown that it is possible to prepare resorcinol/formaldehyde (RF) based PolyHIPE materials by the addition of phosphoric acid to the HIPE containing a continuous phase of both resorcinol and formaldehyde. A rigid salmon-pink coloured monolith was produced within 10 minutes at a curing temperature of 60 °C. At 40 °C the reaction cured in 20-25 minutes and at room temperature between 50 and 60 minutes. The RF-based PolyHIPE material showed the open-cellular structure that would normally be expected for a PolyHIPE material. The large-scale preparation of the materials encountered problems, such as HIPE gelation and increase in viscosity due to the rapid exothermic reaction between resorcinol and formaldehyde. The gelation and increase in viscosity of the emulsion resulted in the production of a non-uniform sample due to the holes/defects present caused by trapped air pockets between the layers of the emulsion. The preparation container was placed in a mixture of ice/water to dissipate the heat and slow down the reaction rate. This decreased the HIPE viscosity and allowed for a more uniform PolyHIPE sample to

be produced. Kevlar fibres were added to the resorcinol/formaldehyde continuous phase and a fibre-reinforced RF PolyHIPE material was also produced. The ESEM images showed there was a strong interaction between the RF matrix and the Kevlar fibre. The TGA traces showed that the RF material was thermo-oxidatively more stable than the standard S/DVB PolyHIPE material

It was also shown that it was possible to prepare 95 % void styrene/DVB- and MMA-based PolyHIPE materials. The S/DVB materials prepared with Span 80 and OSS showed the normal open-cellular PolyHIPE structure. The PolyHIPE material prepared with the OSS showed the presence of large voids, which were also noticed in the 90 % void OSS material. A 95 % void fibre-reinforced S/DVB material using the OSS as surfactant was also prepared. The Kevlar fibre as previously showed a strong interaction with the PolyHIPE matrix. The 95 % void redox-initiated S/DVB material showed a small and narrow pore size distribution, as did the 90 % void material. This was due to the rapid polymerisation time. The morphology of the 95 % void MMA material was similar to that of the 90 % void MMA material. The material had an open-cell morphology of low porosity.

The mechanical test results showed the expected increase in the shear properties of the S/DVB PolyHIPE material when the foam material was prepared using the OSS as surfactant. The reinforcement of the OSS material with Kevlar fibres showed no increase in the mechanical properties of the material under a shear stress. Both the redox-initiated and the MMA-based PolyHIPE material showed no significant change in either shear modulus or strength value. The OSS material also showed the greatest improvement in compressive mechanical properties of the styrene- and MMA-based core materials. With the reinforcement of the OSS material with Kevlar fibres there is further enhancement in both the compressive strength and modulus

value. The redox-initiated and MMA-based PolyHIPE materials again showed no significant improvement in performance compared to the normal S/DVB PolyHIPE material. The RF-based material showed no significant difference in shear modulus or strength value compared to the standard S/DVB material. When the RF material was reinforced with Kevlar fibres there was an increase in both the shear modulus and strength value. A factor which could affect the mechanical performance was the sample uniformity, due to increasing HIPE viscosity and rapid curing time producing holes/defects within the material. The non-reinforced RF material showed a slight decrease in modulus value compared to the standard S/DVB material. The large standard deviation in the results suggested that sample uniformity was affecting the performance of the fibre-free RF material. The fibre-reinforced RF material showed an increase in the compressive modulus that approached the modulus value obtained for the fibre-reinforced OSS material. The RF material showed more than a two-fold increase in the compressive strength value compared to standard S/DVB material. The RF network is therefore a more rigid plastic network in yield than the S/DVB network. The shear and compressive strengths of the PolyHIPE materials produced compared well with a range of industrially available core materials at the same density. However the compressive and shear modulus values of the materials did not compare well with any of the industrially available honeycomb, balsa wood and foam core materials discussed.

Chapter 8

Fluid transport and permeability studies of porous PolyHIPE materials

8.1 Introduction

This chapter will describe an investigation into the fluid transport and permeability behaviour of the 95 % void PolyHIPE materials that were mechanically tested in **chapter 7**. The permeability of the RF-based material will also be investigated. The influence of pore structure, porosity, wettability and fibre reinforcement on the permeability of the materials will also be discussed.

8.1.1 Capillarity in porous media

A defining feature of PolyHIPE materials, as discussed in **chapter 1**, is their ability to uptake fluids by capillary action. Capillarity is an important factor in the transport of fluids [138]. Capillary behaviour in porous media generally involve a solid and a

liquid phase, and one way to evaluate the surface tension of a solid is the measurement of the contact angle between the solid and liquid phase. **Figure 8.1** shows schematically a liquid drop placed on a smooth solid surface.

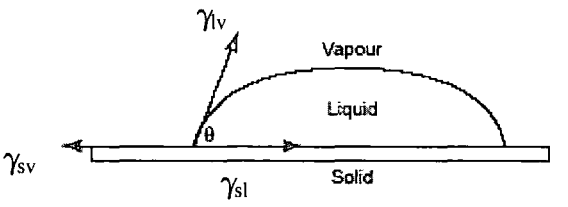

Figure 8.1 *Equilibrium at a line of contact.*

The liquid will remain a drop with an angle of contact, θ, between the solid-liquid and the liquid-vapour phases. This behaviour leads to Young's equation as shown in **equation 8.1**.

$$\gamma_{lv}\cos\theta = \gamma_{sv} - \gamma_{sl} \qquad \textbf{Equation 8.1}$$

Where γ_{lv}, γ_{sv} and γ_{sl} are the surface tensions at the liquid-vapour, solid-vapour and the liquid-solid interfaces respectively.

If the solid surface posseses some roughness it cannot be proven that the measured contact angle is the equilibrium angle. Wenzel suggested a modified form of Young's equation shown in **equation 8.2**.

$$\gamma_{lv}\cos\theta_a = r(\gamma_{sv} - \gamma_{sl}) \qquad \textbf{Equation 8.2}$$

Where θ_a is the average "apparent" contact angle, [136] and, r, the ratio of true-to-apparent solid. Although the case of a rough surface has been investigated, there has been very little focus on porous structures. Lunkwitz et al. [137] derived an alternative expression from Young's equation that considered the surface porosity of the material and produced a corrected value for the contact angle (**see equation 8.3**)

$$\cos\theta = \cos\theta' - \frac{4\varepsilon}{1-\varepsilon}\frac{\cos\theta'+1}{\cos\theta'-1} \qquad \textbf{Equation 8.3}$$

Where θ' is now the contact angle observable on a porous structure and ϵ is the surface porosity of the materials. They studied microporous membranes, of different porosity, made from poly(tetrafluoroethylene), using the fluids water and methylene iodide. They corrected the measured values using **equation 8.3** and found them to be similar to the reported values of PTFE for water and methylene iodide.

It is difficult to measure the contact angle of porous medium as the angle changes over time, due to movement of the liquid front by capillary action and spreading of the liquid droplet as shown in **figure 8.2**.

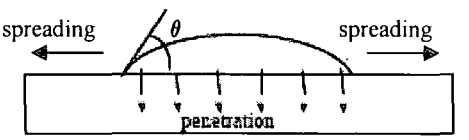

Figure 8.2 *Movement of a liquid front on a porous material due to capillary action.*

8.1.1.1 Wettability and spreading

In most cases if the contact angle is les than 90° then the liquid is said to wet the solid. In cases when no value of θ can be found the liquid is said to wet the solid perfectly. If the contact angle is said to be greater than 90° the liquid is said to not to wet the solid or is non-wetting. When the liquid wets the solid perfectly the imbalance of the forces can lead to a spreading coefficient defined in **equation 8.4** (138).

$$S_{ls} \equiv \gamma_{sv} - \gamma_{lv} - \gamma_{sl} \qquad \textbf{Equation 8.4}$$

8.1.2 Pore structure

8.1.2.1Porosity

The porosity can be referred to as the voidage of the material and in the case of PolyHIPE materials this can be controlled by the volume of the internal phase used during the emulsification process. The voids are generally interconnected and these interconnects can contribute to transport of fluid across the porous medium. There are several methods to evaluate the pore structure and porosity of the material. Optical methods such as microscopy can be used to measure surface porosity. This method was used by Lunkwitz et al. [139] to define the surface porosity for their derived relationship shown in **equation 8.3**. Optical methods can also be used to evaluate void size, but this method will not give an accurate overall pore size distribution due to the large presence of interconnecting windows, especially in PolyHIPE materials. Mercury intrusion porosimetry (MIP) is where the porous material is immersed in mercury to evaluate the bulk volume of the sample. As mercury does not wet most materials a pressure must be applied to allow the liquid to penetrate into the pores. MIP can lead to interconnect size and volume distribution curves from which the average and median interconnect diameters can be calculated. In the case of PolyHIPE materials the median and average interconnect diameters determined from MIP, will give a more accurate value of interconnect compared to void size of the material. Generally, void size can be determined from optical methods such as microscopy. The porosity and the surface area of the material can also be determined. However, the surface area values calculated from MIP are not reliable, if there are meso- and micropores present.

Imbibition methods involve the porous material being immersed in a wetting fluid under vacuum, until the fluid imbibes into the pore space. The sample is then

weighed before and after imbibition. The two weights and the density of the fluid allow for the calculation of the pore volume. The porosity of the material can also be calculated from the same method.

Gas adsorption and density methods are other methods to evaluate the porosity of the material.

8.1.2.2 Permeability

Permeability is the term used for the conductivity of a porous medium with respect to permeation of a Newtonian fluid [138].

The unit of permeability is the "Darcy". A porous material has a permeability equal to 1 Darcy if a pressure difference of 1 atmosphere will produce a flow rate of 1 cm^3s^{-1} of a fluid with 1 cP viscosity through a cube having sides 1 cm in length. Therefore 1 Darcy is equal to 0.987 μm^2. The permeability, k, is defined by Darcy's law which is a linear relationship similar to Newton's law of viscosity or Fick's law of diffusion **(see equation 8.5)**.

$$Q = -\left(\frac{kA\Delta P}{\mu L}\right) \qquad \textbf{Equation 8.5}$$

Q = Volumetric flow rate (discharge, m^3s^{-1})

A= Cross sectional area of sample (m^2)

ΔP = Pressure drop (Pa or $kgm^{-1}s^{-2}$)

L = Length of sample in flow direction (m)

μ = Viscosity of fluid (cP or $kgm^{-1}s^{-1}$)

The pressure drop present in Darcy's law is obtained by measuring the hydrostatic pressure exerted by a column of fluid. Permeability values can be obtained from one measure of flow rate at a given pressure according to Darcy's law but there is usually a considerable experimental error. It is more common practice to obtain several

measurements at low flow rates or pressures, plot flow rate against pressure drop and fit a straight line to the data points. According to Darcy's law this line must pass through the origin. Scattering of the points may cause the line to deviate from the origin. If the data points cannot be fitted with a straight line then Darcy's law is not being obeyed and the system may need to be investigated to analyse the problem.

8.2 Experimental

8.2.1Materials

PolyHIPE discs were stamped using a cork borer from slices of PolyHIPE materials prepared in **chapter 7**. The discs prepared were 25 mm in diameter and with a thickness of 2 mm. The kerosene (low odour) was supplied by Aldrich Chemicals.

8.2.2 Instrumentation

The Swinnex filter holders were supplied by Millipore and the instrumental setup for the measurement of the permeability of the PolyHIPE materials is shown in **figure 8.3**. The pore structure of the PolyHIPE materials was characterised by mercury intrusion porosimetry (MIP) using an AutoPore III 9420 porosimeter.

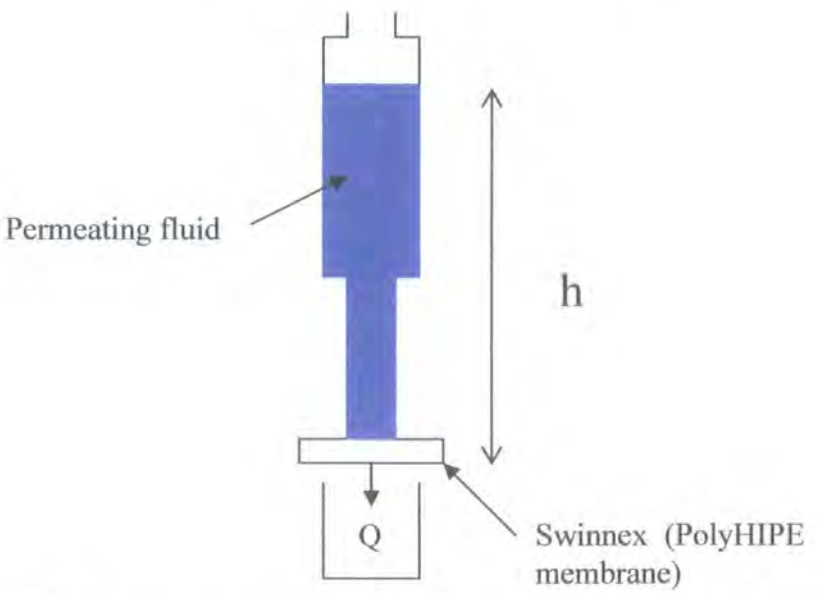

Figure 8.3 *Instrumental set-up for the measurement of the permeability of the PolyHIPE materials.*

8.2.3 Permeability tests

The discs prepared as out-lined in **8.2.1** were placed in the Swinnex membrane holders which were attached to the instrumental set-up shown in **figure 8.3**. The membranes were initially washed twice with water and then with propan-2-ol and then washed through again with de-ionised water or kerosene until a constant discharge was obtained at the highest pressure drop. The discharge of the fluid was then measured at four different heights of fluid (25, 30, 35 and 40 cm) after one minute. This was repeated three times for each different height. The pressure drop was the hydrostatic pressure exerted by a column of fluid calculated using **equation 8.6**.

$$\Delta P = \rho g h \qquad \textbf{Equation 8.6}$$

Where ρ is the density of the permeating fluid (kgm^{-3}), g is the gravitational constant of acceleration (9.8 ms^{-2}) and h is the height of the column of fluid (m).

The flow discharge was then plotted against pressure drop as described in **8.1.1.2**. The permeability coefficient was then calculated from the gradient of the graph using **equation 8.5** where the viscosity of water and kerosene are 1 cP and 10 cP [140] respectively. This method was repeated for both water and kerosene as the permeating fluid.

8.2.4 Contact angle measurements

The contact angle was measured directly by the sessile drop method [139]. A thin slice (~ 2 mm thickness) of the PolyHIPE material was placed on the goniometer stage. The surface of the PolyHIPE material was then levelled by raising or lowering the stage using the goniometer eye piece. A drop of the fluid was placed on the surface of the material using a Pasteur pipette. The contact angle was then measured by

aligning the tangent to the drop profile using the goniometer eyepiece. Any change in the contact angle after a time period of one minute was observed and recorded.

8.3 Results and discussion

8.3.1 Permeability results

Figure 8.4 shows the flow rate against pressure drop chart for the 95 % void styrene- and MMA-based PolyHIPE materials with water as the permeating fluid.

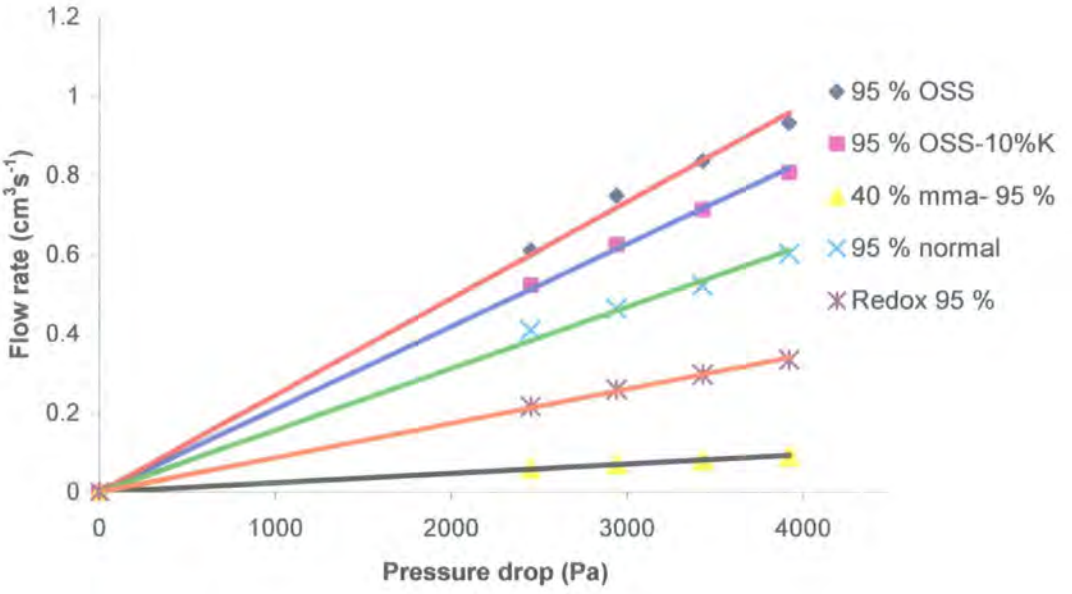

Figure 8.4 *Flow rate against pressure drop chart for the styrene- and MMA-based PolyHIPE materials when water is the permeating fluid.*

All of the materials show linear behaviour, indicating they can be described by Darcy's law. The graph shows a decreasing trend in the gradient and therefore the permeability coefficient from the non-reinforced OSS PolyHIPE material to the MMA-based PolyHIPE material.

Figure 8.5 shows the flow rate against pressure drop for the 95 % void styrene- and MMA-based materials when kerosene is the permeating fluid.

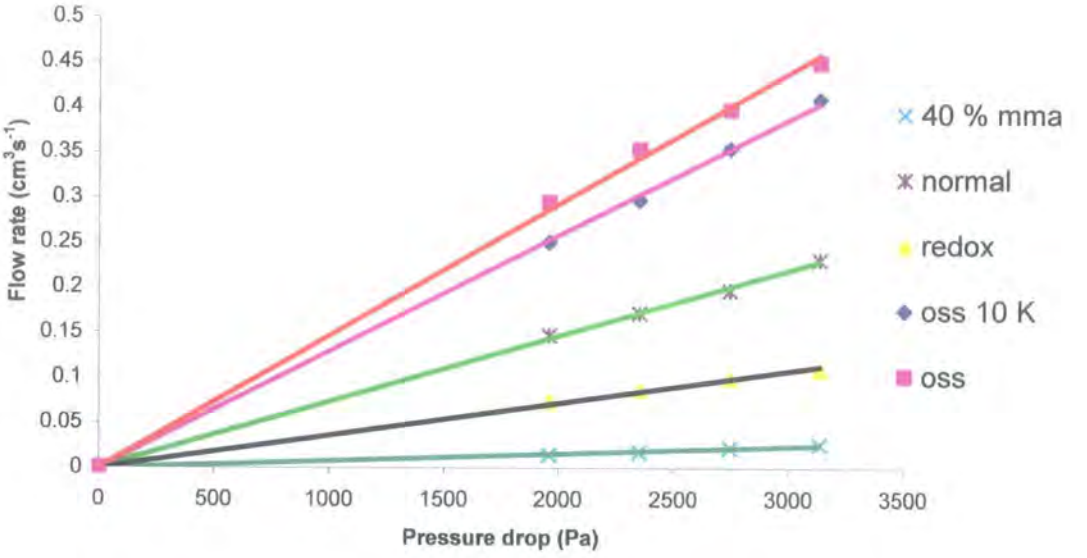

Figure 8.5 *Flow rate against pressure drop for the 95 % void styrene- and MMA-based PolyHIPE materials with kerosene as the permeating fluid.*

The trend is similar to the trend that was observed when water was the permeating fluid. There is a decreasing gradient and therefore permeability coefficient going from the non-reinforced OSS PolyHIPE material to the MMA-based PolyHIPE material. For each of the materials tested there is an increase in the flow discharge when kerosene is the permeating fluid.

For the RF-based PolyHIPE material when water was used as the permeating fluid, no significant discharge was obtained at the highest-pressure drop. **Figure 8.6** shows the flow rate against pressure drop for the RF-based PolyHIPE material when kerosene is the permeating fluid.

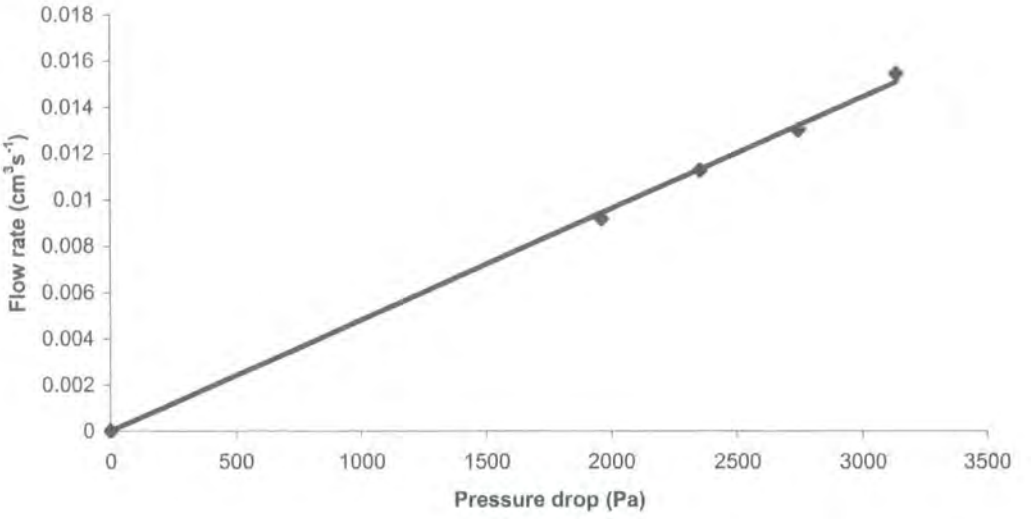

Figure 8.6 *Flow rate against pressure drop for the RF-based PolyHIPE material with kerosene as the permeating fluid.*

The RF-based PolyHIPE material shows linear behaviour according to Darcy's law. The flow discharge from the RF-based material is lower than that obtained for the MMA-based PolyHIPE material. **Table 8.1** shows the permeability coefficients calculated for all the PolyHIPE materials tested when water and kerosene are used as the permeating fluids.

Table 8.1 Permeability coefficients obtained for the PolyHIPE materials tested

Permeating fluid	Water		Kerosene	
Sample name	k (10^{-13} m^2)	k (Darcy)	k (10^{-13} m^2)	k (Darcy)
OSS	9.78	0.99	59.5	6.0
OSS 10K	8.51	0.86	51.0	5.2
Normal	6.27	0.64	30.46	3.1
Redox	3.51	0.36	14.9	1.5
40 % MMA	0.97	0.09	3.22	0.32
RF	No data	No data	1.89	0.19

There is a decreasing trend in permeability coefficient from the non-reinforced OSS PolyHIPE material to the 40 % MMA PolyHIPE material, when either water or kerosene is used as the permeating fluid. The nature of the permeating fluid has no effect on the permeability coefficient trend of the materials; however there is a significant increase in the value of k obtained when the permeating fluid is changed from water to kerosene. There was no permeability coefficient obtained when water was the permeating fluid with the RF-based material. This was due to wettability problems of the RF material. This suggests that the RF PolyHIPE material is a more hydrophobic material compared to S/DVB PolyHIPE material. The coefficient value obtained when kerosene was the permeating fluid was 0.19 Darcy. This is close to the value reported in the patent by Sherrington et al. (0.1 Darcy) [17].

It was observed that there are two factors influencing the results obtained. They are the pore structure of the materials and the interaction of the PolyHIPE materials with the permeating fluid.

8.3.1.1 Influence of pore structure

Mercury intrusion porosimetry was used to evaluate the pore structure of the materials tested. **Figure 8.7** shows the log differential intrusion against interconnect diameter for the styrene- and MMA-based PolyHIPE materials.

The foam produced using the optimised surfactant system as was observed in the ESEM images shown in **chapters 5** and **7**, has a large interconnect size distribution due to the presumed increase in HIPE stability producing larger interconnecting windows on polymerisation. From the log differential intrusion curve, the majority of the interconnect sizes lie between 6.5 – 9.5 μm for the OSS foams with the Kevlar fibres present but between 5 - 8 μm for the non-reinforced OSS material. The presence of the Kevlar fibres may cause coalescence of the emulsion around the

areas in contact with fibre accounting for the slight increase in the interconnect size. The normal PolyHIPE prepared using the standard formulation shows two peaks where the majority of the interconnect sizes lie. The larger of the two peaks lies between 4-6 μm, with a smaller peak at around 8 μm.

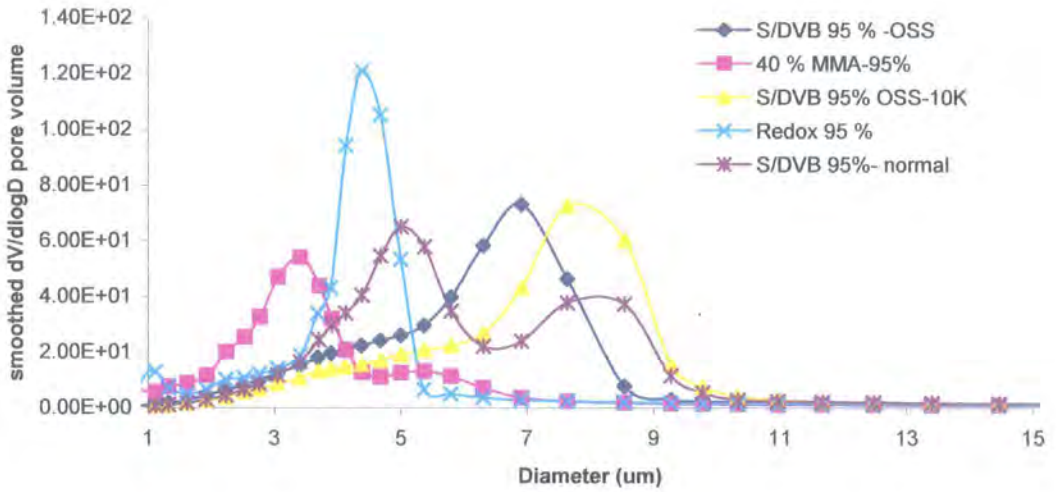

Figure 8.7 *Log differential intrusion against interconnect diameter curves for the styrene- and MMA-based PolyHIPE materials.*

The presence of the two main regions of interconnect size obtained for the standard S/DVB PolyHIPE material suggests that some coalescence of the emulsion droplets occurred during polymerisation. The foam produced using the redox initiation system instead of potassium persulfate has a very narrow interconnect size distribution and a smaller average interconnect size than the standard system. The faster curing time allows less time for coalescence to occur and therefore a narrow interconnect size distribution is obtained as was discussed in **chapter 5**. The morphology of the MMA-based PolyHIPE foam as shown by the ESEM images in **chapters 4** and **7** consists of an open-cell structure with interconnects of an extremely small nature

showing the structure to be almost closed cell. The porosimetry data confirm the presence of interconnects of smaller diameter than that present in the foam prepared from the standard formulation. From the log differential intrusion against diameter curve the majority of the interconnect sizes for the MMA-based material lie between 2-4 μm. **Figure 8.8** shows the log differential intrusion curve for the RF-based PolyHIPE material.

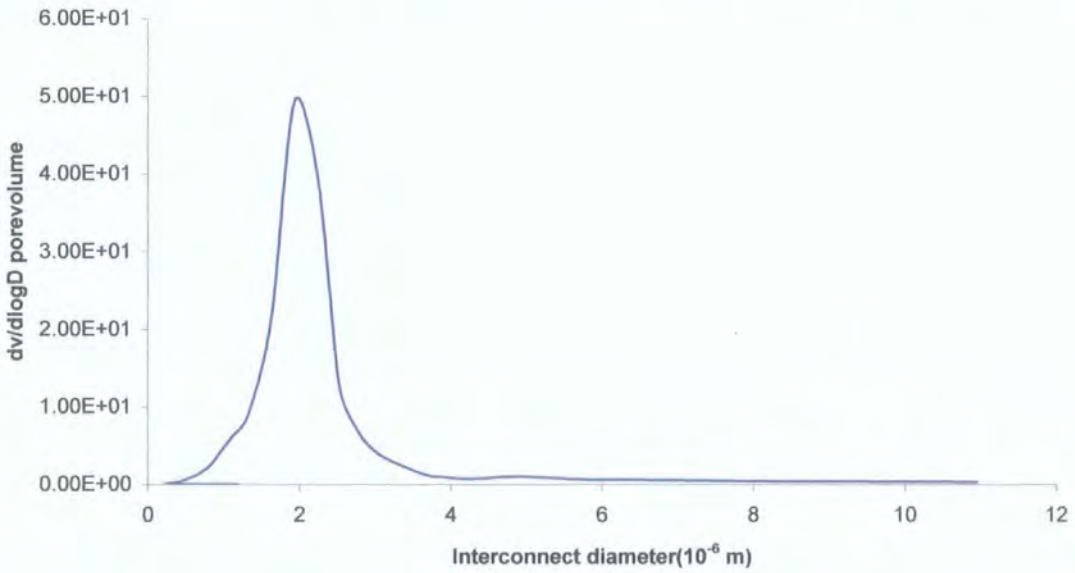

Figure 8.8 *Log differential intrusion against interconnect diameter for the RF-based PolyHIPE material.*

The RF-based PolyHIPE material shows a narrow interconnect size distribution due to the short curing time of the material. From the log differential intrusion against interconnect diameter curve the majority of the pore sizes lie in the range 1.5 – 2.5 μm. **Table 8.2** shows the average and median interconnect diameter values calculated from the mercury intrusion porosimetry.

Table 8.2 Average and median pore diameters obtained from mercury intrusion porosimetry

Sample name	Average interconnect diameter (μm)	Median interconnect diameter (volume) (μm)
OSS	4.2	5.8
OSS 10K	5.1	6.9
Normal	4.4	4.3
Redox	2.3	4.1
40 % MMA	1.7	2.9
RF	1.6	1.8

Figures 8.9 and **8.10** show a graph comparing the average and median interconnect diameter to the permeability coefficient obtained when the permeating fluid is water.

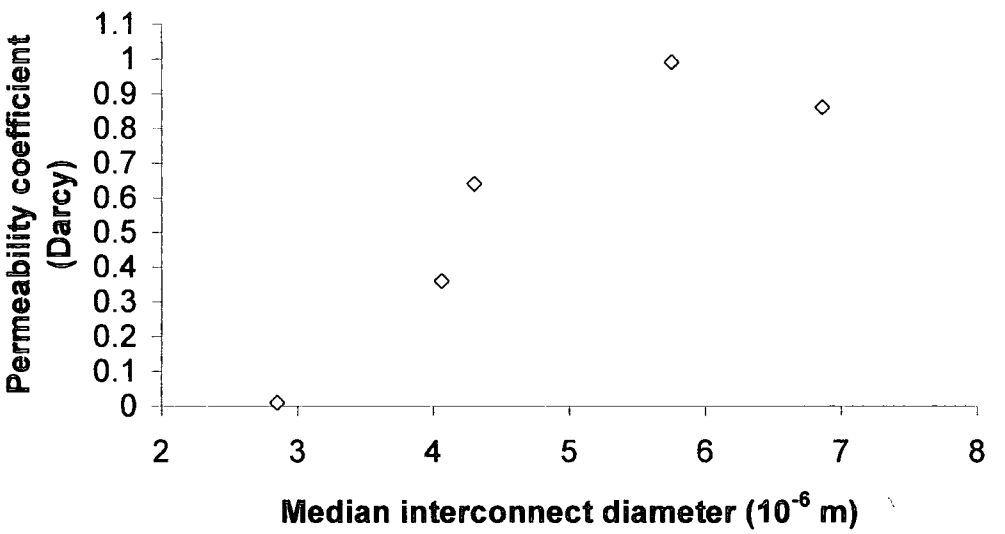

Figure 8.9 *Permeability coefficients against median interconnect diameter where water is the permeating fluid.*

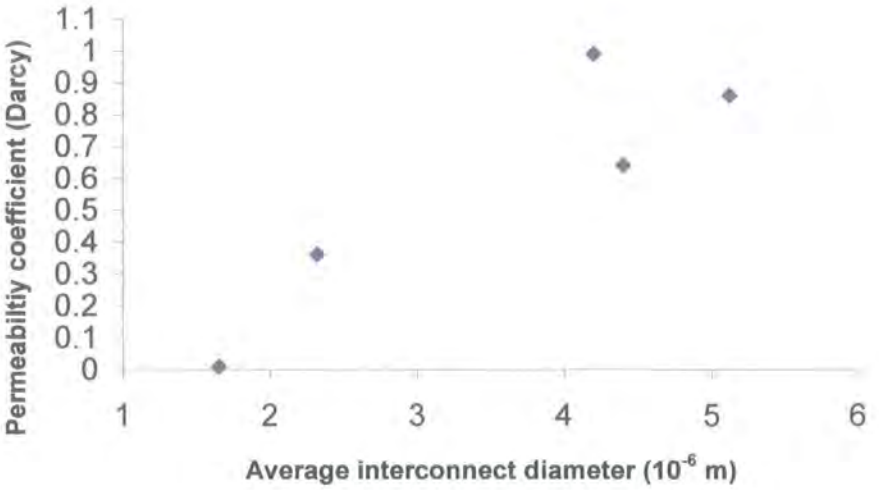

Figure 8.10 *Permeability coefficients against average interconnect diameter when the permeating fluid is water.*

The average and median interconnect diameter produce slightly different trends with the value of permeability coefficient. This is thought to be due to the difference in the calculation of the interconnect diameter values. The median diameter is calculated from the 50 percentile point on any volume, area or length distribution curve whereas the average interconnect diameter assumes that the interconnects are cylindrical and is calculated from the relationship 4V/A [141].

The only major difference in the trends is the value of the 95 % void S/DVB material prepared with the OSS. The average interconnect diameter is lower than that of the 95 % void S/DVB material prepared with Span 80, whereas the median interconnect diameter is greater. The median interconnect diameter produces the more expected trend with permeability increasing with increasing interconnect diameter, except for the fibre-reinforced OSS PolyHIPE material where the permeability and wettability of the fibre present must also be taken account and will affect the permeability of the composite as a whole. The trend for both the median and average interconnect

diameter when kerosene is the permeating fluid is similar to the trend observed when water was the permeating fluid. The trend for both the median and average interconnect diameter is shown in **figure 8.11** and **figure 8.12**.

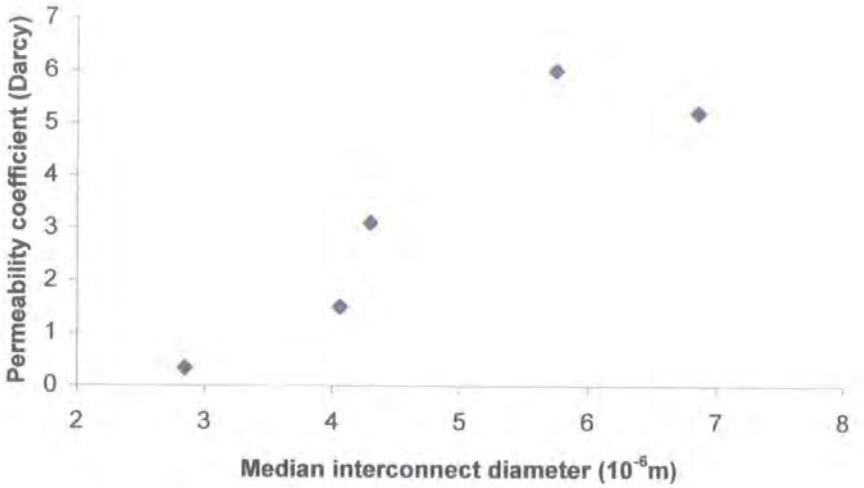

Figure 8.11 *Permeability coefficients against median interconnect diameter when kerosene is the permeating fluid.*

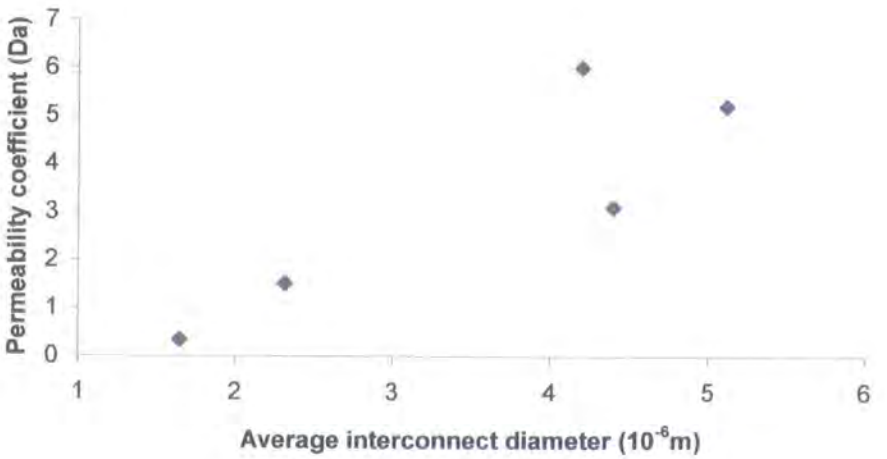

Figure 8.12 *Permeability coefficients against average interconnect diameter when kerosene is the permeating fluid.*

Figure 8.11 shows an increasing permeability coefficient with increasing interconnect diameter with the exception of the fibre-reinforced OSS PolyHIPE material for the same reasons discussed previously. As was observed when water was the permeating fluid the average interconnect diameter obtained for the fibre free OSS PolyHIPE material is smaller than that of the standard S/DVB PolyHIPE material. The rest of the PolyHIPE materials tested show an increasing permeability coefficient with increasing average interconnect diameter.

8.3.1.2 Influence of porosity

As discussed in **chapter 1**, the volume of internal (droplet) phase added to the monomer phase will govern the density and the overall porosity of the PolyHIPE material produced. The overall porosity of the sample also affects the permeability of the material. **Figure 8.13** shows the flow discharge against pressure drops chart of a 90 and 95 % void * S/DVB material prepared with Span 80 where water was the permeating fluid.

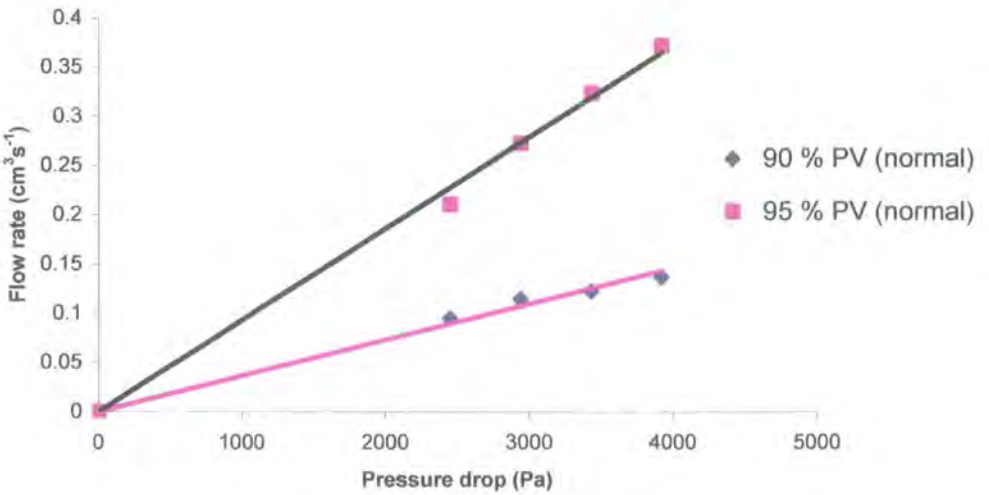

Figure 8.13 *Flow rate against pressure drop of a 90 and 95 % void S/DVB PolyHIPE material.*

** This is a nominal porosity and is calculated from the water/oil ratio e.g. 90/10 water/oil is a 90 % void material*

Figure 8.13 shows that by increasing the overall porosity of the material from 90 to 95 % the permeability of the material increases and over a two fold increase in the discharge of permeating fluid at each pressure drop tested is obtained.

As discussed in **chapter 2**, the mould substrate can influence the porosity and open-cell nature of the PolyHIPE surface against which it is produced. A glass substrate will generally give a closed-cell material whereas substrates such as PVC, PP and PE affect the open-cell nature of the material at the surface. A PTFE substrate produced a more open-cell material compared to other substrates, but the material produced did show areas which were closed-cell in nature (**see figure 2.7**). This effect on the surface porosity can also affect the permeability of the material. **Figure 8.14** shows the flow discharge against pressure drop chart for a redox initiated S/DVB material prepared from PTFE plate moulds and a sample produced from a slice removed from the centre of the redox intiated sample produced for mechanical testing. The permeating surface of this material has not been in contact with the mould substrate.

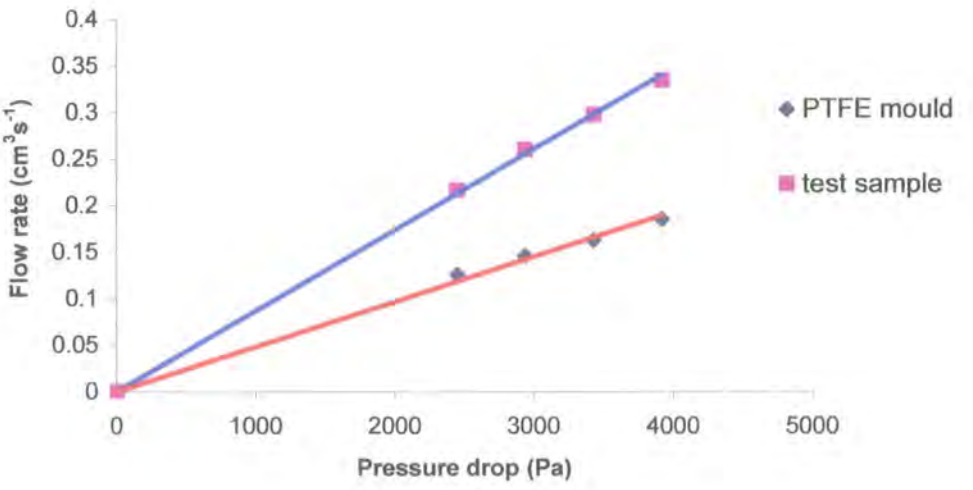

Figure 8.14 *Flow rate against pressure drop for a redox-initiated S/DVB material prepared from a PTFE mould and a redox-initiated S/DVB material cut from the mechanical test samples.*

Figure 8.14 shows that the sample cut from the mechanical test sample has a larger gradient and therefore greater permeability compared to the PolyHIPE material produced from the PTFE mould.

8.3.1.3 Influence of wettability: contact angle measurements

The influence of the pore structure and the porosity of a PolyHIPE material on its permeability values has already been described. The wettability of the material from which the PolyHIPE is made can also be a determining factor in the permeability value obtained. The contact angle of water was measured on both the RF and S/DVB material prepared with a redox initiator. After placement of the water drop on the RF PolyHIPE surface, there was no instant wetting of the PolyHIPE surface. The initial contact angle obtained was 121°. After one minute the angle had receded to 113° due to the influence of the porous nature of the material as discussed in **8.1.1**. The values show that water is a non-wetting liquid for the RF PolyHIPE materials. After placement of the water drop on the S/DVB PolyHIPE material the wetting of the surface occurred instantly. The initial contact angle was 23° and after one minute had receded to 16° due to the porous nature of the material. This value is lower than the reported value of 86° for pure polystyrene [140]. This is could be due either to the presence of residual calcium chloride or capillary action drawing the water into the material, or both effects. It is difficult to describe the contact value obtained for porous materials as an equilibrium contact angle due to the movement of the wetting front by capillary action. It is a dynamic contact angle. On addition of the kerosene droplet, there was instant wetting of both the RF and S/DVB PolyHIPE surface and no contact angle was observable. This is possibly a combination of the wettabillity and the porous nature of the material. The instant spreading of the kerosene droplet

suggests that kerosene is a more wetting liquid for both materials compared to water and correlates with the larger permeability coefficients obtained for kerosene.

8.3.1.4 Influence of fibre reinforcement

In **8.3.1.1** the Kevlar fibre-reinforced PolyHIPE material prepared with the OSS did not follow the expected increasing permeability trend with increasing median interconnect diameter. The fibre-reinforced PolyHIPE material showed a decrease in permeability compared to the fibre free OSS PolyHIPE material even though it had greater median pore diameter. This was said to be due to the wettability and the presence of the fibres within the composite material. There are a few examples in the literature investigating the wetting behaviour of fibres. Fotheringham et al. [141] investigated the wetting behaviour of PP fibres using an ESEM. **Figure 8.15** shows an ESEM image of wetting of the PP fibres by water.

Figure 8.15 ESEM *image of fibre wetting by water* [141].

They found that the contact angle was in the region of 85-95°, indicating the hydrophobic property of the polypropylene fibres. With the addition of oil droplets

[141], [142] they found that the oil wet the surface immediately with the droplet forming a barrel shape as shown in **figure 8.16 (a)** and **(b).**

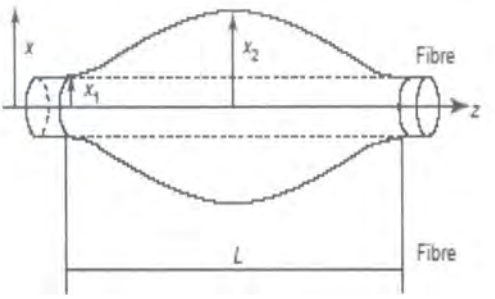

(a) (b)

Figure 8.16 *Fibre wetting by oil, (a) ESEM image, (b) oil droplet profile*[142].

The contact angles were obtained by an analytical expression derived from the oil droplet profile as shown in **figure 8.16 (b)**. They found that the contact angles are between 15 and 25° indicating the affinity of the polypropylene fibres for oil. The permeability of the fibre-reinforced composite can be either be affected by the reduced porosity of the material due to the presence of the fibres or the interaction of the permeating fluid with the fibre surface.

8.4 Conclusions

In this chapter it has been shown that it is possible to calculate permeability coefficients for different PolyHIPE materials using Darcy's law for both water and kerosene as the permeating fluid. It was also shown that the permeability of the materials was influenced by the pore structure, porosity, wettability and the fibre reinforcement of the materials. It was found that permeability of the PolyHIPE materials increased with increasing median pore diameter with the exception of fibre-reinforced OSS material due to the presence of the fibres additionally affecting the permeability of the materials. Increasing the porosity of the material from 90 to 95 %

also increased the permeability of the material. The surface porosity was also found to affect the permeability of the material. A sample where the permeating surface had been in contact with the PTFE mould substrate was found to have a lower permeability than that of a S/DVB material where the permeating substrate had not been in contact with the mould substrate. The permeability coefficients obtained when kerosene was present as the permeating fluid were significantly higher compared to the permeability values obtained when water was present. In fact it was not possible to calculate a permeability coefficient for the RF material as there was significant flow discharge of water obtained at the highest pressure drop. Contact angle measurements showed that water was a non-wetting fluid for the RF based material with an initial contact angle of 121° and a decrease due to movement of the wetting front by capillary action to 113°. This was compared to the S/DVB material where the water droplet wet the surface instantly with an initial contact angle of 23° and a decrease to 16° after one minute. So it was concluded that the RF material was more hydrophobic compared to the S/DVB material. In the case of kerosene it was found that the liquid wet both the RF and S/DVB material instantly with no contact angle observable and therefore accounted for the larger permeability coefficient values obtained for kerosene.

Chapter 9

An investigation into the production of porous materials with anisotropic properties

9.1 Introduction

It has already been shown that is possible to enhance the mechanical properties of PolyHIPE materials by i) the addition of active fillers such as fibres, which reinforce the cellular matrix of the PolyHIPE material; ii) changing the chemical composition of the material by the addition of more rigid monomers such as methyl methacrylate (MMA), iii) the removal of the plasticisation effect of the surfactant Span 80 by the use of an optimised surfactant system. In this chapter work on the production of a porous material with possible anisotropic properties will be described. The three methods investigated were,

1) The preparation of PolyHIPE materials with shape-memory properties.
2) The curing of a HIPE in a centrifugal field.

3) The addition of high aspect ratio filler particles that could be removed to leave a porous material with anisotropic properties.

The shape memory effect would allow to us to heat and stretch a PolyHIPE material to leave an elongated cell structure on cooling. This material would hopefully show anisotropic properties, as it would have different mechanical behaviour in the direction of the elongated cells, relative to at 90 ° to the direction of the elongation. Placing the HIPE in a centrifugal field would possibly elongate the internal phase droplets during polymerisation to leave an elongated cell structure on polymerisation followed by removal of the internal phase.

If a high aspect ratio filler material is added in a high enough concentration to a mixture of monomers, it is hoped that they would arrange themselves in an ordered assembly and on removal would leave an anisotropic structure within the polymer matrix. The production of an ordered arrangement at high concentrations will depend on the shape of the material. It was decided that fillers with a high aspect ratio (needle-like) would have the best chance of forming such an arrangement.

9.1.1 Shape-memory materials

9.1.1.1 Introduction

Lendlein et al. [143] have described a wide range of shape-memory materials, which have been described as stimuli-responsive materials. The change in shape created by a change in temperature is called a thermally induced shape-memory effect. This involves heating and deforming, then cooling the material to hold the deformed shape. On re-heating the material above a certain temperature the material regains its original dimensions. Thermo-responsive materials will be the main focus of this introduction. **Figure 9.1** shows a schematic representation of the thermally induced one-way shape-memory effect.

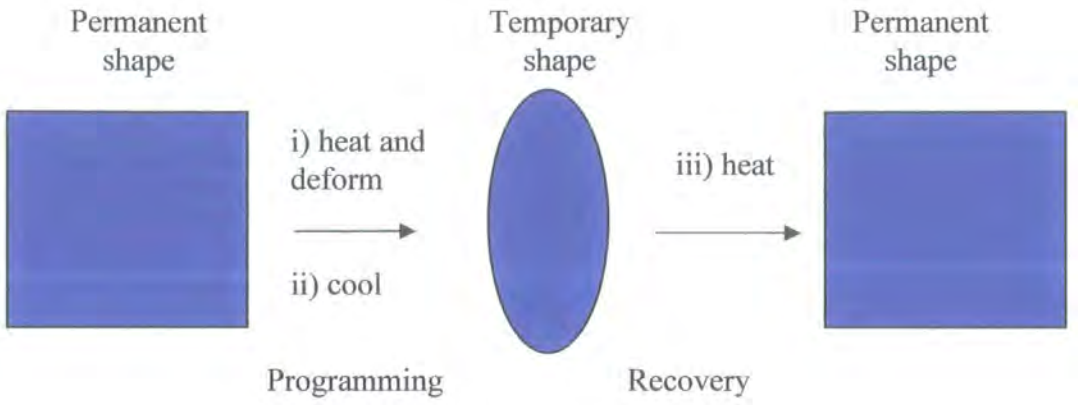

Figure 9.1 *Schematic representation of the thermally induced one-way shape-memory effect.*

First the polymer is processed to receive its permanent shape. Afterwards the polymer is heated above a certain temperature then deformed and the temporary shape is fixed on cooling. This process is called programming. The permanent shape has now been stored as the sample holds the temporary shape. Heating the shape memory material above a transition temperature T_{trans} activates the shape memory effect. This is called the recovery process as the recovery of the permanent shape and dimensions is observed. Further programming by mechanical deformation can return the temporary shape, but it may not match the first temporary shape. Metal alloys are reported to show shape-memory properties, but for this introduction the shape memory effect in polymers will be discussed.

In the glassy state all movements of the polymer are frozen. The transition to the rubber-elastic state occurs with increasing thermal energy. This allows segmental motion and enables the chains to take up their lowest energy conformation. The flow or movement of the polymer chains can be stopped completely by the presence of cross-links. The cross-links can either be chemical or physical. Such cross-linked

materials are generally referred to as elastomers [143]. Chemically cross-linked polymers form insoluble materials, which swell in good solvents. Thermoplastic elastomers are triblock (ABA) copolymers consisting of a glassy thermoplastic A and an elastomeric B block [4]. Thermoplastic elastomers contain physical net-points. A requirement for the formation of the net-points is the existence of a certain morphology of a phase-separated material. The highest thermal transition is related to the hard segment forming phase. If this is not exceeded theses domains will stabilise the permanent shape by acting as physical net-points in the material. In addition to the net-points, networks can contain flexible components in the form of amorphous chains. If the glass transition temperature of these segments is below the working temperature, the networks will be elastic. They show entropy elasticity and can be stretched with a loss of entropy [143]. The distance between the net-points increases during stretching and they become orientated. As soon as the external force is released the material returns to its original shape and gains back the entropy, which the material had lost.

9.1.1.2 Molecular mechanism of the shape-memory effect for polymers

An elastomer will exhibit the shape memory effect if the material can be stabilised in the deformed state. This can be achieved by using the network chains as a molecular switch. For this to happen, the flexibility of the segments should be a function of the temperature. The one possibility of a switch function is a thermal transition of the network chains (T_{trans}). At temperatures above T_{trans} the chains become flexible, whereas movement of the chains below this transition is partially limited. If T_{trans} is a melting point T_m, crystallisation of the switching segment can be initiated by cooling after stretching above the transition temperature. The crystallisation is always incomplete which means that a certain amount of chains remain amorphous. The

crystallites formed prevent the segment chains from regaining their permanent random coil-like structures immediately and from recovering the permanent shape spontaneously. The permanent shape of shape-memory networks is stabilised by covalent networks, whereas the permanent shape of shape memory thermoplasts is governed by the highest thermal transition T_{perm}. If T_{trans} is a glass transition temperature (T_g) and the increase in temperature is greater than the transition temperature of the switching segment, these segments are flexible and can be deformed elastically.

Figure 9.2 shows a schematic represenation of the molecular mechanism of the thermally induced shape-memory effect for a covalently cross-linked polymer with $T_{trans} = T_m$

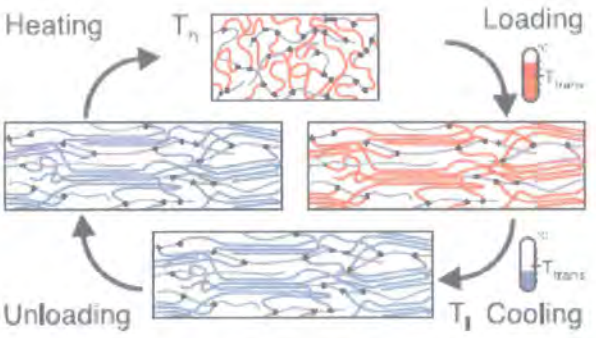

Figure 9.2 *Schematic representation of the molecular mechanism of the thermally induced shape memory effect for an AB covalently cross-linked network with* $T_{trans} = T_m$ [144].

The review by Lendlein et al. [143], gives a detailed overview of the different physically cross-linked shape-memory polymers, such as linear block copolymers, where the mechanism of the thermally induced shape-memory effect is based on the phase segregated morphology as discussed previously, with one of the phases acting

as a molecular switch. Through the formation of physical net-points, the phase with the highest thermal transition will provide the mechanical strength and will record the permanent shape. Physically cross-linked shape-memory polymers are divided into two categories if the shape-memory effect is due either to a melting temperature T_m or a glass transition T_g.

9.1.1.3 Chemically cross-linked shape-memory polymers

There are two methods of cross-linking with which to produce chemically cross-linked shape-memory polymers [143]. The first is polycondensation or polyaddition by free radical polymerisation with a di – or tri-functional cross-linker, where the chemical, thermal and mechanical properties of the polymer network can be adjusted by the choice of monomers and the cross-linker content. The second is the cross-linking process by a radical mechanism of linear polymers initiated by ionising radiation.

They described the memory effect of polyethylene treated with ionising radiation. A chemically cross-linked network was formed by low doses of irradiation. Polyethylene chains were oriented by the application of a mechanical stress above the melting temperature of the polyethylene crystals. Cooling below its crystallisation temperature forms the polyethylene crystals and these fix the temporary shape. Heating the material above the melting temperature, results in the material returning to the permanent shape during the irradiation process. HDPE, LDPE and copolymers of PE and poly(vinyl acetate) are also covalently cross-linked this way.

Lendlein also explained that poly(vinyl chloride) can show shape-memory behaviour. When PVC is heated under vacuum, hydrogen chloride is eliminated. The material can then be cross-linked in an HCl atmosphere. This resulting material showed a shape-memory effect. The recovery was observed when the volume change was

measured on compression above the glass transition temperature. The weakly dehydrochlorinated (0.6 %) sample showed no recovery with the highest relative increase in volume change occurring with a degree of dechlorination of 12.9 and 22.5 %.

They also described the formation of shape-memory networks by the copolymerisation of mono-functional monomers with low-molecular weight or oligomeric cross-linkers. Covalently cross-linked copolymers made from stearyl (meth)acrylate and N, N'–methylenebisacrylamide as a cross-linker exhibit a shape-memory effect. The thermal transition is the melting point of the crystalline domains formed by the stearyl side chains. The melting/switching temperature for shape-memory behaviour varied with stearyl acrylate content. Stretching the sample at 60 °C and then cooling programmed the temporary shape. The permanent shape was recovered when the sample was heated above the switching temperature. Copolymer networks can also be obtained by radical copolymerisation of poly(octadecyl vinyl ether) diacrylates or dimethacrylates with butyl acrylate. The octadecyl can crystallise because of phase separation. The materials recovery was said to be complete.

Butyl acrylate has also been used to produce an AB polymer biodegradable network structure with oligo(ϵ-caprolactone) diols [144], which have been functionalised with methacrylate end groups. The PCL switching segments were incorporated covalently within the network. Lendlein et al. [144] chose n-butyl acrylate because of the low T_g of pure poly(n-butyl acrylate). Shaping the material above the transition temperature and then cooling led to the crystallisation of the PCL segment. The temporary shape is fixed by physical cross-links. Heating the material above the transition temperature causes the crystallites to melt and the material returns to its original dimensions. The molecular weight of the oligo(ϵ-caprolactone) dimethacrylate and the content of butyl

acrylate are the molecular parameters for controlling crystallinity as well as the switching temperature. They varied the cross-link density of the material by varying the weight content of butyl acrylate. For the oligo(ϵ-caprolactone), M_n = 2,000 g/mol, the butyl acrylate content was varied from 11 to 90 w/w % and 20 to 71 % w/w for the dimethacrylate, M_n = 10,000 g/mol. For M_n = 2000 g/mol and a butyl acrylate content of 11 % w/w the AB network formed had a T_m of 23 °C. The corresponding homo-network of the oligo(ϵ-caprolactone) dimethacrylate had a melting point of 32 °C. All other networks tested were found to be completely amorphous. For the networks produced with oligo (ϵ-caprolactone) dimethacrylate with M_n = 10,000 g/mol, the T_m decreased from 51 to 45 °C with increasing butyl acrylate content. None of the investigated materials showed a glass transition between – 20 and 70 °C. The elastic modulus of both the different molecular weight networks decreased with butyl acrylate content. **Figure 9.3** shows photographs of the recovery process during the shape memory effect of the AB polymer network formed with oligo(ϵ-caprolactone) dimethacrylate and butyl acrylate at 70 °C. The permanent shape (rod) is regained within 20 seconds after heating to above the melting temperature of the crystallites. Busby et al. [145], [146], [147] have shown it is possible to prepare cellular PolyHIPE materials containing poly(ϵ – caprolactone) diacrylate (M_n = 500 and 2000) as cross-linker with styrene and MMA as comonomers. On the basis of this and Lendlein's work, it could be possible to prepare PolyHIPE materials, which showed shape-memory properties. The permanent shape would represent the normal open-cellular structure of a PolyHIPE material. After stretching the material above T_{trans} and cooling the temporary structure should represent an elongated cell structure in the direction of the strain. On reheating the PolyHIPE material above the T_{trans} the PolyHIPE material would regain its permanent shape.

Lendlein et al. [143] also described other biocompatible and biodegradable multi-block copolymers. They consisted of a crystallisable hard segment (T_m) of poly(p-dioxane) and an amorphous switching segment, poly[(L-lactide)-co-glycolide], which exhibits a glass transition temperature.

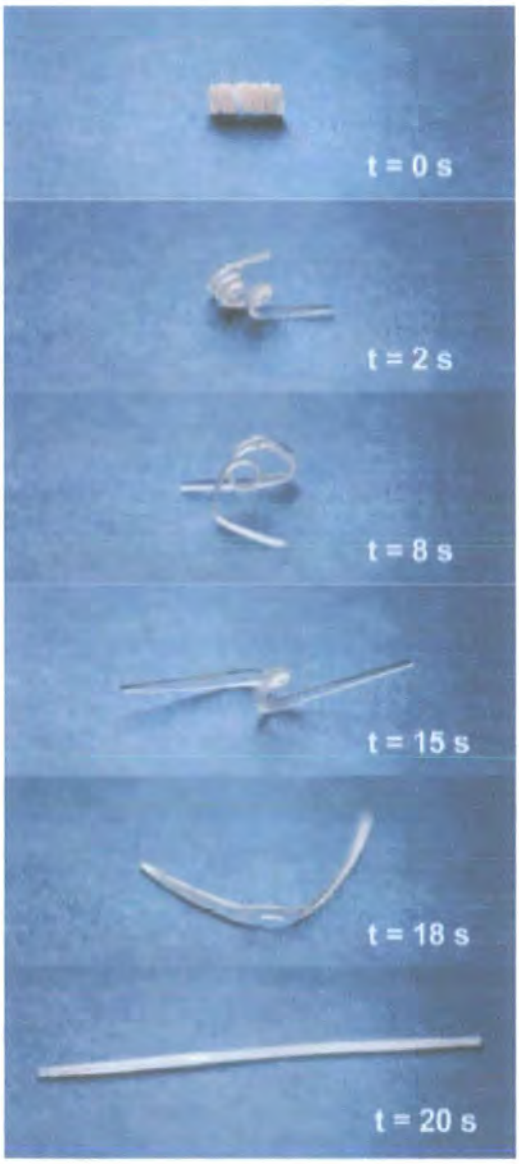

Figure 9.3 *The macroscopic shape memory effect of AB-polymer networks. The permanent shape is a rod and the temporary shape is a spiral. The photographs show the transiton from the temporary to permanent shape at 70 °C* [144].

9.2 Experimental

9.2.1 Materials and instrumentation

9.2.1.1 Materials

Poly(ϵ – caprolactone) diol (M_n = 2000 g/mol) and acryloyl chloride (96 %) were obtained from Aldrich Chemicals. The triethylamine (99 %) was obtained from Lancaster Chemicals.

The monomers styrene (99 %), 2-ethylhexyl acrylate (98 %) and divinylbenzene (80 %) and the surfactant sorbitan monooleate (Span 80) were obtained from Aldrich Chemicals. Each of the monomers was purified prior to HIPE preparation by passing through a column of basic activated aluminium oxide. The initiators potassium persulfate (99 + %) and 2,2'-azobisisobutyronitrile (98 %) (AIBN) were obtained from Aldrich Chemicals. The particle fillers aragonite and wollastonite (particle size distribution unknown) were purchased from Speciality Minerals and OTAVI Minerals GmBH respectively. The calcium chloride dehydrate (99 + %) and the ammonium chloride (99.5 + %) were purchased from Aldrich Chemicals.

9.2.1.2 Instrumentation

NMR spectra were carried on a Varian 500 spectrometer with $CDCl_3$ as solvent. MALDI- tof spectra of samples immobilised in a mixture 2,5- dihydroxybenzoic acid or dithranol were recorded using a Voyager-DE STR MALDI. Elemental analysis (C, H and N) was performed using an Exeter Analytical E-440 elemental analyser. ESEM images were recorded from a FEI Philips XL30 Environmental Scanning Electron Microscope. The DSC traces were recorded on a Perkin-Elmer 1 Differential Scanning Calorimeter.

9.2.2 Synthesis of Macromonomer

The preparation of the poly(ϵ – caprolactone) diacrylate (PCLDA) was carried out as described by Busby et al. [145], [146], [147]. The poly(ϵ – caprolactone) diol (20 g, ≈10 mmol OH groups) was dissolved in 200 ml DCM containing triethylamine (6.3 ml, 45 mmol). This mixture was then placed in a round-bottomed flask and cooled to ice temperature. The whole unit was purged with nitrogen as the flask cooled to ice temperature. Acryloyl chloride (6.0 ml, 74 mmol) in 30 ml DCM was added drop-wise over 1 hour to the contents of the round-bottomed flask under constant stirring at ice temperature. The system was then left stirring for a further 20 hours by which time it had returned to room temperature. The resulting yellow solution was extracted with 30 ml portions of 3 wt % KOH aqueous solutions followed by the same amount of 1 % HCl solution until in both cases a colourless aqueous layer was obtained. The extracted organic layer was then dried over $MgSO_4$ and placed on a rotary evaporator to remove the majority of the DCM, then concentrated *in vacuo* to a constant mass.

Mass and yield: 16.5 g, 83 %

^{1}H NMR: (500 MHz, $CDCl_3$), δ ppm = 6.4 (dd, $J_{Ha\text{-}Hc}$ = 16 Hz, $J_{Ha\text{-}Hb}$ = 2 Hz), 6.10 (dd, $J_{Ha\text{-}Hc}$ = 17 Hz, JHb-Hc = 10 Hz), 5.8, (dd, $J_{Hb\text{-}Hc}$ = 9 Hz, $J_{Ha\text{-}Hb}$ = 1 Hz), 4.20 (t, J = 5 Hz), 4.15 (t, J = 7Hz [-CO_2CH_2-]), 4.06 (t, J = 7 Hz, [-CH_2OCH_2-]), 3.70 (t, J = 5 Hz, [-$OCCH_2$-]), 2.30 (t, J = 8 Hz, [-CH_2CO_2]), 1.65 and 1.45 are mulitplets due to [-$OCCH_2CH_2CH_2CH_2$-].

^{13}C NMR: (125 MHz, $CDCl_3$), δ ppm 173.7, 166.5 [-CO_2CH_2-], 130.8, 128.8 [C=C], 69.3 [-CO_2CH_2-], 64.6, 64.36, 64.33, 63.05 [-CH_2OCH_2-], 34.3, 28.6, 25.8, 25.7, 24.8, 24.7 [-$OCCH_2CH_2CH_2CH_2$-].

MALDI-tof MS of PCLDA: m/z 1377, 1606, 1834, 2063 [(M_n)+ Na^+], 1166, 2307, 2535, 2764, 2992, 3219, 3448, 3676, 3792 [(M_n)+ K^+].

Elemental analyis: calculated for $C_{109.6}H_{180}O_{38.2}$- C, 62.5 %; H, 8.5 %, found- C, 50.4 %; H, 7.2 %

DSC: T_m = 34.5 and 47.1 °C, ΔH_m = 6.0 and 55.5 Jg-1, T_{cry} = 4.1 °C, ΔH_{cry} = -61.5 Jg $^{-1}$.

9.2.3 HIPE preparation and polymerisation

A monomer phase consisting of macromonomer PCLDA (0.6 g, 0.28 mmol), styrene (2.8 g, 26.8 mmol), 2 – ethylhexyl acrylate (1.6 g, 8.7 mmol) and the surfactant Span 80 (1 g, 2.3 mmol) was placed in a three-necked round-bottomed flask. The system was purged with nitrogen for 10 minutes prior to HIPE preparation. An aqueous phase consisting of 45 g water, calcium chloride dihydrate (0.5 g, 3.4 mmol) and potassium persulfate (0.1 g, 0.37 mmol) was added drop-wise under constant stirring (300 rpm) until a HIPE had formed. The HIPE was then placed in a PTFE plate mould and cured at 60 °C for 48 hours. The resulting material was washed with water and propan-2-ol in a soxhlet apparatus and then dried *in vacuo* for 48 hours. **Table 9.1** shows the varying monomer phase compositions used for the PCL PolyHIPE preparations. Each experiment was carried out only once.

Table 9.1 Monomer phase composition for PolyHIPE preparation

Sample code	Styrene (g)	EHA (g)	PCLDA (g)	DVB (g)
257 RJC	/	3.75	1.25	/
258RJC	2.8	1.6	0.6	/
259RJC	3.8	0.6	0.6	/
260RJC	2.8	1.0	0.6	0.6
261RJC	2.3	1.6	0.6	0.5
262RJC	2.25	1.85	0.6	0.3
263RJC	2.55	1.6	0.6	0.25

9.2.4 Shape-memory properties

A strip of ≈ 2-5 cm of the PolyHIPE material prepared as outlined in **9.2.3** was clamped at either end of the sample (**see figure 9.4**). The initial length of the material of the material was measured using a ruler to the nearest mm. The sample was heated above $T_{trans,}$ then stretched by weighting, and then cooled. The length of the sample in its temporary structure was then measured as previously. The sample was then clamped and heated above T_{trans} to regain the permanent shape. The length of the sample was then measured as already stated and the percent recovery (% R) was calculated as shown in **equation 9.1**.

$$\%R = \frac{l_0 - l_f}{l_0 - l_i} \times 100 \qquad \textbf{Equation 9.1}$$

where,

l_i = initial length of sample (mm)

l_0 = length of sample after heating, stretching and then cooling (mm)

l_f = length of sample obtained reheating above T_{trans} (mm)

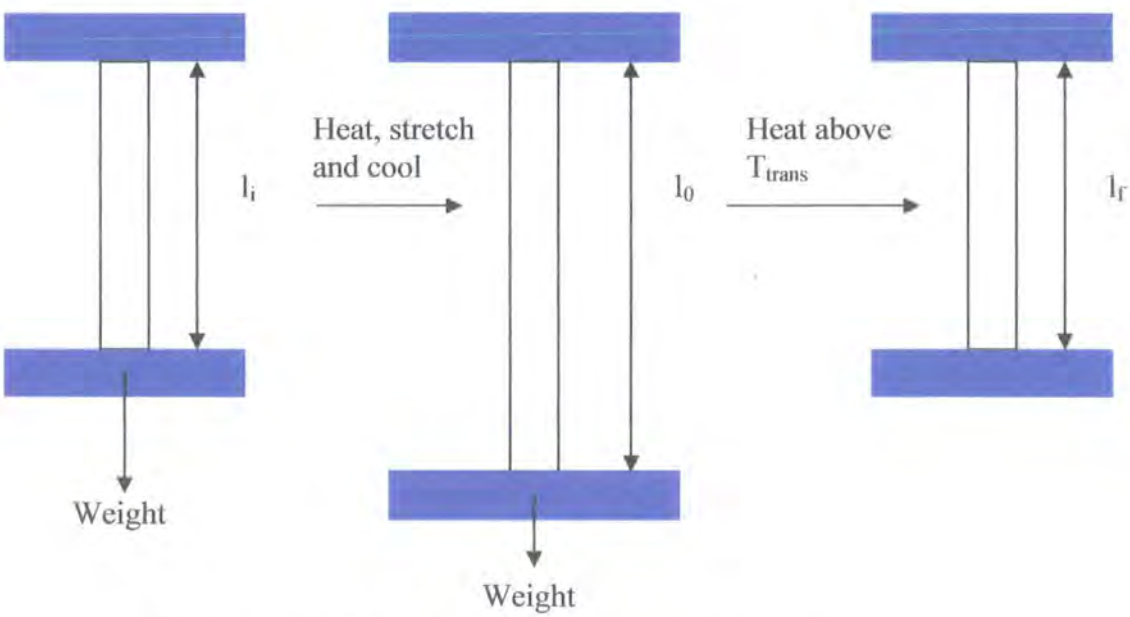

Figure 9.4 *Schematic of the shape memory test set-up*

9.2.5 Centrifugal curing

Resorcinol (8.3 g, 75.38 mmol) and formaldehyde (12.2 g, 40 % aq, 150.3 mmol) were mixed together in a polyethylene bottle until all of the resorcinol had dissolved. The amphoteric surfactant Miranol (2.3 g) was then added to the solution. To this mixture cyclohexane (180 ml, 1.75 mol) was then added, under constant mechanical stirring, until a high internal phase emulsion had formed. After HIPE formation, the catalyst phosphoric acid (3 g, 50 % aq, 15.3 mmol) was added to the emulsion. The PE bottle containing the HIPE was then weighed and placed within the centrifuge sample holder. A PE bottle containing an amount of water, of equal weight to the HIPE, was then placed in the opposite side of the sample holder. The HIPE was left in the centrifuge to cure at speeds of either 1,000 or 10, 000 rpm and at temperatures of either 20 or 45 °C for up to 1 hour. The material was removed from the centrifuge and the remaining water and cyclohexane were removed *in vacuo* at 50 °C. Each experiment was carried out only once, unless complete separation of the HIPE occurred and in this case the experiment was carried out until a PolyHIPE material was obtained.

9.2.6 Addition of filler particles

The monomer phase consisted of styrene (9 g, 86.4 mmol), divinylbenzene (1 g, 7.68 mmol) and the oil soluble initiator 2,2'-azobisisobutyronitrile (AIBN) (0.1 g, 0.61 mmol). The filler particle was then added to the monomer phase until a high enough concentration was reached to produce a viscous slurry of monomer and filler. This mixture was then cured in the oven at 60 °C. The top and bottom surfaces of the monolith were then removed to allow easier removal of the filler from the polymer matrix. The filler particles were removed by washing the monolith in water in a

soxhlet apparatus for 48 hours or by washing with dilute or concentrated HCl for a certain period of time. Each experiment was carried out only once.

9.3 Results and discussion

9.3.1 Macromonomer synthesis

Acrylate groups have the characteristic resonances in the ^1H nmr at δ5.8, 6.1 and 6.4 ppm [148] and these can be seen in **figure 9.6 (a).**

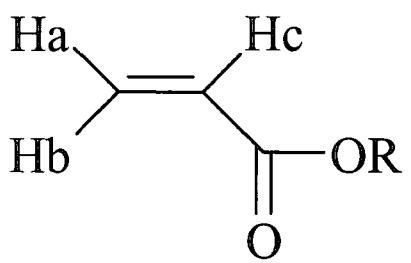

Figure 9.5 *Assignment of H's in acrylate groups.*

From **figure 9.5** it can be seen that H_c occurs at 6.1 ppm because the coupling constants obtained are characterictic of *trans* (17 Hz) and *cis* (10 Hz) and H_c is the only proton without geminal coupling. The doublet of doublets at δ5.8 ppm shows geminal couplng (1 Hz) and a J_2 constant of 9 Hz. As the latter value is less than 12 Hz, this coupling constant is characteristic of *cis* and this peak was therefore assigned to H_a. The doublet of doublets at δ6.4 ppm again shows geminal coupling (2 Hz) but this time has a J_2 coupling constant of 16 Hz, which being greater than 15 Hz is characteristic of *trans* and was assigned to H_b.

The extent of conversion of the diol to diacrylate was established using MALDI-tof mass spectrometry. This is illustrated where each peak of the starting material was shifted by the molecular weight of two acrylate groups (2 x H_2C=CH-CO-) minus two protons (108 a.m.u). **Figures 9.7 (a)** and **(b)** show the MALDI-tof MS for the PCL diol and the PCL diacrylate. It can be shown from both spectra that there are peaks at

[(M_n) + 108] but no peaks existed for the mono-substituted material at peaks at [(M_n) + 54]. The two sets of peaks present in **figure 9.7 (b)**, are due to the diacrylate flying with both sodium and potassium ions during analysis. The difference between the two sets of m/z peaks is 16 and corresponds to the difference in atomic mass of sodium and potassium.

The difference in carbon and hydrogen values obtained from elemental analysis could not be explained. The material was placed in a dessicator *in vacuo* in the presence of P_2O_5 for a period of two weeks but no change in % C or % H values were obtained.

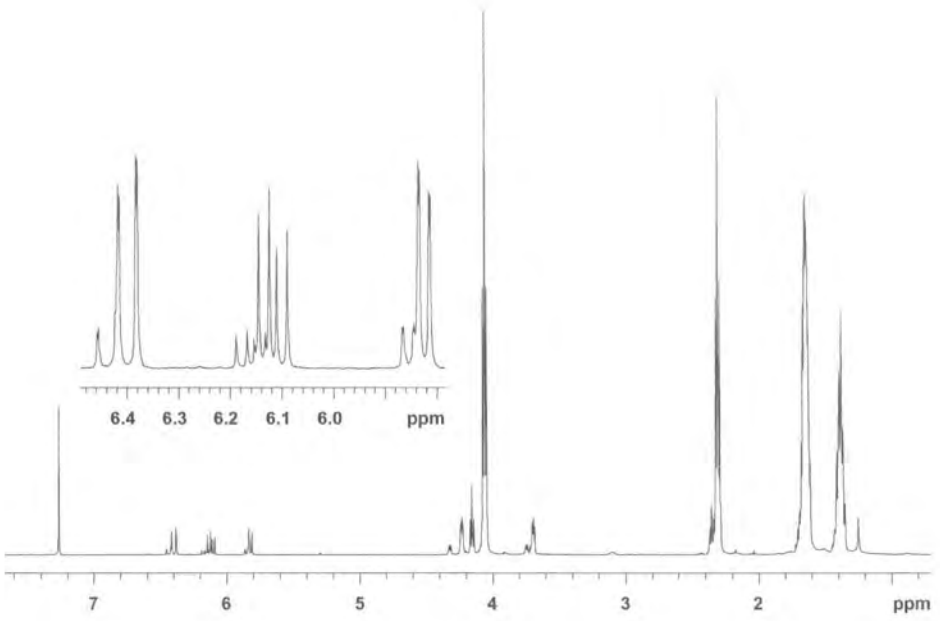

(a)

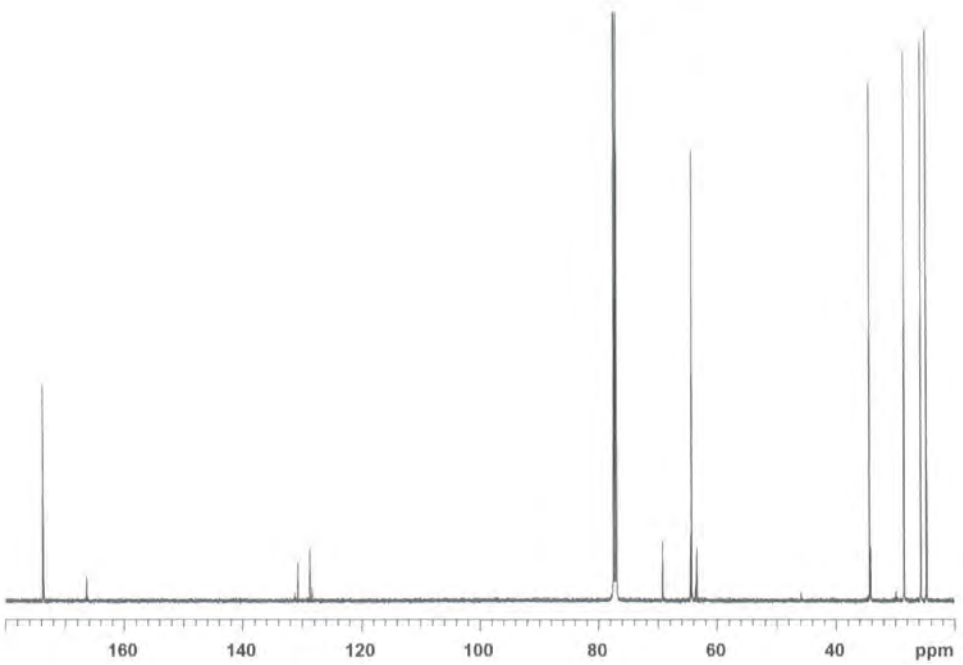

(b)

Figure 9.6 *NMR spectra of PCL diacrylate, (a) ^{1}H and (b) ^{13}C.*

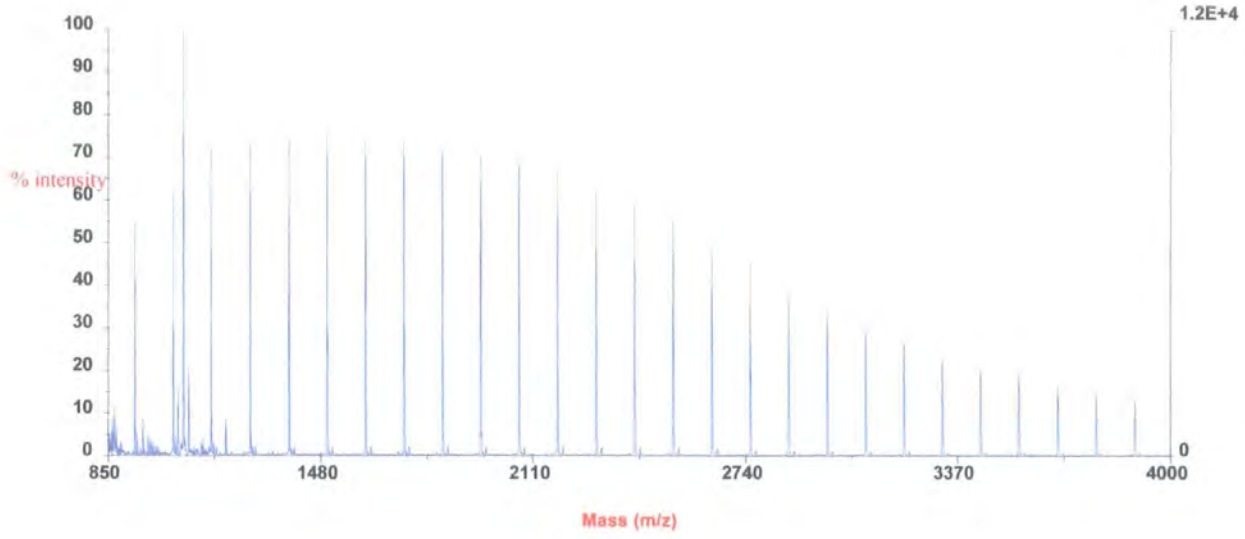

(a)

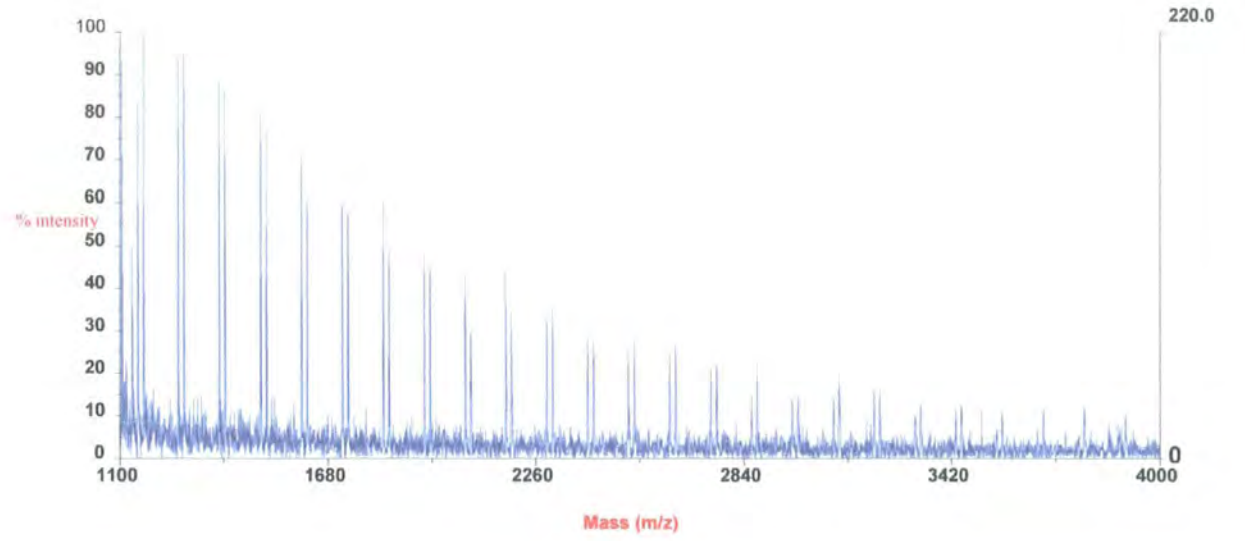

(b)

Figure 9.7 *Maldi-tof spectrun of (a) poly(ε-caprolactone) diol (M_n = 2,000 g/mol) and (b) poly(ε-caprolactone) diacrylate macromonomer.*

9.3.2 PolyHIPE preparation

In initial experiments, such as 257RJC, EHA and PCLDA were the only two monomers present in the continuous phase. In these cases HIPE preparation was difficult due to the increased viscosity of the monomer phase and also the increasing difficulty of dissolution of the solid PCLDA in the EHA. At high concentrations of PCLDA, gelation of the monomer phase occurred. This was possibly due to the high reactivity of both of the acrylates present. The inhibitor hydroquinone was added to the monomer phase. This prevented gelation of the monomer phase and a HIPE could be formed. The HIPE formed then phase separated on curing and no PolyHIPE was produced. The addition of styrene to the monomer phase and the reduction in PCLDA content in 258RJC resulted in a HIPE, which produced a PolyHIPE material that was elastomeric in nature. On drying under vacuum at 25 °C there was noticeable shrinking in size of the PolyHIPE material produced in 258RJC. This is probably due to the drying process being conducted above the glass transition temperature of the PolyHIPE material. The PolyHIPE material produced was opaque in nature after drying. The material also reduced in size, by around 50 %, when placed in the freeze drier. In this case cracks appeared within the sample during the drying process. An increase in styrene content (259RJC) produced a more rigid/plastic material. The material produced was not opaque in nature and, although there was a reduction in the flexibility of the sample, the PolyHIPE material still reduced in size when drying under vacuum. The addition of the cross-linker DVB prevented the material from shrinking during the drying process. The material produced was more rigid in nature than 258RJC, and the flexibility increased with decreasing DVB content from 11 – 5 wt %.

9.3.3 Shape-memory properties

The materials produced using the monomer compositions in 258RJC and 259RJC showed the greatest shape-memory behaviour. The programming and recovery process (258RJC) can be shown in the photographs presented in **figure 9.9**. The blue arrows represent the programming process and the red arrows the recovery process. The video of this process can also be observed (**see attached CD**). The PolyHIPE material produced from 258RJC recovered its permanent shape in seconds. The shape-memory effect is determined by the crystallisation of the PCL segment, this prevents the material regaining its permanent covalent network. The temporary shape is fixed by physical cross-links. Heating above the transition temperature will cause the crystallites to melt and the material to regain the permanent shape.

When the styrene content of the material (259RJC) is increased, a shape memory effect is still observed. The photographs in **figure 9.10** show the programming and recovery process for the PolyHIPE material prepared from 259RJC. The T_g of both 258 and 259RJC were estimated using the Fox equation (**see chapter 1, equation 1.8**). Using the T_g values of 373 K for cross-linked polystyrene [128], 223 K [128] for EHA and 213 K [149] for the poly(ϵ-caprolactone). For 258RJC the possible T_g of the material was calculated to be 285 K, or 12 °C and for 259 RJC the T_g of the PolyHIPE was calculated to be 318 K or 45 °C. This shows that it is possible to prepare either an elastomeric or a rigid foam material with shape-memory properties. The materials containing DVB showed no deformation when subjected to the same treatment as for the previous materials. The material snapped when clamped or stretched due to its rigid/brittle nature. The material should generally show some elasticity at the working temperature so that deformation can take place. The addition of the DVB increases the cross-linking density and therefore the T_g of the material.

Tables 9.2, 9.3 and 9.4 show the percent recovery of each material on reheating after stretching and cooling. The percent recovery of both the PolyHIPE materials remains above 85-90 % after at least three cycles. After repeated heating and stretching small tears appeared in the sample, which eventually led to sample destruction on further stretching. The reproducible nature of the shape-memory process leads to the advantage of producing a material that can be switched between two different morphologies to change the mechanical behaviour of the material. **Figure 9.11** shows the morphology of the permanent shape and the temporary shape of the material obtained after heating, stretching and cooling. The permanent shape is the normal open-cellular structure expected of a PolyHIPE material.

Table 9.2 Percent recovery measurements for the PolyHIPE material 258RJC

Cycle	l_i (mm)	l_0 (mm)	l_f (mm)	Recovery (%)
1	40	55	42	86.7
2	42	55	42	100
3	42	68	42	100
4	42	73	42	100
5	42	74	42	100

Table 9.3 Percent recovery measurements for the PolyHIPE material 258RJC

Cycle	l_i (mm)	l_0 (mm)	l_f (mm)	Recovery (%)
1	41	63	43	91
2	43	60	44	94
3	44	65	46	91

The temporary structure has an elongated cellular structure in the direction of the deformation. This could lead to possible anisotropic behaviour where the foam material may exhibit enhanced mechanical properties in the direction of the elongation. The deformation exerted during the programming process can be used to produce properties in addition to an anisotropic morphology. If a triaxial stress were exerted on the foam material possible inversion of the cellular network would produce a re-entrant type structure (**see figure 9.8**), which is characteristic of a class of materials that are known as auxetic foams. Evans et al. give a detailed overview of the behaviour and types of auxetic materials available [(2)].

Table 9.4 Percent recovery measurements for the PolyHIPE material 259RJC

Cycle	l_i (mm)	l_0 (mm)	l_f (mm)	Recovery (%)
1	34.0	50	35	93.8
2	35	47	36	91.7
3	36	55	37	94.7
4	37	58	42	76.2
5	42	60	42	100

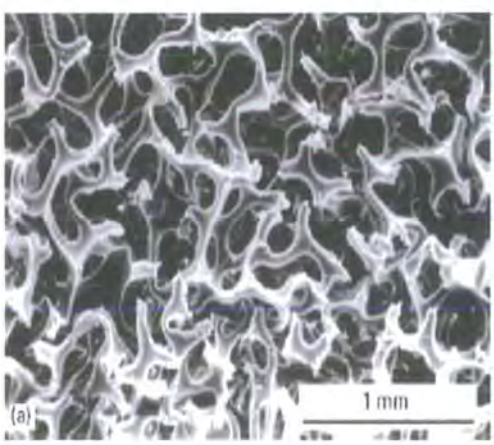

Figure 9.8 *Micrograph image of an auxetic foam with a re-entrant type structure. (152)*

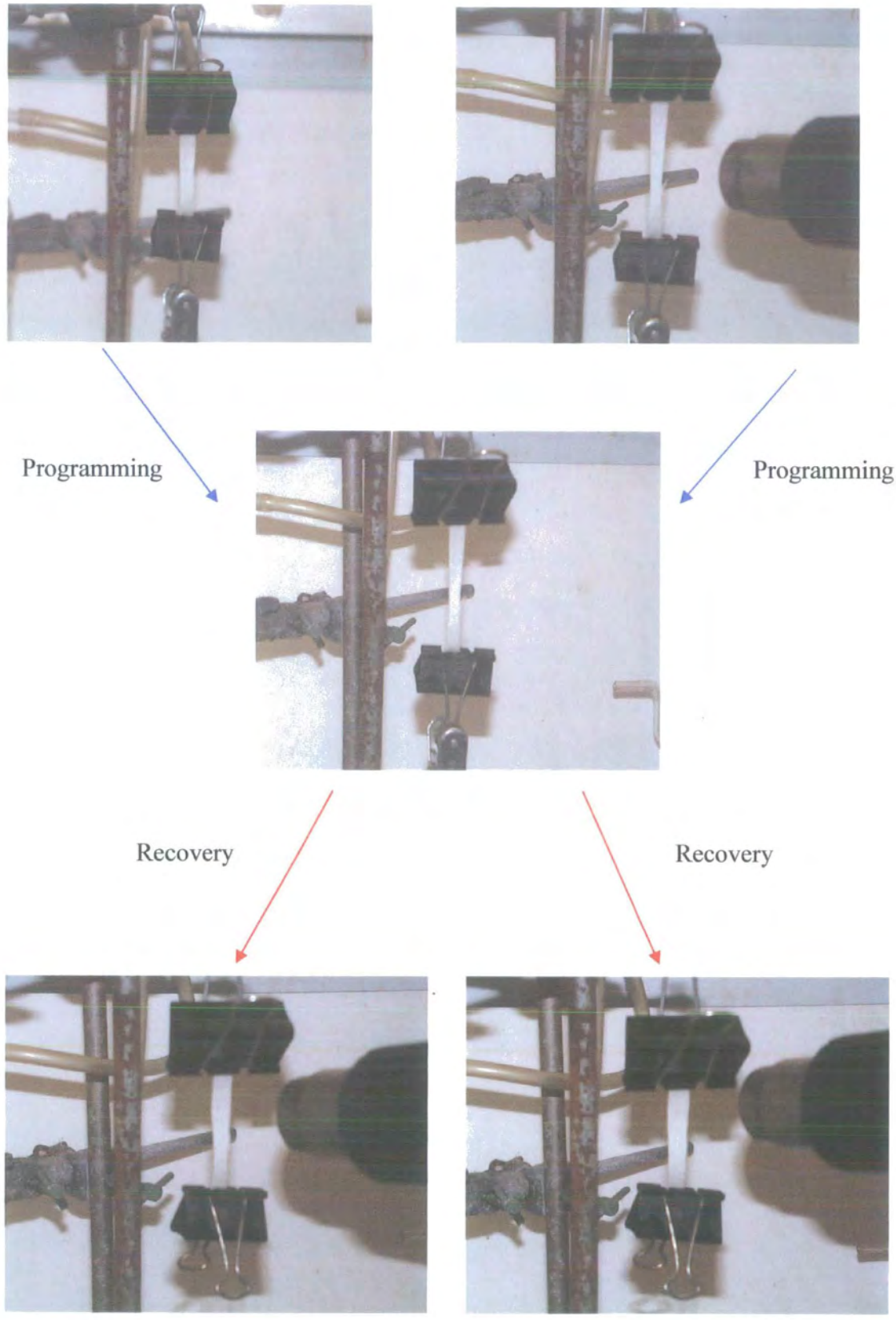

Figure 9.9 *Photographs of the shape memory effect of* 258RJC.

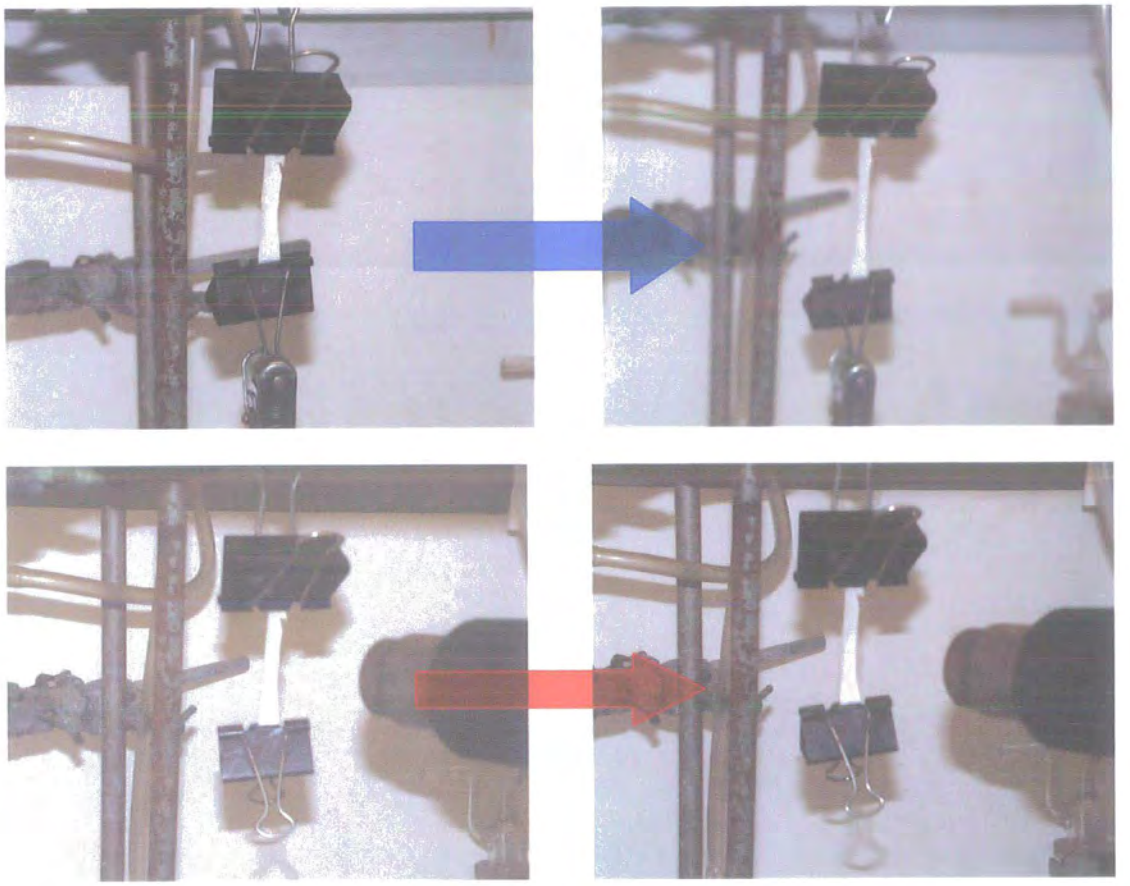

Figure 9.10 *Photographs of the shape memory effect of* 259RJC *(blue = programming process of heating and stretching above the* T_{trans} *and then cooling to produce the temporary elongated cell structure, red = recovery process of the permanent structure on reheating the material above* T_{trans}*)..*

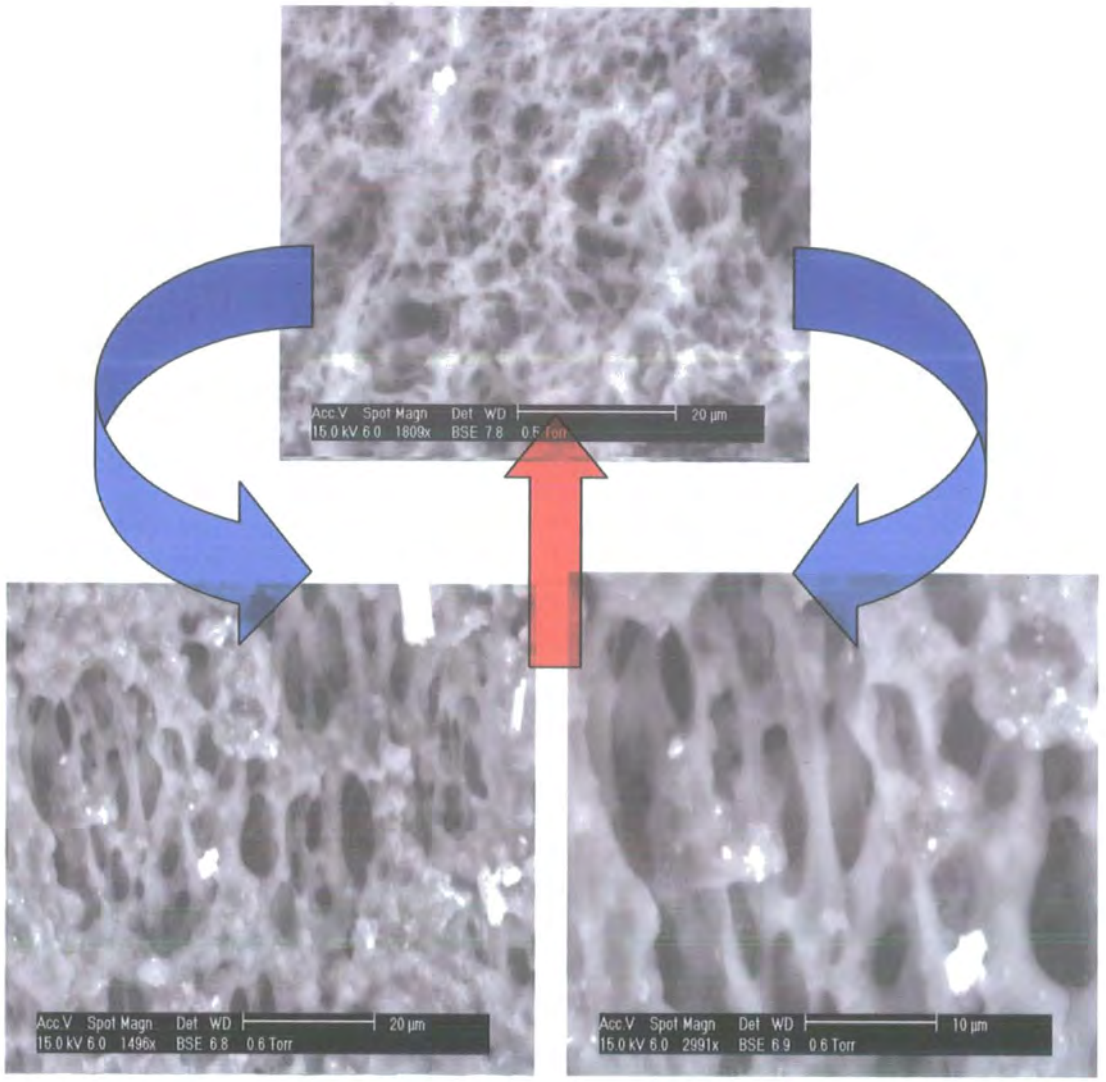

Figure 9.11 *Morphology of the material before and after the shape memory process (258RJC) (blue = programming process of heating and stretching above the* T_{trans} *and then cooling to produce the temporary elongated cell structure, red = recovery process of the permanent structure on reheating the material above* T_{trans}*).*

9.3.4 Centrifugal curing

The RF-based material was used due to the rapid curing time (10 minutes at 60 °C) of the RF reaction. The monolith produced at a speed of 1000 rpm was homogenous in nature and there were no signs of phase separation due to the centrifugal force. There was no effect on the morphology of the RF material when the material was cured at a speed of 1,000 rpm at room temperature. The ESEM image in **figure 9.12** shows no possible elongation of the HIPE droplets by the application of the centrifugal force during curing.

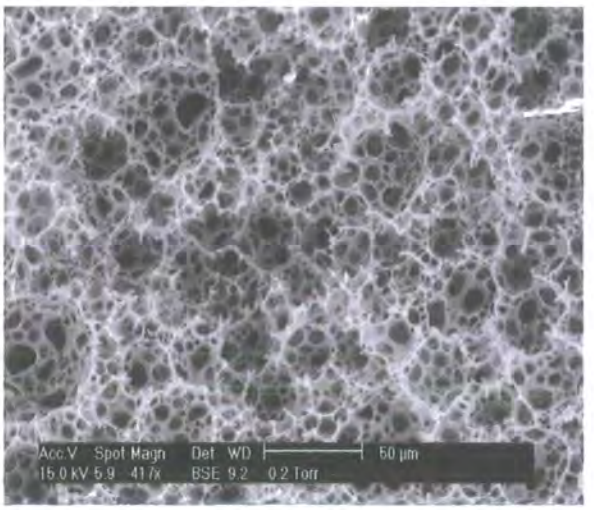

Figure 9.12 *ESEM image of the RF PolyHIPE material after curing at 1000 rpm and at room temperature.*

The speed used was increased to 10,000 rpm, the maximum speed available with the centrifuge. **Figure 9.13** shows schematically the different regions produced within the PE bottle after curing at a speed of 10,000 rpm at room temperature. Area 1 was a region of dense red/pink-coloured polymer, which was very tough and physically hard in nature. Area 2 was a region of softer material, which was lighter in colour compared to the material present in area 1. Area 3 was a layer of the solvent cyclohexane. The centrifugal force drives the HIPE to phase separation with the denser continuous phase existing at the bottom of the PE bottle.

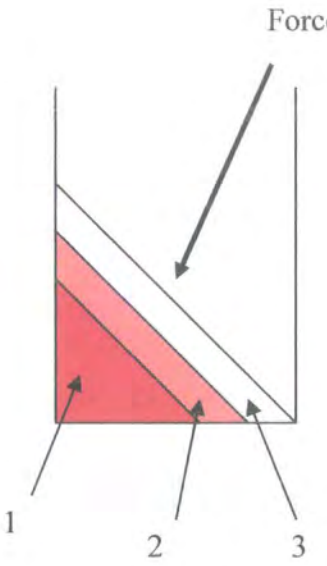

Figure 9.13 *Schematic of the material produced after curing within a centrifugal force (see text for description of areas 1-3).*

Figure 9.14 shows an ESEM image of the polymer material existing in area 1.

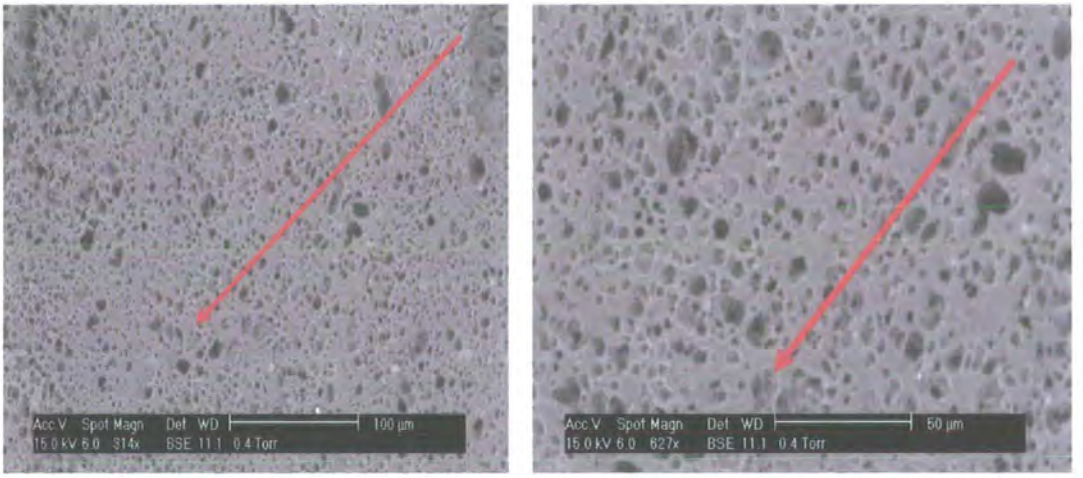

Figure 9.14 *ESEM images of the RF material present in area 1 after curing in the centrifuge.*

The material was fractured or cut in the direction of the force, which is shown by the pink arrow present on the ESEM images. There is no sign that the droplets have been elongated due to the centrifugal force applied. There may be a possible alignment of the voids/pores rather than a physical deformation in the shape of the droplets during curing. A stronger centrifugal force may be needed to produce any observable droplet

elongation; however this may result in greater phase separation of the emulsion. To eradicate the problem of phase separation, the centrifuge was heated to 45 °C prior to placement of the PE bottle containing the HIPE within the centrifuge. As discussed previously, the RF-based PolyHIPE material cures in 25 – 30 minutes at a polymerisation temperature of 45 °C. The material was cured at the same centrifugal speed as previously for a period of thirty minutes. The material produced consisted of the same three regions as previously stated. This suggests that phase separation of the HIPE is instantaneous on application of the centrifugal force. This method was far less effective in preparing an elongated cellular structure compared to the shape-memory PolyHIPE materials.

9.3.5 Addition of filler particles

The aim of this section of work was to add to a monomer phase of styrene and DVB high aspect ratio fillers, which could be then removed from the cured polymer material by washing/leaching from the matrix. If the filler were present in a high concentration then the particles would hopefully align in an ordered arrangement to leave a structure that was anisotropic in nature when the filler particles were removed. This technique was tried with conventional salt crystals such as calcium chloride and ammonium chloride, which could be easily removed from the material by washing with water in a soxhlet apparatus. **Figure 9.15** shows the structure of the S/DVB material after removal of the calcium chloride salt particles.

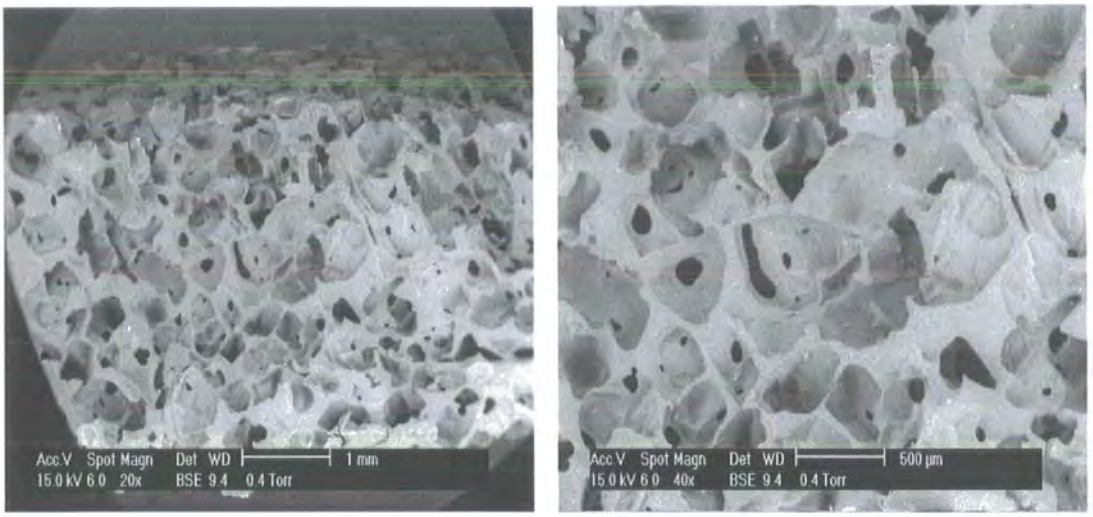

Figure 9.15 *ESEM images of the porous S/DVB material produced after removal of calcium chloride salt particles.*

The ESEM images show that it is possible to prepare a rigid porous material by removal of the calcium chloride salt particles with water. The pore size of the material is around 100 µm with a void/cell size between 300-500 µm. The ammonium chloride particles were also added and removed in the same way as the calcium chloride particles. **Figure 9.16** shows ESEM images of the material produced after removal of the ammonium chloride particles.

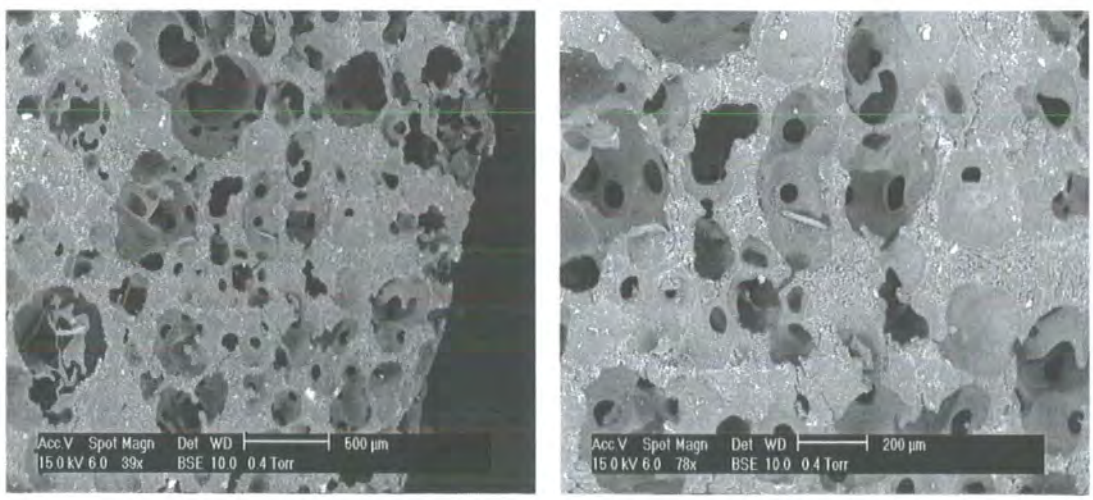

Figure 9.16 *ESEM images of the S/DVB material obtained after removal of the ammonium chloride crystals.*

The removal of the ammonium chloride particles with water also produces a rigid porous material. Again the pore size of the material is large (100 – 200 μm) compared to the S/DVB PolyHIPE material. The only difference compared to the material produced from the removal of the calcium chloride particles is the absence of any noticeable cell/void shape containing the pores. At high concentrations it was expected that crystals might pack together in an ordered arrangement to produce a porous material with possible anisotropic behaviour. This was not observed from the ESEM images. This is possibly due to the high size or shape distribution of the salt crystals present as shown in the ESEM images in **figure 9.17**.

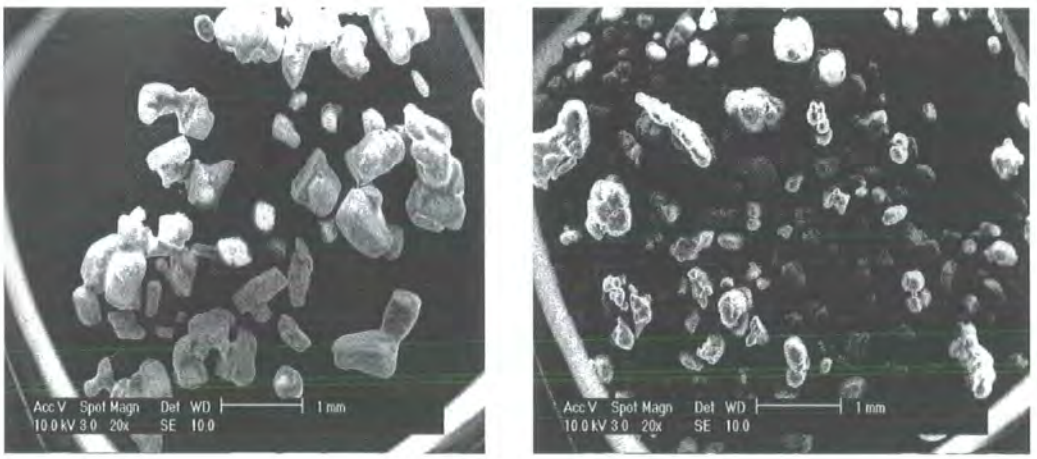

(a) (b)

Figure 9.17 *ESEM images of (a) calcium chloride and (b) ammonium chloride fillers.*

Although no anisotropic structure was observed, it was shown that it was possible to prepare porous materials by the removal of solid particles or crystals from a cured monomer phase. An Internet search was then carried out for filler shapes with a high aspect ratio, such as fibres or needle shaped crystals, which could be dissolved out of the cured monomer phase. The two filler materials identified were the minerals wollastonite and aragonite. Wollastonite is a naturally occurring calcium silicate mineral, and is unique due to its acicular (needle-like) shape (**see figure 9.18 (a)**). This is due to the repeating twisted chain structure of three silica tetrahedral units (**see**

figure 9.18 (b)). Wollastonite surfaces in contact with water hydrolyse to form calcium hydroxide and are subject to dissociation in acid, especially hydrochloric acid. Aragonite, which is crystallised calcium carbonate (calcite), also exists in an acicular form (**see figure 9.18(c)**).

(a)

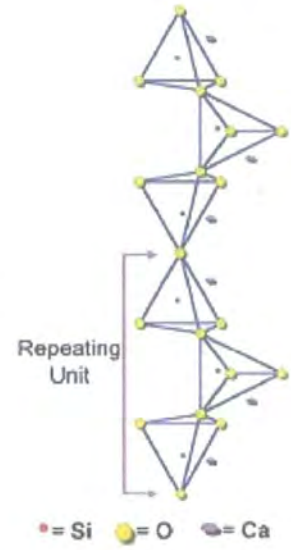

(b)

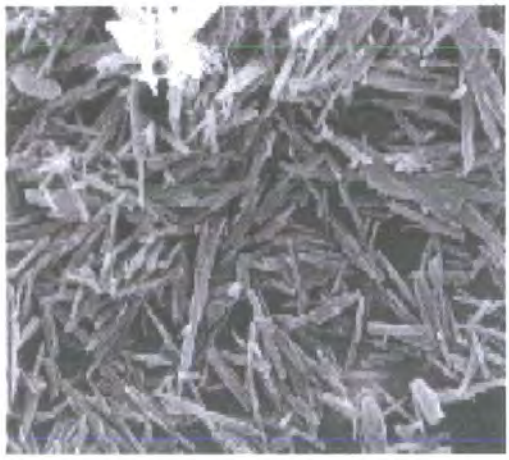

(c)

Figure 9.18 (a) *Acicular form of wollastonite, (b) structure of wollastonite and (c) acicular form of aragonite.*

The S/DVB material produced on the addition of wollastonite was a rigid/hard grey-coloured material. The S/DVB material containing the wollastonite was left in concentrated HCl for one week. There were no noticeable signs of dissolution of the wollastonite from the S/DVB material by the HCl. **Figure 9.19 (a)** and **(b)** shows ESEM images of the S/DVB material containing the wollastonite filler. The material was cut at both the bottom and the top of the monolith so that the acid could penetrate and dissolve the filler. **Figure 9.19 (a)** is the top surface of the monolith and **figure 9.19 (b)** is a fractured surface which shows the morphology of the material beyond the top surface.

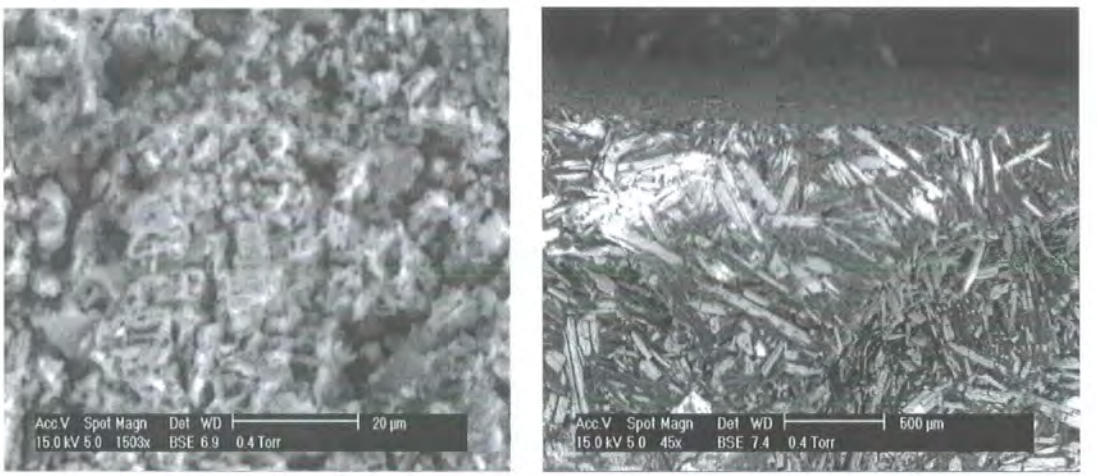

(a) (b)

Figure 9.19 *ESEM images of the S/DVB material containing the wollastonite filler, (a) top cut surface, (b) fractured surface.*

The ESEM image of the top surface shows a porous material but of a different morphology compared to the materials containing the ammonium chloride and calcium chloride filler particles. The fractured surface shows the presence of wollastonite crystals even though the material had been submerged in concentrated

HCl for one week. If the crystals had been dissolved due to the hydrochloric acid no anisotropic structure would have been observed, as the crystals do not fall into any type of ordered structure within the S/DVB material. The addition of the aragonite crystals at high concentration produced a mixture of monomer and filler, which was paste-like and viscous in nature prior to polymerisation. After polymerisation the monolith had expanded in dimensions and was difficult to remove from the PE bottle. The monolith was washed in concentrated HCl for one week and then in water for 48 hours. After the washing procedure there was no sign of any removal of the aragonite from the polymer material. The filler materials themselves were dispersed in HCl and water for one week to observe the solubility of each material. The wollastonite mixed/dispersed easily in both water and the HCl but after one week there was still a significant amount of material dispersed within both the HCl and the water. The HCl/wollastonite solution had turned a light yellow/green colour, which suggested that some of the material may have dissolved but this may be a slow process. The aragonite material did not disperse easily within the water or the HCl. The material remained on the surface of both the water and the HCl.

9.4 Conclusions

In this investigation it has been shown that it is possible to prepare PolyHIPE materials that have shape-memory properties. The shape-memory effect produces a PolyHIPE material with an elongated cell temporary structure. This material may now behave anisotropically due to the possible enhanced mechanical properties in the direction of the elongated cells. If this material is then heated up above its T_{trans} the permanent structure is then regained. It was shown that it was possible to prepare both elastomeric and more rigid plastic materials that showed shape-memory properties. The shape-memory process for both materials was reproducible in nature showing percent recovery between 85 and 100 % for up to 5 cycles. The shape-memory effect was suggested to be due to the crystallisation of the PCLDA (switching segment) and the recovery process was due to heating the material above the melting temperature of the PCLDA to reproduce the permanent structure. The addition of DVB to the formulation produced a material, which was rigid in nature but showed no shape-memory properties.

The use of centrifugal curing did not produce a PolyHIPE material with an elongated cell structure. ESEM images showed there might be possible alignment of the voids in the direction of the centrifugal force. A RF material was produced which consisted of three areas. A hard/dense RF PolyHIPE material which was dark red in colour, a weaker, less dense material which was light pink in colour and a layer of cyclohexane. The centrifugal force was forcing the HIPE to phase separate with the heavier polymer material to the bottom right- hand side of the PE bottle and the lighter cyclohexane layer remaining on the surface. The temperature of the centrifuge

was increased to try and reduce the extent of phase separation but there was no change in the material produced.

The addition of calcium chloride and ammonium chloride filler particles, at high concentrations, to a monomer phase of styrene and DVB produced porous foam materials after removal of the particles with water. The material produced showed no anistropic nature in the pore structure. It was hoped that at high concentrations the particles may assume an ordered arrangement and when removed would leave that order within the pore structure. This was not the case for the ammonium and calcium chloride salt crystals. High aspect ratio fillers such as wollastonite and aragonite were thought to have a high chance of producing an ordered arrangement at high concentrations due to their needle like shape. Both materials produced were washed in concentrated HCl and water and from physical observations and ESEM images no significant dissolution of the particles occurred. ESEM images showed that the wollastonite filler particles did not form an ordered arrangement as was hoped, they also showed there may be some removal of the particles at the surface of the material but complete removal of the particles may be extremely slow.

Chapter 10

Conclusions and future work

10.1 Conclusions

As discussed in **chapter 1**, the main aim of the project was to prepare lightweight uniform PolyHIPE materials for structural applications, by the polymerisation of the continuous phase of a high internal phase emulsion. For the PolyHIPE foams to be used as viable core materials varying the mechanical properties compared to a standard styrene/divinylbenzene material was investigated and the PolyHIPE materials produced were also compared to commercially available core materials. The main conclusions are listed below.

10.1.1 Mould testing

From the mould tests results it was shown that PTFE produced the most uniform PolyHIPE materials compared to glass, PVC, PP and PE. From ESEM images it was shown that the open-cell nature and the porosity of the PolyHIPE surface in contact with the mould substrate was adversely affected compared to the fractured surface of the material. Mould release agents such as vacuum grease, PTFE spray and a PTFE substrate called Tygflor were also used to enhance sample uniformity and reduce

adherence to the mould substrate. The mould release agents Tygflor and the PTFE spray enhanced sample uniformity from the flat PVC mould. From the mould test results it was decided that the optimum moulding technique for large scale production was to use a PVC mould coated with PTFE spray.

10.1.2 Acrylate- and methacrylate-based PolyHIPE materials

It was shown it was possible to prepare elastomeric PolyHIPE materials from monomers such as EHA and BA at a concentration in the monomer phase of up to 80 % w/w. Compressive mechanical testing showed that the modulus of the PolyHIPE materials decreased with increasing elastomer concentration compared to the standard S/DVB PolyHIPE material. It was also possible to prepare more rigid/glassy PolyHIPE materials using monomers such as BMA and MMA. Only materials with a MMA concentration of 40 % w/w could be prepared due the decreased stability of the HIPE at higher MMA concentrations. PolyHIPE materials of up to 80 % w/w BMA were prepared. Compressive mechanical test results showed the expected increase in compressive modulus with increasing MMA concentration compared to the standard S/DVB material.

The compressive test results also showed that at low concentrations (20-40 % w/w) of both BA and BMA the yield strength of the material increased compared to the standard S/DVB material. This was also evident when comparing the different acrylate- and methacrylate-based materials at a monomer concentration of 20 % w/w. The addition of the acrylate- and methacrylate-based monomers reinforced the foam material in yield with the effect increasing as the side-chain length was shortened, from EHA to the more rigid side-chain in MMA. The methacrylate-based materials showed a greater reinforcement in yield strength compared to their acrylate counterparts, due to the presence of the methyl group in the backbone.

PolyHIPE materials were also prepared using multifunctional methacrylates EGDMA and TMPTM as alternative cross-linkers to DVB. There was a significant change in the compressive properties compared to the standard S/DVB material at a concentration of 10 % w/w EGDMA and TMPTM. Further increases in the methacrylate cross-linker concentration led to a decrease in the modulus of the PolyHIPE material.

10.1.3 Optimisation of surfactant system and curing time

In this work it has been shown that is possible to prepare S/DVB PolyHIPE materials at an internal phase volume of 90 and 95 % using an alternative co-surfactant system containing Span 20 (6.3 % w/w), CTAB (0.4 % w/w) and DDBSS (0.3 %) at a lower weight percent level of the monomer phase compared to the standard 20 % w/w Span 80 used to prepare S/DVB PolyHIPE materials. The replacement of Span 80 with the OSS resulted in an increase in the compressive, flexural and shear properties of the S/DVB PolyHIPE material. This increase in the mechanical properties was said to be due to the absence of the plasticisation effect of the surfactant Span 80.

It was not possible to prepare acrylate or methacrylate-based PolyHIPE materials using Span 20 within the co-surfactant system. Replacing Span 20 with Span 80 at a higher concentration in the co-surfactant system (8.3 % w/w) resulted in PolyHIPE materials prepared from 80 % EHA, 40 % MMA and 10 % EGDMA.

It has also been discussed that it is possible to prepare 90 and 95 % void S/DVB PolyHIPE materials using a redox initiator. The most efficient redox couple contained iron (II) sulfate heptahydrate, ascorbic acid and hydrogen peroxide, which resulted in the cure of the HIPE within four hours at a polymerisation temperature of 60 °C. This was compared to the standard thermal initiation using potassium persulfate which cured the HIPE within 24 hours at 60 °C. Increasing the polymerisation temperature reduced the curing time of both the redox and potassium persulfate initiated materials

although the uniformity of the sample was adversely affected. There was no difference in either the shear or compressive modulus or strength of the redox initiated material compared to the standard potassium persulfate initiated S/DVB PolyHIPE material. It was not possible to prepare either MMA- or EGDMA-based PolyHIPE materials using this redox initiator due to phase separation of the emulsion on addition of the hydrogen peroxide.

10.1.4 Resorcinol/formaldehyde and urea/formaldehyde based PolyHIPE materials

It has been shown during the work that it is possible to prepare PolyHIPE materials by step-growth polymerisation by using resorcinol/formaldehyde and urea/formaldehyde chemistry. The rigid RF PolyHIPE material was cured in 10 minutes at 60 °C, by adding a phosphoric acid catalyst to the HIPE, and was salmon-pink in colour with an open-cell morphology. To prepare the UF PolyHIPE materials a UF based resin was used as a pre-polymer and the HIPE could be cured within 72 hours using ammonium chloride and within 24 hours using hydrochloric acid as catalyst. The PolyHIPE prepared from ammonium chloride was elastomeric and open-cell in nature compared to the more rigid open-cell material prepared using hydrochloric acid as catalyst.

TGA analysis showed that the RF PolyHIPE material was thermally more stable than the standard S/DVB PolyHIPE material, whereas the UF PolyHIPE material decomposed at a lower temperature than that of the S/DVB material.

Shear and compressive core tests showed that the RF material had a greater compressive strength compared to the standard S/DVB material. However there was no significant difference in either the compressive modulus or the shear properties of the RF material compared to the S/DVB PolyHIPE material. It was not possible to

prepare UF materials for compressive and shear core testing due to processing problems on a large-scale setup.

10.1.5 Fibre-reinforcement of PolyHIPE materials

It has been shown that by addition of fibres such as Kevlar, PP and viscose to a S/DVB monomer phase that it was possible to prepare 90 % void fibre-reinforced composite materials. ESEM images showed that the adhesion of the PolyHIPE matrix to the fibre was greatest with the Kevlar fibres, followed by PP and viscose showing the least adhesion. In addition, fibre pull-out from the PolyHIPE matrix was observed with the latter. Flexural mechanical testing showed an increase in the flexural modulus and strength compared to the fibre-free material with the addition of Kevlar and PP fibres but no significant increase in modulus or strength with the addition of the viscose fibres. With increasing fibre volume there was an increase in flexural modulus of the material but a decrease in the flexural strength due to the increasingly brittle nature of the foam. Addition of Kevlar fibres to the 95 % void S/DVB PolyHIPE material prepared from the OSS, showed no significant change in both the compressive and shear properties compared to the fibre-free PolyHIPE material. Addition of the Kevlar fibres to the RF material resulted in an increase in both the shear properties and the compressive modulus compared to the fibre-free material. However there was no significant difference compared to the compressive strength of the fibre-free material.

10.1.6 Comparison with commercially available core materials

It was shown from the compressive and shear core tests that the fibre-free S/DVB PolyHIPE materials prepared with the OSS and the 10 % w/w Kevlar-reinforced OSS, together with the fibre-free and fibre-reinforced RF materials competed well with the shear and compressive strength of the commercially available core materials examined.

10.1.7 Preparation of anisotropic porous materials

From the work discussed it has been shown that is possible to prepare poly(ϵ-caprolactone)/EHA/styrene-based PolyHIPE materials with possible anisotropic properties. This was possible due to the materials exhibiting what is known as a shape-memory effect. It was possible to heat, stretch and cool the PolyHIPE material to produce and hold an elongated cell structure in the direction of the stretch. It was thought that this material would exhibit anisotropic behaviour in the direction of the elongated cells. On re-heating, the PolyHIPE material regained its permanent shape and the isotropic open-cell structure within seconds. The percent recovery of the permanent shape of the material was between 75-100 % after at least five cycles.

Other methods such as curing a HIPE in a centrifugal field or the addition and removal of high aspect ratio fillers from a S/DVB polymer matrix failed to provide porous materials with any order or anisotropy.

10.1.8 Permeability studies of PolyHIPE materials

From the permeability studies it was shown that it was possible to obtain permeability coefficient values for the PolyHIPE materials by using Darcy's law for permeating fluids such as water and kerosene. It was shown that the permeability of the material was affected by the pore structure, porosity and surface porosity, fibre reinforcement and the wettability of the PolyHIPE material. Contact angle measurements with both kerosene and water on the S/DVB and RF based materials showed that the RF material was more hydrophobic compared to the S/DVB and that kerosene wet both the RF and S/DVB material to a greater degree than water. This explained the much higher permeability coefficients obtained for kerosene compared to water. In the case of the RF material, water was said to be a non-wetting liquid due the contact angle being greater than 90° (121°). It was also discussed that it was difficult to describe the

contact angle measured as an equilibrium contact angle due to the movement of the wetting front by capillary action. It was to be considered a dynamic contact angle.

10.2 Future work

10.2.1 Mould testing

Other investigations could involve improving HIPE stability to produce thinner, pinhole or defect free membranes especially at higher polymerisation temperatures. Investigation into the packing of HIPE droplets at the HIPE /mould interface and its influence on the surface morphology would also be interesting from an academic point of view. A recent application of the observations reported in this thesis, have involved preparing EHA-based PolyHIPE membranes with a thickness of 100 μm for electrochemical sensor applications [150]. Other applications of the mould tests experiments could involve preparing membranes for filtration based applications such as water purification.

10.2.2 Improving mechanical performance and fibre-reinforcement

In this investigation the addition of the fibres occurred prior to HIPE preparation and this limited the fibre volume to 10 % w/w of the monomer phase. Addition of the fibres after HIPE preparation could be investigated and may lead to higher fibre volumes being incorporated and therefore a further increase in the flexural rigidity of the material could be obtained. From an engineering aspect, injection moulding of the HIPE/fibre mixture could lead to possible alignment of the fibres and therefore an anisotropic material and enhanced mechanical properties in the direction of the aligned fibres.

Other fibres such as glass, carbon or PE could be used as reinforcement and their effect on the mechanical properties of the material investigated. Fibres could also be

incorporated with the MMA-based PolyHIPE material to observe if any further enhancement in the compressive properties of the material were obtained.

Addition of monomers such as maleimide or bismaleimides which are already known to enhance the mechanical properties of the PolyHIPE materials [74], [75], [76] could be used to prepare PolyHIPE materials on a large scale to observe any affect on the bulk mechanical properties of the material. Other methods such as preparation and testing of PolyHIPE materials containing epoxy resin, urethane or nylon based chemistry could be investigated.

Other methods of preparing anisotropic materials could also be investigated. Such as injection moulding of a HIPE containing fibres as previously discussed, to provide an anisotropic fibre-reinforced material. Heating and deforming other types of foam materials (e.g. polyurethanes) under a constant tension, then cooling, can lead to materials with an anisotropic structure (**see figure 10.1**) and a Poisson's ratio of greater than one [151].

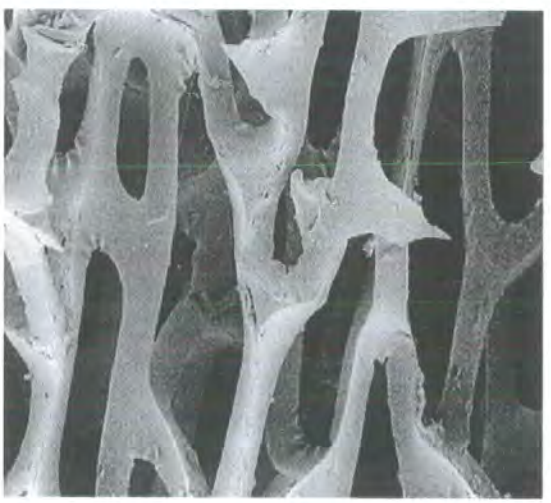

Figure 10.1 *SEM image of a polyurethane foam with anisotropic structure and Poisson's ratio greater than 1* [151].

Deformation of the PCL-based PolyHIPE material by the application of a triaxial compressive force may produce an inverted cell temporary structure and a PolyHIPE material which may show auxetic behaviour.

10.2.3 Permeability studies

Other future work could involve investigating gas permeability as it was not possible to perform the experiments due the difficulty and time involved in preparing a test rig. Other wetting and non-wetting liquids could be tested and compared to values obtained for water and kerosene. A different experimental set-up could be investigated and the permeability coefficient values compared to the values obtained in **chapter 8**.

References

1) L.E. Neilson, Mechanical Properties of Polymers, 2nd edition, Reinhold Publishing, New York, 1962.

2) K.E. Evans, A. Alderson, *Adv. Mater*, **12**, 617 (2000).

3) D.W. Hadley, I.M. Ward, An Introduction to the Mechanical Properties of Solid Polymers, 3rd edition, John Wiley & Sons Ltd, New York, 2000.

4) G. Cowie, Polymers: Chemistry and Physics of Modern Materials, 2nd edition, Chapman and Hall, New York, 1991.

5) T.G. Fox, *Bull. Am. Phys. Soc*, **1**, 123 (1956).

6) L.J. Gibson, M.F. Ashby, Cellular Solids: Structure and Properties, 1st edition. Pergamon Press, New York, 1988.

7) N. Fell, S, Forster, F. Ramsteiner, *Polym. Testing*, **20**, 661 (2001).

8) D. Barby, Z. Haq, U.S. 4, 522. 953, 1985.

9) K.J. Lissant, Emuslions and Emulsion Technology Part1, Marcel Dekker Inc, New York, 1974.

10) W.C. Griffin, *J. Soc. Cosmet. Chem*, **1**, 326 (1949).

11) W.C. Griffin, *J. Soc. Cosmet. Chem*, **5**, 249 (1954).

12) J.A. Kitchener, P.R. Musslewhite, "The Theory and Stability of Emulsions", in: P. Sherman (ed.), "Emulsion Science".

13) N.R. Cameron, Ph.D thesis, University of Strathclyde, 1995.

14) H.H. Chen, E. Ruckenstein, *J. Coll. Interf. Sci*, **145**, 260 (1991).

15) M.P. Aronson, M.F. Petko, *J. Coll. Interf. Sci*, **159**, 149 (1993).

16) J. Kizling, B. Kronberg, *Coll. Surf*, **50**, 131 (1990).

17) A.R Elmes, K. Hammond, D.C. Sherrington, U.S. 4,985,468, 1991.

18) D. Barby, Z. Haq, Eur. Pat. Appl. EP 68830, 1983.

19) D. Barby, Z. Haq, U.S. 4,797,310, 1989.

20) P.G. Cummins, D.P. Gregory, Z. Haq, E.J. Staples, Eur. Pat. Appl. EP 240342, 1987.

21) Z. Bhumgara, *Filtr. Sep*, **32**, 245 (1995).

22) K. Allmer, E. Berggren, E. Eriksson, A. Larsson, I. Porrvik, PCT Int. Appl. WO 9719347, 1997.

23) J.M. Williams, D.A. Wrobleski, *J. Mater. Sci*, **24**, 4062 (1989).

24) J.C. Dyer, B. Hird, P.K. Wong, S.M. Beshouri, PCT Int. Appl. WO 9621474, 1976.

25) C.J.C. Edwards, D.P. Gregory, M. Sharples, Eur. Pat. Appl. EP 239360, 1987.

26) C.J.C. Edwards, D.P. Gregory, M. Sharples, U.S. 4,788,225, 1988.

27) J.C. Dyer, T.A. Desmarais, PCT Int. Appl. WO 9640824, 1996.

28) J.C. Dyer, T.A. Desmarais, U.S. 5,633,291, 1997.

29) T.C. Roetker, T.A. Desmarais, B.A. Yeazell, PCT Int. Appl. WO 9946319, 1997.

30) B.T.A. Chang, P.K. Wong, T.V. Mai, PCT Int. Appl. WO 9737745.

31) N.R. Cameron, D.C. Sherrington, *J. Mater. Chem*, **7**, 2209 (1997).

32) S.M. Beshouri, U.S. 5200433, 1993.

33) S.M. Beshouri, U.S. 5334621, 1994.

34) S.A. Goldman, J.J. Scheibel, U.S. 5500451, 1996.

35) R.P. Adamski, S.M. Beshouri, V.G. Chamupathi, PCT Int. Appl. WO 9745456, 1997.

36) R.M. Bass, T.F. Brownscombe, PCT Int. Appl WO 9745479, 1997.

37) T.F. Brownscombe, R.M. Bass, L.S. Corley, U.S. 5,290,820, 1994.

38) T.F. Brownscombe, R.M. Bass, L.S. Corley, U.S. 5,358,974, 1994.

39) T.F. Brownscombe, W.P. Gergen, R.M. Bass, M. Mores, P.K. Wong, U.S. 5,189,070, 1993.

40) T.A. Desmarais, T.M. Shively, J.C. Dyer, B. Hird, S.T. Dick, PCT Int. Appl. WO 0050498, 2000.

41) T.A. Desmarais, T.M. Shively, J.C. Dyer, B. Hird, S.T. Dick, PCT Int. Appl. WO 0050502, 2000.

42) K. Kadonaga, A. Mitsuhashi, H. Fujimaru, M. Sasabe, K. Takahashi, M. Izubayashi, PCT Int. Appl. WO 0136493, 2001.

43) T.A. Desmarais, T.M. Shively, J.C. Dyer, PCT Int. Appl. WO 0050501, 2000.

44) A.M. Nyitray, J.M. Williams, *J. Cell. Plastics*, **25**, 217 (1989).

45) A.M. Nyitray, J.M. Williams, D. Onn, A. Witek, *Mater. Res. Soc. Symp. Proc*, **171**, 99 (1990).

46) J.M. Williams, Jr., A.M. Nyitray, M.H. Wilkerson, U.S. 4,966,919, 1990.

47) J.M. Williams, A.M. Nyitray, M.H. Wilkerson, U.S. 5,037,859, 1991.

48) J.M. Williams, M.H. Wilkerson, *Polymer*, **31**, 2162 (1990).

49) W.R. Even, D.P. Gregory, *MRS Bull*, **19**, 29 (1994).

50) R. Butler, C.M. Davies, A.I. Cooper, *Adv. Mater*, **13**, 1459 (2001).

51) H. Deleuze, R. Faivre, V. Herroguez, *Chem. Commun*, 2822 (2002).

52) S.W. Mork, J.H. Solc, C.P. Park, PCT Int. Appl. WO 9909070, 1999.

53) H. Tai, A. Sergienko, M.S. Silverstein, *Polymer*, **42**, 4473 (2001).

54) Z. Haq, U.S. 4,536,521, 1985.

55) N.R. Cameron, D.C. Sherrington, I. Ando, H. Kurosu, *J. Mater. Chem*, **6**, 719 (1996).

56) J.V. Crivello, *J. Org. Chem*, **46**, 3056 (1981).

57) K. Jones, B.R. Lothian, A. Martin, G. Taylor, Z. Haq, Eur. Pat. Appl. EP 156541, 1985.

58) K. Jones, B.R. Lothian, A. Martin, G. Taylor, Z. Haq, U.S. 4,612,334, 1986.

59) K. Jones, B.R. Lothian, A. Martin, G. Taylor, Z. Haq, U.S. 4,611,014, 1986.

60) K. Jones, B.R. Lothian, A. Martin, G. Taylor, Z. Haq, U.S. 4,668,709, 1987.

61) B.C. Benicewicz, G.D. Jarvinen, D.J. Kathios, B.S. Jorgensen, J. *Radioanal. Nucl. Chem*, **31**, 235 (1998).

62) J.F. Brown, N.R. Cameron, P. Kranjc, *J. Org. Lett*, **4**, 2497 (2002).

63) R.V. Law, D.C. Sherrington, C.E. Snape, *Macromolecules,* **30**, 2868 (1997).

64) A. Mercier, H. Deleuze, O. Mondain-Monval, *Actual. Chim*, 56 (2000).

65) A. Mercier, H. Deleuze, O. Mondain-Monval, *React. Funct. Polym*, **46**, 67 (2000).

66) A. Mercier, H. Deleuze, O. Mondain-Monval, *Macromol. Chem. Phys*, 202 (2001).

67) J.M. Williams, D.A. Wrobleski, *Langmuir*, **4**, 656 (1988).

68) L. Albiston, N.R. Cameron, D.P. Gregory, D.C. Sherrington, *Colloid Polym. Sci*, **274**, 592 (1996).

69) D.P. Gregory, M. Sharples, I.M. Tucker, Eur. Pat. Appl. EP 299672, 1989.

70) A.J. Gray, M.H. Wilkerson, J.M. Williams, *Langmuir*, **6**, 437 (1990).

71) A. Barbetta, N.R. Cameron, S.J. Cooper, *Chem. Commun*, 221 (2000).

72) A. Barbetta, N.R. Cameron, *J. Mater. Chem*, **10**, 2466 (2000).

73) P. Hainey, I.M. Huxham, B. Rowatt, D.C. Sherrington, L. Tetley, *Macromolecules*, **24**, 117 (1991).

74) P.G. Apen, J.R. Duke, M.A. Hoisington, *Polm. Mater. Sci. Eng*, **74**, 240 (1996).

75) P.G. Apen, J.R. Duke, M.A. Hoisington, *Polymer*, **38**, 3347 (1997).

76) P.G. Apen, J.R. Duke, M.A. Hoisington, *Polymer*, **39**, 4369 (1998).

77) N.R. Cameron, D.C. Sherrington, *Macromolecules*, **30**, 5860 (1997).

78) Z. Haq, Eur. Pat. Appl. EP 110678, 1984.

79) Z. Haq, U.S. 4,473,611, 1984.

80) J.C. Dyer, T.A. Desmarais, R.J. McChain , E.C. Smith, M. Tremblay, PCT Int. Appl. WO 0238657, 2002.

81) J.E. Mark, H. Sun, G.S. Sur, *Eur. Polym. J*, **38**, 2373 (2002).

82) J.J. Bartos III, M.H. Wilkerson, J.M. Williams, *J. Mater. Sci*, **25**, 5134 (1990).

83) D. Zenkert, An Introduction to Sandwich Construction, 2nd edition, EMAS, Warley, 1995.

84) H.G. Allen, Analysis and Design of Structural Sandwich Panels, 1st edition, Pergamon Press, New York, 1969.

85) http://www.euro-composites.com.

86) http://www.tubus-bauer.com.

87) http://www.hexcel.com.

88) K.A. Arora, A.J. Lesser, T.J. McCarthy, *Macromolecules*, **31**, 4614 (1998).

89) http://www-alice.ges.de/trd/gallery/rad/rad.html.

90) http://www.alcanairex.com.

91) http://www.diabgroup.com

92) http://www.atc-chem.com.

93) http://www.roehm.com.

94) http://www.npl.co.uk/cmmt/metal_foams/pdf_files/industrial_review.pdf.

95) http://www.alulight.com.

96) http://www.cymat.com

97) http://www.incosp.com.

98) X. Badiche, J.-D. Bartout, H. Bernet, Y. Bienvenu, M. Croset, S. Forest, P. Ienny, *Mat. Sci. Eng., A*, **A289**, 276 (2000).

99) B.C. Alen, U.S. 3,087,807, 1963.

100) P.W. Hardy, G.W. Peisker, U.S. 3,300,296, 1967.

101) http://www.baltek.com.

102) http://boatdesign.net/articles/foam-core, T. Gundberg, Foam Core Materials in the Marine Industry.

103) L.J. Gibson, O. Kesler, T.M. McCormack, R. Miller, *Int. J. Solids. Struct*, **38**, 4901 (2001).

104) http://www.mdacomposites.org/materials/htm.

105) G.S. Hollister, C. Thomas, Fibre Reinforced Materials, 1st edition, Elsevier, New York, 1966.

106) R. Nicholls, Composite Construction Materials Handbook, 1st edition, Prentice-Hall, New Jersey, 1976.

107) M. Palumbo, E. Tempesti, *Appl. Compos. Mater*, **8**, 343 (2001).

108) H. Shen, S. Nutt, *Composites Part A*, **34**, 899 (2003).

109) H. Shen, S. Nutt, *Composites Part A*, **34**, 941 (2003).

110) T.C. Cotgreave, J.B. Shorthall, *J. Mater. Sci*, **12**, 708 (1977).

111) P.C. LeBaron, T.J. Pinnavaia, Z. Wang, *Appl. Clay. Sci*, **15**, 11 (1999).

112) T. Lan, T.J. Pinnavaia, *Chem. Mater*, **6**, 2216 (1994).

113) E.P. Giannelis, P.B. Messersmith, *Chem. Mater*, **6**, 1719 (1994).

114) T.J. Pinnavaia, Z. Wang, *Chem. Mater*, **10**, 3769 (1998).

115) F.J. Guild, A.J. Kinloch, *J. Mater. Sci*, **30**, 1689 (1995).

116) D.L. Hunston, A.J. Kinloch, S.J. Shaw, *Polymer*, **24**, 1341 (1983).

117) D.L. Hunston, A.J. Kinloch, S.J. Shaw, *Polymer*, **24**, 1355 (1983).

118) M. Fischer, G.P. Hellman, *Macromolecules*, **29**, 2498 (1996).

119) A.M. Donald, E.J. Kramer, *J. Appl. Polym. Sci*, **27**, 3729 (1982).

120) E.P. Giannelis, W. Krawiec, L.G. Scanlon, R.A. Vaia, S. Vasudevan, *Adv. Mater*, **7**, 154 (1995).

121) J.S. Choi, C. Chun, S.J. Lee, *Macromol. Res*, **11**, 104 (2003).

122) Y.S. Choi, I.J. Chung, Y.K. Kim, K.H. Wang, M. Xu, *Polymer*, **44**, 6387 (2003).

123) P. Aranda, E. Ruiz-Hitzky, *Appl. Clay. Sci*, **15**, 119 (1999).

124) P. Aranda, E. Ruiz-Hitzky. *Chem. Mater*, **4**, 1395 (1992).

125) Comprehensive Polymer Science, Volume 3: Chain Polymerisation, Part I, ed. G.C. Eastmond, A. Ledwith, S. Russo, P. Sigwalt, 1st edition, Pergamon Press, Oxford, 1989.

126) BS 4370: Part 4, "Determination of the modulus of elasticity and strength of a rigid cellular material of polymeric origin", 1991.

127) ASTM C365-00, "Standard test method for flat-wise compressive properties of sandwich cores".

128) Polymer Handbook, ed. J. Brandrup, E.A. Grulke, E.H. Immergut, 4th edition, Wiley Interscience, 1999, USA.

129) http://www.fpl.fs..fed.us/documnts/pdf1996/conne96apdf, A.H. Conner, "Urea-Formaldehyde Adhesive resins".

130) Comprehensive Polymer Science, Volume 5: Step Polymerisation, ed. G.C. Eastmond, A. Ledwith, S. Russo, P. Sigwalt, 1st edition, Pergamon Press, Oxford, 1989.

131) D.D. Werstler, *Polymer*, **27**, 750 (1986).

132) D.D. Werstler, *Polymer*, **27**, 757 (1986).

133) A.W. Christiansen, *J. App. Polym. Sci*, **75**, 1760 (2000).

134) ASTM C273-00, "Standard Test Method for the Shear Properties of Sandwich Core Materials".

135) R.T. Conley, Thermal Stability of Polymers, 1st edition, Marcel Dekker, New York, 1970.

136) F.A.L. Dullien, Porous media: Fluid Transport and Pore Structure, 1st edition, Academic Press, London, 1979.

137) W. Burger, K. Lunkwitz, J. Troger, *J. Coll. Interf. Sci*, **194**, 281 (1997).

138) http://www.resintechgroup.com/tables/viscosity.html.

139) P.A. Webb, C. Orr, Analytical Methods in Fine Particle Technology, 1st edition, Micrometrics Instrument Corporation, USA, 1997.

140) G.C. Perry, R.G. Craig, F.A. Peyton, *J. Phys. Chem*, **64**, 541 (1960).

141) A.F. Fotheringham. R.R. Mather, Q. Wei, R.D. Yang, *J. Aerosol. Sci*, **33**, 1589 (2002).

142) J. Buckman, A.F. Fotheringham. R.R. Mather, Q. Wei, R.D. Yang, *Oil. Gas. Sci. Technol*, **58**, 593 (2003).

143) S. Kelch, A. Lendlein, *Angew. Chem. Int. Ed*, **41**, 2034 (2002).

144) R. Langer, A. Lendlein, A.M. Schmidt, *Proc. Natl. Acad. Sci*, **98**, 842 (2001).

145) W. Busby, Ph. D thesis, University of Durham, 2001.

146) W. Busby, N.R. Cameron, C.B. Jahoda, *Biomacromolecules*, **2**, 154 (2001).

147) W. Busby, N.R. Cameron, C.B. Jahoda, *Polym. Int*, **51**, 871 (2002).

148) I. Fleming, D.H. Williams, Spectroscopic Methods in Organic Chemistry, 5th edition, McGraw-Hill, UK, 1995.

149) D.K. Armani, C. Liu, *J. Micromech, Microeng*, **10**, 80 (2000).

150) N.R. Cameron, R.J. Carnachan, R. Kataky, M. Swan, C. Zhao, *Adv. Mater*, 2004 (submitted).

151) R.S. Lakes, T. Lee, *J. Mater. Sci*, **9**, 2397 (1997).

152) N. Chan, K.E. Evans, *J. Mater. Sci*, **21**, 5725 (1997).

153) A.I. Cooper, H. Zhang, *Chem. Mater*, **14**, 4017 (2002).

154) Y.C. Ko, J.D. Lindsay, U.S. Pat. Appl, 20040087926, (2004).

155) G. Akay, Z. Bhumgara, R.J. Wakeman, *Chem. Eng. Res. Des*, **73**, 782 (1995).

156) S. Bose, P.A. Mahanwar, *J. Min. Mater. Char. Eng*, **3**, 23 (2004).

157) W. Yang, W. Shi, Z. Li, B. Xie, J. Feng, M. Yang, *J. Elastom. Plast*, **36**, 251, (2004).